



REPORT

SURFACE WAVE MEASUREMENTS

CALIFORNIA STRONG MOTION INSTRUMENTATION PROGRAM STATIONS SANTA CLARA, SANTA CRUZ, SAN BENITO AND MONTEREY COUNTIES, CALIFORNIA

GEOVision Project No. 18045

Prepared for

State of California
Department of Conservation
California Geological Survey
Strong Motion Instrumentation Program
801 K Street
Sacramento, CA 94612

Prepared by

GEOVision Geophysical Services, Inc.
1124 Olympic Drive
Corona, California 92881

Report 18045-01

June 22, 2018

TABLE OF CONTENTS

1	INTRODUCTION	1
2	OVERVIEW OF SURFACE WAVE METHODS	4
3	FIELD PROCEDURES	11
3.1	SITE PREPARATION AND SURVEY CONTROL.....	11
3.2	MASW SURVEY	12
3.3	ARRAY MICROTREMOR SURVEY	14
3.4	HVSR MEASUREMENTS.....	16
4	DATA REDUCTION AND MODELING	17
4.1	MASW DATA REDUCTION	17
4.2	ARRAY MICROTREMOR DATA REDUCTION	18
4.3	HORIZONTAL/VERTICAL SPECTRAL RATIO MEASUREMENTS.....	21
4.4	SURFACE WAVE MODELING	22
5	RESULTS	27
6	REFERENCES	28
7	CERTIFICATION	31

APPENDICES

APPENDIX A	SITE REPORTS.....	32
	CE.47126.....	33
	CE.47179.....	44
	CE.47189.....	54
	CE.47377.....	67
	CE.47404.....	88
	CE.47405.....	99
	CE.47524.....	109
	CE.47567.....	119
	CE.47762.....	129
	CE.48906.....	140
	CE.57203.....	153
	CE.57218.....	163
	CE.57370.....	176
	CE.57371.....	186
	CE.58135.....	198

LIST OF TABLES

TABLE 1 CSMIP STATIONS	3
TABLE 2 SURFACE WAVE TECHNIQUES UTILIZED AT EACH CSMIP STATION	11
TABLE 3 SUMMARY OF RESULTS	27

LIST OF FIGURES

FIGURE 1 CSMIP STATIONS.....	2
FIGURE 2 RELATIONSHIP BETWEEN THE WAVELENGTH OF SURFACE WAVES AND INVESTIGATION DEPTH	4
FIGURE 3 TYPICAL SASW SETUP	5
FIGURE 4 MASKING OF WRAPPED PHASE SPECTRUM AND RESULTING DISPERSION CURVE	6
FIGURE 5 COMPARISON OF RAYLEIGH AND LOVE WAVE F-V TRANSFORMS	7
FIGURE 6 COMPARISON OF F-V TRANSFORMS BETWEEN VERTICAL AND RADIAL HORIZONTAL COMPONENT RAYLEIGH WAVE SEISMIC DATA AT SEISMIC STATION CE.13924	8
FIGURE 7 TYPICAL MASW FIELD LAYOUT	12
FIGURE 8 GEOMETRICS GEODE SEISMOGRAPH	13
FIGURE 9 4 LB HAMMER, 12 LB SLEDGEHAMMER, AND 240 LB AWD USED FOR MAS _R W ACQUISITION	13
FIGURE 10 HAMMER IMPACT ALUMINUM SOURCE AND WOOD TRACTION PLANK USED FOR MAS _L W ACQUISITION	14
FIGURE 11 ARRAY TYPES UTILIZED FOR ARRAY MICROTREMOR MEASUREMENTS	15
FIGURE 12 NESTED TRIANGLE AND L-SHAPED ARRAYS USED FOR ARRAY MICROTREMOR MEASUREMENTS	15
FIGURE 13 NANOMETRICS TRILLIUM COMPACT SEISMOMETER USED FOR HVSR MEASUREMENTS.....	16
FIGURE 14 MICROMED TROMINO® ENGR SEISMOMETER USED FOR HVSR MEASUREMENTS	17
FIGURE 15 COMPARISON OF RAYLEIGH WAVE F-V TRANSFORMS FROM 48 AND 12 CHANNEL RECEIVER GATHERS AT SEISMIC STATION CE.13080.....	18
FIGURE 16 EXAMPLE OF ESAC DATA REDUCTION.....	19
FIGURE 17 EXAMPLE OF ReMi™ PROCESSING WITH DISPERSION CURVE PICKED ALONG LOWER ENVELOPE OF RAYLEIGH WAVE ENERGY.....	20
FIGURE 18 EXAMPLE HVSR DATA FROM SEISMIC STATION CE.47405	21
FIGURE 19 INFLUENCE OF DENSITY ON V _S MODELS.....	23
FIGURE 20 INFLUENCE OF POISSON'S RATIO ON V _S MODELS DERIVED FROM RAYLEIGH WAVE DISPERSION DATA	25
FIGURE 21 INFLUENCE OF NON-UNIQUENESS ON ESTIMATED V _{S30}	26

1 INTRODUCTION

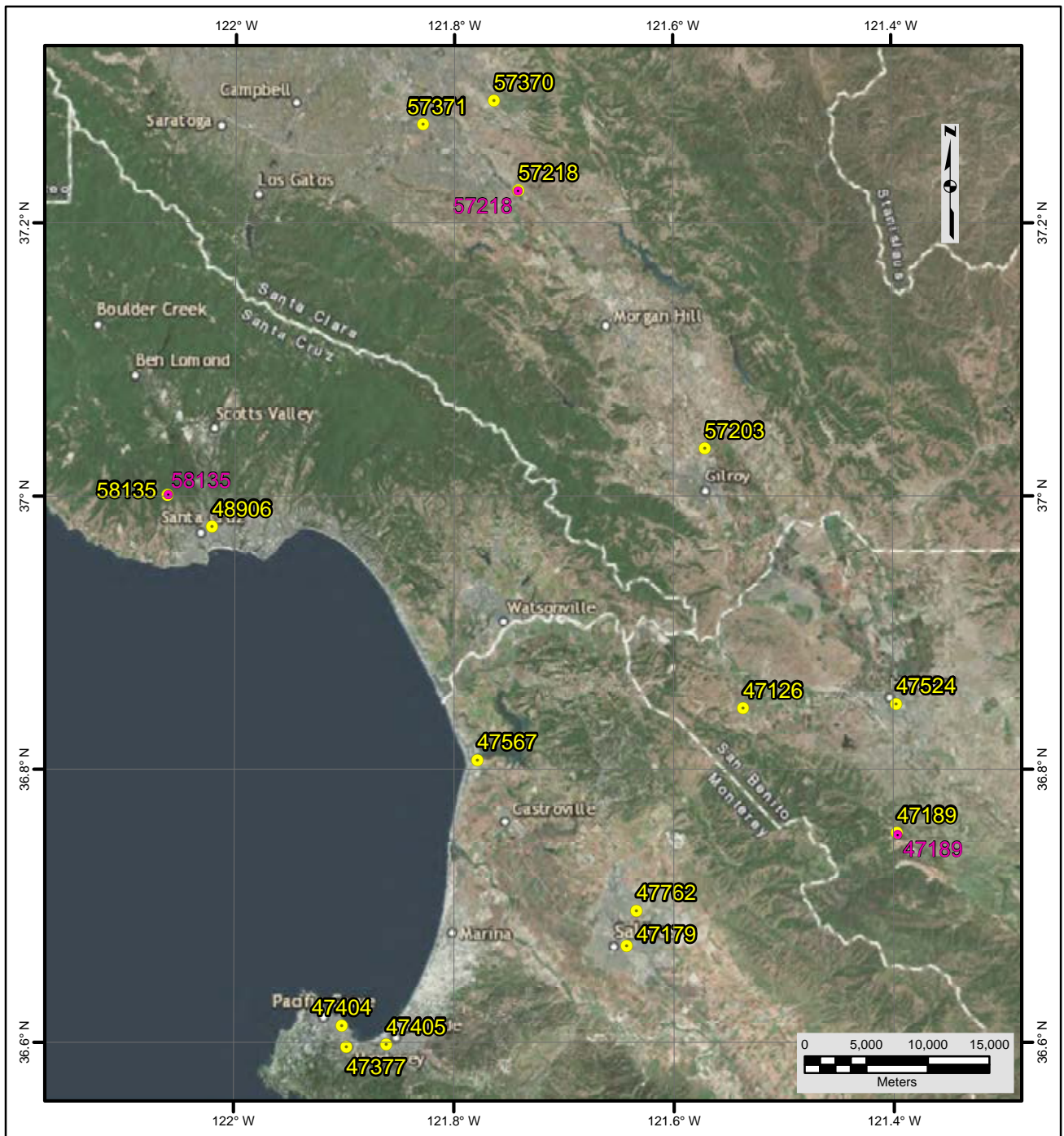
In-situ seismic measurements using active and passive (ambient noise) surface wave techniques were performed at fifteen (15) California Strong Motion Instrumentation Program (CSMIP) stations in Santa Clara, Santa Cruz, San Benito, and Monterey Counties, California from March 3rd to March 21st, 2016. The purpose of this investigation was to provide a shear (S) wave velocity profile to a minimum depth of 40 meters (m) and an estimate of the average S-wave velocity of the upper 30 m (V_{S30}) for each CSMIP site. The active surface wave technique utilized during this investigation consisted of the multi-channel analysis of surface waves (MASW) method. The passive surface wave techniques utilized consisted of the single station horizontal/vertical spectral ratio (HVSr) and array microtremor methods. The location and description of the CSMIP stations characterized during this investigation are summarized in Figure 1 and Table 1.

V_{S30} is used in the NEHRP provisions and the Uniform Building Code (UBC) to separate sites into classes for earthquake engineering design (BSSC, 1994). The average shear wave velocity of the upper 100 ft (V_{S100ft}) is used in the International Building Code (IBC) for site classification. These site classes are as follows:

- Class A – hard rock – $V_{S30} > 1500$ m/s (UBC) or $V_{S100ft} > 5,000$ ft/s (IBC)
- Class B – rock – $760 < V_{S30} \leq 1500$ m/s (UBC) or $2,500 < V_{S100ft} \leq 5,000$ ft/s (IBC)
- Class C – very dense soil and soft rock – $360 < V_{S30} \leq 760$ m/s (UBC)
or $1,200 < V_{S100ft} \leq 2,500$ ft/s (IBC)
- Class D – stiff soil – $180 < V_{S30} \leq 360$ m/s (UBC) or $600 < V_{S100ft} \leq 1,200$ ft/s (IBC)
- Class E – soft soil – $V_{S30} < 180$ m/s (UBC) or $V_{S100ft} < 600$ ft/s (IBC)
- Class F – soils requiring site-specific evaluation

At many sites, active surface wave techniques with the utilization of portable energy sources, such as hammers and weight drops, are sufficient to obtain a S-wave velocity model to a depth of 30 m. At sites with high ambient noise levels and/or very soft soils, these energy sources may not be sufficient to image to 30 m and a larger energy source, such as a bulldozer, is necessary. Alternatively, passive surface wave techniques, such as the array microtremor technique or the refraction microtremor method of Louie (2001), can be used to extend the depth of investigation at sites that have adequate ambient noise conditions. It should be noted that two-dimensional passive surface wave arrays (e.g. triangular, circular, or L-shaped arrays) will provide better accuracy than linear arrays.

This report contains the results of the active and passive surface wave measurements conducted at 15 CSMIP station sites. An overview of the surface wave methods is given in Section 2. Field and data reduction/modeling procedures are discussed in Sections 3 and 4, respectively. Results are presented in Section 5. References and our professional certification are presented in Sections 6 and 7, respectively.



File Name: 18045_ALL
Date: 5/29/2018

Legend

- CSMIP Station
- CSMIP Station Corrected Location

NOTES:

1. WGS 1984 Coordinate System
2. Image Source: Esri, DigitalGlobe, GeoEye, Earthstar Geographics, CNES/Airbus DS, USDA, USGS, AEX, Getmapping, Aerogrid, IGN, IGP, swisstopo, and the GIS User Community



**FIGURE 1
SITE LOCATION MAP
ALL STATIONS**



Table 1 CSMIP Stations

No.	Station Number	Station Name	Latitude	Longitude	Location	Address
1	47126	San Juan Bautista – Fire Station	36.8453	-121.5369	San Juan Bautista Fire Station	311 2 nd St., San Juan Bautista
2	47179	Salinas – City Yard	36.6715	-121.6432	Salinas City Service and Building Yard	John and Work St, Salinas
3	47189	Hollister – SAGO South	36.7526	-121.3963	Hollister Hills Rec. Area	7800 Cienega Rd, Hollister
4	47377	Monterey – City Hall	36.5974	-121.8979	Monterey City Hall	580 Pacific St., Monterey
5	47404	Monterey – Hawthorne & Lighthouse	36.6129	-121.9019	City of Monterey Building Maintenance #12	582 Hawthorne St., Monterey
6	47405	Monterey – Hwy 1 & Dela Vina	36.5991	-121.8615	Monterey Fire Station #3	401 Dela Vina Ave., Monterey
7	47524	Hollister – South & Pine	36.8483	-121.3973	Glorietta Warehouse Freefield	711 Sally St., Hollister
8	47567	Moss Landing – Hwy 1 & Dolan Rd A	36.8076	-121.7789	PG&E Substation	Dolan Rd, Moss Landing
9	47762	Salinas – County Hospital Grounds	36.6973	-121.6342	Natividad Hospital Freefield	1441 Constitution Blvd, Salinas
10	48906	Santa Cruz – County Office Bldg Grounds	36.9781	-122.0211	Santa Cruz County Office Building Freefield	701 Ocean St., Santa Cruz
11	57203	Gilroy – Hwy 101 & Cohansey	37.0355	-121.5714	St. Louise Regional Hospital Freefield	9400 No Name Uno, Gilroy
12	57218	San Jose – Hwy 101 & Metcalf Rd	37.2241	-121.7417	PG&E Substation	150 Metcalf Rd, San Jose
13	57370	San Jose – San Felipe & Villages Pkwy	37.2903	-121.7640	San Jose Fire Station #11	2840 Villages Parkway, San Jose
14	57371	San Jose – Monterey Hwy & Skyway Dr.	37.2730	-121.8289	San Jose Fire Station #18	4430 South Monterey Rd, San Jose
15	58135	Santa Cruz – UCSC Lick Elect Shop	37.0014	-122.0615	UC Santa Cruz, Lick Electronics Lab	McLaughlin Drive (UC Santa Cruz), Santa Cruz

Note. Stations CE.47189, CE.57218, and CE.58135 relocated with modified station coordinates presented in table above and pertinent data reports.

2 OVERVIEW OF SURFACE WAVE METHODS

Both active and passive (ambient noise) surface wave techniques were utilized during this investigation. Active surface wave techniques include the spectral analysis of surface waves (SASW) and multi-channel array surface wave (MASW) methods. Passive surface wave techniques include the HVSR technique and the array and refraction microtremor methods.

The basis of surface wave methods is the dispersive characteristic of Rayleigh and Love waves when propagating in a layered medium. The Rayleigh wave phase velocity (V_R) depends primarily on the material properties (V_S , mass density, and Poisson's ratio or compression wave velocity) over a depth of approximately one wavelength. The Love wave phase velocity (V_L) depends primarily on V_S and mass density. Rayleigh and Love wave propagation are also affected by damping or seismic quality factor (Q). Rayleigh wave techniques are utilized to measure vertically polarized S-waves (S_V -wave); whereas, Love wave techniques are utilized to measure horizontally polarized S-waves (S_H -wave).

Surface waves of different wavelengths (λ) or frequencies (f) sample different depths (Figure 2). As a result of variance in the shear stiffness of the distinct layers, waves with different wavelengths propagate at different phase velocities; hence, dispersion. A surface wave dispersion curve is the variation of V_R or V_L with λ or f (Figure 2).

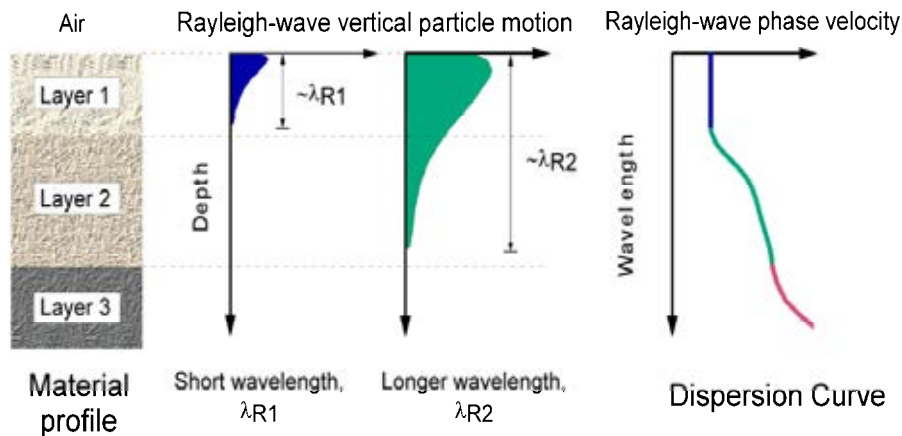


Figure 2 Relationship between the wavelength of surface waves and investigation depth

The SASW and MASW methods are in-situ seismic methods for determining shear wave velocity (V_S) profiles (Stokoe et al., 1994; Stokoe et al., 1989; Park et al., 1999a and 1999b, Foti, 2000). Surface wave techniques are non-invasive and non-destructive, with all testing performed on the ground surface at strain levels in the soil in the elastic range ($< 0.001\%$). SASW testing consists of collecting surface wave phase data in the field, generating the dispersion curve, and then using iterative forward or inverse modeling to calculate the shear wave velocity profile. MASW testing consists of collecting multi-channel seismic data in the field, applying a wavefield transform to obtain the dispersion curve, and data modeling to obtain the V_S profile.

A detailed description of the SASW field procedure is given in Joh, 1996. A typical SASW setup is shown in Figure 3. A vertical dynamic load is used to generate horizontally-propagating Rayleigh waves and a horizontal force is used to generate Love waves. The ground motions are monitored by two, or more, vertical (Rayleigh wave) or horizontal (Love wave) receivers and recorded by the data acquisition system capable of performing both time and frequency-domain calculations. Theoretical, as well as practical considerations, such as signal attenuation, necessitate the use of several receiver spacings to generate the dispersion curve over the wavelength range required to evaluate the stiffness profile. To identify and/or minimize phase shifts due to differences in receiver coupling and subsurface variability, the source location is reversed. To develop a V_S model to a 30-meter depth using Rayleigh wave methods, energy sources typically include: small hammers (rock hammer or 3 lb hammer) for short receiver intervals; 10 to 20 lb sledgehammers for intermediate separations, and accelerated weight drops (AWD) or an electromechanical shaker for larger spacings. More energetic sources, such as bulldozers or seismic vibrators (VibroseisTM), can be used to characterize velocity structure to depths of 100 m or more. Energy sources for shallow imaging using Love waves include a hammer and horizontal traction plank, portable hammer impact aluminum source, and inclined or horizontal accelerated weight drop systems. Energy sources for deeper imaging using Love waves include horizontal seismic vibrators. Generally, high frequency (short wavelength) surface waves are recorded across receiver pairs spaced at short intervals, whereas low frequency (long wavelength) surface waves require greater spacing between receivers. Dispersion data averaged across greater distances are often smoother because effects of localized heterogeneities are averaged.

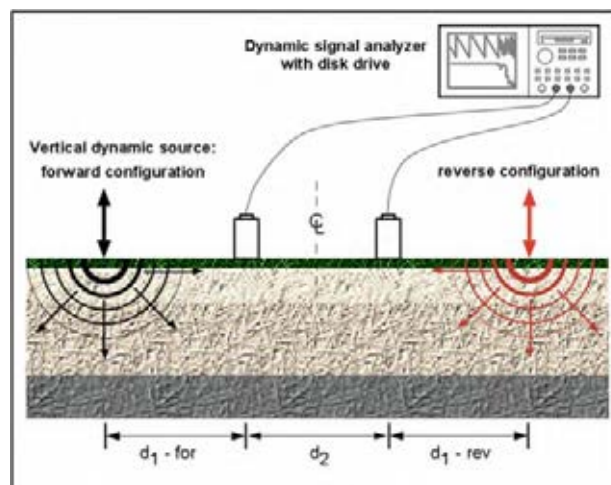


Figure 3 Typical SASW setup

After the time-domain motions from the two receivers are converted to frequency-domain records using the Fast Fourier Transform, the cross-power spectrum and coherence are calculated. The phase of the cross-power spectrum represents the phase differences between the two receivers as the wave train propagates past them. It ranges from $-\pi$ to π in a wrapped form and must be unwrapped through an interactive process called masking. Phase jumps are specified, near-field data (wavelengths longer than two times the distance from the source to first receiver) and low-coherence data are removed. The experimental dispersion curve is calculated from the unwrapped phase angle and the distance between receivers by:

$$V_{R/L} = f * d_2 / (\Delta\phi / 2\pi)$$

where V_R = Rayleigh wave phase velocity
 V_L = Love wave phase velocity
 f = frequency
 d_2 = distance between receivers
 $\Delta\phi$ = the phase difference in radians

Figure 4 demonstrates phase unwrapping of the cross power spectrum during SASW data reduction.

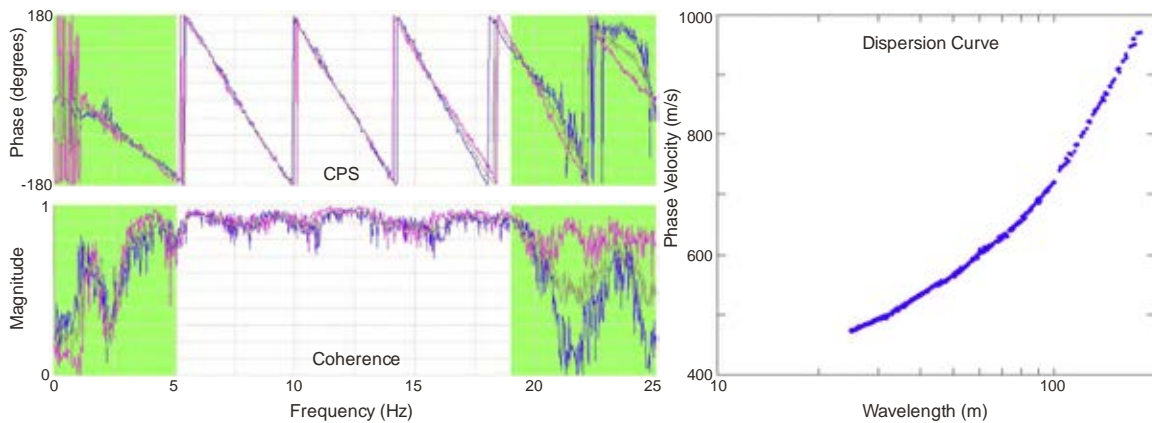


Figure 4 Masking of wrapped phase spectrum and resulting dispersion curve

A detailed description of the MASW method is given by Park, 1999a and 1999b. Ground motions are recorded by 24, or more, geophones typically spaced 1 to 3 m apart along a linear array and connected to a seismograph. Energy sources are the same as those outlined above for SASW testing. When applying the MASW technique to develop a one-dimensional (1-D) V_S model, the surface-wave data, preferably, are acquired using multiple-source offsets at both ends of the array. The most commonly applied MASW technique is the Rayleigh-wave based MASW method, which we refer to as MAS_{RW} to distinguish from Love-wave based MASW (MAS_{LW}). MAS_{RW} and MAS_{LW} acquisition can easily be combined with P- and S-wave seismic refraction acquisition, respectively. MAS_{RW} data are generally recorded using a vertical source and vertical geophone, but may also be recorded using a horizontal geophone with radial (in-line) orientation. MAS_{LW} data are recorded using transversely orientated horizontal source and transverse horizontal geophone.

A wavefield transform is applied to the time-history data to convert the seismic record from time-offset space to frequency-phase velocity space in which the surface-wave dispersion curve can be easily identified. Common wave-field transforms include: the frequency-wavenumber ($f-k$) transform, slant-stack transform ($\tau-p$), frequency domain beamformer, and phase-shift transform. Occasionally, SASW analysis procedures are used to extract surface wave dispersion data, from fixed receiver pairs, at smaller wavelengths than can be recovered by wavefield transformation. Construction of a dispersion curve, over the wide frequency/wavelength range necessary to develop a robust V_S model while also limiting the maximum wavelength based on an established near-field criterion (e.g. Yoon and Rix, 2009; Li and Rosenblad, 2011), generally

requires multiple source offsets. Although, the vast majority of MASW surveys record Rayleigh waves, it has been shown that Love wave techniques can be more effective in some environments, particularly shallow rock sites and sites with a highly attenuative, low velocity surface layer (Xia, et al., 2012; **GEOVision**, 2012; Yong, et al., 2013; Martin, et al., 2014). Figure 5 provides an example of frequency-velocity (f-v) transforms of MAS_RW and MAS_LW data from site CE.13929 (Yong, et al., 2013) where the fundamental mode Love wave was much more easily interpreted.

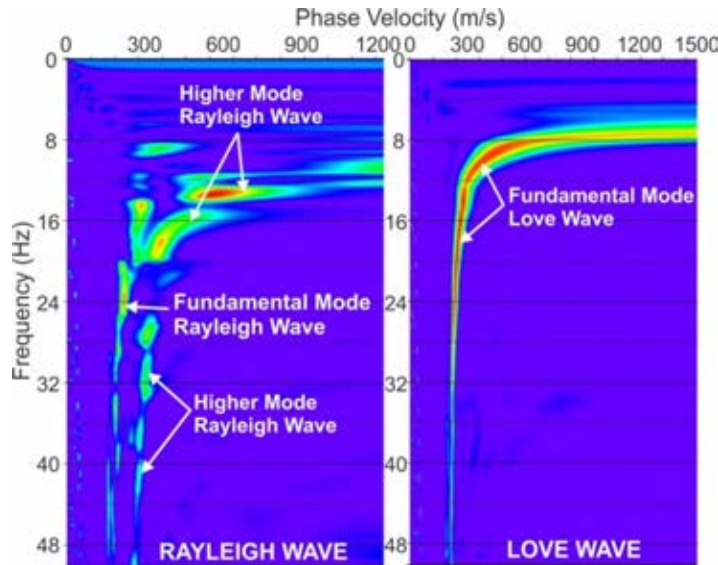


Figure 5 Comparison of Rayleigh and Love wave f-v transforms

Rayleigh wave techniques, however, are generally more effective at sites where velocity gradually increases with depth because larger energy sources are readily available for generation of Rayleigh waves. Rayleigh wave techniques are generally more applicable to sites with high velocity layers and/or velocity inversions because the presence of such structures is more apparent in the Rayleigh wave dispersion curves than in Love wave dispersion curves. Rayleigh wave techniques are preferable at sites with a high velocity surface layer because Love waves do not theoretically exist in such environments. Occasionally, the horizontal radial component of a Rayleigh wave may yield higher quality dispersion data than the vertical component because different modes of propagation may have more energy in one component than the other. Recording both the vertical and horizontal components of the Rayleigh wave is particularly useful at sites with complex modes of propagation or when attempting to recover multiple Rayleigh wave modes for multi-mode modeling as demonstrated in Dal Moro, et al, 2015. Figure 6 provides example f-v transforms of vertical and horizontal radial component Rayleigh wave data from site CE.13924 where the horizontal component data yields a better-defined dispersion curve at low frequencies than the vertical component data. Joint inversion of Rayleigh and Love wave data may yield more accurate V_s models and also offer a means to investigate anisotropy, where S_V - and S_H -wave velocity are not equal, as shown in Dal Moro and Ferigo, 2011.

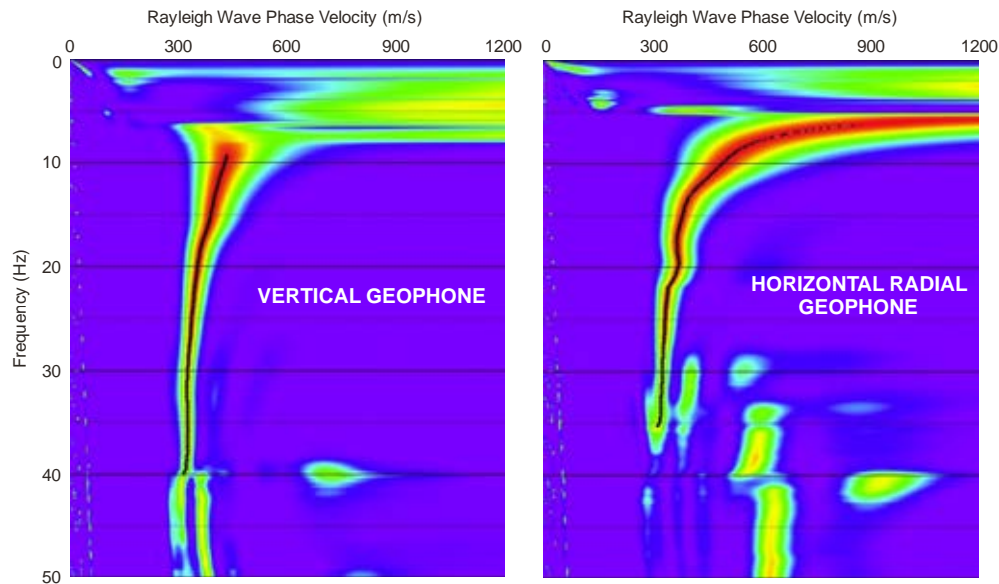


Figure 6 Comparison of f - v transforms between vertical and radial horizontal component Rayleigh wave seismic data at seismic station CE.13924

A detailed discussion of the array microtremor method can be found in Okada, 2003. This technique uses 4, or more, receivers aligned in a 2-dimensional array. Unlike the SASW and MASW techniques, which uses an active energy source (i.e. hammer), the microtremor (ambient vibration, passive surface wave) technique records background noise emanating from ocean wave activity, wind noise, traffic, industrial activity, construction, etc. Triangle, circle, semi-circle, and “L” shaped arrays are commonly used, although any 2-dimensional arrangement of receivers can be used. For investigation of the upper 100 m, receivers typically consist of 1 to 4.5 Hz geophones. The nested triangle array, which consists of several embedded equilateral triangles, is often used as it provides accurate dispersion curves with a relatively small number of geophones. With this array, the outer side of the triangle should be equal to or greater than the desired depth of investigation. The “L” array is useful at sites located at the corner of perpendicular intersecting streets. Typically, 30, or more, 30-second noise records are acquired for analysis. The surface wave dispersion curve is typically estimated from array microtremor data using various f - k methods such as beam-forming (Lacoss, et al., 1969), and maximum-likelihood (Capon, 1969), and the spatial-autocorrelation (SPAC) method, which was originally based on work by Aki, 1957. The SPAC method has since been extended and modified (Ling and Okada, 1993 and Ohori *et al.*, 2002) to permit the use of noncircular arrays, and is now collectively referred to as extended spatial autocorrelation (ESPAC or ESAC). Further modifications to the SPAC method permit the use of irregular or random arrays (Bettig *et al.*, 2001). Although it is common to apply SPAC methods to obtain a surface wave dispersion curve for modeling, other approaches involve direct modeling of the coherency data, also referred to as SPAC coefficients (Asten, 2006 and Asten, *et al.*, 2015).

The refraction microtremor technique (ReMi™), a detailed description of which can be found in Louie (2001), differs from the more established array microtremor technique in that it uses a linear receiver array rather than a two-dimensional array. Refraction microtremor field procedures typically consist of laying out a linear array of at least 24, 4.5 Hz geophones and recording 20, or more, 30 second noise records. These noise records are reduced using the

software package SeisOpt® ReMi™ v2.0 by Optim™ Software and Data Services. This package is used to generate and combine the slowness (p) – frequency (f) transform of the noise records. The surface wave dispersion curve is picked at the lower envelope of the surface wave energy identified in the p-f spectrum. It should be noted that other data reduction techniques such as seismic interferometry and ESAC can also be used to extract surface wave dispersion curves from linear array, passive surface wave data.

The horizontal-to-vertical spectral ratio (HVSR) technique was first introduced by Nogoshi and Igarashi (1971) and popularized by Nakamura (1989). This technique utilizes single-station recordings of ambient vibrations (microtremor or noise) made with a three-component seismometer. In this method, the ratio of the Fourier amplitude spectra of the horizontal and vertical components is calculated to determine the frequency of the maximum HVSR response (HVSR peak frequency), commonly accepted as an approximation of the fundamental frequency (f_0) of the sediment column overlying bedrock. The HVSR peak frequency associated with bedrock is a function of the bedrock depth and S-wave velocity of the sediments overlying bedrock. The theoretical HVSR response can be calculated for an S-wave velocity model using modeling schemes based on surface wave ellipticity, vertically propagating body waves, or diffuse wavefields containing body and surface waves. The HVSR frequency peak can also be estimated using the quarter-wavelength approximation:

$$f_0 = \frac{\bar{V}_s}{4z}$$

where f_0 is the site fundamental frequency and \bar{V}_s is the average shear-wave velocity of the soil column overlying bedrock at depth z .

The active and passive surface wave techniques complement one another as outlined below:

- SASW/MASW techniques image the shallow velocity structure which cannot be imaged by the microtremor technique and are needed for an accurate V_s model and V_{S30}/V_{S100ft} estimate.
- Microtremor techniques often perform well in noisy environments where SASW/MASW depth investigation may be limited.
- In a high noise environment, the microtremor technique will extend the depth of investigation of SASW/MASW soundings.

The dispersion curves generated from the active and passive surface wave soundings are generally combined and modeled using iterative forward and inverse modeling routines. The final model profile is assumed to represent actual site conditions. Several options exist for the Rayleigh wave forward solution: a formulation that takes into account only fundamental-mode Rayleigh wave motion, one that includes all stress waves and incorporates receiver geometry in an SASW test named the 3-D solution (Roesset et al., 1991), one that computes an effective mode for an MASW test but assumes a plane Rayleigh wave and no body wave effects, and a multi-mode solution that models different Rayleigh wave modes. Both fundamental mode and multi-mode forward solutions are available for modeling of Love wave data.

The theoretical model used to interpret the dispersion curve assumes horizontally layered, laterally invariant, homogeneous-isotropic material. Although these conditions are seldom

strictly met at a site, the results of active and/or passive surface wave testing provide a good “global” estimate of the material properties along the array. The results may be more representative of the site than a borehole “point” estimate.

It may not always be possible to develop a coherent, fundamental mode dispersion curve over sufficient frequency range for modeling due to dominant higher modes with the higher modes not clearly identifiable for multi-mode modeling. It may, however, be possible to identify the Rayleigh wave phase velocity of the fundamental mode at 40 m wavelength (V_{R40}) in which case V_{S30} can at least be estimated using the Brown et al., 2000 relationship:

$$V_{S30} = 1.045V_{R40}$$

This relationship was established based on statistical analysis of a large number of surface wave data sets from sites with control by velocities measured in nearby boreholes and has been further evaluated by Martin and Diehl, 2004, and Albarello and Gargani, 2010.

As with all surface geophysical methods, inversion of surface wave dispersion data does not yield a unique V_S model and there are multiple possible solutions that may equally well fit the experimental data. Based on our experience at other sites, the shear wave velocity models (V_S and layer thicknesses) determined by surface wave testing are within 20% of the velocities and layer thicknesses that would be determined by other seismic methods (Brown, 1998). The average velocity of the upper 30 m or 100 ft, however, is much more accurate, often to better than 5%, because it is not sensitive to the layering in the model. V_{S30} does not appear to suffer from the non-uniqueness inherent in V_S models derived from surface wave dispersion curves (Martin et al., 2006, Comina et al., 2011). Therefore, V_{S30} is more accurately estimated from inversion of surface wave dispersion data than the resulting V_S models.

3 FIELD PROCEDURES

3.1 Site Preparation and Survey Control

Active and passive surface wave sounding and HVSR measurement locations were established by **GEOVision** personnel after review of site conditions and accessibility. A summary of the geophysical techniques utilized at each site is presented as Table 2.

Table 2 Surface Wave Techniques Utilized at each CSMIP Station

Station No.	Active Surface Wave		Passive Surface Wave			
	MAS _R W	MAS _L W	Nested Triangle Array	L-shaped Array ¹	Linear	HVSR
47126	✓			✓		✓
47179	✓		✓			✓
47189	✓	✓				✓
47377	✓	✓	✓			✓
47404	✓		✓	✓		✓
47405	✓			✓		✓
47524	✓			✓		✓
47567	✓		✓			✓
47762	✓			✓		✓
48906	✓		✓			✓
57203	✓			✓		✓
57218	✓	✓		✓		✓
57370	✓			✓		✓
57371	✓			✓		✓
58135	✓				✓	✓

1. Two linear arrays can be extracted as needed.

When possible, a 70.5 to 94 m long MASW array was established at each site. Four sites (CE.47126, CE.47404, CE.48906, and CE.57370) only had space for arrays with length of 47 m, or less. This was not considered an issue because the microtremor arrays achieved the desired depth of investigation. Active-source Rayleigh wave data was acquired at each site as specified in the scope of work; however, it was also necessary to acquire active-source Love wave data at three (3) sites (CE.47189, CE.47377, and CE.57218) due to complex Rayleigh wave propagation.

The primary passive surface wave array established at each site consisted of a nested triangle or L-shaped array. The scope of work specified that L-shaped arrays be used with at least 22 geophones per leg and a 100 m length for the legs. Due to space limitations and/or ambient vibration conditions nested triangle arrays were utilized at five (5) of the 15 sites (CE.47179, CE.47377, CE.47404, CE.47567, and CE.48906). The array dimensions (typically 48 m length for the sides of the largest triangle) were sufficient to image to the specified 40 m depth. Additionally, it is preferable to use triangular or circular arrays when possible because they have better azimuthal coverage than L-shaped arrays. It was only possible to deploy a linear array for microtremor measurements at CE.58135 as there was insufficient space to deploy a 2-D array. Array microtremor measurements were not made at site CE.47189, which is located on the side of a hill, because there was no noise sources or space to deploy a 2-D array. Finally, it was not possible to deploy L-arrays with both legs having a length of over 100 m at 5 sites (CE.47126, CE.47405, CE.47762, CE.57370, CE.57371) due to limited space and the need to reduce the number of driveways that the array crossed. At two of these sites one leg of the array was longer than 100 m. The other sites typically had leg lengths of 69 and 72 m, which are still considered sufficient to image velocity structure to over 40 m depth.

At least one HVSR measurement was made near the testing arrays or in close proximity to the seismic station. At sites where field observations and geologic maps indicated that bedrock could be present in the upper 30 m or that there could be significant lateral velocity variability, additional HVSR measurement locations were established along the surface wave testing arrays to demonstrate that velocity structure was sufficiently one-dimensional in nature. Typically, one-hour of ambient vibration measurements were made at the primary HVSR measurement location with 20- to 30-minute recording durations for secondary measurement locations.

The locations of the surface wave and HVSR measurement locations were surveyed using a Trimble Pro XRS submeter GPS system and are summarized in the data reports presented for each site in Appendix A.

3.2 MASW Survey

A typical MASW field layout is shown in Figure 7. The seismic data acquisition system consisted of two 24-channel Geometrics Geode signal enhancement seismographs combined to form a 48-channel system and a laptop computer running Geometrics Seismodule Controller Software (Figure 8). Other seismic equipment utilized during this investigation consisted of: Geospace 4.5 Hz vertical and horizontal geophones, seismic cables, hammer switches, and multiple energy sources including a 240-lb accelerated weight drop (AWD), 4 lb hammer, 12 and 20 lb sledgehammers, an aluminum plate, horizontal traction plank, and hammer-impact aluminum shear wave seismic source (Figure 9).

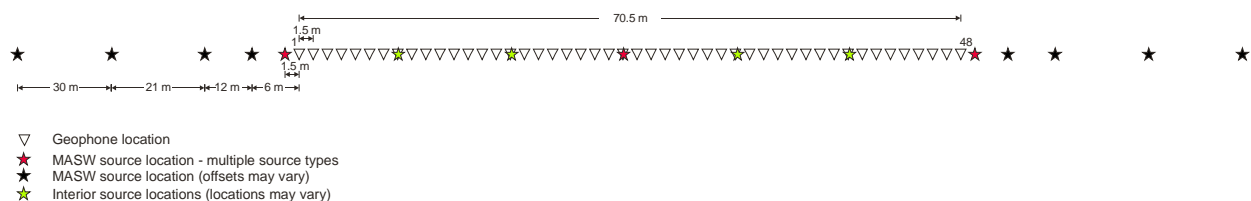


Figure 7 Typical MASW field layout



Figure 8 Geometrics Geode seismograph

MAS_RW data were acquired along a linear array of 48 vertical geophones spaced 1.5 to 2 m apart for an array length of 70.5 or 94 m; except for sites discussed in the previous section. When possible, multiple source locations were occupied at various offsets (up to 30 m) from each end of the array. Multiple sites, however, had limited space of off-end source locations. Additional, interior source locations were located at a 6- to 12-geophone interval. The 4-lb hammer and 12-lb sledgehammer were often used for the near offset source locations and the center source location (geophone 24). The 12-lb hammer was also used for all other interior source locations. The AWD was used for all off-end source locations, where necessary and possible, and the 20-lb sledgehammer was used in areas inaccessible to the AWD. Data from the transient impacts (hammers) were averaged 5 times, or more, to improve the signal-to-noise ratio.



Figure 9 4 lb hammer, 12 lb sledgehammer, and 240 lb AWD used for MAS_RW acquisition

MAS_LW data were also acquired along the same array used for MAS_RW data acquisition at three sites (CE.47189, CE.47377, and CE.57218) because the Rayleigh wave method appeared to be ineffective. Horizontal, transverse orientation 4.5 Hz geophones were used for Love wave

acquisition. A horizontal traction plank weighted down by a vehicle or a hammer impact aluminum S-wave seismic source and 12- or 20-lb sledgehammer (Figure 10) were used as the energy source for Love wave data acquisition. Love wave seismic data were obtained by striking each end of the source to facilitate identification of S-waves and Love waves, which are expected to have reversed polarity on the two seismic records. The seismic data were typically acquired using a 0.25 ms sample rate (fine sample rate required for seismic refraction analysis) and 1 s record length (long record length required for surface wave analysis). The final seismic record at each shot point was the result of stacking 5 to 15 shots to increase the signal to noise ratio. All seismic records were stored on a laptop computer with file names and acquisition parameters documented on a field log.



Figure 10 Hammer impact aluminum source and wood traction plank used for MAS_LW acquisition

3.3 Array Microtremor Survey

The passive surface wave equipment consisted of one or two Geometrics Geode signal enhancement seismographs, Geospace 4.5 Hz vertical geophones, and seismic cables. Array microtremor measurements were made using two types of arrays: 37 channel nested triangle array (Figure 11) using 4.5 Hz geophones and 48 channel L-shaped array using 4.5 Hz (Figure 11). At one site (CE.58135) it was only possible to acquire passive-source surface wave data along the linear array used for MASW data acquisition. At one rock site (CE.47189), there were not clear ambient vibration sources in the site vicinity. The site is also located on the side of a hill and it was not possible to deploy a 2-D array and, therefore, array microtremor measurements were not made. An L-shaped array yields two linear arrays that can be analyzed separately, if needed. Passive surface wave data were acquired using nested triangle arrays at sites where there was sufficient accessible open space to deploy the array. L-shaped arrays were utilized when only the perimeter of a site or the sidewalks of intersecting streets were accessible. Passive surface wave data were not generally acquired along linear arrays during this investigation. Photographs of the array microtremor equipment are presented in Figure 12. Ambient vibration (noise) measurements were generally recorded along each array for about 60 minutes at a 2 ms sample rate (120, 30 second records). Data were stored on a laptop computer for later processing. The field geometry and associated files names were documented in field data acquisition forms.

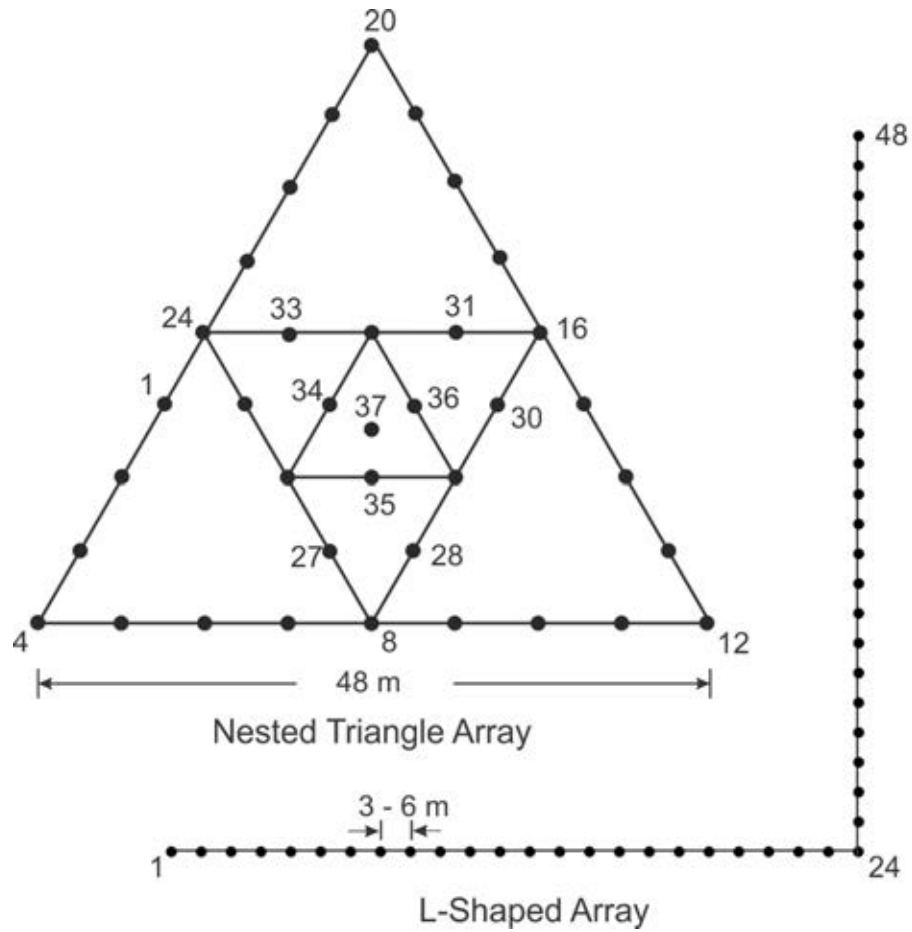


Figure 11 Array types utilized for array microtremor measurements



Figure 12 Nested triangle and L-shaped arrays used for array microtremor measurements

3.4 HVSR Measurements

The seismic systems used to acquire HVSR data consisted of a Nanometrics Trillium Compact 120 second seismometer coupled to a Nanometrics Centaur data acquisition unit (referred to herein as Trillium) and a MOHO Tromino® ENG Y (herein referred to as Tromino) as shown in Figures 13 and 14. The Trillium was coupled to the ground using an aluminum cradle with or without spikes depending upon whether the system was deployed on concrete or on soil. The Tromino was coupled to the ground using either geophone spikes adapted for measurements on soil or aluminum legs adapted for measurements on hard surfaces. The Trillium was set up at location near the seismic station with measurements made for the duration of array microtremor acquisition (~ 1 hour) with ambient noise data recorded at 100 samples per second. Microtremor data were stored in the Centaur data acquisition system and downloaded as miniseed format files at the end of each field day. HVSR measurements were occasionally made at additional locations, at sites with expected shallow rock or lateral velocity variability using a Tromino, to demonstrate that bedrock depth was not highly variable across the site. These microtremor measurements were made for 20 to 30 minutes at each measurement location with data recorded at 128 samples per second. Recordings were stored in the instrument's internal memory, downloaded to a laptop computer, viewed in the software package (Grilla) provided by Micromed, and reformatted to an ASCII file for further analysis. It should be noted that the Trillium is expected to provide the most reliable HVSR data in deep sedimentary basins and can yield reliable results at frequencies as low as 0.1 Hz, although such measurements require a long recording interval at night. On the other hand, the Tromino is designed for rapid, short duration deployment in shallow basins and will not yield reliable results at frequencies less than about 1.5 Hz in low noise environments.



Figure 13 Nanometrics Trillium Compact seismometer used for HVSR measurements



Figure 14 Micromed Tromino® ENGR seismometer used for HVSR measurements

4 DATA REDUCTION AND MODELING

4.1 MASW Data Reduction

Prior to data reduction, seismic records were reviewed to identify relevant geologic structures that could be constrained during data modeling; the most pertinent being approximate depth to high Poisson's ratio saturated sediments identified from P-wave refraction first arrival data in MAS_RW seismic records. It is important to constrain the approximate depth to and P-wave velocity of the saturated zone when modeling Rayleigh wave dispersion data in order to develop a V_S model as accurate as possible. A similar data reduction sequence is used for both MAS_RW and MAS_LW data.

The MASW data were reduced using the software Seismic Pro Surface V9.0 developed by Geogiga using the following steps:

- Input seismic record into software.
- Enter receiver spacing, geometry, offset range used for analysis, etc.
- Apply wavefield transform to seismic record to convert the data from time – offset to frequency – phase velocity space.
- Identify and pick Rayleigh wave dispersion curve.
- Repeat for all seismic records.
- Apply near-field criteria (maximum wavelength equal 1 to 1.3 times the source to midpoint of receiver array distance for Rayleigh wave data and 1.5 times the source to midpoint of receiver array distance for Love wave data).
- Merge multiple dispersion curves extracted from the MASW data collected along each seismic spread (different source types, source locations, different receiver offset ranges, etc.).
- Convert dispersion curves to required format for modeling.
- Calculate a representative dispersion curve for the combined MASW dispersion data using a moving average polynomial curve fitting routine.

A unique data acquisition and data reduction procedure used by **GEOVision** for 1-D MASW soundings is the use of multiple source types and source locations during data acquisition and the extraction of multiple (>50) dispersion curves from the different source locations and limited offset range receiver gathers associated with each source location. The use of such a data acquisition and processing strategy ensures that the modeled dispersion curve covers as wide a frequency/wavelength range as possible and is representative of average conditions beneath the array.

As an example, Figure 15 presents the frequency-phase velocity images of the seismic record offset 1 m from the near geophone at site CE.13080. The image on the left is from a seismic record collected using the AWD source with all 48 channels used for analysis. The image on the right is from a seismic record collected using a 4 lb hammer source with only the near 12 channels used for analysis in order to extract higher frequency (smaller wavelength) dispersion data. The 48-channel receiver gather only recovers the fundamental mode Rayleigh wave at frequencies less than 30 Hz with the 1st higher mode Rayleigh wave dominant at higher frequencies. The receiver gather comprised of the nearest 12 geophones recovers the fundamental mode Rayleigh wave to a frequency of greater than 100 Hz.

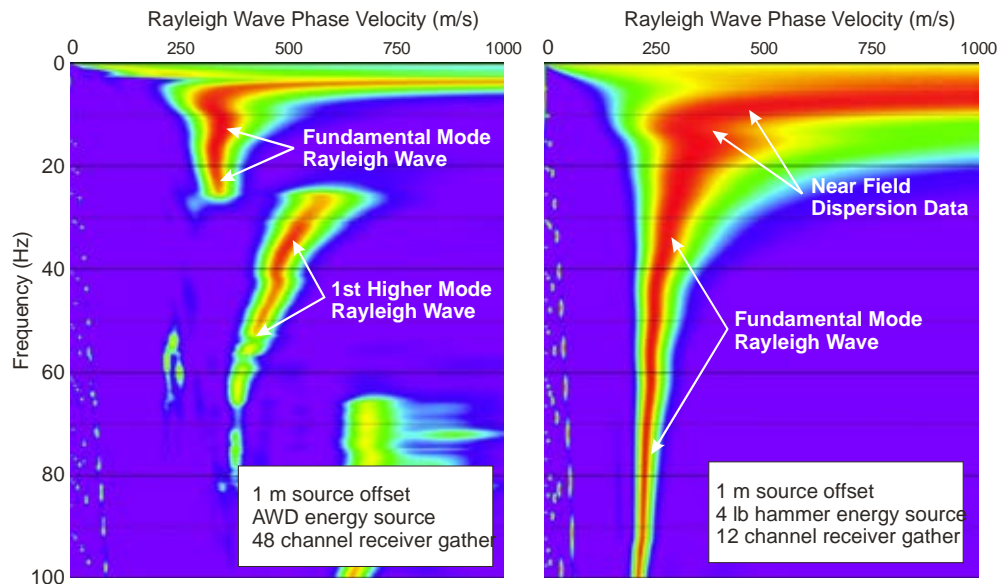


Figure 15 Comparison of Rayleigh wave *f-v* transforms from 48 and 12 channel receiver gathers at seismic station CE.13080.

4.2 Array Microtremor Data Reduction

Array microtremor data collected along nested triangle, L-shaped, and linear arrays were reduced using the ESAC method. Array microtremor data collected along several linear arrays (e.g. linear leg of L-shaped array) were also reduced using the ReMiTM method but not used for site characterization.

The processing sequence for implementation of the ESAC method in the SeisImager software package is as follows:

- Input all seismic records for a dataset into software.

- Load geometry (x and y positions) for each channel in seismic records.
- Calculate the SPAC coefficients for each seismic record and average.
- For each frequency calculate the RMS error between the SPAC coefficients and a Bessel function of the first kind and order zero over a user defined phase velocity range and velocity step.
- Plot an image of RMS error as a function for frequency (f) and phase velocity (v).
- Identify and pick the dispersion curve as the continuous trend on the f-v image with the lowest RMS error.
- Convert dispersion curves to appropriate format for modeling.
- Combine multiple passive dispersion curves, as appropriate.
- Calculate a representative dispersion curve for the passive dispersion data using a moving average polynomial curve fitting routine.

Figure 16 provides an example result from ESAC data processing. The velocity-frequency image shows the degree of fit of the Bessel function to the SPAC coefficients. The receiver offset versus coherence plot shows the best fitting Bessel function for the SPAC coefficients at 1.7 Hz, which, in this case, is at a velocity of 463 m/s.

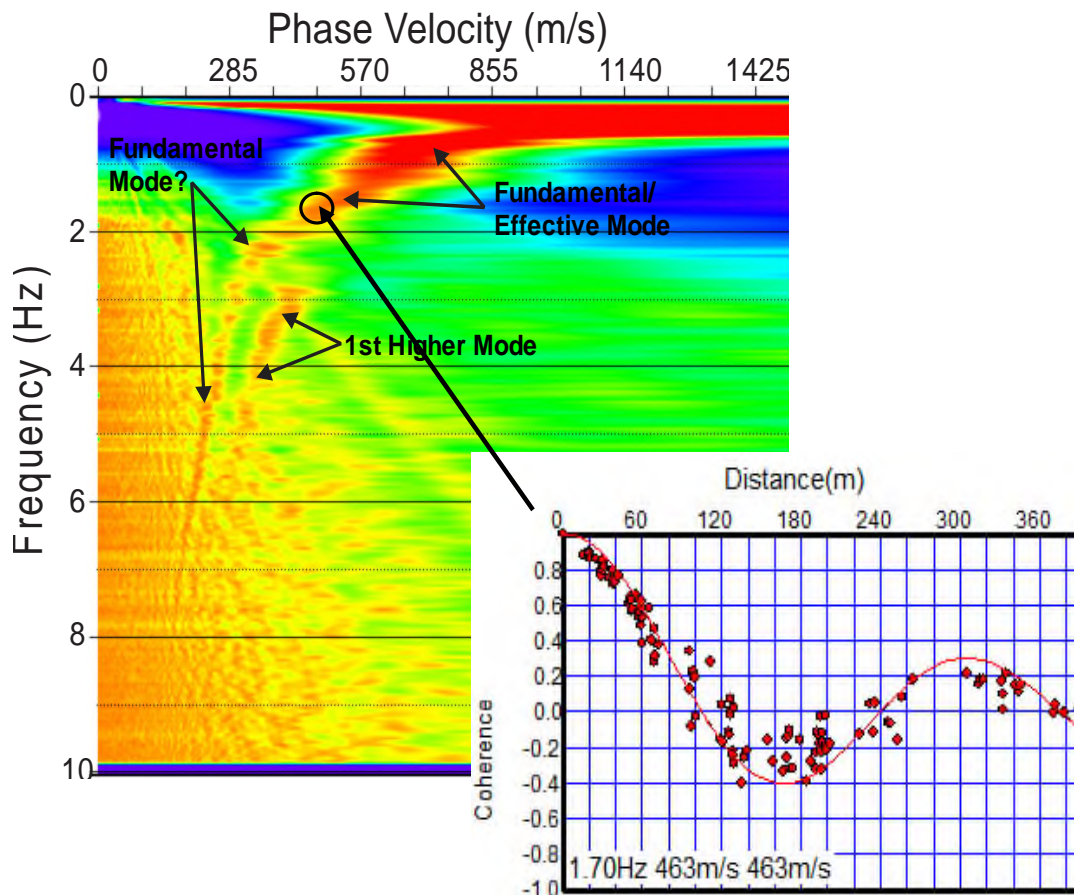


Figure 16 Example of ESAC data reduction

Selected, linear array microtremor data were reduced using both the Optim™ Software SeisOpt® ReMi™ v5.0 data analysis package and ESAC method described above; however, this data was not used for site characterization. Data reduction steps using the ReMi™ software included the following:

- Conversion of SEG-2 format field files to SEG-Y format.
- Data preprocessing which includes trace-equalization gaining and DC offset removal.
- Inputting receiver geometry.
- Computing the velocity spectrum of each record by p-f transformation in both forward and reverse directions.
- Combining the individual p-f transforms (either all or selected) into one image.
- Picking and saving the dispersion curve.
- Conversion of the dispersion curve to appropriate format for modeling.
- Combination of dispersion curve with other passive dispersion curves as appropriate.

An example of the interpretation of linear array microtremor data collected at seismic station CE.12092 is presented as Figure 17. The ReMi™ technique requires that the dispersion curve is interpreted along the lower envelope of the surface wave energy, which is subjective. Analysis of linear array microtremor data using the ESAC technique is not subjective; however, the resulting dispersion curve is only accurate if the multi-directional noise criteria are adequately satisfied.

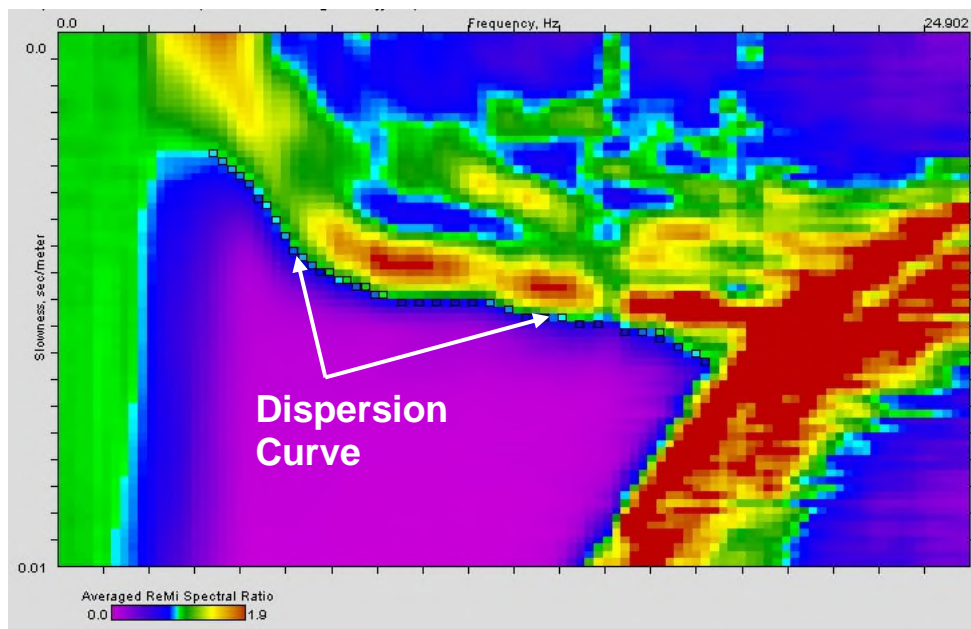


Figure 17 Example of ReMi™ processing with dispersion curve picked along lower envelope of Rayleigh wave energy

4.3 Horizontal/Vertical Spectral Ratio Measurements

HVSR data were reduced using the Geopsy Version 2.9.1 software package (<http://www.geopsy.org>) developed by Marc Wathelet, ISTERre, Grenoble, France with the help of many other researchers.

Microtremor data recorded by the Trillium were exported to miniseed format. Microtremor data recorded by the Tromino were exported to an ASCII file using the software package Grilla, provided with the instrument. Upon export, a 0.3-Hz low-cut filter was automatically applied to the Tromino data. Data files were then loaded into the Geopsy software package, where data file columns containing the vertical and horizontal (north and east) components and the sample rate were specified. HVSR was typically calculated over a frequency range dependent upon the observed site response and using a time window length of 30 to 200 s. Time windows were automatically picked. Fourier amplitude spectra were calculated after applying a 10% cosine taper and smoothed by the Konno and Ohmachi filter with a smoothing coefficient value of 30 to 40. The vertical amplitude spectra were divided by the root-mean-square (RMS) of the horizontal amplitude spectra to calculate the HVSR for each time window and the average HVSR of all time windows. Time windows containing clear transients (nearby foot or vehicular traffic) or yielding poor quality results were then deleted and the computations repeated. The average HVSR peak frequency and standard deviation from all time windows used for analysis is computed and presented along with the standard deviation of the HVSR amplitudes for all time windows.

Figure 18 presents example HVSR data from seismic station CE.47405. The colored lines are the HVSR for each 120 s time window used for analysis. The solid black line is the average HVSR response and the dashed lines represent the HVSR standard deviation.

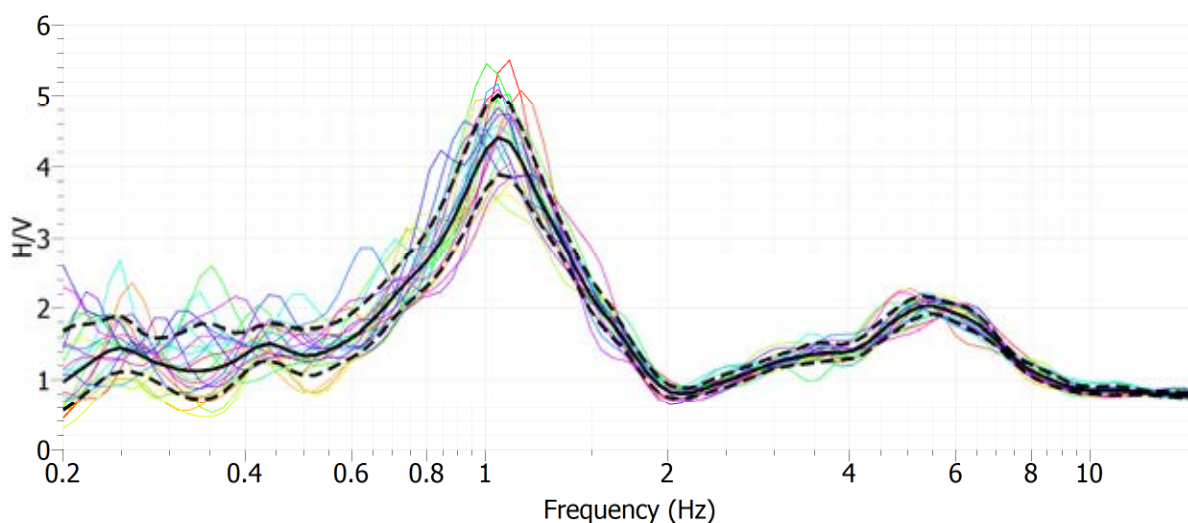


Figure 18 Example HVSR data from seismic station CE.47405

4.4 Surface Wave Modeling

The representative dispersion curves from the active and passive surface wave data at each sounding location were combined as appropriate and the moving average polynomial curve fitting routine in WinSASW V3 was used to generate a composite representative dispersion curve for modeling. During this process the active surface wave data were generally given equal weight to the combined passive surface wave data in the overlapping wavelength range and the combined weight of any linear passive arrays used for analysis was always less than that of the 2D arrays. An equal logarithm wavelength sample rate was used for the representative dispersion curve to reflect the gradual loss in model resolution with depth.

V_S models developed from combined MASW and 2-D array microtremor dispersion data are much more robust and reliable than those that utilize linear microtremor arrays; therefore, linear microtremor arrays were not used for site characterization. At site CE.58135 array microtremor data could only be acquired using a linear array; however, this array did not yield useable Rayleigh wave dispersion data. The mean and coefficient of variation (COV) of V_{R40} or V_{L50}/V_{L55} were calculated from the active and/or passive surface wave dispersion data for use in estimating the error in V_{S30} . The scatter in V_{R40} , V_{L50} , or V_{L55} is a function of measurement and analytical errors as well as the lateral velocity variability beneath the measurement array(s). V_{R40} can also be used to estimate V_{S30} using the Brown, et al., 2000 relationship presented previously.

The final composite representative dispersion curve for each site was loaded into an inverse modeling software package to develop a V_S model. During this process an initial velocity model was generated based on general characteristics of the dispersion curve and the inverse modeling routine utilized to adjust the layer V_S until an acceptable agreement with the observed data was obtained. Layer thicknesses were adjusted and the inversion process repeated until a V_S model was developed with low RMS error between the observed and calculated dispersion curves. Multiple V_S models were developed to demonstrate model non-uniqueness, particularly regarding depth and velocity of the half space when there was a sharp impedance contrast (e.g. bedrock unit). Typically, the V_S model with intermediate depth to rock was selected for the purpose of site characterization unless HVSr data indicated another V_S model was more appropriate. V_{S30} was estimated from the resulting V_S models as the ratio of 30 m and the travel time of an S-wave through the 30 m soil/rock column. At sites where rock was encountered within the depth of investigation, the predicted HVSr peak based on the diffuse field assumption was computed for all V_S models using the software package *HV-Inv* Release 2.3 Beta, which is summarized in García-Jerez, et al., 2016, and compared to the observed HVSr peaks.

Rayleigh wave dispersion data were modeled using either the fundamental mode, effective mode or multi-mode solutions in the WinSASW V3, Seisimager WaveEq, Geogiga Surface Plus, or Geopsy software packages. One site (CE.48906) required an effective mode solution to model a smooth transition from fundamental to 1st higher mode Rayleigh wave at low frequencies. Two sites (CE.47377 and CE.47404) required a multi-mode Rayleigh wave inversion. Love wave dispersion data collected at three sites (CE.47189, CE.47377, and CE.57218), two of which could only be characterized using Love wave data, were modeled using the fundamental mode Love wave solution in the Seisimager software package. Data inputs into the modeling software include layer thickness, S-wave velocity, P-wave velocity or Poisson's ratio (Rayleigh wave

only), and mass density. P-wave velocity and mass density only have a very small influence (i.e. less than 10% providing realistic parameters used) on the S-wave velocity model generated from a surface wave dispersion curve. However, realistic assumptions for P-wave velocity, which is significantly impacted by the location of the saturated zone, and mass density will significantly improve the accuracy of the S-wave velocity model.

Constant mass density values of 1.7 to 2.4 g/cm³ were used in the V_S profiles for subsurface soils depending on P- and S-wave velocity. Within the normal range encountered in geotechnical engineering, variation in mass density has a negligible effect on the estimated V_S from surface wave dispersion data (Foti et al, 2015). Figure 19 demonstrates the effect of density on the resulting V_S model. V_S models are developed for a synthetic model with identical dispersion curves the only variable being constant density (i.e. no reflectivity associated with density) in one model, realistic variation in density with seismic velocity and depth in another model, and an unrealistic amount of density variation in the final model. Relative to the V_S model with realistic density variation, V_{S30} is overestimated by about 1.5% in the V_S model with constant density and underestimated by about 4.5% in the V_S model with an unrealistic amount of density variation. Based on this example, we conclude that the use of realistic density variation in the V_S models will result in an error in V_{S30} associated with density on the order of about 1%.

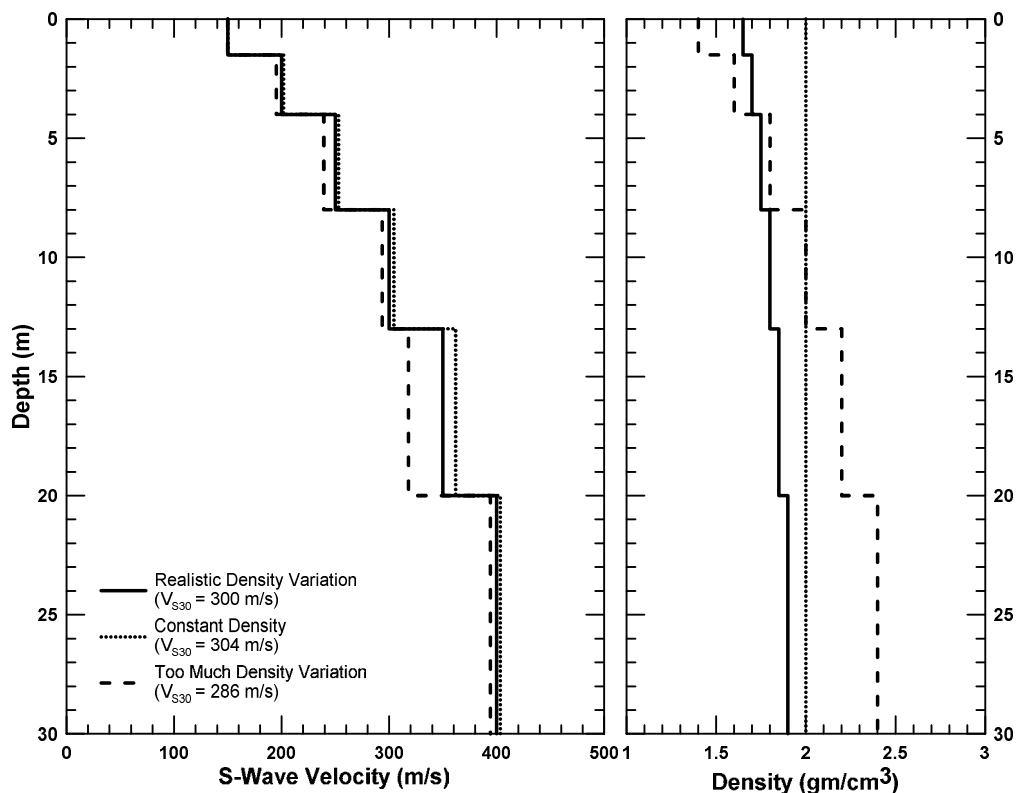


Figure 19 Influence of density on V_S models

During modeling of Rayleigh wave dispersion data, the compression wave velocity (V_P) for unsaturated sediments and weathered rock was estimated using a Poisson's ratio (ν) of 0.3 and the relationship:

$$V_P = V_S [(2(1-\nu))/(1-2\nu)]^{0.5}$$

Poisson's ratio has a larger affect than density on the estimated V_S from Rayleigh wave dispersion data. Achenbach (1973) provides approximate relationship between Rayleigh wave velocity (V_R), V_S and ν :

$$V_R = V_S [(0.862 + 1.14 \nu)/(1 + \nu)]$$

Using this relationship, it can be shown that V_S derived from V_R only varies by about 10% over possible 0 to 0.5 range for Poisson's ratio where:

$$\begin{aligned} V_S &= 1.16V_R \text{ for } \nu = 0 \\ V_S &= 1.05V_R \text{ for } \nu = 0.5 \end{aligned}$$

The common range of the Poisson's ratio for unsaturated sediments and rock is about 0.25 to 0.35, although there can be exceptions. Over this range, V_S derived from modeling of Rayleigh wave dispersion data will vary by about 5%. An intermediate Poisson's ratio of 0.3 was, therefore, often selected for modeling to minimize any error associated with the assumed Poisson's ratio.

To reduce errors associated with expected high Poisson's ratio of saturated sediments, seismic refraction first arrival data were reviewed in the MAS_RW seismic records to determine if there was any evidence of a refractor associated with the top of the saturated zone in the upper 20 to 30 m. If a saturated zone refractor was identified, interactive layer based modeling was conducted to estimate the depth to and V_P (>1,500 m/s) of the saturated sediments, which was then constrained when modeling the dispersion data. Poisson's ratio of saturated, soft sediments can be slightly less than 0.5, and gradually decrease with depth as the sediments become stiffer. It should be noted that Poisson's ratio only affects V_S models developed from Rayleigh wave dispersion data and not those developed from Love wave dispersion data.

Figure 20 demonstrates the effect of Poisson's ratio on the resulting V_S model. V_S models are developed for a synthetic model with identical dispersion curves the only variable being constant Poisson's ratio, which is allowed to vary from 0.1 to 0.495. There is a 20% variation in V_{S30} for V_S models with constant Poisson's ratio over the 0.1 to 0.495 range, but only 6% variation in V_{S30} for V_S models with Poisson's ratio over the common 0.25 to 0.35 range for unsaturated sediments and rock. Therefore, the error in V_{S30} associated with assumed Poisson's ratio may only be on the order of 3% providing the depth to and V_P of the saturated zone is constrained and a Poisson's ratio near 0.3 is used for unsaturated sediments when modeling Rayleigh wave dispersion data.

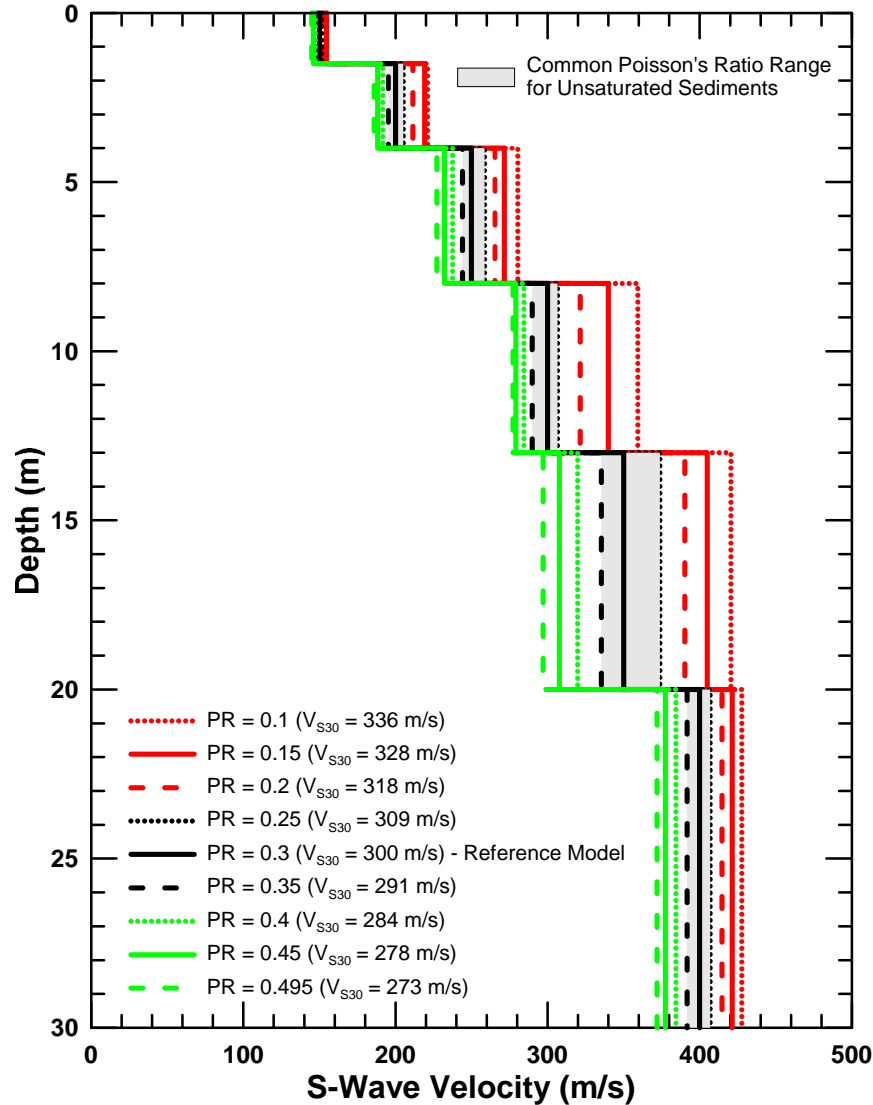


Figure 20 Influence of Poisson's ratio on V_S models derived from Rayleigh wave dispersion data

When modeling surface wave dispersion data, multiple V_S models exist that fit equally well to the observed dispersion curve; referred to as non-uniqueness. Non-uniqueness has been found to have very little effect on estimated V_{S30} as shown in the example presented as Figure 21. Comina et al., 2011 demonstrate that the coefficient of variation (COV) in V_{S30} due to non-uniqueness is often less than about 2%. In this example from station CE.13929, characterized as part of Yong, et al., 2013, multiple V_S models are presented with effectively identical Love wave dispersion curve yet only result in about 2% variation in V_{S30} . The variation in V_{S30} would have been greater had multiple models been generated that fit within error bars defined by the scatter in the dispersion data. However, we address this component of error using the scatter in V_{R40} or V_{L50}/V_{L55} .

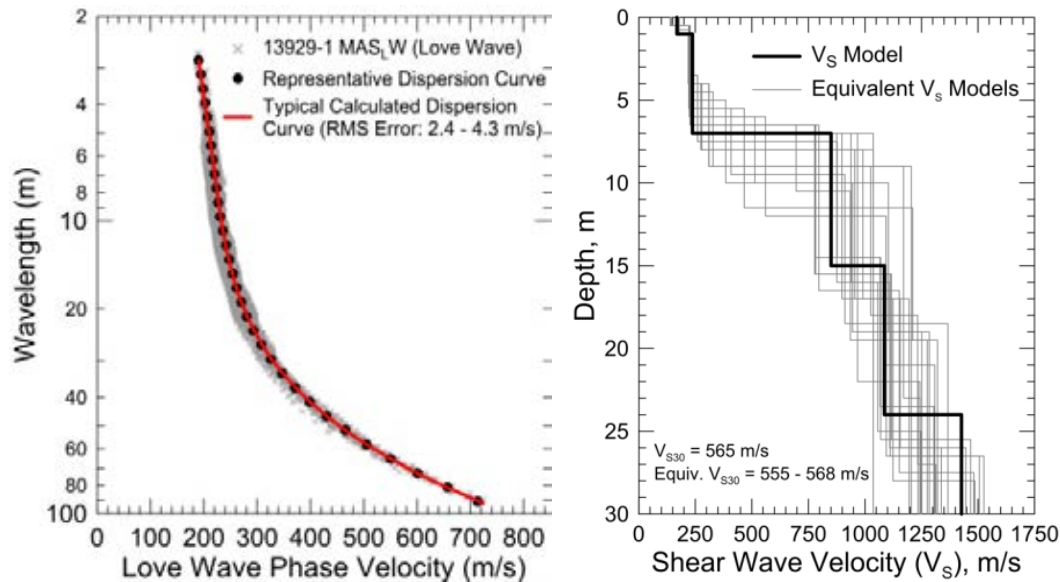


Figure 21 Influence of non-uniqueness on estimated V_{S30}

The error in V_{S30} is the combined effect of assumed density and Poisson's ratio on the resulting V_S models, the error in V_{S30} associated with non-uniqueness, and error in the dispersion curves which is accounted for using the scatter in V_{R40} or V_{L50} . Therefore, the estimated error in V_{S30} , which includes some effects of the lateral velocity variability beneath the testing arrays, was computed as the sum of the following rounded to the nearest 5 m/s: an estimated error of 3% from the realistic assumed layer Poisson's ratios in the model (Rayleigh wave modeling only), 1% error from the realistic assumed layer densities in the model, 2% for the variation in V_{S30} associated with non-uniqueness, and the coefficient of variation (COV) in V_{R40} or V_{L50} between the active and/or passive surface wave dispersion data. In general, resulting errors are slightly less than 10% of V_{S30} . We believe that these error estimates are conservative because they include some component of the lateral velocity variability beneath the testing arrays. In many cases the estimated V_{S30} may fall within the actual range of V_{S30} present beneath the testing array(s). It is of interest to note that V_{S30} estimates based on V_{R40} are generally within 10% of those estimated from the V_S models at the sites.

5 RESULTS

Data reports for each site are presented in Appendix A. These reports include the following:

- Site name and location.
- V_{S30} and estimated error.
- NEHRP Site Class.
- Geomatrix Code.
- HVSr Peak Frequency
- Geologic and site conditions.
- Description of testing arrays.
- Tabulated V_S model(s).
- Discussion and comments.
- Site map showing the approximate location of the seismic station and testing arrays.
- Geologic map.
- Photographs of surface wave testing.
- Plots of HVSr data.
- A composite plot of all dispersion data reduced from the active and passive surface wave data along with a discussion of data sets used for site characterization.
- Plots of field, representative and calculated dispersion data and V_S models.
- Calculated HVSr for V_S models as appropriate.

The V_{S30} , estimated error in V_{S30} , and NEHRP site class for the seismic stations characterized during this investigation are summarized in Table 3.

Table 3 Summary of Results

Station No.	V_{S30} (m/s)	Estimated Error (m/s)	NEHRP Site Class
47126	288	20	D
47179	266	25	D
47189	505	25	C
47377	572	55	C
47404	825	80	B
47405	379	25	C
47524	228	20	D
47567	288	20	D
47762	237	15	D
48906	297	25	D
57203	323	30	D
57218	445	25	C
57370	436	30	C
57371	282	25	D
58135	408	35	C

6 REFERENCES

- Achenbach J, 1973, *Wave Propagation in Elastic Solids*, Elsevier, Amsterdam, Netherlands.
- Aki K, 1957, Space and time spectra of stationary stochastic waves, with special reference to microtremors. *Bull. Earthq. Inst. Univ. Tokyo*, v. 35, pp. 415–457.
- Albarello D and Gargani G, 2010, “Providing NEHRP soil classification from the direct interpretation of effective Rayleigh-wave dispersion curves”, *Bulletin of the Seismological Society of America*, Vol. 100, No. 6, p 3284-3294.
- Asten M, 2006, Site shear velocity profile interpretation from microtremor array data by direct fitting of SPAC curves, in *Proceedings of the Third Int. Symp. Effects of Surface Geol. Seismic Motion*, Vol. 2, LCPC Edition, Grenoble, France, August 30–September 01, Paper No. 99, 1069-1080.
- Asten M, Stephenson W and Hartzell, S, 2015, The use of wavenumber normalization in computing spatially averaged coherencies (krSPAC) of microtremor data from asymmetric arrays, *Proceedings 6th International Conference on Earthquake Geotechnical Engineering*, Christchurch, New Zealand, 9 p.
- Bettig B, Bard PY, Scherbaum F, Riepl J, Cotton F, Cornou C and Hatzfeld D, 2001, Analysis of dense array noise measurements using the modified spatial auto-correlation method (SPAC): application to the Grenoble area, *Bollettino di Geofisica Teorica ed Applicata*, Vol 42, p 281–304.
- Brown L, 1998, Comparison of V_s profiles from SASW and borehole measurements at strong motion sites in Southern California, Master’s thesis, University of Texas, Austin.
- Brown L, Diehl J and Nigbor R, 2000, A simplified method to measure average shear-wave velocity in the top 30 m (V_{s30}), *Proc. 6th International Conference on Seismic Zonation*, 1–6.
- BSSC, 2003, *NEHRP recommended provisions for seismic regulations for new buildings and other structure (FEMA 450), Part I: Provisions*, Building Seismic Safety Council, Federal Emergency Management Agency, Washington D.C.
- Capon J, 1969, High-resolution frequency-wavenumber spectrum analysis, *Proc. Institute of Electrical and Electronics Engineers (IEEE)*, Vol. 57, no. 8, p 1408–1418.
- Comina C, Foti S, Boiero D, and Socco LV, 2011, Reliability of $V_{s,30}$ evaluation from surface-wave tests, *J. Geotech. Geoenviron. Eng.*, p 579–586.
- Dal Moro G, Moura R, Moustafa A, 2015, Multi-component joint analysis of surface waves, *Journal of Applied Geophysics*, Vol. 119, p 128-138.
- Dal Moro G and Ferigo F, 2011, Joint Analysis of Rayleigh- and Love-wave dispersion curves: Issues, criteria and improvements, *Journal of Applied Geophysics*, Vol. 75, p 573-589.
- Ellefsen K, 2003, Seg2_edit: a program for editing and manipulating SEG-2 files, *U.S. Geol. Surv. Open-File Rept. 03-141*, 11 pp.
- Foti S, 2000, Multistation Methods for Geotechnical Characterization using Surface Waves, Ph.D. Dissertation, Politecnico di Torino, Italy.

- Foti S, Lai C, Rix G and Strobbia C, 2015, Surface Wave Methods for Near-Surface Site Characterization, CRC Press, Boca Raton, Florida, 467 p.
- GEOVision, Inc (2012): EPRI (2004, 2006) ground-motion model (GMM) review project: Shear wave velocity measurements at seismic recording stations, <http://www.epri.com/abstracts/Pages/ProductAbstract.aspx?ProductId=000000003002000719>.
- Imai T, Fumoto H, and Yokota K, 1976, P- and S-Wave Velocities in Subsurface Layers of Ground in Japan, Oyo Corporation Technical Note N-14.
- International Committee of Building Officials, 2000 International Building Code, ICC, Hauppauge, NY, Section 1615.1.1
- García-Jerez A, Piña-Flores J, Sánchez-Sesma F, Luzón, F, Perton, M, 2016, A computer code for forward computation and inversion of the H/V spectral ratio under the diffuse field assumption, *Computers & Geosciences*, In Press.
- Joh S, 1996, Advances in interpretation and analysis techniques for spectral-analysis-of-surface-waves (SASW) measurements, Ph.D. Dissertation, University of Texas, Austin.
- Joh S, 2002, WinSASW V2.0, Data Interpretation and Analysis for SASW Measurements, Department of Civil Engineering, Chung-Ang University, Anseong, Korea.
- Lacoss R, Kelly E and Toksöz M, 1969, Estimation of seismic noise structure using arrays, *Geophysics*, v. 34, pp. 21-38.
- Li J and Rosenblad B, 2011, Experimental study of near-field effects in multichannel array-based surface wave velocity measurements, *Near Surface Geophysics*, Vol. 9, 357-366.
- Ling S and Okada H, 1993, An extended use of the spatial correlation technique for the estimation of geological structure using microtremors, *Proc. the 89th Conference Society of Exploration Geophysicists Japan (SEGJ)*, pp. 44–48 (in Japanese).
- Louie J, 2001, Faster, Better: Shear-Wave Velocity to 100 Meters Depth from Refraction Microtremor Arrays, *Bulletin of the Seismological Society of America*, vol. 91, no. 2, p. 347-364.
- Martin A and Diehl J, 2004, Practical experience using a simplified procedure to measure average shear-wave velocity to a depth of 30 meters (V_{s30}), *Proceedings of the 13th World Conference on Earthquake Engineering*, Vancouver, B.C., Canada, August 1-6, 2004, Paper No. 952.
- Martin A, Shawver J and Diehl J, 2006, Combined use of Active and Passive Surface Wave Techniques for Cost Effective UBC/IBC Site Classification, *Proceedings of the 8th National Conference on Earthquake Engineering*, San Francisco, California, Paper No. 1013.
- Martin A, Yong A and Salomone L, 2014, Advantages of active Love wave techniques in geophysical characterization of seismographic station sites – case studies in California and the Central and Eastern United States, *Proceedings of the Tenth U.S. National Conference on Earthquake Engineering, Frontiers of Earthquake Engineering*, July 21-25, Anchorage, Alaska.
- Nakamura Y, 1989, A method for dynamic characteristics estimation of subsurface using microtremor on the ground surface, *Quart. Reprt Rail. Tech. Res. Inst.*, Vol. 30, no. 1, p 25–33.

- Nogoshi M and Igarashi T, 1971, On the amplitude characteristics of microtremor (part 2), *J. Seismol. Soc. Japan*, Vol. 24, p 26–40 (in Japanese).
- Ohori M, Nobata A, and Wakamatsu K, 2002, A comparison of ESAC and FK methods of estimating phase velocity using arbitrarily shaped microtremor arrays, *Bull. Seismol. Soc. Am.*, v. 92, no. 6, p. 2323–2332.
- Okada H, 2003, The Microtremor Survey Method, *Society of Exploration Geophysics Geophysical Monograph Series*, Number 12, 135p.
- Park C, Miller R and Xia J, 1999a, Multimodal analysis of high frequency surface waves, *Proceedings of the Symposium on the Application of Geophysics to Engineering and Environmental Problems '99*, 115-121.
- Park C, Miller R and Xia, J, 1999b, Multichannel analysis of surface waves, *Geophysics*, Vol 64, No. 3, 800-808.
- Rix G, 1988, Experimental study of factors affecting the spectral-analysis-of surface-waves method, Ph.D. Dissertation, University of Texas, Austin.
- Roesset J, Chang D and Stokoe K, 1991, Comparison of 2-D and 3-D Models for Analysis of Surface Wave Tests, *Proceedings, 5th International Conference on Soil Dynamics and Earthquake Engineering*, Karlsruhe, Germany.
- Stokoe K, Rix G and Nazarian S, 1989, In situ seismic testing with surface waves, *Proceedings, Twelfth International Conference on Soil Mechanics and Foundation Engineering, Vol. 1*, Rio de Janeiro, Brazil, pp. 330-334.
- Stokoe K, Wright S, Bay J and Roesset J, 1994, Characterization of Geotechnical Sites by SASW Method, *ISSMFE Technical Committee 10 for XIII ICSMFE, Geophysical Characteristics of Sites*, A.A. Balkema Publishers/Rotterdam & Brookfield, Netherlands, pp. 146.
- Xia J, Xu Y, Luo Y, Miller R, Cakir R and Zeng C, 2012, Advantages of using Multichannel analysis of Love waves (MALW) to estimate near-surface shear-wave velocity, *Surveys in Geophysics*, 841–860.
- Yong A, Martin A, Stokoe K and Diehl J, 2013, ARRA-funded V_{S30} measurements using multi-technique method approach at strong-motion stations in California and Central-Eastern United States, Open-File Report 2013-1102, United States Geological Survey, <http://pubs.usgs.gov/of/2013/1102/>.
- Yoon S and Rix G, 2009, Near-field effects on Array-based surface wave methods with active sources, *Journal of Geotechnical and Geoenvironmental Engineering*, Vol. 135, no. 3, 399-406.

7 CERTIFICATION

All geophysical data, analysis, interpretations, conclusions, and recommendations in this document have been prepared under the supervision of and reviewed by a **GEOVision** California Professional Geophysicist.

Reviewed and approved by



6/22/2018

Antony Martin

Date

California Professional Geophysicist, P. GP 989

GEOVision Geophysical Services

- * This geophysical investigation was conducted under the supervision of a California Professional Geophysicist using industry standard methods and equipment. A high degree of professionalism was maintained during all aspects of the project from the field investigation and data acquisition, through data processing interpretation and reporting. All original field data files, field notes and observations, and other pertinent information are maintained in the project files and are available for the client to review for a period of at least one year.

A professional geophysicist's certification of interpreted geophysical conditions comprises a declaration of his/her professional judgment. It does not constitute a warranty or guarantee, expressed or implied, nor does it relieve any other party of its responsibility to abide by contract documents, applicable codes, standards, regulations or ordinances.

APPENDIX A

SITE REPORTS

Report

Geophysical Site Characterization

SMIP Station CE.47126

Station Name: San Juan Bautista - Fire Station

Location: San Juan Bautista Fire Station/City Hall, 311 2nd Street, San Juan Bautista, California

Latitude: 36.8453

Longitude: -121.5369

V_{s30}: 288 m/s

Estimated Error in V_{s30}: ± 20 m/s

NEHRP Site Class: D

Geomatrix Code: AHC

HVSR Peak Frequency: ~1.6 Hz

Site Geology: Site located on Holocene alluvium less than 0.5 km from outcrops of Oligocene San Lorenzo Formation (Figure 2). Seismic station located about 150 m southwest of the San Andreas fault zone.

Site Conditions: Suburban site with low traffic noise from nearby roads. Relatively flat terrain in site vicinity.

Geophysical Methods Utilized: MAS_RW, array microtremor, HVSR

Geophysical Testing Arrays:

1. Array 1: 48-channel “L” shaped array utilizing 4.5 Hz vertical geophones spaced 3 m apart used to acquire passive surface wave data. The S-N and W-E linear segments of array have lengths of 60 and 81 m, respectively (Figure 1).
2. Array 2: 48 channel MAS_RW array utilizing 4.5 Hz vertical geophones spaced 0.75 m apart for a length of 35.25 m, forward and reverse shot locations with multiple source offsets (1.5 m on the low end and 1.5 m to 10 m off the high end of the array), and multiple interior source locations. 4 and 12 lb hammers were used as energy sources (Figure 1).
3. One HVSR location near seismic station (Figure 1).

Table 1 Location of Geophysical Testing Arrays

Location	Latitude	Longitude
Seismic Station CE.47126	36.84530	-121.53690
Array 1 Passive, Northeast End of Array	36.84520	-121.53639
Array 1 Passive, Corner of Array	36.84566	-121.53711
Array 1 Passive, Southwest End of Array	36.84524	-121.53756
Array 2 MASW, Northwest End of Array	36.84562	-121.53711
Array 2 MASW, Southeast End of Array	36.84543	-121.53679
HVSR Location 1	36.84537	-121.53704

Notes: 1) WGS84 Coordinate System (decimal degrees)

S-Wave Velocity Model:

Table 2 V_s Model

Depth to Top of Layer (m)	Layer Thickness (m)	S-Wave Velocity (m/s)	Inferred P-Wave Velocity (m/s)	Assumed Poisson's Ratio	Assumed Density (g/cm ³)
0	1	166	311	0.300	1.80
1	1.5	200	373	0.300	1.80
2.5	2.5	264	494	0.300	1.90
5	10	319	596	0.300	1.95
15	12	282	1600	0.484	1.90
27	18	418	1650	0.466	1.95
45	27	520	1700	0.448	2.00
72	>18	672	1750	0.414	2.10

Notes: 1) Depth to saturated zone fixed at about 15 m based on seismic refraction data.
 2) Depth of investigation is about 75 m.
 3) Bottom layer is a half space.

Observations/Discussion:

H/V Spectral Ratio

HVSR data collected using both Nanometrics Trillium Compact (Trillium) and MOHO Tromino ENGR (Tromino) seismographs. The HVSR data reveals an approximate 1.6 Hz peak (Figure 4), which may be associated with a geologic structure(s) within the depth of investigation of the surface wave sounding. Both the Trillium and Tromino yield similar HVSR peaks. However, HVSR amplitudes from the Trillium ambient vibration data are higher at frequencies less than 2 Hz and considered more reliable (Figure 7).

Array Microtremor Data

Noise conditions at the site (multi-directional noise sources) appeared sufficient for successful application of passive surface wave techniques. Over 60 minutes (127, 30 second seismic records) of ambient vibration data were acquired with an L-shaped array (Array 1). The ESAC technique was used to extract surface wave dispersion data from the ambient vibration data. To better characterize error, dispersion curves were generated from approximate 15 minute time segments of the ambient vibration data and also from the complete data set. The minimum and maximum Rayleigh wavelength extracted from Array 1 were about 9.5 and 195 m, respectively. No attempt was made to extract surface wave dispersion data from the linear legs of the L-shaped array because 2D arrays will yield more reliable dispersion data than linear arrays.

MASW Data

MASW data acquisition was limited to a 35.25 m long array (48 geophones spaced 0.75 m apart) in a grass area in front of the city hall building (Array 2). Rayleigh wave dispersion data were interpreted from 10 MAS_RW seismic records collected at 10 different source locations using 4-lb hammer and 12-lb sledgehammer energy sources. Maximum source offset was 1.5 m at the northwest end of the array and 10 m at the southeast end of the array. Using variable receiver offset ranges, over 50 dispersion curves were extracted and combined for analysis. To minimize near field effects, the maximum Rayleigh wavelength data extracted from the MAS_RW data set was set equal to one times the distance between the source and midpoint of the active receiver array. There is nominally about 30 to 40 m/s of scatter in MAS_RW dispersion data, which is likely in part due to lateral velocity variation. The minimum Rayleigh wavelength phase velocity data extracted from a 48-channel MAS_RW receiver gather was about 5 m. Reducing data from smaller hammer sources using a limited offset range receiver gather (i.e. less active geophones) allowed for extraction of surface wave dispersion data to a minimum wavelength of about 3 m.

Modeling

Surface wave dispersion data from active and passive surface wave data sets are in excellent agreement over the approximate 9 to 28 m overlapping wavelength range (Figure 5). The phase velocity of a 40 m wavelength Rayleigh wave (V_{R40}) is 273 m/s with a coefficient of variation (COV) of 1% from ESAC analysis of the ambient vibration data collected along Array 1. Representative dispersion curves were generated for each surface wave data set using a moving average, polynomial curve fitting routine. These individual representative dispersion curves were combined and a composite representative dispersion curve generated for the combined data set for modeling. Error bars for the composite representative dispersion curve were estimated based on the scatter in the dispersion data.

The composite representative dispersion curve was inverted using an iterative non-linear least squares inversion routine and fundamental mode Rayleigh wave assumption to derive V_S models. Realistic estimates of Poisson's ratio and density were used to make models as accurate as possible. High Poisson's ratio, saturated sediments were constrained at a depth of about 15 m with $V_P > 1,600$ m/s based on interactive, layer-based analysis of seismic refraction first arrival data. Poisson's ratio of the saturated sediments was set to gradually decrease with depth as the sediments became stiffer, a common observation in borehole velocity logs. Model layer thicknesses increased with depth to reflect the reduction in model resolution with depth. Several

V_S models were developed with almost identical calculated dispersion curves to demonstrate the non-uniqueness inherent in the inversion of surface wave dispersion data; especially at layer boundaries where an abrupt change in seismic velocity occurs or associated with high velocity layers or velocity inversions.

Theoretical HVSR, based on the diffuse field assumption, was computed for all V_S models using the software package *HV-Inv* Release 2.3 and the assumption that the noise field consists of only Rayleigh waves and both Rayleigh and Love waves.

Results

V_S models are presented as Figure 6. Surface wave depth of investigation is about 75 m based on $\lambda_{\max}/2.5$. The HVSR peak frequency computed from the V_S models is in good agreement with observed HVSR data regardless of whether the noise field consists of Rayleigh and Love waves or only Rayleigh waves (Figure 7).

V_{S30} is 288 m/s (NEHRP Site Class D). The average V_S of the upper 75 m (V_{S75}) is 382 m/s. The estimated error in V_{S30} , which includes some effects of the lateral velocity variability beneath the testing arrays, is about 20 m/s. This is computed based on the sum of the following rounded to the nearest 5 m/s: an estimated error of 3% from the realistic assumed layer Poisson's ratios in the model, 1% error from the realistic assumed layer densities in the model, 2% for the variation in V_{S30} associated with non-uniqueness, and the 1% COV in V_{R40} from the passive-source surface wave dispersion data. V_{S30} is between 284 and 291 m/s for the equivalent V_S models, demonstrating that non-uniqueness does not have a large impact on estimated V_{S30} . Interestingly, V_{S30} estimated from V_{R40} using the Brown et al., 2000 relationship ($V_{S30} \cong 1.045V_{R40}$, assuming V_{R40} represents the fundamental mode Rayleigh wave) is 285 m/s, only 1% different than that estimated from the V_S model.



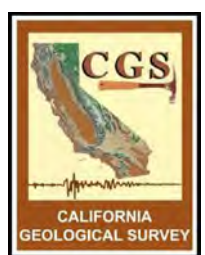
File Name: 18045_47126
Date: 5/29/2018

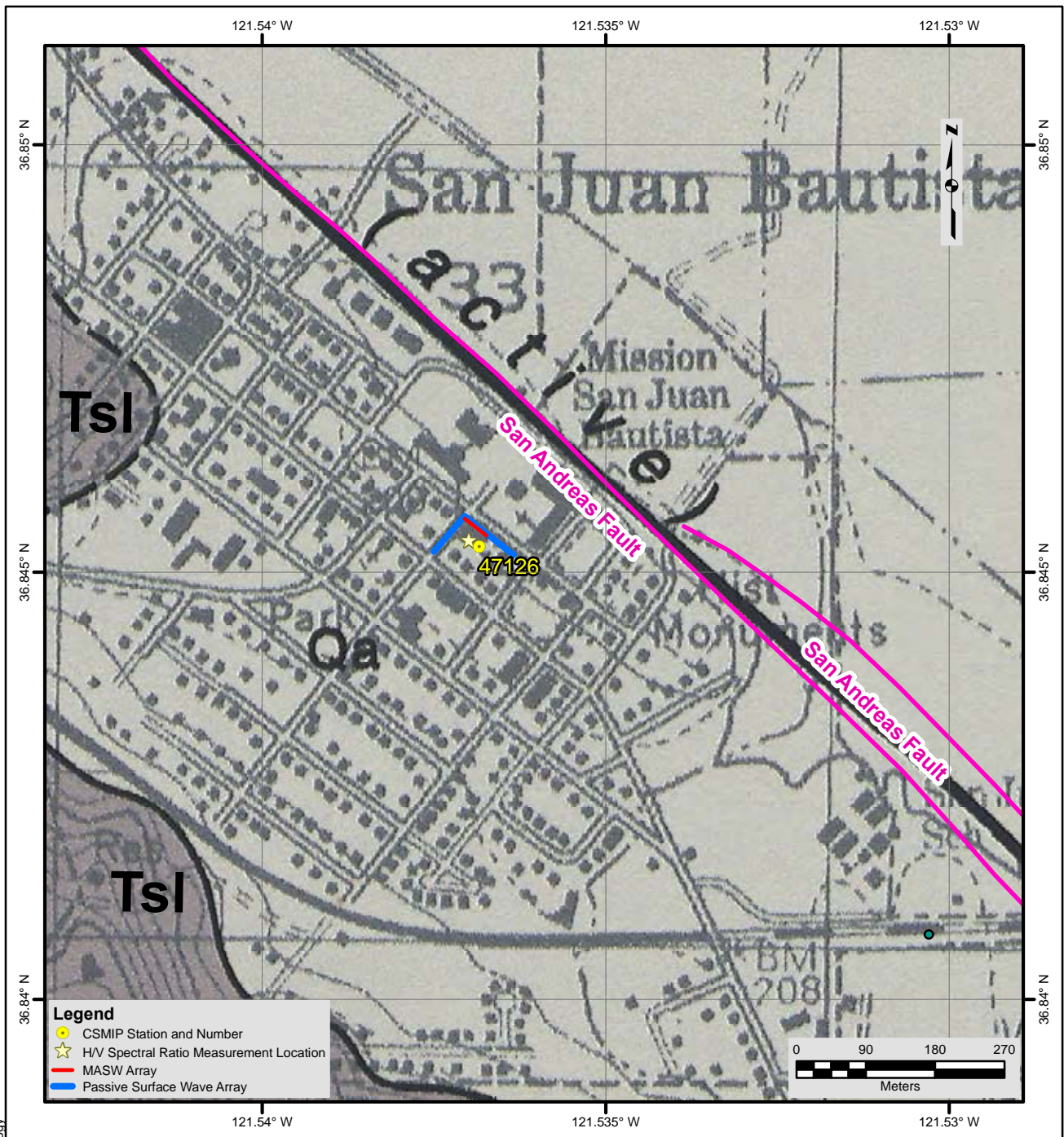
- Legend**
- CSMIP Station and Number
 - ★ H/V Spectral Ratio Measurement Location
 - MASW Array
 - Passive Surface Wave Array

- NOTES:**
1. WGS 1984 Coordinate System
 2. Image Source: Esri, DigitalGlobe, GeoEye, Earthstar Geographics, CNES/Airbus DS, USDA, USGS, AEX, Getmapping, Aerogrid, IGN, IGP, swisstopo, and the GIS User Community



**FIGURE 1
SITE MAP
CE • 47126**





Description of Geologic Map Units

Qa = Quaternary (Holocene) Alluvial gravel and sand of San Benito River
 Tsl = Tertiary (Oligocene) San Lorenzo Formation

NOTES:

1. WGS 1984 Coordinate System
2. Geologic Map of the Prunedale & San Juan Bautista Quadrangles, Monterey & San Benito Counties, California by Thomas W Dibblee, Jr., 2006

File Name: 18045_47126-Geology
Date: 5/29/2018



**FIGURE 2
 GEOLOGIC MAP
 CE • 47126**





View inside fire station of CE.47126 seismic station



Looking southeast along MASW Array 2

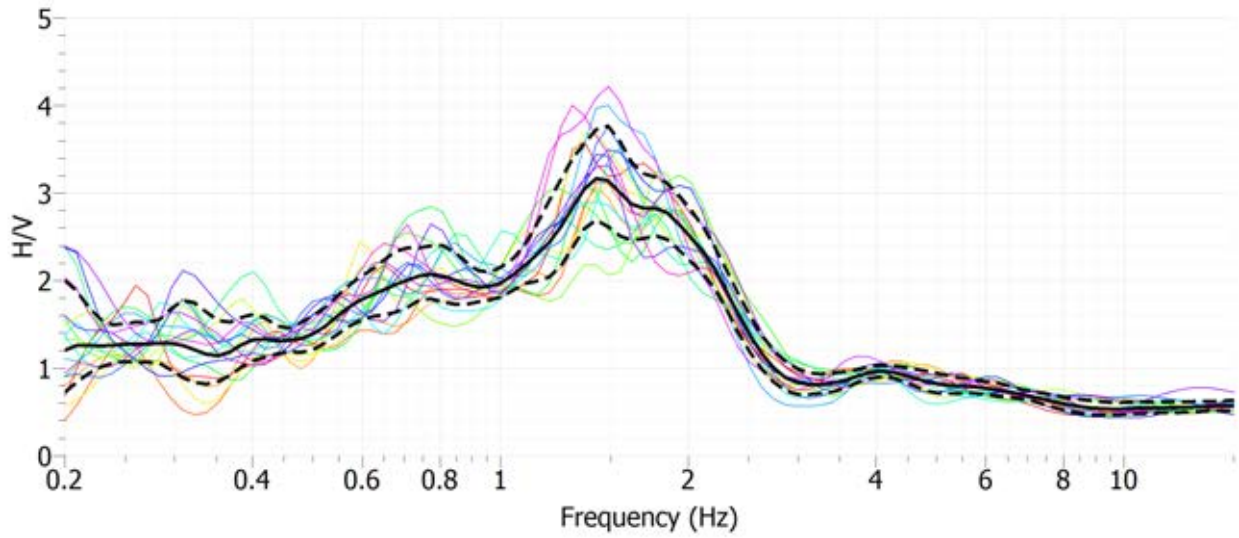


Looking south towards city hall from the corner of passive surface wave Array 1

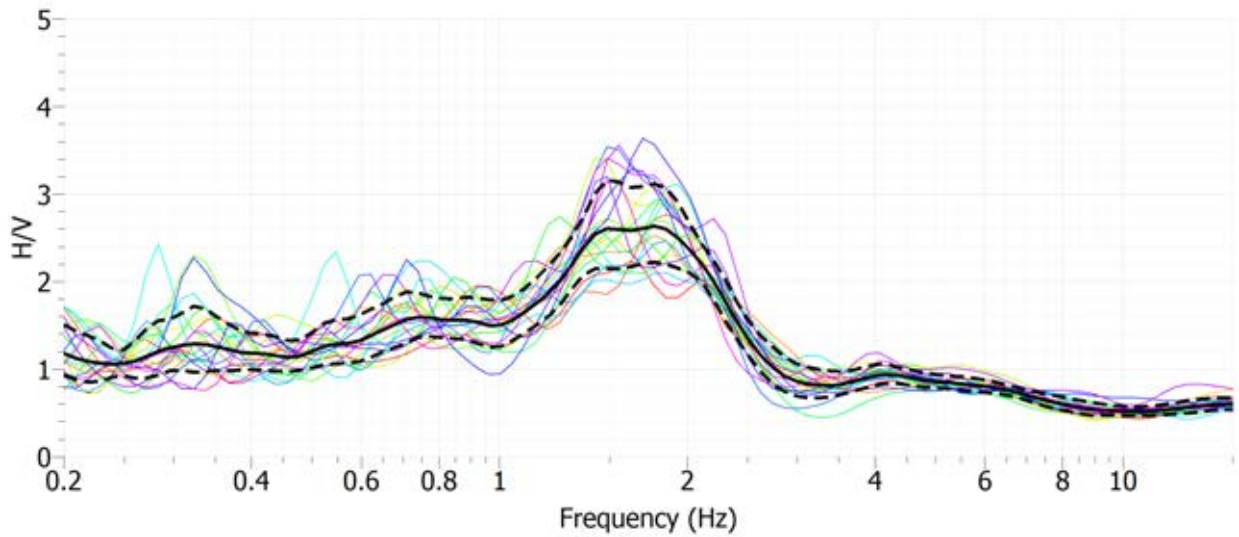


Looking towards fire station from HVSr Location 1

Figure 3 Site CE.47126 Photographs



Site CE.47126, HVSr Location 1, Nanometrics Trillium Compact Sensor



Site CE.47126, HVSr Location 1, MOHO Tromino ENGR Sensor

Figure 4 H/V Spectral Ratio of Ambient Vibration Data, Site CE.47126

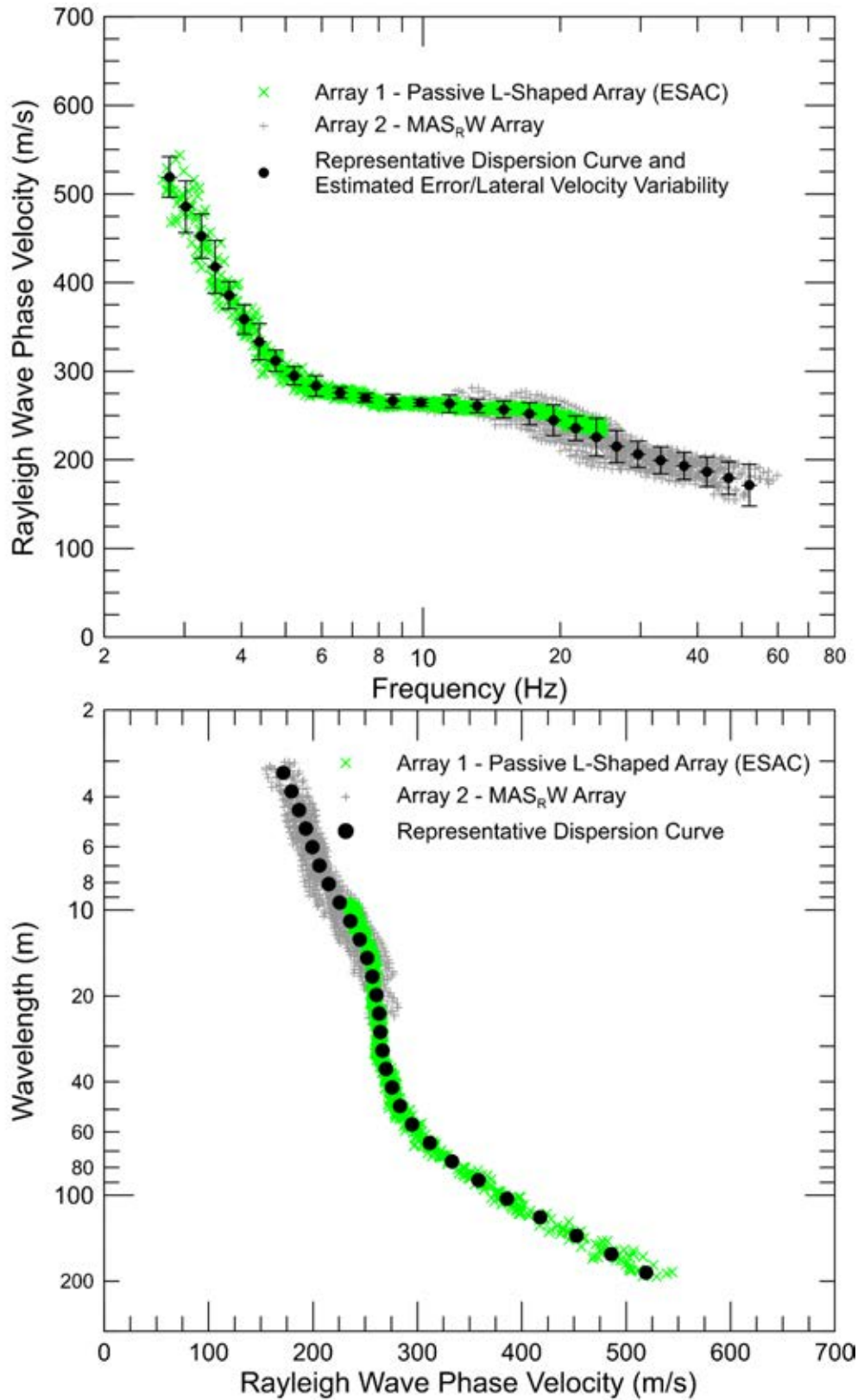


Figure 5 CE.47126 – Rayleigh wave dispersion curves derived from active- and passive-source surface wave data

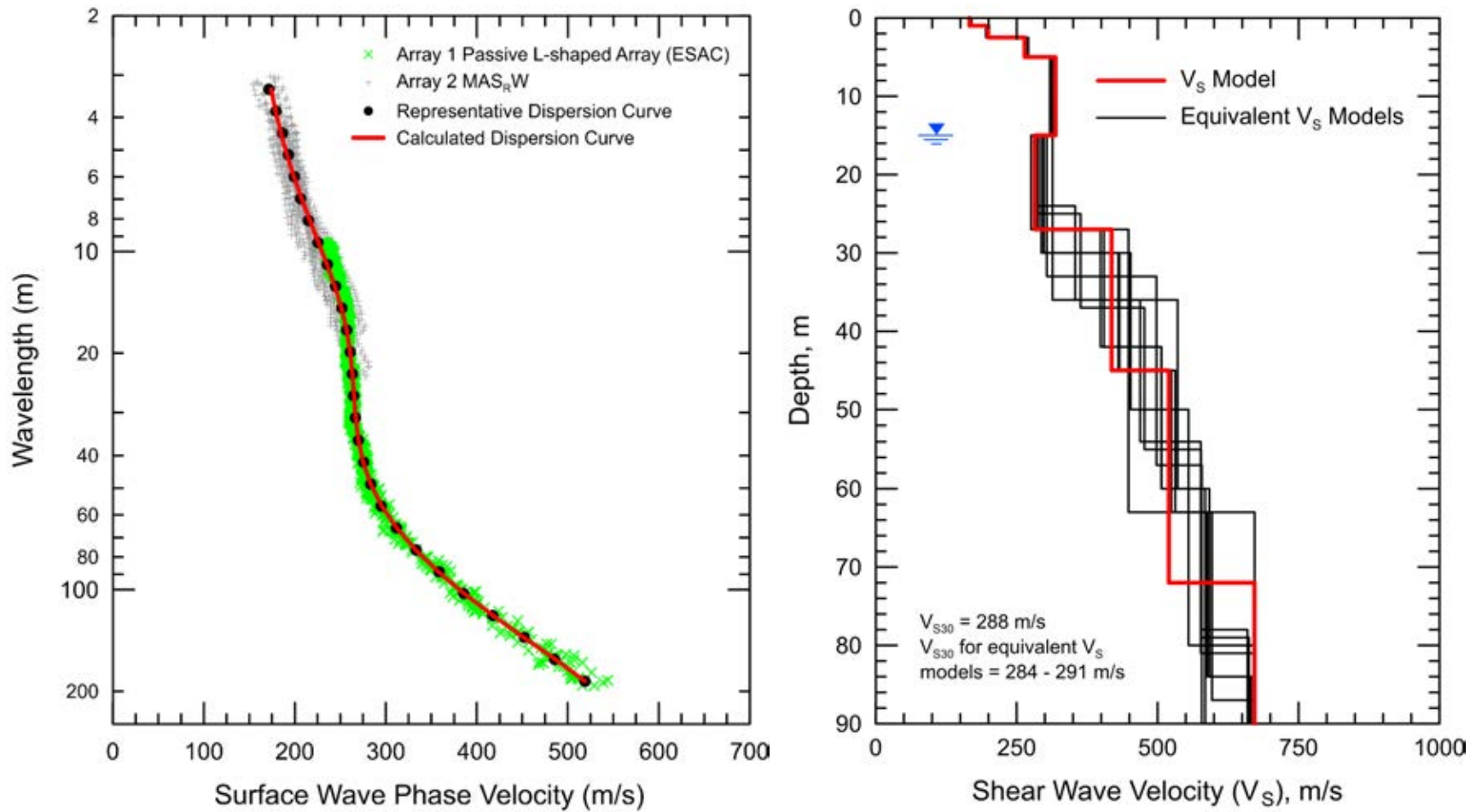


Figure 6 CE.47126 - Field, representative and calculated surface wave dispersion data (left) and associated V_S models (right)

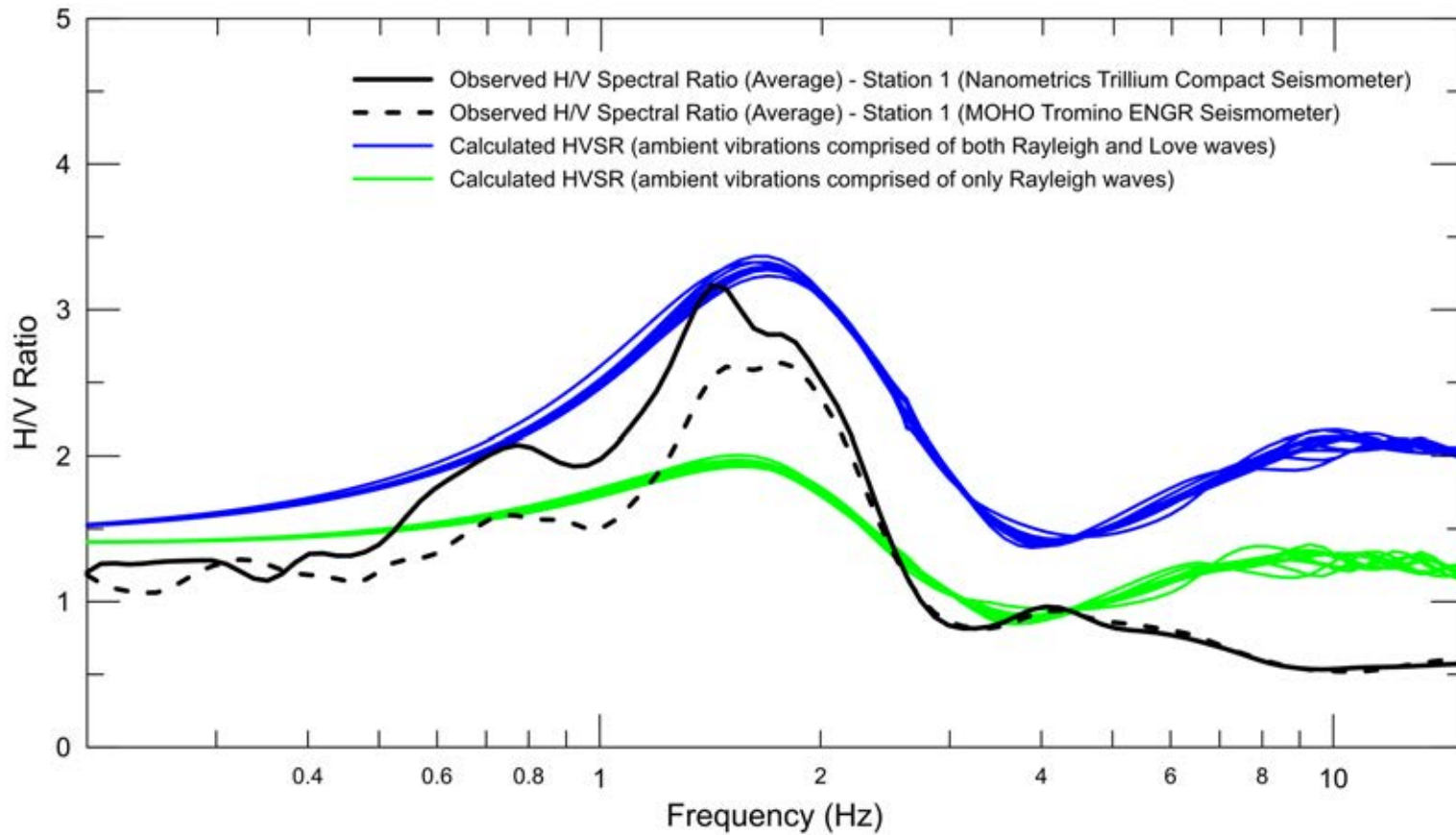


Figure 7 CE.47126 – Calculated HVSR response based on diffuse field assumption

Report Geophysical Site Characterization SMIP Station CE.47179

Station Name: Salinas – City Yard

Location: Salinas City Service and Building Yard, John Street and Work Street, Salinas, CA

Latitude: 36.6715

Longitude: -121.6432

V_{s30}: 266 m/s

Estimated Error in V_{s30}: ± 25 m/s

NEHRP Site Class: D

Geomatrix Code: AHD

HVSR Peak Frequency: Primary peak at 0.25 Hz, possible weak peak at 1.2 Hz

Site Geology: Station located on Holocene alluvium (Figure 2) more than 5 km from outcrops of Mesozoic granodiorite and metasedimentary rocks.

Site Conditions: Suburban site with moderate traffic noise from nearby roads. Flat terrain in site vicinity.

Geophysical Methods Utilized: MAS_RW, array microtremor, HVSR

Geophysical Testing Arrays:

1. Array 1: 37-channel, nested triangle array utilizing 4.5 Hz vertical geophones with 48 m maximum length of outer side of array (Figure 1).
2. Array 2: 48 channel MAS_RW array utilizing 4.5 Hz vertical geophones spaced 1.5 m apart for a length of 70.5 m, forward and reverse shot locations with multiple source offsets (1.5 m off both ends of the array) and multiple interior source locations (Figure 1). A 4-lb hammer and 12-lb hammers were used at interior and offset source locations and an accelerated weight drop (AWD) was used for the offset source locations.
3. One HVSR location near Array 1 (Figure 1).

Table 1 Location of Geophysical Testing Arrays

Location	Latitude	Longitude
Seismic Station CE.47179	36.67150	-121.64320
Array 1 Passive, Southwest Corner of Triangle Array	36.67075	-121.64309
Array 1 Passive, North Corner of Triangle Array	36.67118	-121.64300
Array 1 Passive, Southeast Corner of Triangle Array	36.67090	-121.64258
Array 2 MASW, Southwest End of Array	36.67076	-121.64307
Array 2 MASW, Northeast End of Array	36.67138	-121.64289
HVSR Location 1	36.67106	-121.64288

Notes: 1) WGS84 Coordinate System (decimal degrees)

S-Wave Velocity Model:

Table 2 V_s Model

Depth to Top of Layer (m)	Layer Thickness (m)	S-Wave Velocity (m/s)	Inferred P-Wave Velocity (m/s)	Assumed Poisson's Ratio	Assumed Density (g/cm ³)
0	2.5	165	309	0.300	1.70
2.5	3.5	224	418	0.300	1.80
6	5	308	576	0.300	1.90
11	7	241	451	0.300	1.85
18	37	327	1700	0.481	1.90
55	>5	440	1800	0.468	2.00

Notes: 1) Depth to saturated zone fixed at about 18 m based on seismic refraction data.
 2) Depth of investigation is about 60 m.
 3) Bottom layer is a half space.

Observations/Discussion:

H/V Spectral Ratio

HVSR data collected at a single location using both Nanometrics Trillium Compact (Trillium) and MOHO Tromino ENGR (Tromino) seismographs. The HVSR data from both sensors reveals a 0.25 Hz peak (Figure 4), which would be associated with a geologic structure(s) at a depth much greater than the expected depth of investigation of the surface wave sounding. The amplitude of the 0.25 Hz peak is lower in ambient vibration data recorded by the Tromino because this instrument is not designed to reliably detect HVSR peaks associated with deep geologic structures. Both the Trillium and Tromino also detect a possible, weak 1.2 Hz HVSR peak (Figure 4).

Array Microtremor Data

Noise conditions at the site (multi-directional noise sources) appeared sufficient for successful application of passive surface wave techniques. A nested triangle array (Array 1) was utilized at this site because of limited site access. The presence of railroad tracks and curved roads limited the application of an L-shaped array. A nested triangle array has better azimuthal coverage (three azimuths for every sensor spacing) than a L-shaped array (two azimuths in the leg directions and one azimuth between receivers on different legs) and, therefore, should perform better in a variety of noise conditions. Over 50 minutes (108, 30 second seismic records) of ambient vibration data were acquired into Array 1. The ESAC technique was used to extract surface wave dispersion data from the ambient vibration data. To better characterize error, dispersion curves were generated from approximate 13.5 minute time segments of the ambient vibration data and also from the complete data set. The minimum and maximum Rayleigh wavelength extracted from Array 1 were about 7 and 150 m, respectively.

MASW Data

MASW data acquisition was conducted using a 70.5 m long receiver array (Array 2). Rayleigh wave dispersion data were interpreted from 17 MAS_RW seismic records collected at 7 different source locations using 4-lb hammer, 12-lb sledgehammer, and AWD energy sources. Due to limited space the maximum source offset was 1.5 m at each end of the array. Using the 12 seismic records and variable receiver offset ranges, over 60 dispersion curves were extracted and combined for analysis. To minimize near field effects, the maximum Rayleigh wavelength data extracted from the MAS_RW data set was set equal to 1.3 times the distance between the source and midpoint of the active receiver array. There is nominally about 20 m/s of scatter in MAS_RW dispersion data, which is likely in part due to lateral velocity variation. The minimum Rayleigh wavelength phase velocity data extracted from a 48-channel MAS_RW receiver gather was about 4 m. Reducing data from smaller hammer sources using a limited offset range receiver gather (i.e. less active geophones) allowed for extraction of surface wave dispersion data to a minimum wavelength of about 2 m.

Modeling

Surface wave dispersion data from active and passive surface wave data sets are in good agreement over part but not all of the 7 to 55 m overlapping wavelength range (Figure 5). The dispersion curve from Array 1 appears to be affected by higher mode Rayleigh waves between a frequency of about 6 and 9 Hz (wavelength of 27 to 46 m) as shown in Figure 5. The nature of the dispersion curves would tend to indicate that there is a high velocity layer and/or velocity inversion in the shallow subsurface. There are two options for modeling such data: 1) use the MASW dispersion data over the 6 to 9 Hz frequency range and model with the fundamental mode assumption (used for data analysis) or 2) use the array microtremor data over this frequency range and model with the effective mode assumption.

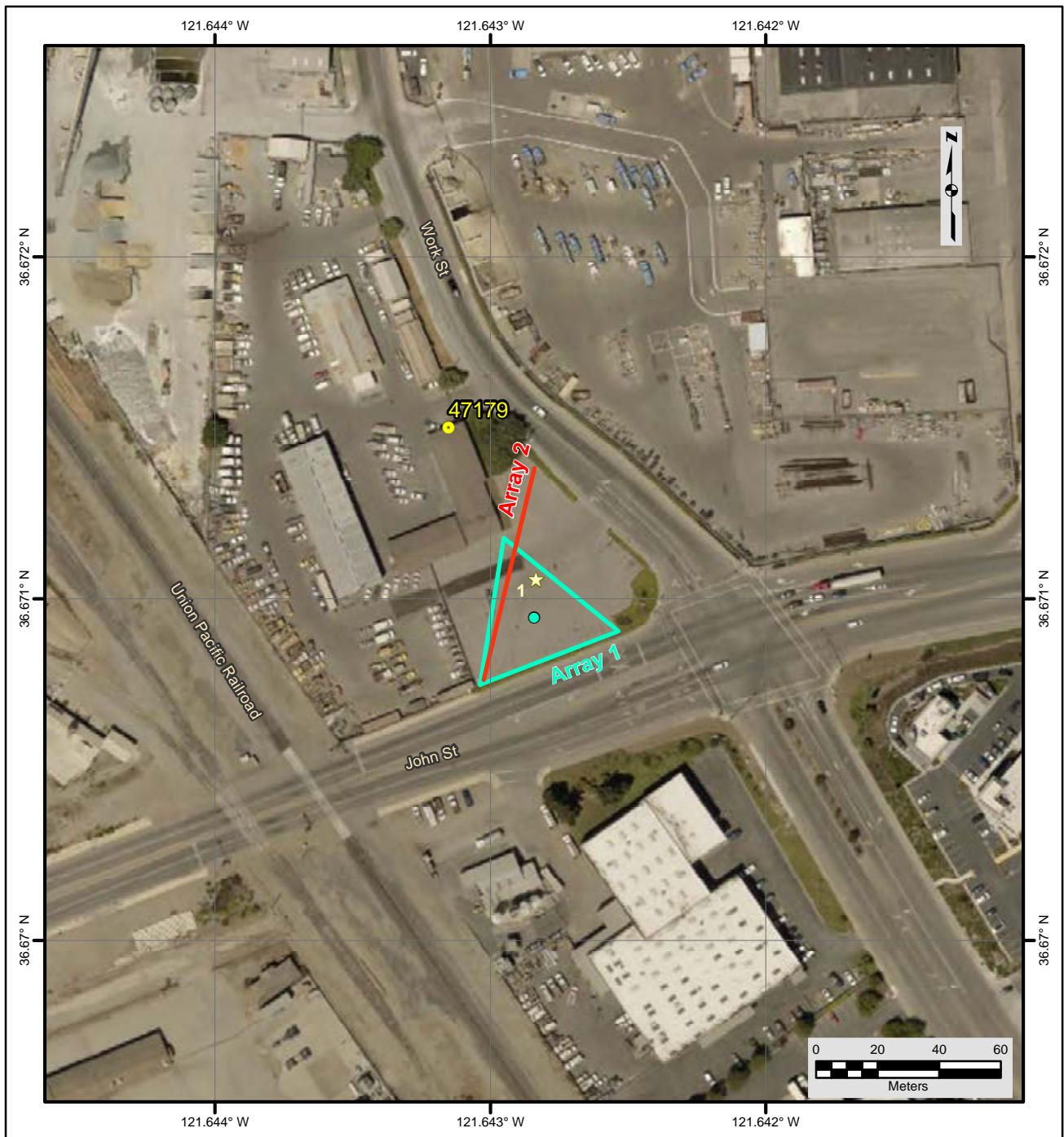
The phase velocity of a 40-m wavelength Rayleigh wave (V_{R40}) is 247 m/s with a coefficient of variation (COV) of 2.5% from 8 dispersion curves extracted from the MASW data. V_{R40} was not evaluated for microtremor array because higher mode Rayleigh waves appear to affect the dispersion curve at this wavelength. Representative dispersion curves were generated for each

surface wave data set (dispersion data over 6 to 9 Hz frequency range removed from Array 1) using a moving average, polynomial curve fitting routine. These individual representative dispersion curves were combined and a composite representative dispersion curve generated for the combined data set for modeling. Error bars for the composite representative dispersion curve were estimated based on the scatter in the dispersion data.

The composite representative dispersion curve was inverted using an iterative non-linear least squares inversion routine and fundamental mode Rayleigh wave assumption to derive V_S models. Realistic estimates of Poisson's ratio and density were used to make models as accurate as possible. High Poisson's ratio, saturated sediments were constrained at a depth of about 18 m with $V_P > 1,600$ m/s based on interactive, layer-based analysis of seismic refraction first arrival data and a possible water table seismic reflector. Poisson's ratio of the saturated sediments was set to gradually decrease with depth as the sediments became stiffer, a common observation in borehole velocity logs. Model layer thicknesses increased with depth to reflect the reduction in model resolution with depth. Several V_S models were developed with almost identical calculated dispersion curves to demonstrate the non-uniqueness inherent in the inversion of surface wave dispersion data; especially at layer boundaries where an abrupt change in seismic velocity occurs or associated with high velocity layers or velocity inversions.

Results

V_S models are presented as Figure 6. There is likely much more non-uniqueness associated with the high velocity layer and underlying velocity inversion than shown in the Figure. Global inversion routines are better suited for exploring non-uniqueness associated with such geologic structure. Surface wave depth of investigation is about 60 m based on $\lambda_{\max}/2.5$. V_{S30} is 266 m/s (NEHRP Site Class D) for the V_S model presented in Table 2. The average V_S of the upper 60 m (V_{S60}) is 299 m/s. The estimated error in V_{S30} , which includes some effects of the lateral velocity variability beneath the testing arrays, is about 25 m/s. This is computed based on the sum of the following rounded to the nearest 5 m/s: an estimated error of 3% from the realistic assumed layer Poisson's ratios in the model, 1% error from the realistic assumed layer densities in the model, 2% for the variation in V_{S30} associated with non-uniqueness, and the 2.5 % COV in V_{R40} from the active-source surface wave dispersion data. V_{S30} is between 265 and 267 m/s for the equivalent V_S models, demonstrating that non-uniqueness does not have a large impact on estimated V_{S30} . Interestingly, V_{S30} estimated from V_{R40} using the Brown et al., 2000 relationship ($V_{S30} \cong 1.045V_{R40}$, assuming V_{R40} represents the fundamental mode Rayleigh wave) is 258 m/s, only 3% different than that estimated from the V_S model.



File Name: 18045_47179
Date: 5/29/2018

Legend

- CSMIP Station and Number
- ★ H/V Spectral Ratio Measurement Location
- MASW Array
- ▭ Passive Surface Wave Triangle Array

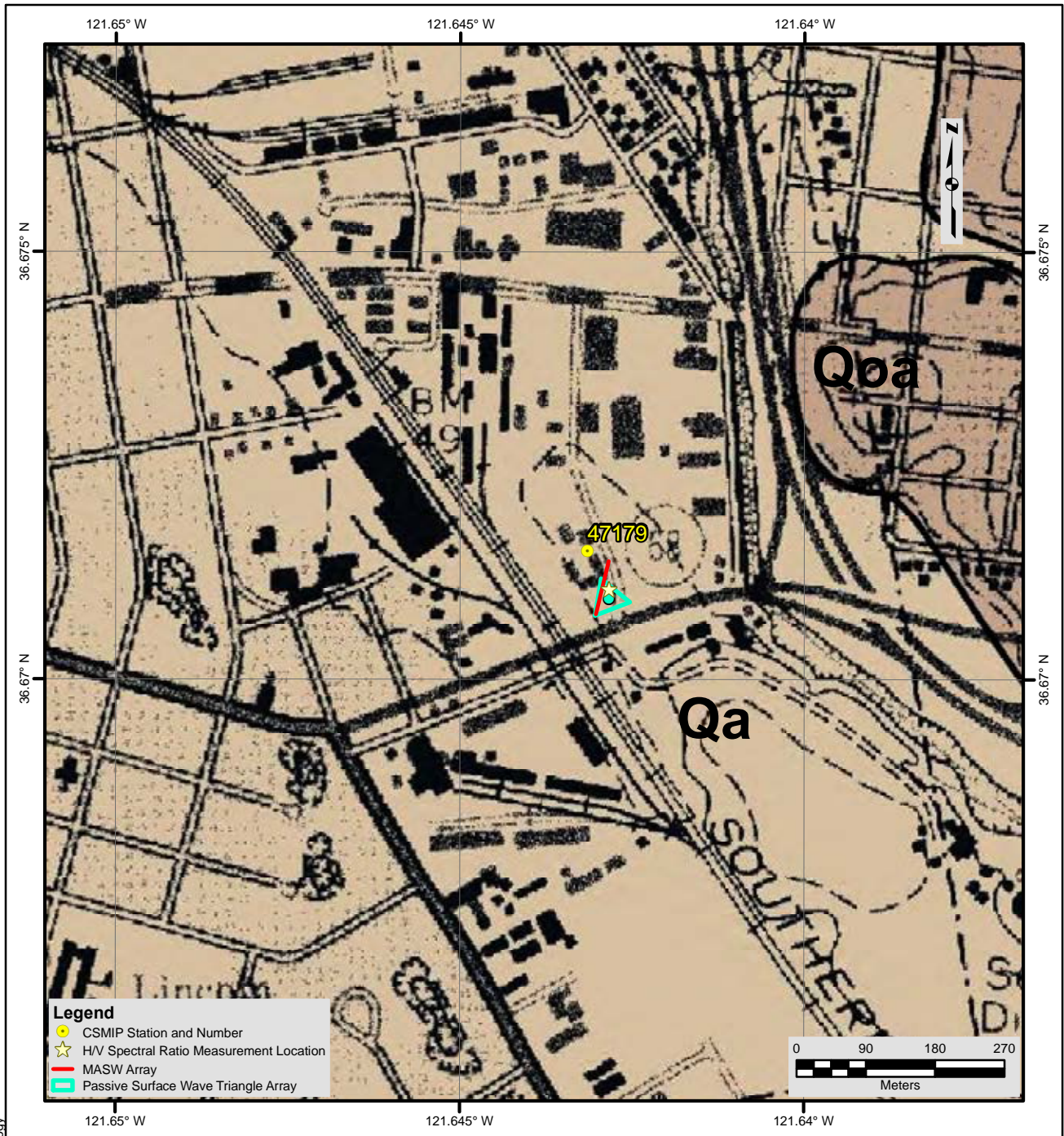
NOTES:

1. WGS 1984 Coordinate System
2. Image Source: Esri, DigitalGlobe, GeoEye, Earthstar Geographics, CNES/Airbus DS, USDA, USGS, AEX, Getmapping, Aerogrid, IGN, IGP, swisstopo, and the GIS User Community



**FIGURE 1
SITE MAP
CE • 47179**





Description of Geologic Map Units

Qa = Quaternary (Holocene) Alluvial gravel, sand, and silt/clay of valley areas and flood plains
 Qoa = Quaternary (Holocene-Pleistocene) dissected older alluvium

NOTES:
 1. WGS 1984 Coordinate System
 2. Geologic Map of the Monterey and Salinas Quadrangles, Monterey County, California by Thomas W Dibblee, Jr., 2007

File Name: 18045_47179-Geology
Date: 5/29/2018



**FIGURE 2
 GEOLOGIC MAP
 CE • 47179**





HVSr measurement location



Looking north along MASW Array 2
towards building housing the seismic station

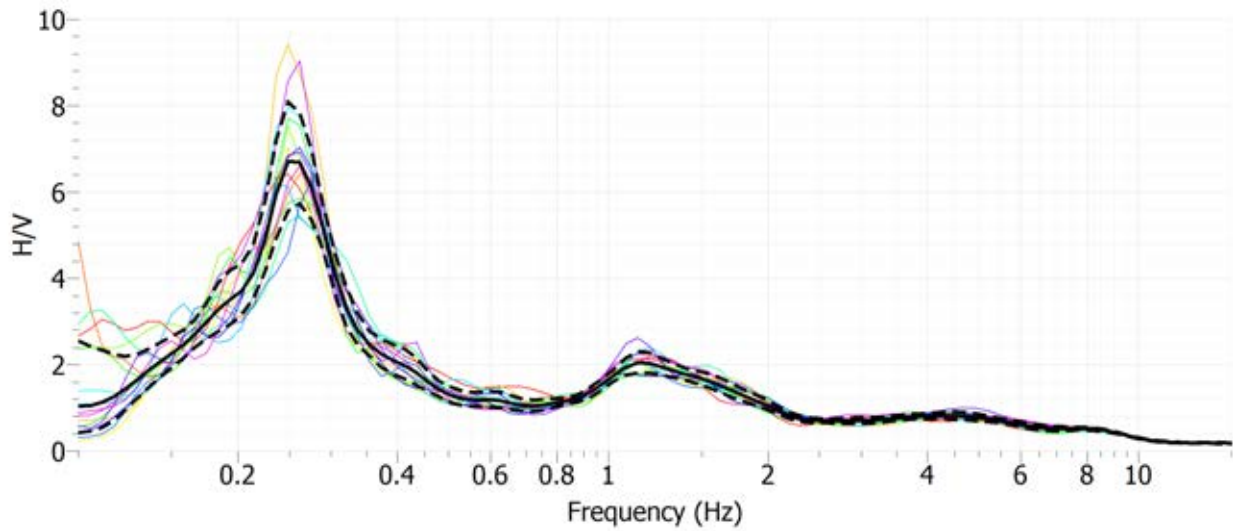


Seismic data acquisition system

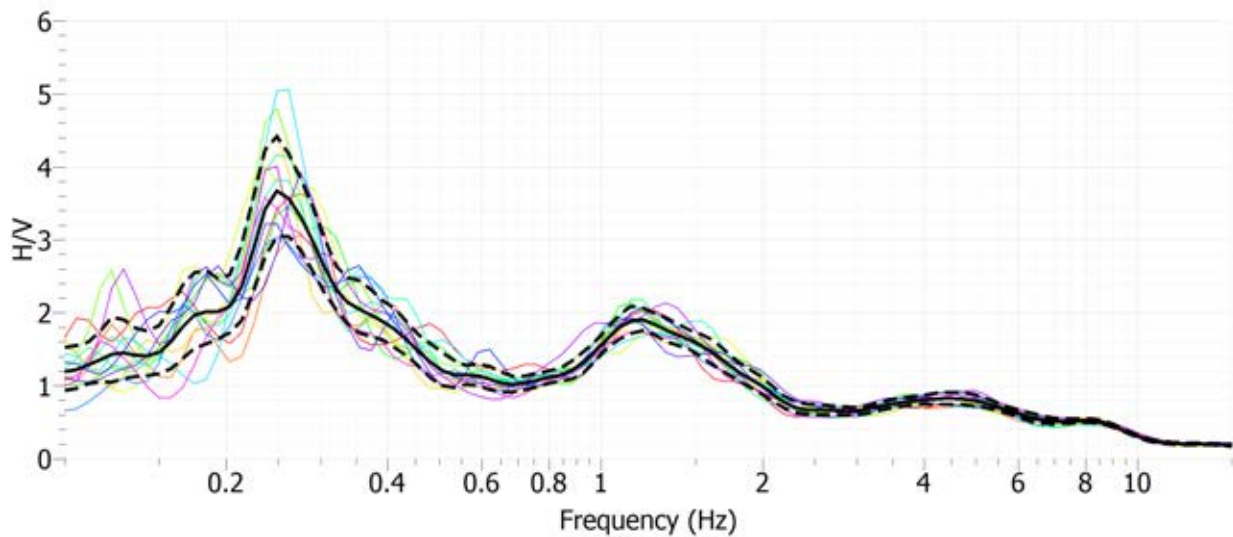


Looking northwest toward center of triangular
passive surface wave Array 1

Figure 3 Site CE.47179 Photographs



Site CE.47179, HVSR Location 1, Nanometrics Trillium Compact Sensor



Site CE.47179, HVSR Location 1, MOHO Tromino ENGR Sensor

Figure 4 H/V Spectral Ratio of Ambient Vibration Data, Site CE.47179

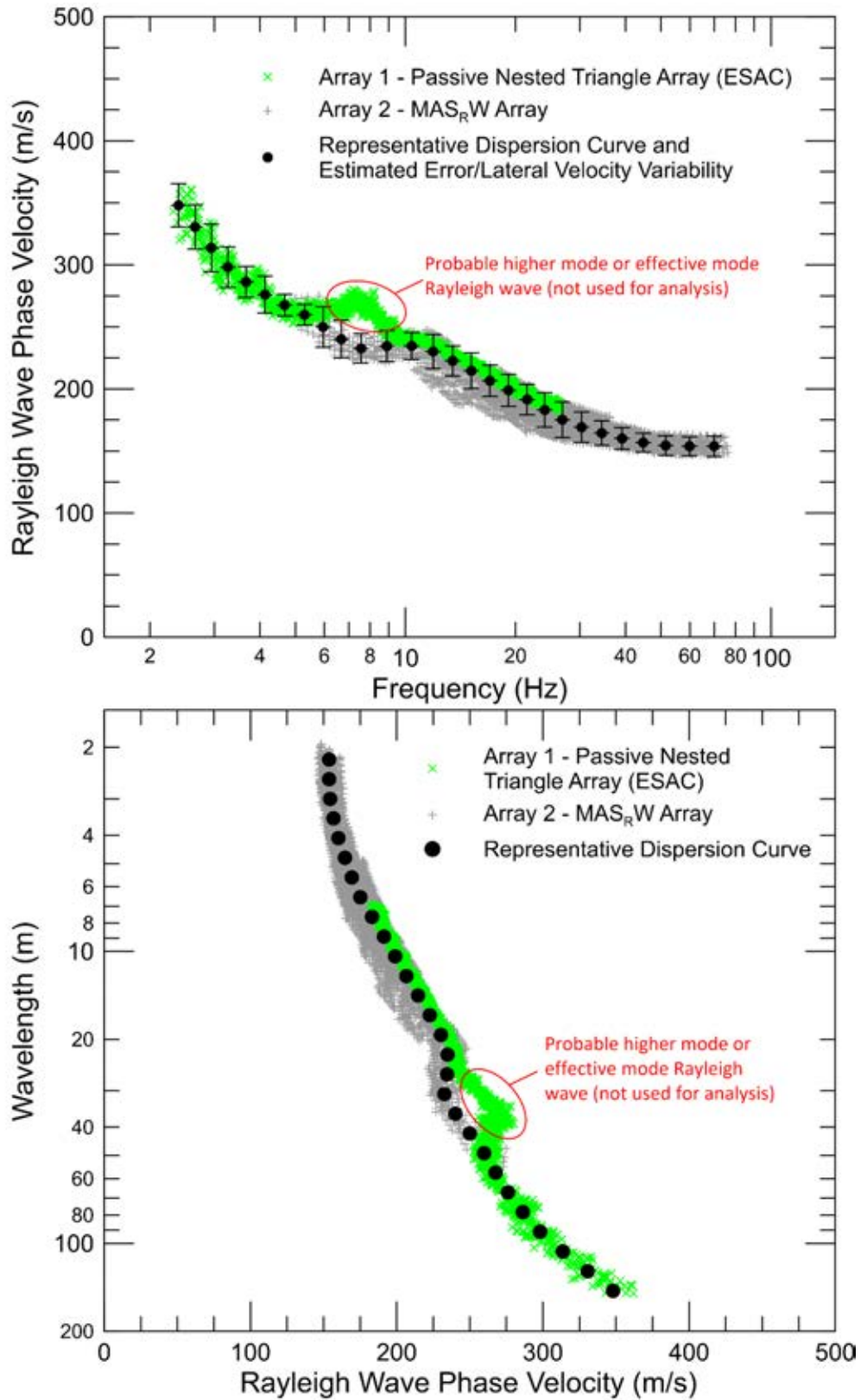


Figure 5 CE.47179 – Rayleigh wave dispersion curves derived from active- and passive-source surface wave data

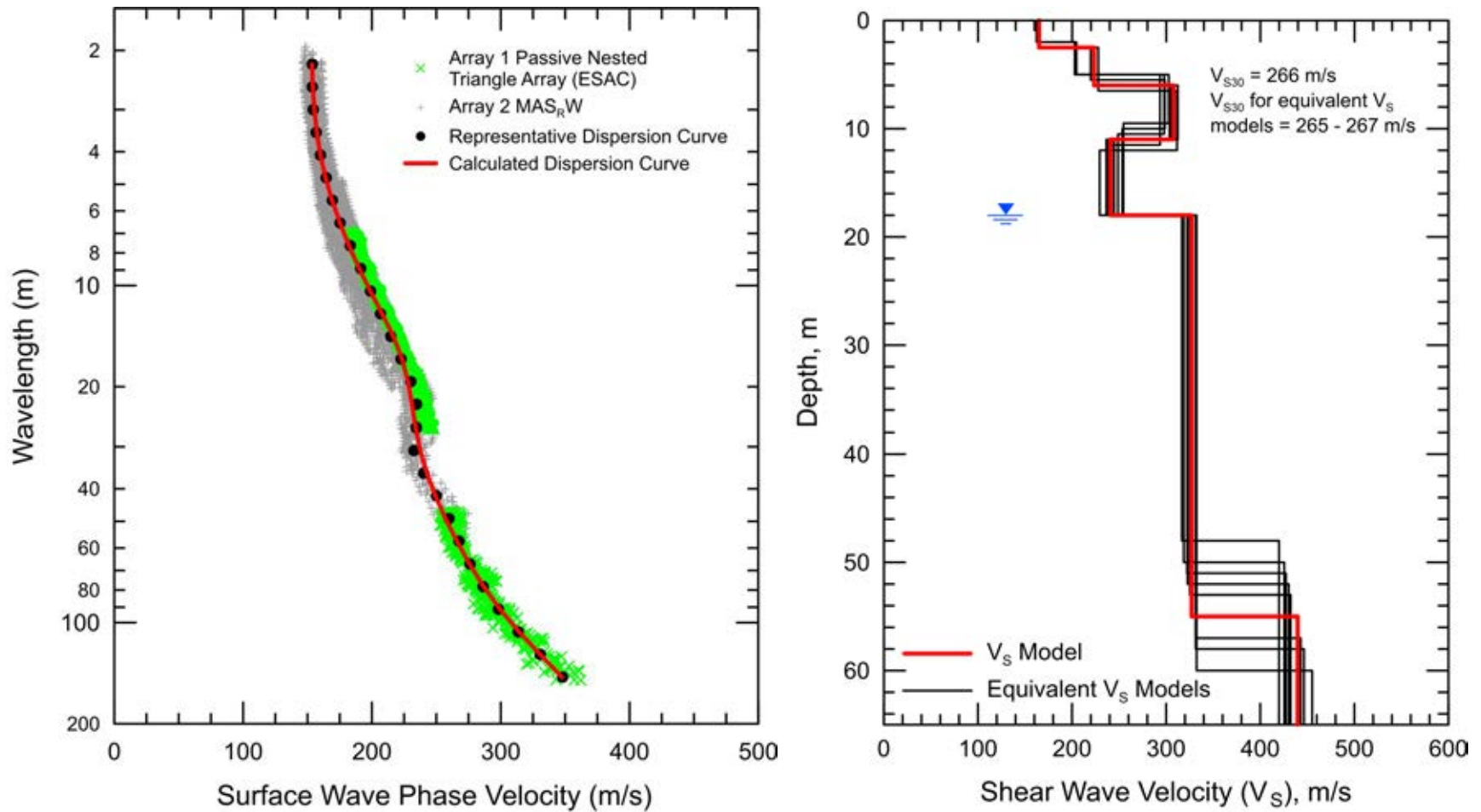


Figure 6 CE.47179 - Field, representative and calculated surface wave dispersion data (left) and associated V_S models (right)

Report

Geophysical Site Characterization

SMIP Station CE.47189

Station Name: Hollister - SAGO South

Location: Hollister Hills State Vehicular Recreation Area, 7800 Cienega Road, Hollister, California

Latitude: 36.75258

Longitude: -121.39627

V_{s30}: 505 m/s

Estimated Error in V_{s30}: ± 25 m/s

NEHRP Site Class: C

Geomatrix Code: IGB

HVSR Peak Frequency: None

Site Geology: Site located in area mapped as Cretaceous granitic rock (Figure 2). The San Andreas fault zone is located about 250 m northeast of seismic station. Site inspection reveals that site is likely located on a thin layer of residual soil overlying intensely weathered granitic rock.

Site Conditions: Rural site with low traffic noise. Hilly terrain in site vicinity.

Geophysical Methods Utilized: MAS_RW, MAS_LW, P- and S-wave seismic refraction, HVSR

Geophysical Testing Arrays:

1. Array 1: 48 channel MAS_RW and P-wave seismic refraction array utilizing 4.5 Hz vertical geophones spaced 2 m apart for a length of 94 m, forward and reverse shot locations with one source offset (2 m at both ends of array) and multiple interior source locations (Figure 1). A 4-lb hammer used as an energy source at the near offset and center shot locations. A 12-lb sledgehammer used for the near-offset and all interior shots locations. A 20-lb sledgehammer used only at the off-end source locations.
2. Array 1: Coincident with array above. 48 channel MAS_LW and S-wave seismic refraction array utilizing 4.5 Hz horizontal geophones spaced 2 m apart for a length of 94 m, forward and reverse shot locations with one source offset (2 m at both ends of array) and multiple interior source locations. A portable aluminum source with 4-, 12- and 20-lb hammers utilized as an energy source. Hammer type dependent upon source location.
3. Two HVSR locations (Figure 1).

Table 1 Location of Geophysical Testing Arrays

Location	Latitude	Longitude
Seismic Station CE.47189 (corrected)	36.75258	-121.39627
MASW Array 1, Southwest End of Array	36.75246	-121.39610
MASW Array 1, Northeast End of Array	36.75275	-121.39511
HVSR Location 1	36.75258	-121.39560
HVSR Location 2	36.75322	-121.39712

Notes: 1) WGS84 Coordinate System (decimal degrees)
 2) Location of seismic station moved to reflect actual approximate location.

S-Wave Velocity Model:

Table 2 V_s Model (Inversion of Love Wave Dispersion Data)

Depth to Top of Layer (m)	Layer Thickness (m)	S-Wave Velocity (m/s)	Assumed Density (g/cm ³)
0	1	101	1.60
1	1	178	1.80
2	4	342	1.90
6	5	506	2.00
11	6	756	2.10
17	7	868	2.15
24	>6	959	2.20

Notes: 1) Depth of investigation is about 30 m.
 2) Bottom layer is a half space.

Table 3 V_s Model (Average S-wave Seismic Refraction Model)

Depth to Top of Layer (m)	Layer Thickness (m)	S-Wave Velocity (m/s)
0.00	0.60	121
0.60	1.19	194
1.79	1.19	310
2.98	1.19	391
4.17	1.19	450
5.36	1.19	498
6.55	1.19	531
7.74	2.50	603
10.24	2.50	712
12.75	2.50	747
15.25	2.50	769
17.75	2.50	799
20.25	2.50	839
22.75	2.50	886
25.25	2.50	934
27.76	2.50	1013

Observations/Discussion:

H/V Spectral Ratio

HVSR data was collected at two locations using a MOHO Tromino ENGR (Tromino) seismograph as shown in Figure 1 and Table 1. About 30 minutes of ambient vibration data were acquired at each HVSR location. HVSR location 2 was located at an alternate MASW testing location that was not necessary to complete. There are no clear peaks in the HVSR data (Figure 4), which appears to confirm that rock is very shallow at the site.

Array Microtremor Data

The seismic station is located on the side of a hill and it was not possible to deploy a 2-D array for microtremor data acquisition. No attempt was made to acquire ambient vibration data using the linear MASW array because the site is located in a rural, low noise environment.

Seismic Refraction and MASW Data

Seismic refraction and MASW data acquisition were conducted along the 94-m long Array 1 (Figure 1). Rayleigh wave dispersion data were interpreted from 14 MAS_RW seismic records collected at 9 different source locations using 4-lb hammer, and 12- and 20-lb sledgehammer energy sources. Maximum source offset was only 2 m at both ends of the array due to limited space. P-wave seismic refraction data was interpreted using the largest energy source utilized at the 9 source locations spaced about 12 m apart. Love wave dispersion data were interpreted from

13 MAS_LW seismic records collected at 9 different source locations using a portable aluminum source with a 4-lb hammer, and 12- and 20-lb sledgehammers. Maximum source offset was only 2 m at both ends of the array due to limited space. S-wave seismic refraction data was interpreted using the largest energy source utilized at the 9 source locations spaced about 12 m apart.

Review of Rayleigh wave (MAS_RW) data indicated that higher modes may be dominant over a wide frequency range. The source of dominant higher mode energy Rayleigh wave data is expected to be associated with a thin low velocity layer overlying much higher velocity sediments/rock. Because of the complex Rayleigh wave propagation, it was not possible to develop an acceptable Rayleigh wave dispersion curve over sufficient wavelength range for modeling. It was, however, possible to estimate the Rayleigh wave phase velocity at 40-m wavelength (V_{R40}), which ranged from about 460 to 500 m/s, averaging 480 m/s. Dominant higher modes were not, however, a significant issue in Love wave (MAS_LW) data. Therefore, modeling of Love wave, rather than Rayleigh wave, phase velocity data was conducted at this site.

Using the 13 seismic records and variable receiver offset ranges, over 90 dispersion curves were extracted from the Love wave seismic records and combined for analysis. To minimize near field effects, the maximum wavelength Love wave extracted from the MAS_LW data set was set equal to the lesser of 1.3 times the distance between the source and midpoint of the active receiver array or 71 m. There is nominally about 40 m/s of scatter in MAS_LW dispersion data, which is likely in part due to lateral velocity variation. The minimum wavelength Love wave phase velocity data extracted from a 48-channel MAS_LW receiver gather is in the 7 to 12 m range. Reducing data from smaller hammer sources using a limited offset range receiver gather (i.e. less active geophones) allowed for extraction of surface wave dispersion data to a minimum wavelength of about 3.5 m.

Seismic Refraction Modeling

The P- and S-wave seismic refraction data for Array 1 were modeled using a tomographic inversion routine with a smooth velocity gradient starting model with results presented in Figure 5.

The P-wave seismic refraction survey design allowed P-wave velocity to be imaged to a maximum depth of about 30 m along Array 1. The seismic refraction model (Figure 5) indicates that P-wave velocity is about 250 to 500 m/s at the surface and increases to 1,000 m/s at a depth of 2 to 8 m, and is greater than 1,750 m/s at a depth below 25 to 28 m. The maximum P-wave velocity in the model is about 2,000 m/s and P-wave velocity may gradually increase with depth below 30 m as weathering decreases.

The S-wave seismic refraction survey design allowed S-wave velocity to be imaged to a maximum depth of about 30 m. The seismic refraction model (Figure 5) indicates that S-wave velocity is about 150 m/s at the surface and increases to 500 m/s at a depth of 4 to 7 m, 750 m/s at a depth of 7 to 15 m, and over 1,000 m/s at a depth of 26 to 28 m. The maximum S-wave velocity in the model is about 1,050 m/s and S-wave velocity may gradually increase with depth below 30 m as weathering decreases. The average S-wave velocity of the upper 30 m (V_{S30}) was estimated between a position of 34 and 68 m on the S-wave refraction model, where depth of

investigation is greatest. Over this interval, V_{S30} ranges from about 550 to 583 m/s, a 6% variation. An average V_S model was developed over the 34 to 68 m distance interval by horizontally averaging the travel time of each model cell and cell thickness and average V_{S30} was determined to be 563 m/s.

The seismic refraction models (Figure 5) indicate that there is lateral velocity variation beneath Array 1 with 6% variation in V_{S30} beneath the central 34 m of the array and likely greater variation beneath the entire array.

Surface Wave Modeling

V_{R40} averages about 480 m/s from limited Rayleigh wave dispersion data extracted from Array 1. The phase velocity of a 50 m wavelength Love wave (V_{L50}) averages 517 m/s with a coefficient of variation (COV) of 1.5 % from 14 dispersion curves reduced from MAS_{LW} data collected along Array 1. A representative dispersion curve was generated for surface wave data set using a moving average, polynomial curve fitting routine. Error bars for the representative dispersion curve were estimated based on the scatter in the dispersion data. Figure 6 presents the Love wave dispersion data and representative dispersion curve.

The representative dispersion curve was inverted using an iterative non-linear least squares (local search) inversion routine with the fundamental mode Love wave assumption to derive V_S models. Realistic estimates of density were used to make models as accurate as possible. Poisson's ratio does not affect Love wave propagation. Model layer thicknesses generally increased with depth to reflect the reduction in model resolution with depth. Multiple V_S models were developed with almost identical calculated dispersion curves to demonstrate the non-uniqueness inherent in the inversion of surface wave dispersion data; especially at layer boundaries where an abrupt change in seismic velocity occurs or associated with high velocity layers or velocity inversions.

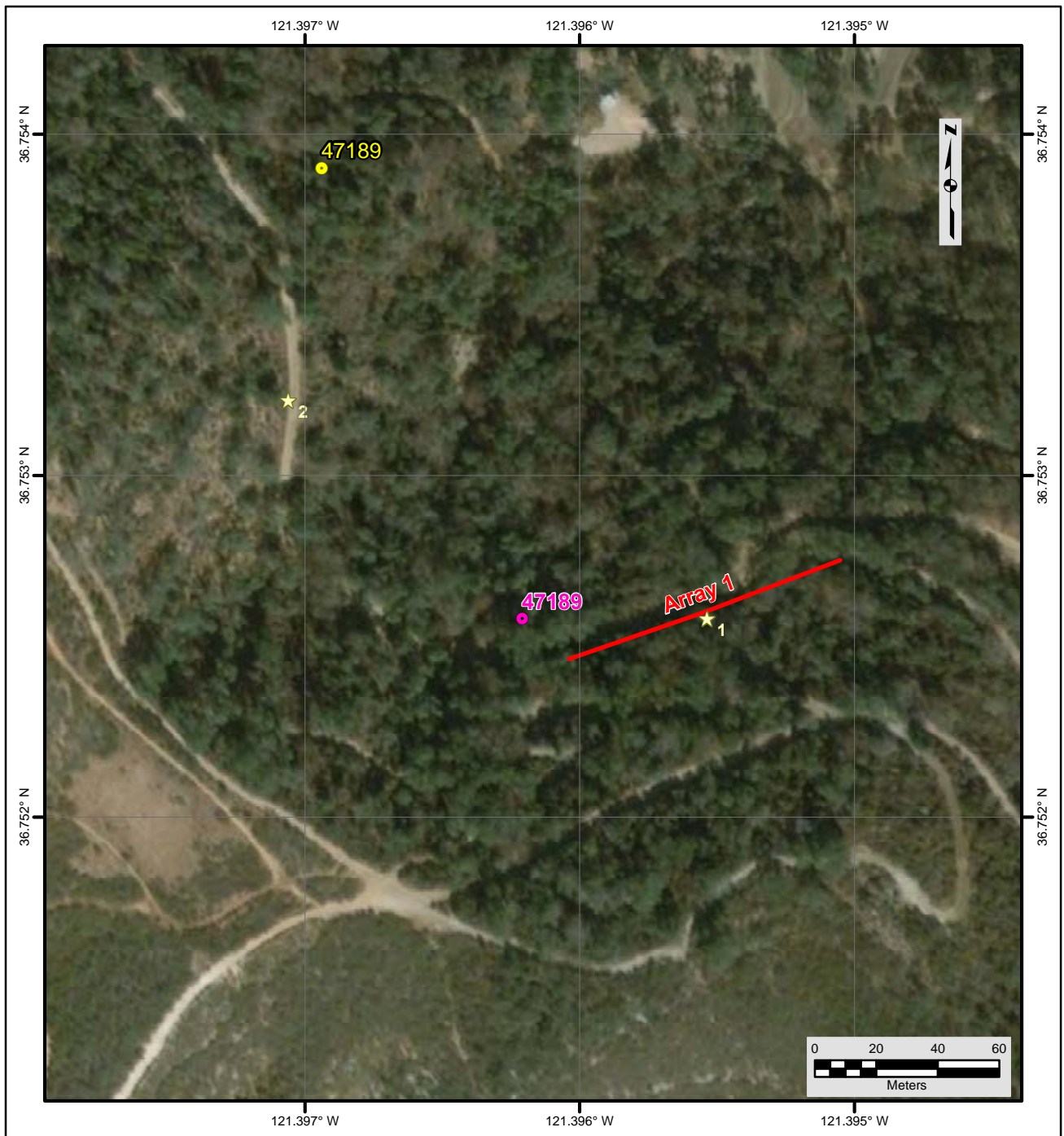
Results

V_S models from inversion of the Love wave dispersion data are presented as Figure 7 and the V_S model selected for purpose of site characterization is presented in Table 2. Also included on the figure is the average V_S model between 34 and 68 m on the S-wave seismic refraction model. The surface wave and seismic refraction models yield similar subsurface velocity structure except between a depth of about 3 and 10 m where seismic refraction V_S is slightly higher. The low S-wave velocity at the surface is likely associated with residual soil, which grades with depth into very intensely weathered to decomposed rock. V_S does not exceed 750 m/s until a depth of about 11 m and competent rock is not present in the upper 30 m. Surface wave depth of investigation is about 30 m based on $\lambda_{max}/2$ to $\lambda_{max}/2.5$.

V_{S30} from the V_S model developed from the Love wave data is 505 m/s (NEHRP Site Class C). The estimated error in V_{S30} , which includes some effects of the lateral velocity variability beneath the testing arrays, is about 25 m/s. This is computed based on the sum of the following rounded to the nearest 5 m/s: 1% error from the realistic assumed layer densities in the model, 2% for the variation in V_{S30} associated with non-uniqueness, and the 1.5 % COV in V_{L50} from the Love wave dispersion data. Average V_{S30} from the central portion of the seismic refraction model is 563 m/s, about 11% higher than that from the Love wave dispersion data. In our

experience, seismic refraction models can overestimate V_{S30} if high velocity layers are present or if out-of-plane refractors occur. In a weathered rock environment, it is plausible that the first-arrival occurs from a structure outside of the vertical plane, thereby, resulting in overestimated V_{S30} .

Interestingly, V_{S30} estimated from V_{R40} using the Brown et al., 2000 relationship ($V_{S30} \cong 1.045V_{R40}$, assuming V_{R40} represents the fundamental mode Rayleigh wave) is 502 m/s, very similar to that from the V_S model developed from Love wave dispersion data. A formal empirical relationship between phase velocity and V_{S30} has not been developed for Love wave data; however, we often find that V_{S30} is between V_{L50} and V_{L55} . At this site V_{L50} is 517 m/s, 2% higher than V_{S30} estimated from the V_S model.



File Name: 18045_47189
Date: 5/29/2018

Legend

- Corrected CSMIP Station
- CSMIP Station and Number
- ★ H/V Spectral Ratio Measurement Location
- MASW Array

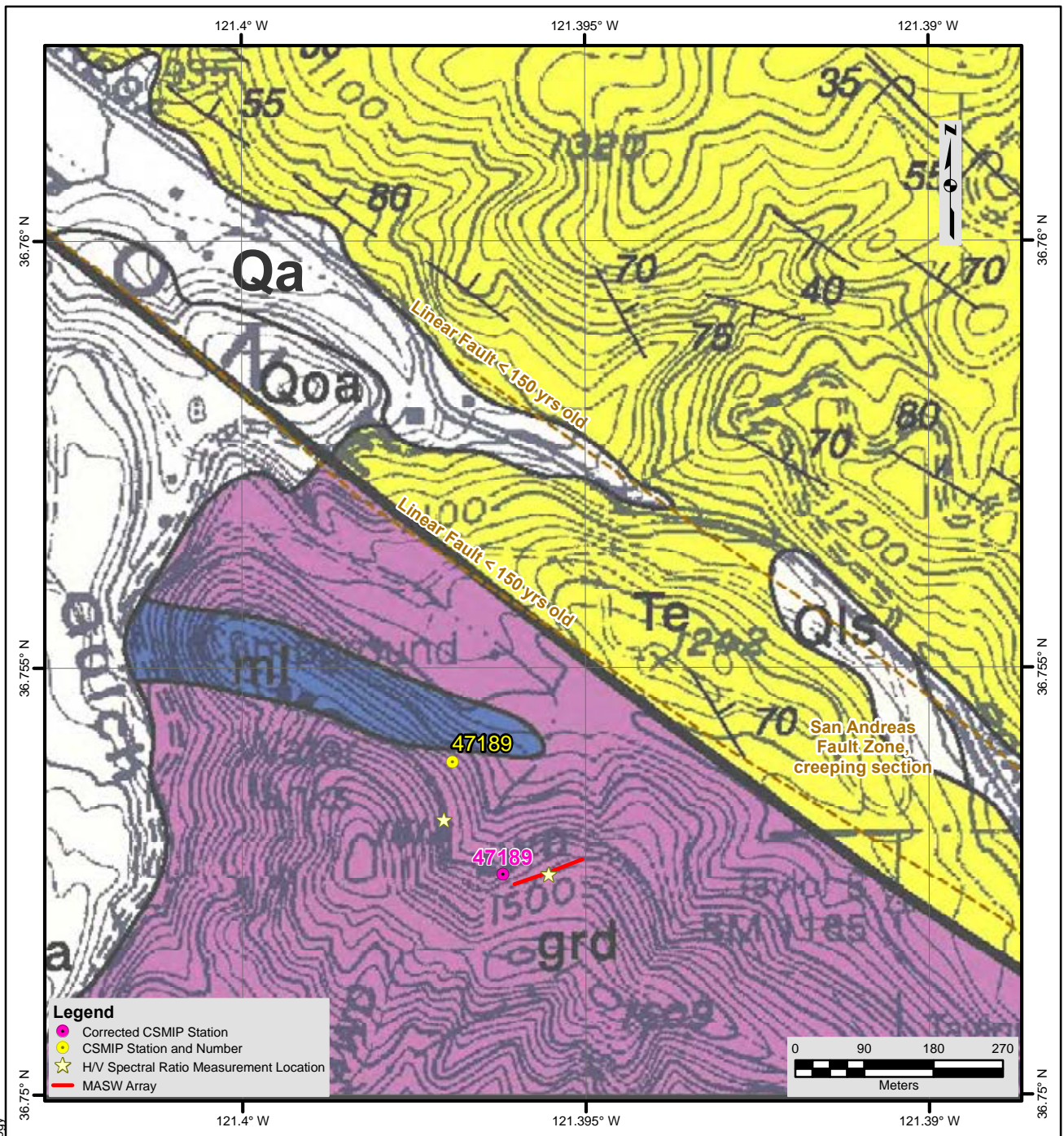
NOTES:

1. WGS 1984 Coordinate System
2. Image Source: Esri, DigitalGlobe, GeoEye, Earthstar Geographics, CNES/Airbus DS, USDA, USGS, AEX, Getmapping, Aerogrid, IGN, IGP, swisstopo, and the GIS User Community



**FIGURE 1
SITE MAP
CE • 47189**





Description of Geologic Map Units

Qa = Quaternary (Holocene) Alluvial pebble, gravel, sand and clay of valley areas
 Qls = Quaternary (Holocene to Pleistocene) Landslide rubble
 Qoa = Quaternary (Pleistocene) Older alluvial terrace gravel and sand
 Te = Tertiary (Pliocene to Miocene) Etchegoin Formation, marine clastic sandstone
 grd = Mesozoic (Cretaceous) Granitic rocks of Salinian basement
 ml = Paleozoic-Mesozoic Meta-sedimentary marble, dolomite and calcite

NOTES:

1. WGS 1984 Coordinate System
2. Geologic Map of the Hollister Quadrangle, Monterey and San Benito Counties, California by Thomas W Dibblee, Jr., 2006



**FIGURE 2
 GEOLOGIC MAP
 CE • 47189**



File Name: 18045_47189-Geology

Date: 5/29/2018



Seismic Station CE.47189



HVSR Sensor location 2

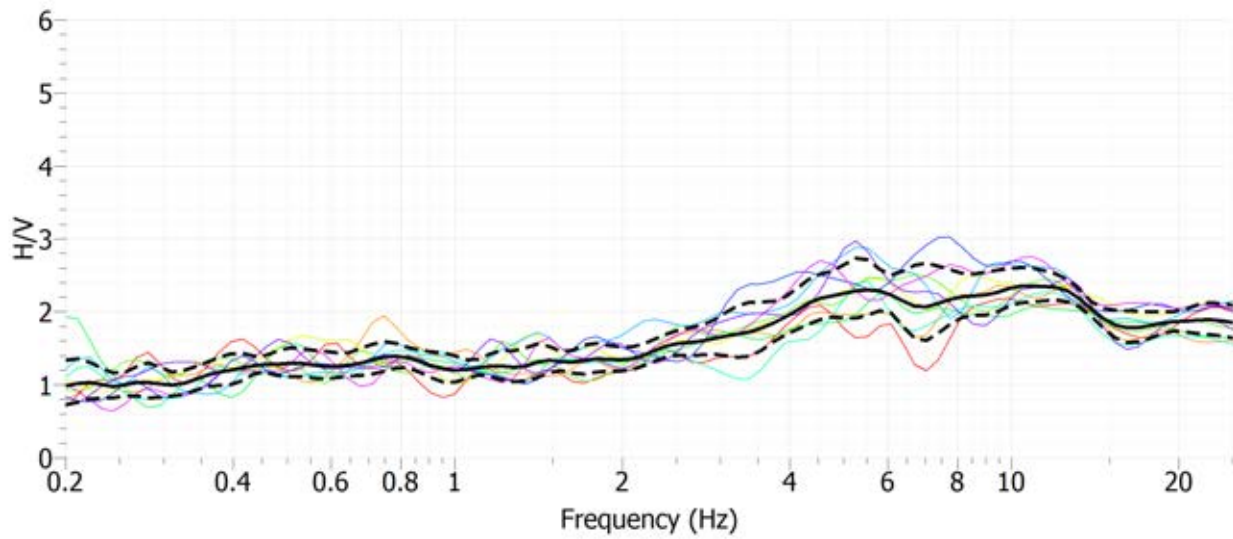


Looking southwest along MASW and seismic refraction Array 1

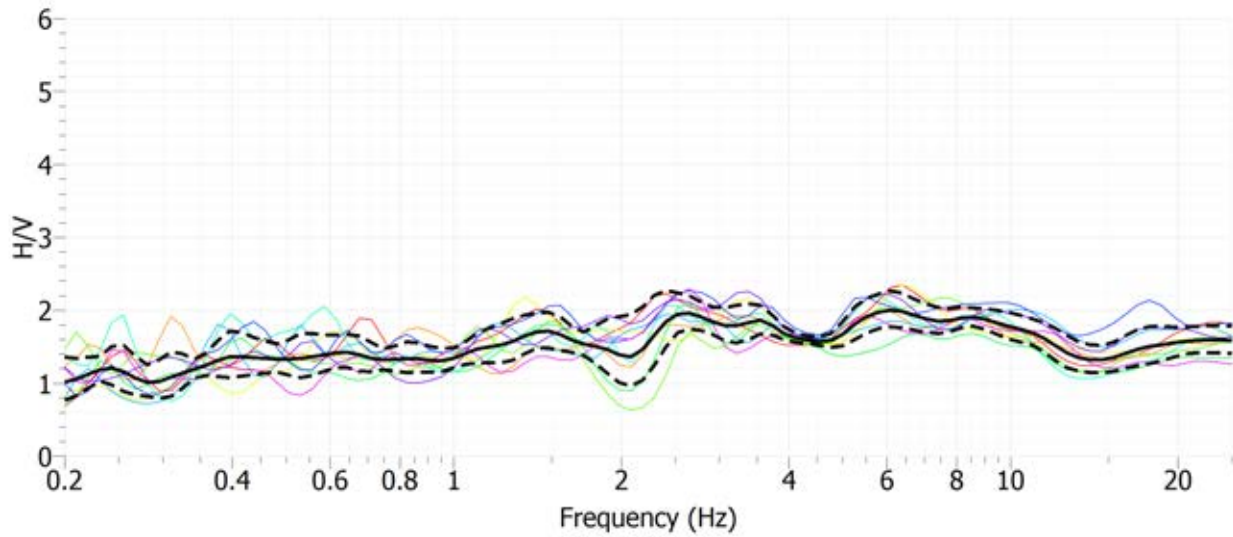


Love wave MASW data acquisition along Array 1

Figure 3 Site CE.47189 Photographs

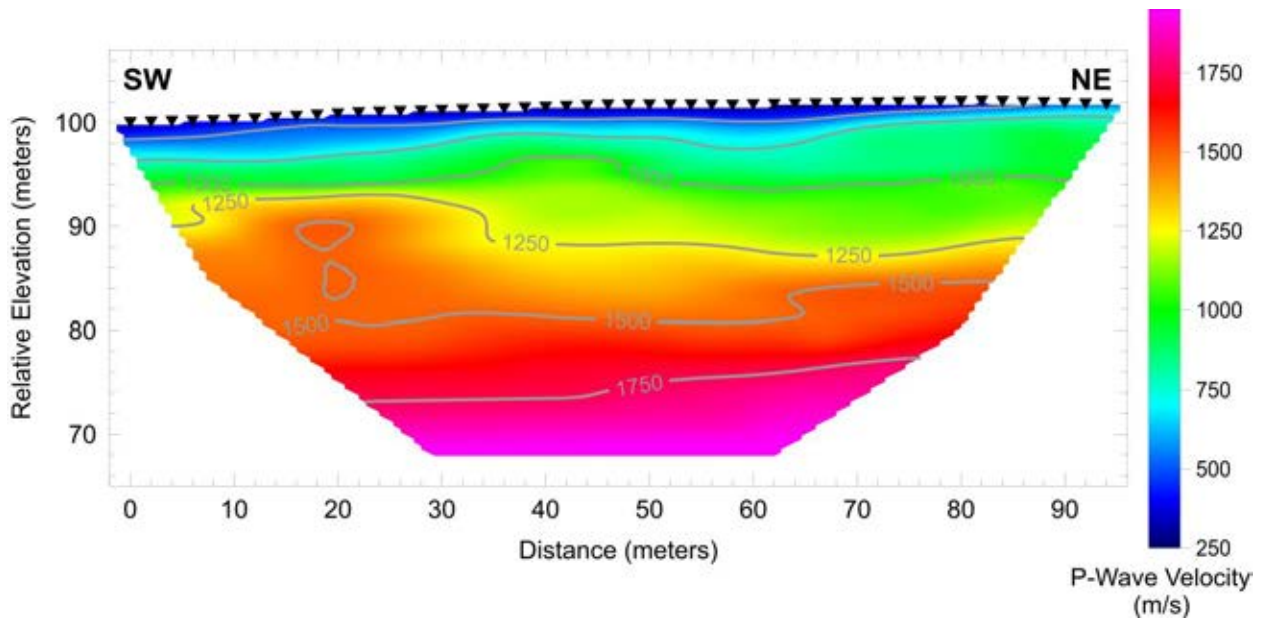


Site CE.47189, HVSR Location 1, MOHO Tromino ENGR Sensor

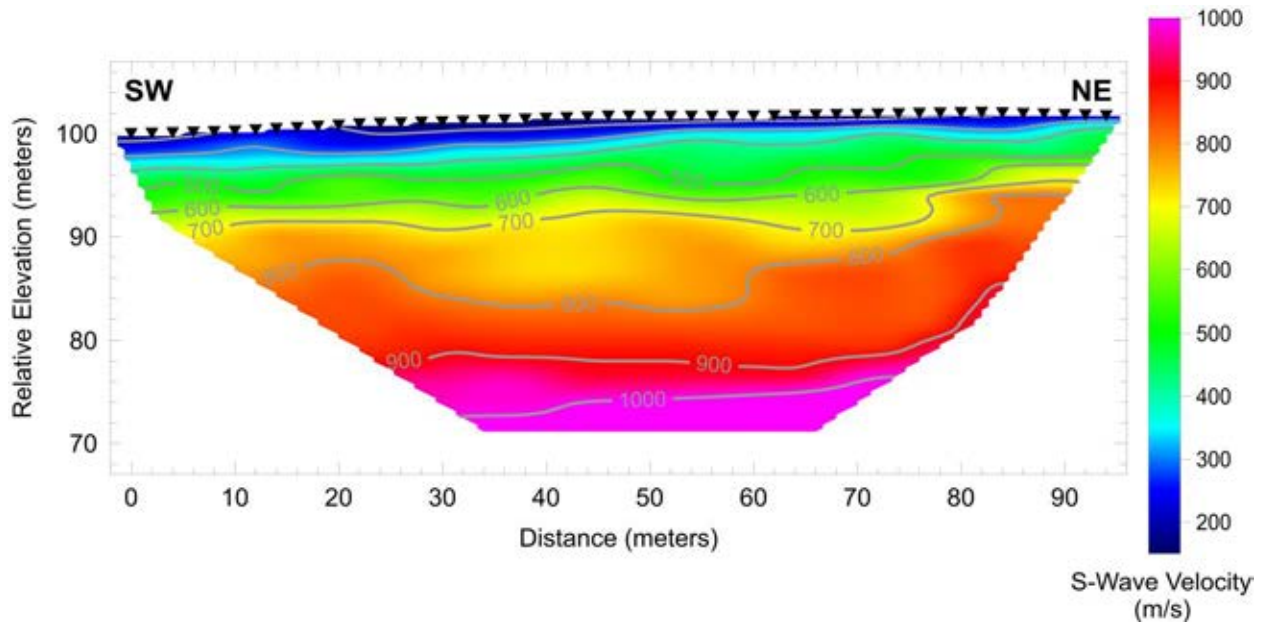


Site CE.47189, HVSR Location 2, MOHO Tromino ENGR Sensor

Figure 4 H/V Spectral Ratio of Ambient Vibration Data, Site CE.47189



Array 1 – P-wave tomographic seismic refraction model developed using a smooth velocity gradient starting model



Array 1 – S-wave tomographic seismic refraction model developed using a smooth velocity gradient starting model

Figure 5 P- and S-wave Seismic Refraction Models, Site CE.47189

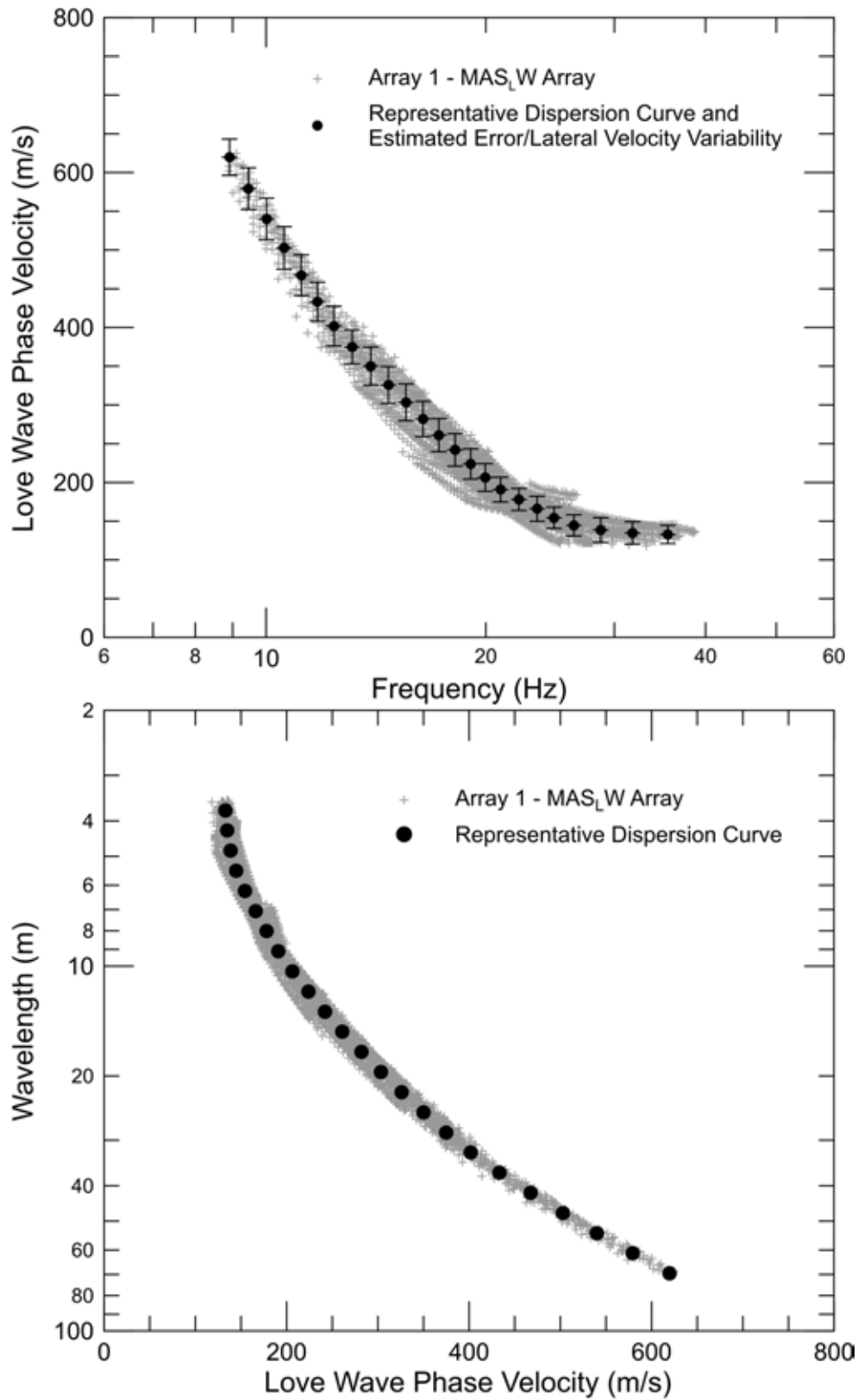


Figure 6 CE.47189 – Love wave dispersion curves derived from active-source surface wave data

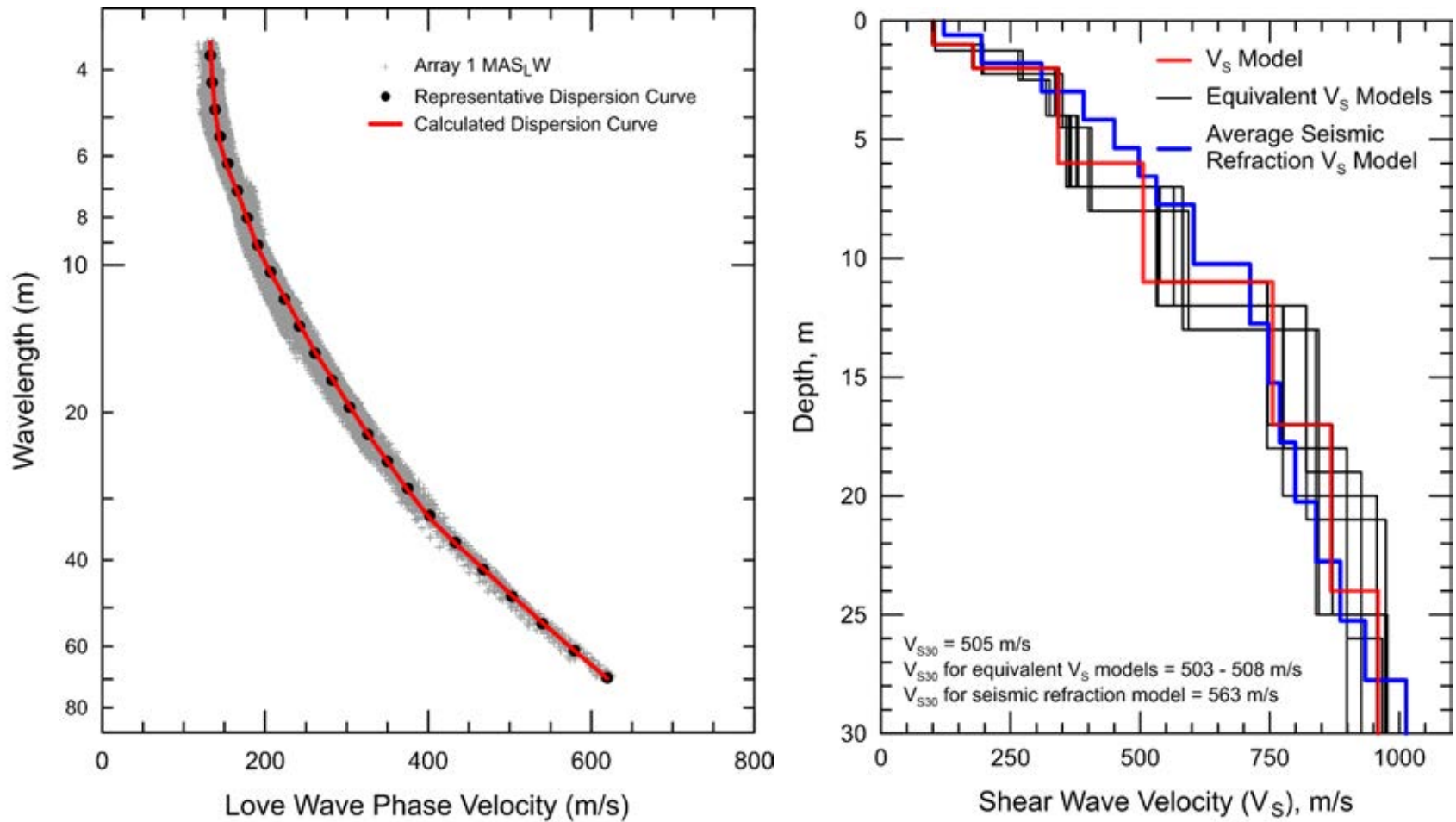


Figure 7 CE.47189 - Field, representative and calculated Love wave dispersion data (left) and associated V_S models (right)

Report

Geophysical Site Characterization

SMIP Station CE.47377

Station Name: Monterey - City Hall

Location: Monterey City Hall, 580 Pacific Street, Monterey, CA

Latitude: 36.5974

Longitude: -121.8979

V_{s30}: 572 m/s

Estimated Error in V_{s30}: ± 55 m/s

NEHRP Site Class: C

Geomatrix Code: AGA

HVSR Peak Frequency: No high amplitude peaks. Inconclusive weak peaks at 3.8, 5.7, and 30 Hz.

Site Geology: Site located near Monterey Bay on area mapped as Mesozoic granitic rock (Figure 2). Quaternary older alluvium and Tertiary Monterey Formation outcrop about 200 m east and south of the site. (Figure 2). Field inspection reveals that residual soil overlies granitic rock.

Site Conditions: Suburban site with traffic and pedestrian noise from nearby streets. Gently sloping terrain in site vicinity.

Geophysical Methods Utilized: MAS_RW, MAS_LW, array microtremor, HVSR

Geophysical Testing Arrays:

1. Array 1: 37 channel, nested triangle array utilizing 4.5 Hz vertical geophones with 48 m maximum length of outer side of array (Figure 1).
2. Array 2: 48 channel MAS_RW array utilizing 4.5 Hz vertical geophones spaced 1.5 m apart for a length of 70.5 m, forward and reverse shot locations with multiple source offsets (1.5 m to 15 m at both ends of array) and multiple interior source locations. A 4-lb hammer and 12-lb sledgehammer were used as energy sources (Figure 1). P-wave seismic refraction data was also acquired on the array.
3. Array 2: 48 channel MAS_LW array utilizing 4.5 Hz horizontal geophones spaced 1.5 m apart for a length of 70.5 m, forward and reverse shot locations with multiple source offsets (1.5 m to 15 m off both ends) and multiple interior source locations. Energy source consisted of a hammer-impact aluminum S-wave source with a 12-lb sledgehammer (Figure 1). Array also used to acquire S-wave seismic refraction data.
4. One HVSR location in vicinity of center of triangle array (Figure 1).

Table 1 Location of Geophysical Testing Arrays

Location	Latitude	Longitude
Seismic Station CE.47377	36.59740	-121.89790
Array 1 Passive, Center of Triangle Array	36.59748	-121.89727
Array 1 Passive, Corner of Triangle Array	36.59740	-121.89698
Array 1 Passive, Corner of Triangle Array	36.59773	-121.89732
Array 1 Passive, Corner of Triangle Array	36.59732	-121.89751
Array 2 MASW, Northeast End of Array	36.59772	-121.89716
Array 2 MASW, Southwest End of Array	36.59711	-121.89736
HVSR Location 1	36.59748	-121.89728

Notes: 1) WGS84 Coordinate System (decimal degrees)

S-Wave Velocity Models:

Table 2 V_s Model (Average S-wave Seismic Refraction Model)

Depth to Top of Layer (m)	Layer Thickness (m)	S-Wave Velocity (m/s)
0.00	0.34	96
0.34	0.69	101
1.03	0.69	139
1.72	0.69	318
2.41	0.69	502
3.10	0.69	551
3.78	0.69	628
4.47	1.44	629
5.92	1.44	640
7.36	1.44	642
8.81	1.44	656
10.25	1.44	672
11.70	1.44	697
13.14	1.44	723
14.59	1.44	737
16.03	1.44	750

Table 3 V_S Model (Inversion of Love Wave Dispersion Data)

Depth to Top of Layer (m)	Layer Thickness (m)	S-Wave Velocity (m/s)	Assumed Density (g/cm ³)
0	0.75	96	1.60
0.75	1.75	258	1.85
2.5	4	529	2.00
6.5	6	598	2.05
12.5	9	686	2.10
21.5	>8.5	779	2.10

Notes: 1) Depth of investigation is about 30 m.
2) Bottom layer is a half space.

Table 4 V_S Model (Multi-Mode Inversion of Rayleigh Wave Dispersion Data)

Depth to Top of Layer (m)	Layer Thickness (m)	S-Wave Velocity (m/s)	Inferred P-Wave Velocity (m/s)	Assumed Poisson's Ratio	Assumed Density (g/cm ³)
0.000	0.552	80	139	0.253	1.70
0.552	2.406	305	531	0.254	1.90
2.958	1.826	372	688	0.293	2.00
4.785	5.315	543	1034	0.310	2.05
10.100	8.262	816	1650	0.338	2.15
18.362	21.277	1156	2014	0.254	2.25
39.639	>6	1393	2822	0.339	2.30

Notes: 1) Depth of investigation is about 45 m.
2) Bottom layer is a half space.

Table 5 V_S Model (Effective Mode Inversion of Rayleigh Wave Dispersion Data)

Depth to Top of Layer (m)	Layer Thickness (m)	S-Wave Velocity (m/s)	Inferred P-Wave Velocity (m/s)	Assumed Poisson's Ratio	Assumed Density (g/cm ³)
0	0.75	108	201	0.300	1.60
0.75	1.75	282	527	0.300	1.80
2.5	4	448	838	0.300	2.00
6.5	6	562	1051	0.300	2.10
12.5	9	852	1594	0.300	2.20
21.5	12.5	952	1779	0.300	2.20
34	>11	1254	2344	0.300	2.30

Notes: 1) Depth of investigation is about 45 m.
2) Bottom layer is a half space.

Table 6 Recommended V_s Model (Joint Inversion of Rayleigh and Love Wave Dispersion Data)

Depth to Top of Layer (m)	Layer Thickness (m)	S-Wave Velocity (m/s)	Inferred P-Wave Velocity (m/s)	Assumed Poisson's Ratio	Assumed Density (g/cm ³)
0.000	0.515	81	168	0.350	1.70
0.515	0.730	191	394	0.346	1.90
1.245	1.785	305	629	0.346	2.00
3.030	7.289	511	1055	0.346	2.05
10.319	6.497	732	1509	0.346	2.15
16.816	17.881	996	2054	0.346	2.25
34.697	>11	1352	2794	0.347	2.30

Notes: 1) Depth of investigation is about 45 m.
2) Bottom layer is a half space.

Observations/Discussion:

H/V Spectral Ratio

HVSR data was collected at a single location using a Nanometrics Trillium Compact seismograph (Trillium) as shown in Figure 1 and Table 1. Over 60 min of ambient vibration data were acquired at the HVSR location. There are no clear, high amplitude peaks in the HVSR data; however, there are inconclusive weak peaks at about 3.8, 5.7 and 30 Hz.

Array Microtremor Data

Noise conditions at the site (multi-directional noise sources) appeared sufficient for successful application of passive surface wave techniques. A nested triangle array (Array 1) was utilized at this site because of limited site access. A nested triangle array has better azimuthal coverage (three azimuths for every sensor spacing) than a L-shaped array (two azimuths in the leg directions and one azimuth between receivers on different legs) and should, therefore, perform better in a variety of noise conditions. A total of 50 minutes (100, 30 second seismic records) of ambient vibration data were acquired into Array 1. The ESAC technique was used to extract surface wave dispersion data from the ambient vibration data. To better characterize error, dispersion curves were generated from approximate 12.5-minute time segments of the ambient vibration data and also from the complete data set. The minimum and maximum Rayleigh wavelength extracted from Array 1 are about 22 and 145 m, respectively.

Seismic Refraction and MASW Data

P- and S-wave seismic refraction and MASW (Rayleigh and Love wave) data were acquired along the 70.5 m long Array 2 (Figure 2). Rayleigh wave dispersion data were interpreted from 16 MAS_RW seismic records collected at 13 different source locations using 4-lb hammer and 12-lb sledgehammer energy sources. Maximum source offset was 15 m at both ends of the array. P-wave seismic refraction data was interpreted using the 12-lb sledgehammer data acquired at the

13 source locations spaced about 9 m apart. Love wave dispersion data were interpreted from 13 MAS_LW seismic records collected at 12 different source locations using a portable, hammer-impact, aluminum source with a 12-lb sledgehammer.

Review of Rayleigh wave (MAS_RW) data indicated that higher modes are likely dominant over a wide frequency range. The source of dominant higher mode energy Rayleigh wave data is expected to be associated with a thin, low velocity soil layer overlying much higher velocity weathered rock. However, it was possible to pick the apparent 1st higher Rayleigh wave mode. Using the 16 seismic records and variable receiver offset ranges, over 60 dispersion curves were extracted and combined for analysis. To minimize near field effects, the maximum Rayleigh wavelength data extracted from the MAS_RW data set was set equal to the lesser of 40 m and 1.3 times the distance between the source and midpoint of the active receiver array. There is nominally about 40 to 80 m/s of scatter in MAS_RW dispersion data, which is likely due to significant lateral velocity variation. The minimum Rayleigh wavelength phase velocity data (1st higher mode) extracted from a 48-channel MAS_RW receiver gather was about 11 to 23 m. Reducing data from smaller hammer sources using a limited offset range receiver gather (i.e. less active geophones) allowed for extraction of surface wave dispersion data to a minimum wavelength of about 2.5 m.

Dominant higher modes were not a significant issue in Love wave (MAS_LW) data. However, Love wave dispersion data was very difficult to interpret due to significant apparent lateral velocity variability beneath the array, which may result in higher error in resulting V_s models and V_{S30} estimates. Using the 13 seismic records and variable receiver offset ranges, over 75 dispersion curves were extracted from the Love wave seismic records and combined for analysis. To minimize near field effects, the maximum Love wavelength extracted from the MAS_LW data set was set equal to the lesser of 1.3 times the distance between the source and midpoint of the active receiver array or 71 m. There is nominally about 60 to 80 m/s of scatter in MAS_LW dispersion data due to significant lateral velocity variability beneath the array. The minimum wavelength Love wave phase velocity data extracted from a 48-channel MAS_LW receiver gather is in the 12 to 45 m range. Reducing data from smaller hammer sources using a limited offset range receiver gather (i.e. less active geophones) allowed for extraction of surface wave dispersion data to a minimum wavelength of about 2 m.

Seismic Refraction Modeling

The P- and S-wave seismic refraction data for Array 2 were modeled using a tomographic inversion routine with starting models based on layer-based, time-term analysis of the seismic refraction first arrival data with results presented in Figure 5.

The P-wave seismic refraction survey design allowed P-wave velocity to be imaged to a maximum depth of about 12 m along Array 2. The seismic refraction model (Figure 5) indicates that P-wave velocity is about 250 m/s at the surface then increases to 1,000 m/s at a depth of about 2 m and is greater than 2,500 m/s at a depth below 4 to 7 m. The maximum P-wave velocity in the model is slightly less than 3,000 m/s. Based on the seismic refraction model, weathered rock is likely located at a depth on the order of 2 m beneath the array.

The S-wave seismic refraction survey design allowed S-wave velocity to be imaged to a maximum depth of about 18 m. The seismic refraction model (Figure 5) indicates that S-wave velocity is about 100 m/s at the surface, increases to 500 m/s at an average depth of about 2 m, and over 700 m/s at a depth of 5 to 12 m. S-wave velocity may gradually increase with depth below 18 m as weathering decreases. The average S-wave velocity of the upper 20 m (V_{S20}) was estimated between a position of 24 and 48 m on the S-wave refraction model, where depth of investigation is greatest. Over this interval, V_{S20} ranges from about 422 to 495 m/s, a 16% variation. An average V_S model was developed over the 24 to 48 m distance interval by horizontally averaging the travel time of each model cell and cell thickness and is presented as Table 2.

The seismic refraction models (Figure 5) indicate that there is lateral velocity variation beneath Array 2 with 16% variation in V_{S20} beneath the central 24 m of the array and likely greater variation beneath the entire array. The high P-wave velocity relative to S-wave velocity indicates that fractures in the weathered rock are likely water filled.

Surface Wave Modeling

A representative dispersion curve was generated for each surface wave data set using a moving average, polynomial curve fitting routine. Error bars for the representative dispersion curve were estimated based on the scatter in the dispersion data. Figure 6 presents the active- and passive-source Rayleigh and Love wave dispersion data and the associated representative dispersion curves. There is significant scatter in the dispersion data due to lateral velocity variability beneath the array as demonstrated by seismic refraction models. Only first higher mode Rayleigh wave data could be extracted from the MAS_{RW} data; however, it appears that fundamental mode or effective mode Rayleigh wave data were extracted from the array microtremor data. The fundamental mode Love wave was recovered from the MAS_{LW} data; however, there is significant uncertainty due to the lateral velocity variability.

V_{R40} averages about 646 m/s from the inferred fundamental or effective mode Rayleigh wave dispersion data extracted from the ambient vibration data (Array 1) using the ESAC technique. The phase velocity of a 50-m wavelength Love wave (V_{L50}) averages 595 m/s with a coefficient of variation (COV) of 3.5 % from 16 dispersion curves reduced from MAS_{LW} data collected along Array 2.

Interpretation of the surface wave dispersion data is complicated by the significant scatter in the dispersion data associated with lateral velocity variability and dominant higher mode Rayleigh wave energy over some frequency ranges. Therefore, multiple data modeling approaches were utilized including inversion of the fundamental mode Love wave data, inversion of the multi-mode Rayleigh wave data, effective mode inversion of the Rayleigh wave data, and joint inversion of the multi-mode Rayleigh and fundamental mode Love wave data.

The Love wave representative dispersion curve was inverted using an iterative, non-linear least squares (local search) inversion routine (Seisimager software package) with the fundamental mode Love wave assumption to derive V_S models. The Rayleigh wave representative dispersion curves were modeled using the multi-mode global inversion routine in the Geopsy software package and the effective mode global and local inversion routines in the Seisimager software

packages. Joint inversion of the Rayleigh and Love wave dispersion data was conducted using the global inversion routine in the Geopsy software package. Realistic estimates of Poisson's ratio and density were used to make models as accurate as possible. Poisson's ratio does not affect Love wave propagation. Model layer thicknesses generally increased with depth to reflect the reduction in model resolution with depth. Multiple V_S models were developed with almost identical calculated dispersion curves to demonstrate the non-uniqueness inherent in the inversion of surface wave dispersion data, especially at layer boundaries where an abrupt change in seismic velocity occurs or associated with high velocity layers or velocity inversions.

Multiple model parameterizations with different layer depth search ranges were used when conducting global inversions in the Geopsy software package in order to more thoroughly search the model space. Figure 7 presents an ensemble of V_S models from multi-mode inversion of the Rayleigh wave dispersion data using a single model parameterization. Most of the V_S models have calculated dispersion curves fitting within the estimated dispersion error and can, therefore, be considered valid. Figure 8 presents an ensemble of V_S models from joint inversion of the Rayleigh and Love wave dispersion data using a single model parameterization. With the exception of the lowest frequency Love wave dispersion data, most of the V_S models have calculated dispersion curves fitting within the estimated dispersion error and can, therefore, be considered valid. Only the V_S model with the lowest misfit from each parameterization is presented for discussion from which a single model is selected for the purpose of site characterization, although ensembles of models can be made available in digital form.

Results

V_S models from inversion of the Love wave dispersion data are presented in Figure 9 and the V_S model selected for comparison with V_S models from other data modeling approaches is presented in Table 3. Also included on the figure is the average V_S model between 24 and 48 m on the S-wave seismic refraction model. The surface wave and seismic refraction models yield similar subsurface velocity structure although the seismic refraction model has slightly higher V_S in the weathered rock below 4 m. The low S-wave velocity at the surface is likely associated with residual soil. Weathered rock is encountered at a depth of about 2.5 m. V_S does not appear to exceed 900 m/s in the upper 30 m; however, we do not have high confidence in long wavelength Love wave dispersion data. Surface wave depth of investigation is about 30 m based on $\lambda_{\max}/2$ to $\lambda_{\max}/2.5$. V_{S30} from the V_S model developed from the Love wave data is 547 m/s (NEHRP Site Class C).

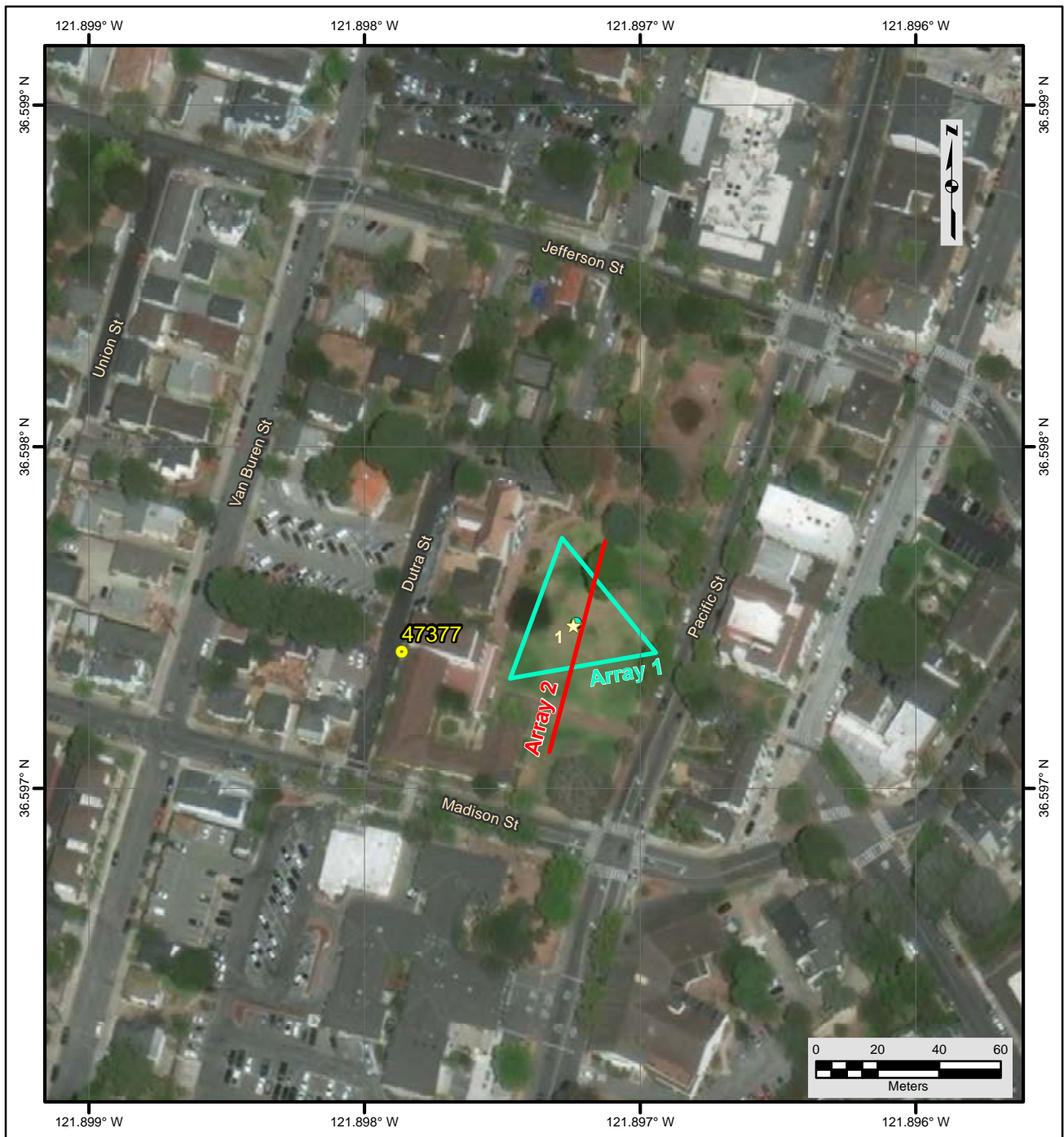
V_S models with the lowest misfit resulting from a global, multi-mode inversion of the Rayleigh wave dispersion data using 5 different model parameterizations are presented in Figure 10 and the V_S model selected for comparison with V_S models from other data modeling approaches is presented in Table 4. Surface wave depth of investigation is estimated to be about 45 to 50 m. V_{S30} from the V_S model selected for discussion is 604 m/s (NEHRP Site Class C).

A V_S model from an effective mode inversion of the Rayleigh wave dispersion data is presented in Figure 11 and Table 5. The lower frequency segment of the first higher mode Rayleigh wave data was not used for effective mode inversion. Surface wave depth of investigation is estimated to be about 45 to 50 m. V_{S30} from the V_S model selected for discussion is 574 m/s (NEHRP Site Class C).

V_S models with the lowest misfit resulting from a global, joint inversion of the Rayleigh and Love wave dispersion data using 5 different model parameterizations are presented in Figure 12 and the V_S model selected for comparison with V_S models from other data modeling approaches is presented in Table 6. Surface wave depth of investigation is estimated to be about 45 to 50 m. V_{S30} from the V_S model selected for discussion is 572 m/s (NEHRP Site Class C).

V_S models from the various data modeling approaches are summarized in Figure 13. The velocity-depth trends are quite similar in the upper 15 m. We believe that the S-wave refraction model would be in better agreement with the surface wave models had a smooth model tomographic inversion been conducted. It should also be noted that the refraction model only reflects average velocity structure beneath the central portion of the array. We expect that the V_S models developed from effective mode Rayleigh wave inversion (Figure 11 and Table 5) and joint Rayleigh and Love wave inversion (Figure 12 and Table 6) best reflect average S-wave velocity beneath the array and recommend that the V_S model from joint Rayleigh and Love wave inversion be used for the purpose of site characterization. V_{S30} from this V_S model is 572 m/s (NEHRP Site Class C). The estimated error in V_{S30} , which includes some effects of the lateral velocity variability beneath the testing arrays, is about 55 m/s. This is computed based on the sum of the following rounded to the nearest 5 m/s: an estimated error of 3% from the realistic assumed layer Poisson's ratios in the model, 1% error from the realistic assumed layer densities in the model, 2% error for the variation in V_{S30} associated with non-uniqueness, and the 3.5% COV in V_{L50} from the Love wave dispersion data. Interestingly, V_{S30} estimated from V_{R40} using the Brown et al., 2000 relationship ($V_{S30} \cong 1.045V_{R40}$, assuming V_{R40} represents the fundamental mode Rayleigh wave) is 675 m/s, about 18% higher than that from V_S model developed from joint inversion of the Rayleigh and Love wave dispersion data. This difference may result from V_{R40} being associated with an effective mode rather than fundamental mode Rayleigh wave. A formal empirical relationship between phase velocity and V_{S30} has not been developed for Love wave dispersion data; however, we often find that V_{S30} is between V_{L50} and V_{L55} . At this site V_{L50} is 595 m/s, 4% higher than V_{S30} estimated from the V_S model.

If the foundation of the structure housing the seismic station is located on weathered rock then the average S-wave velocity between 3 and 33 m, which is 761 m/s, might better represent V_{S30} beneath the seismic station.



File Name: 18045_47377
Date: 5/29/2018

Legend

- CSMIP Station and Number
- ★ H/V Spectral Ratio Measurement Location
- MASW Array
- ▭ Passive Surface Wave Triangle Array

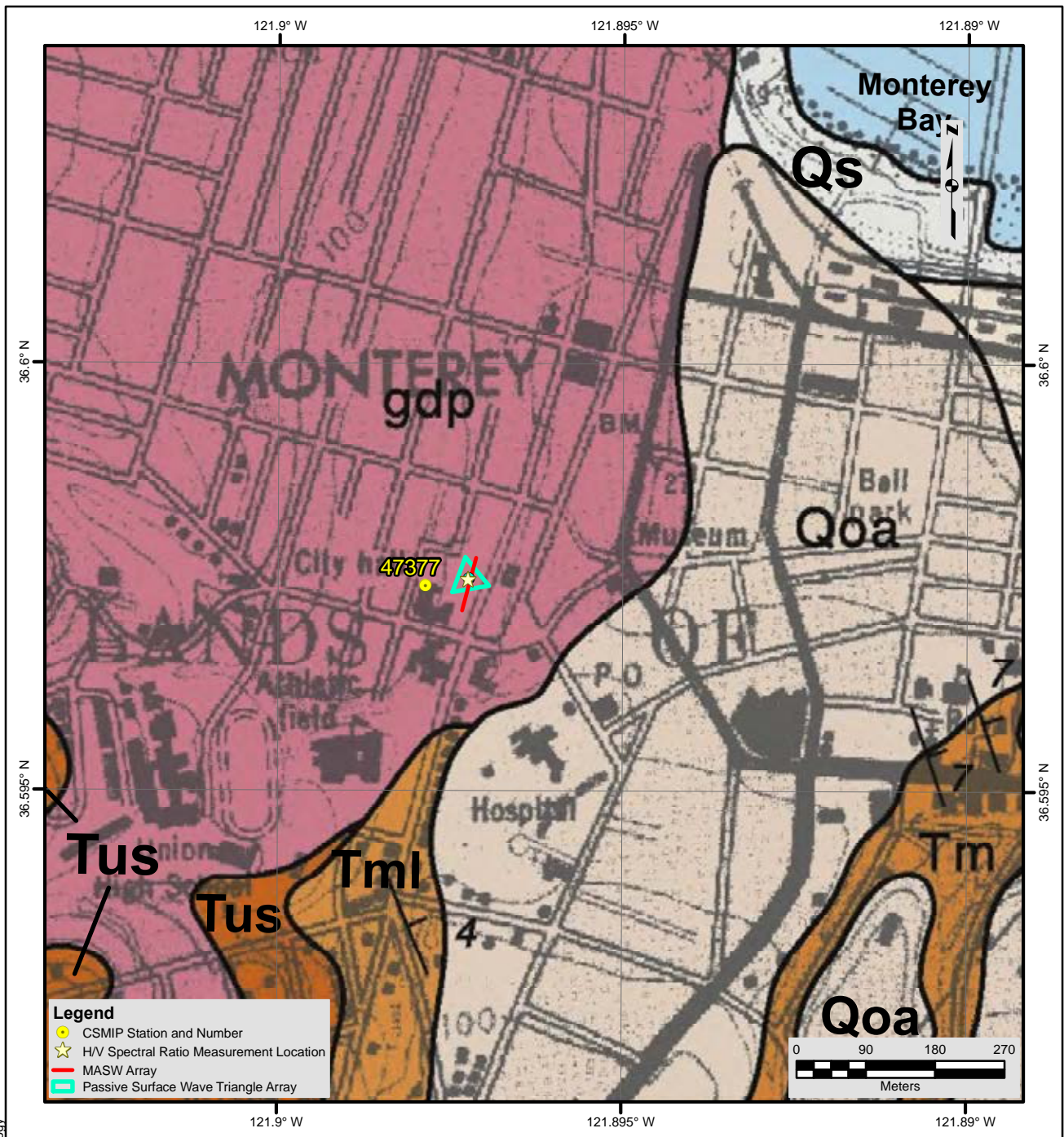
NOTES:

1. WGS 1984 Coordinate System
2. Image Source: Esri, DigitalGlobe, GeoEye, Earthstar Geographics, CNES/Airbus DS, USDA, USGS, AEX, Getmapping, Aerogrid, IGN, IGP, swisstopo, and the GIS User Community



**FIGURE 1
SITE MAP
CE • 47377**





Description of Geologic Map Units

Qs = Quaternary (Holocene) Beach Sand
 Qoa = Quaternary (Holocene to Pleistocene) Dissected older alluvium
 Tm = Tertiary (Miocene) Monterey Formation, Mohnian Stage, upper Miocene
 Tml = Tertiary (Miocene) Monterey Formation, Luisian Stage, middle Miocene
 Tus = Tertiary (Miocene) Marine Sandstone, Los Laureles Sandstone of Bowen
 gdp = Mesozoic granitic rocks of Salinian basement, granodiorite

NOTES:

1. WGS 1984 Coordinate System
2. Geologic Map of the Monterey and Seaside Quadrangles, Monterey County, California by Thomas W Dibblee, Jr., 2007

File Name: 18045_47377-Geology

Date: 5/29/2018



**FIGURE 2
 GEOLOGIC MAP
 CE • 47377**





HVSR measurement location



Looking southwest towards center of MASW Array 2 and building housing seismic station

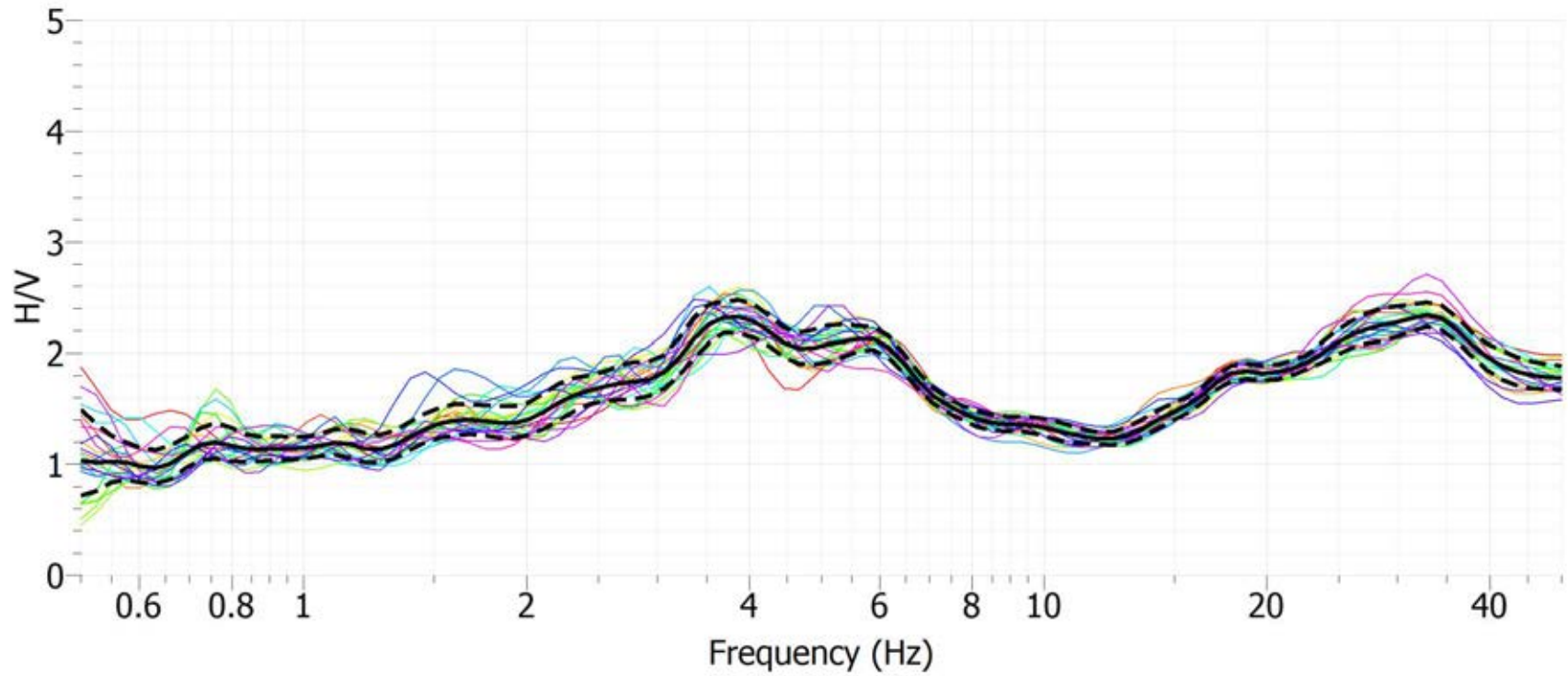


Looking northwest at nested triangle Array 1



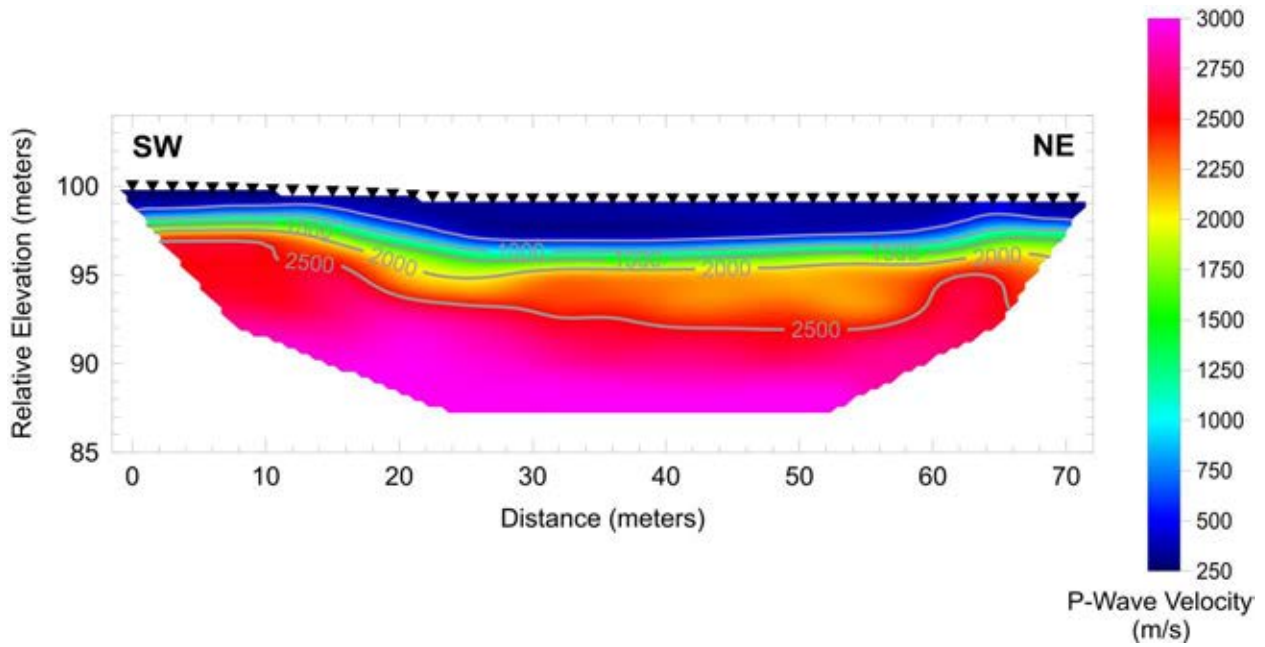
Looking southeast along MASW Array 2

Figure 3 Site CE.47377 Photographs

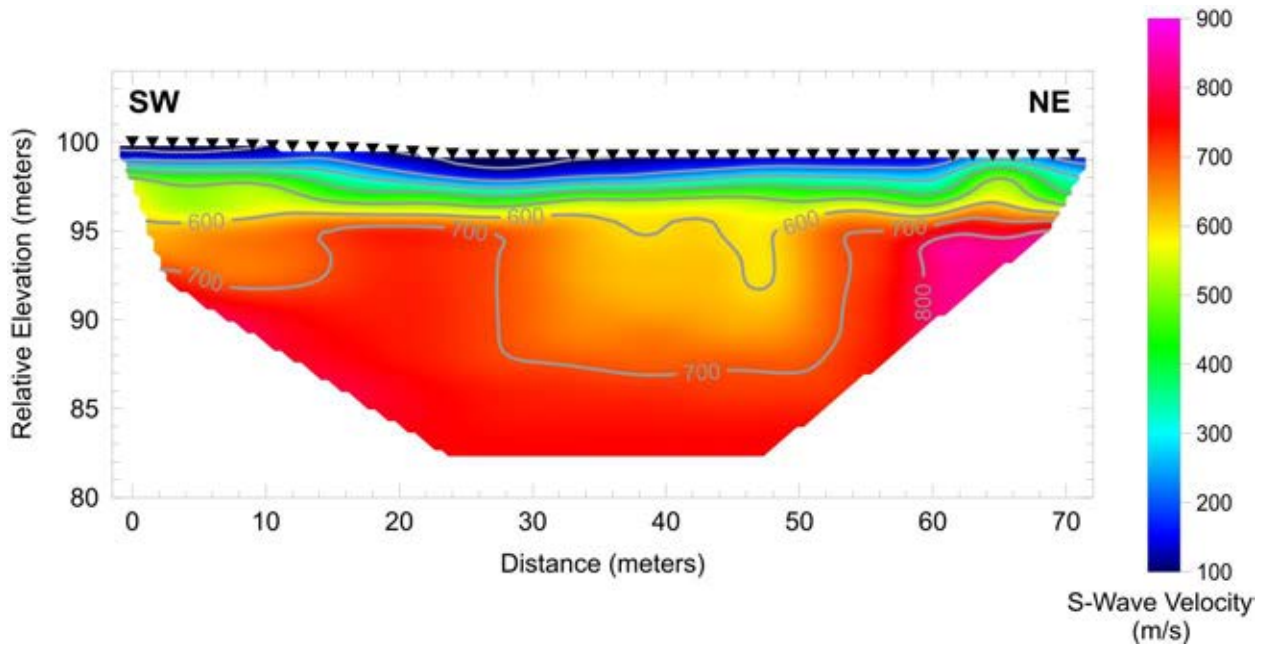


Site CE.47377, HVSR Location 1, Nanometrics Trillium Compact Sensor

Figure 4 H/V Spectral Ratio of Ambient Vibration Data, Site CE.47377



Array 2 – P-wave tomographic seismic refraction model developed using a layer-based starting model



Array 2 – S-wave tomographic seismic refraction model developed using a layer-based starting model

Figure 5 P- and S-wave Seismic Refraction Models, Site CE.47377

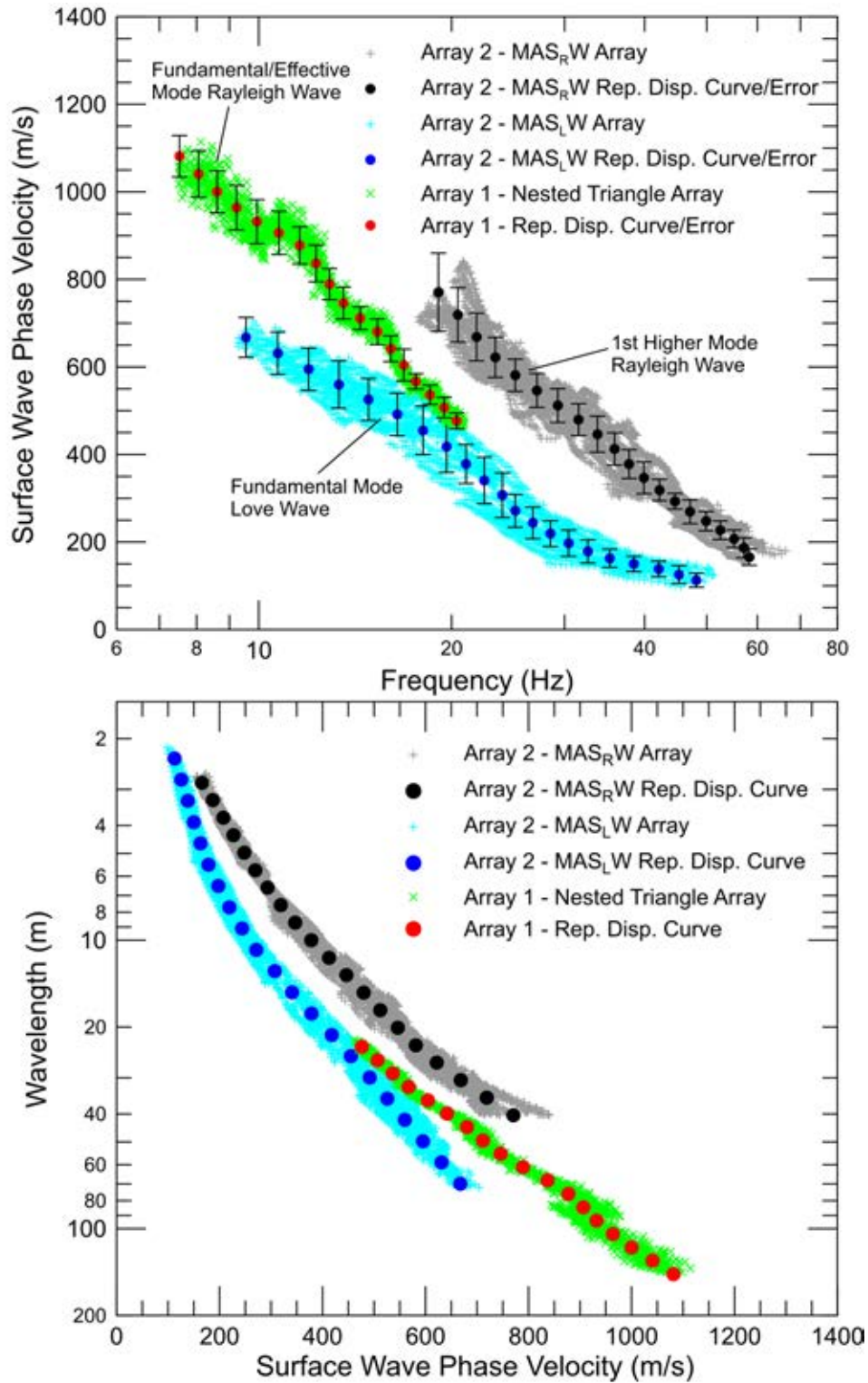


Figure 6 CE.47377 – Rayleigh and Love wave dispersion curves derived from active- and passive-source surface wave data

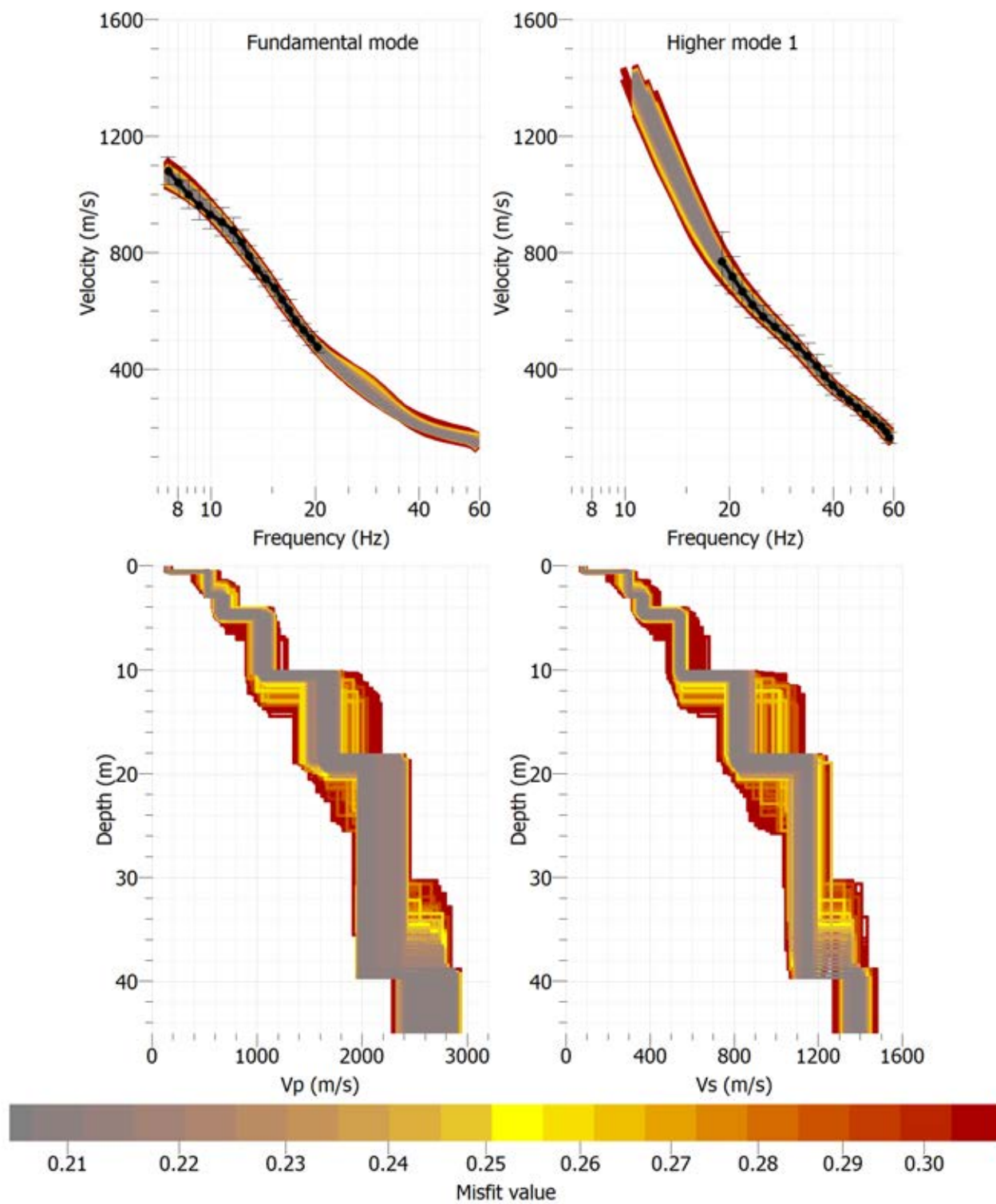


Figure 7 CE.47377 – Ensemble of V_s models resulting from global inversion of fundamental and first higher mode Rayleigh wave

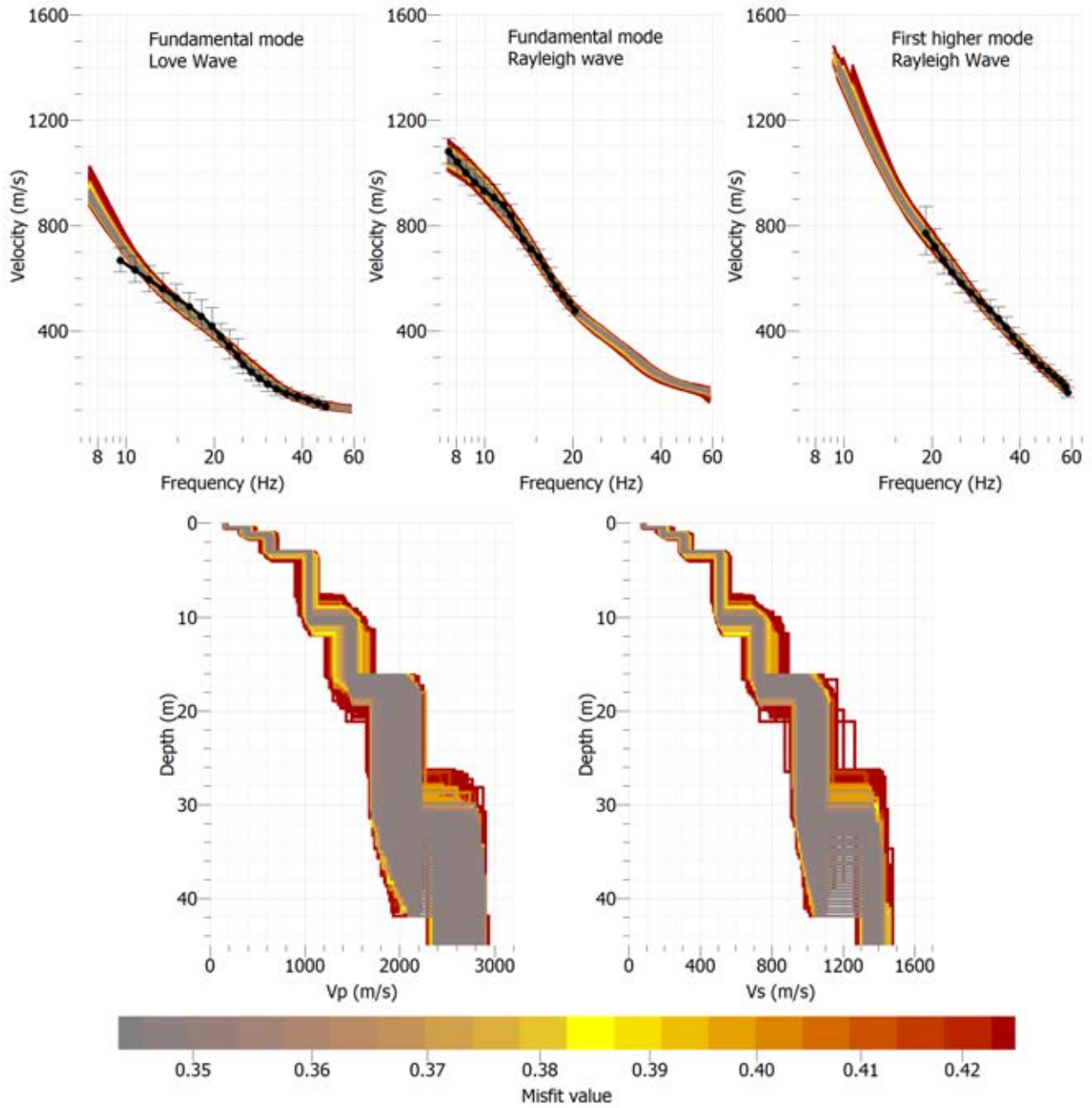


Figure 8 CE.47377 – Ensemble of V_s models resulting from joint global inversion of fundamental mode Love wave and fundamental and first higher mode Rayleigh wave

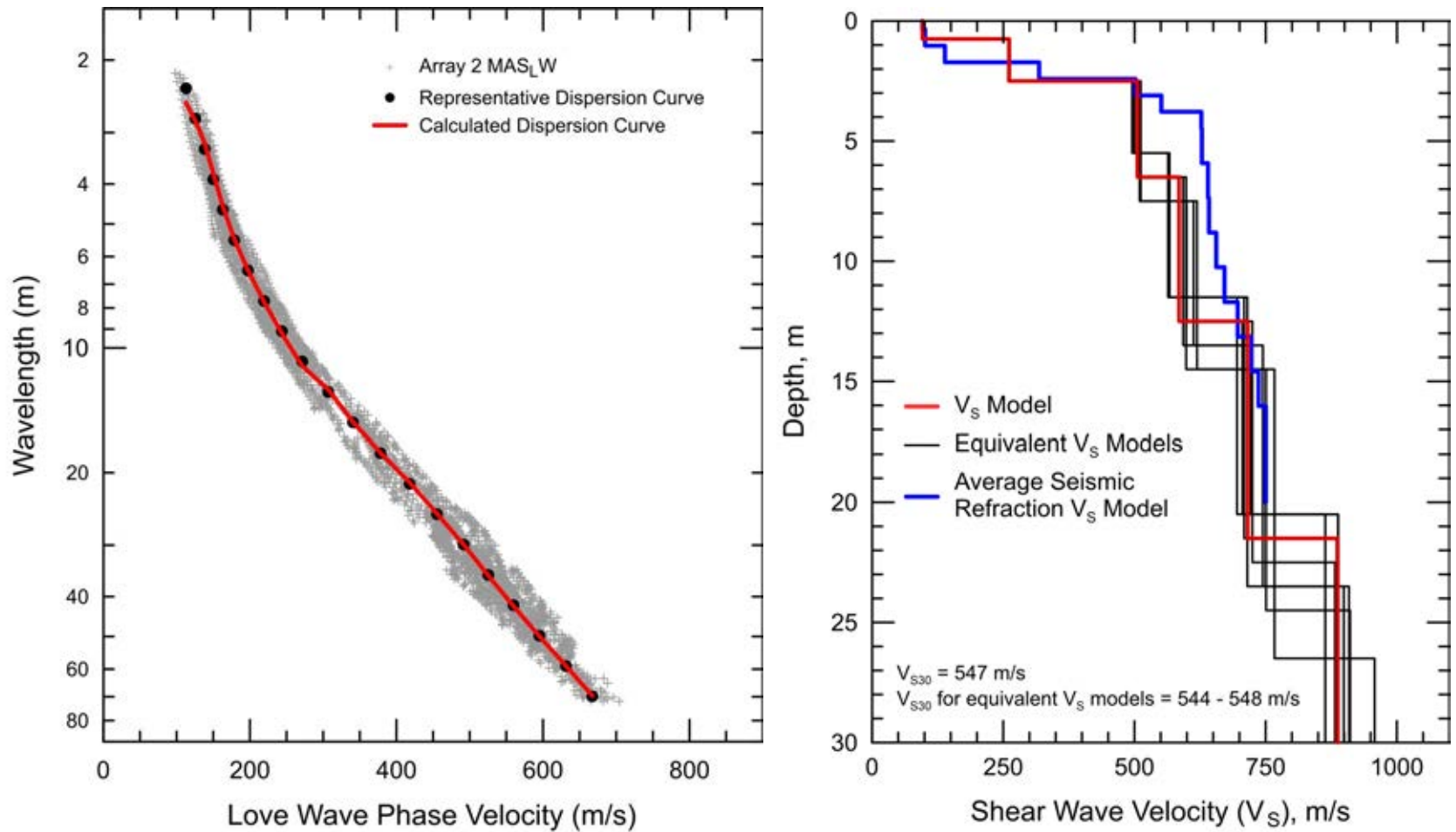


Figure 9 CE.47377 - Field, representative and calculated Love wave dispersion data (left) and associated V_S models (right)

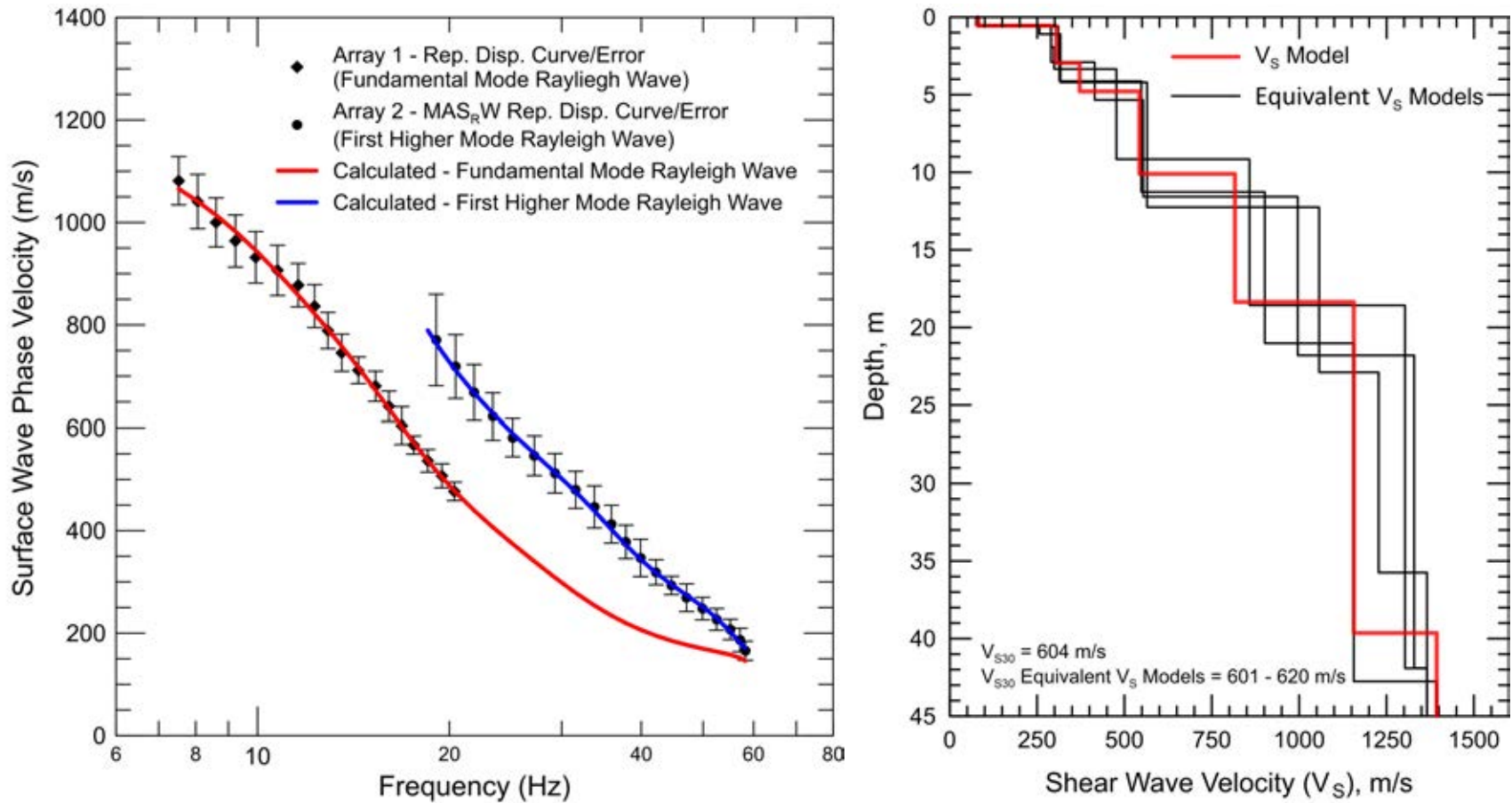


Figure 10 CE.47377 - Field, representative and calculated Rayleigh wave dispersion data (left) and associated V_s models (right) resulting from inversion of Rayleigh wave fundamental and first higher modes

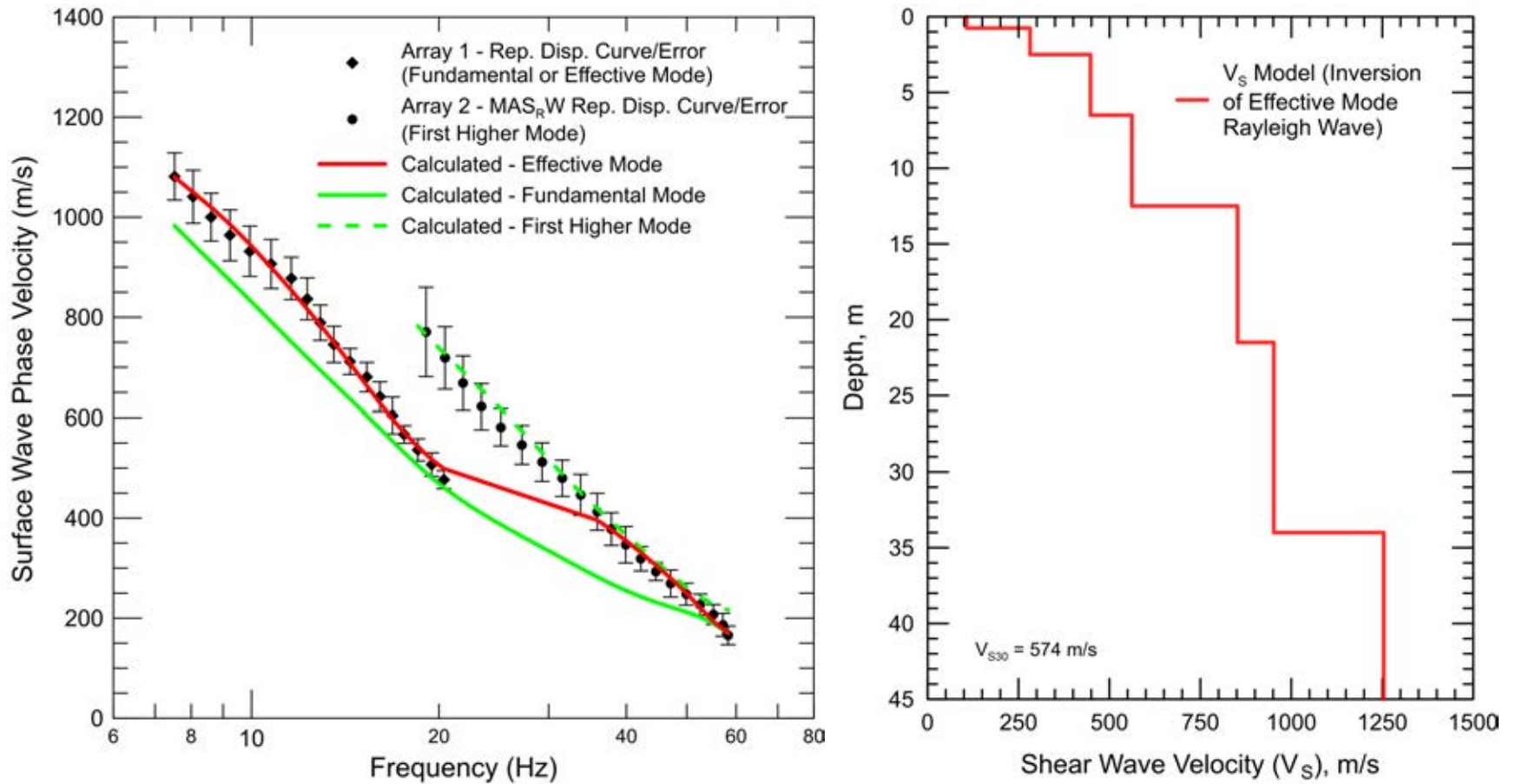


Figure 11 CE.47377 - Field, representative and calculated Rayleigh wave dispersion data (left) and associated V_s model (right) resulting from effective mode inversion of Rayleigh wave dispersion data

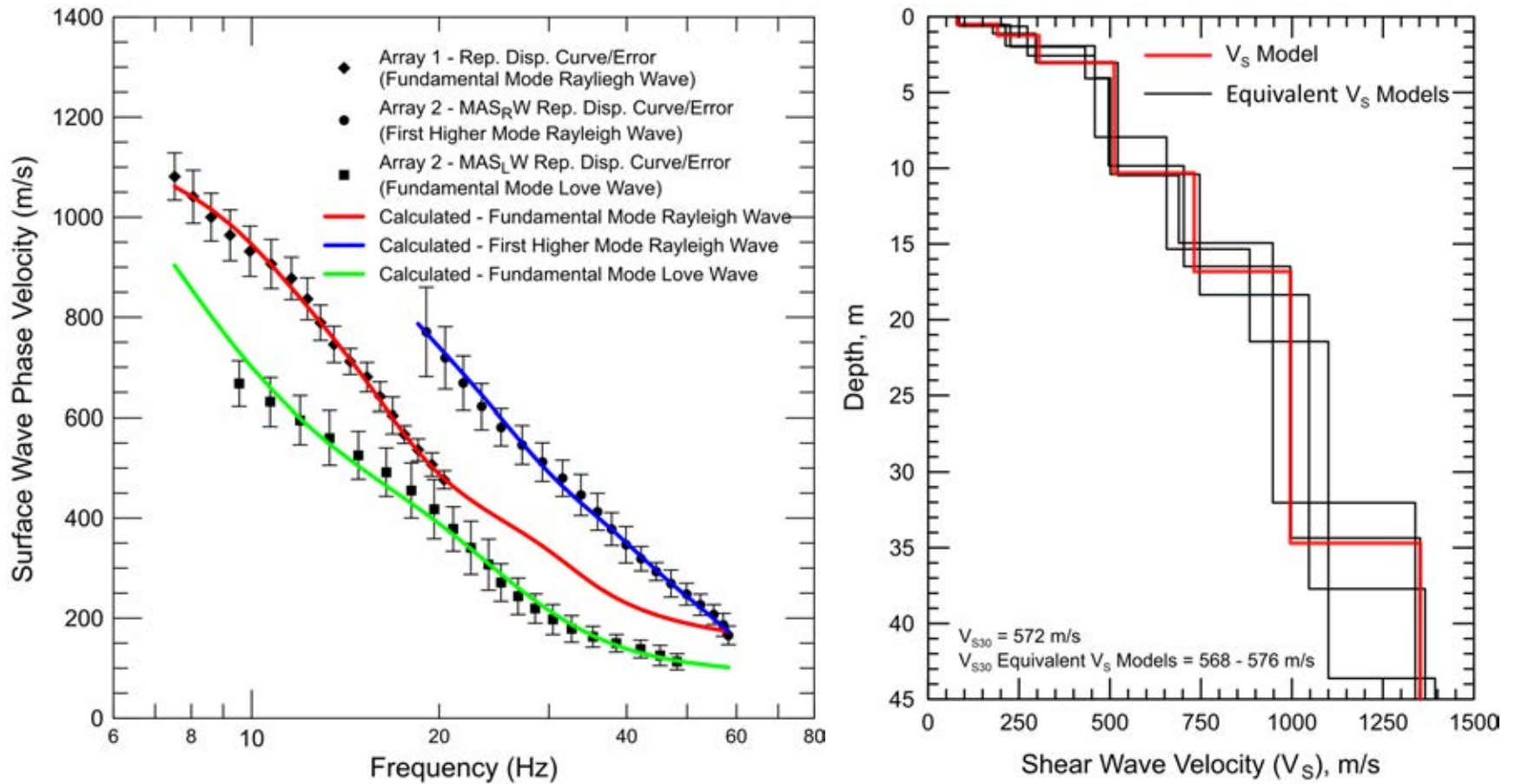


Figure 12 CE.47377 - Field, representative and calculated Rayleigh wave dispersion data (left) and associated V_s model (right) resulting from joint inversion of Love and Rayleigh wave dispersion data

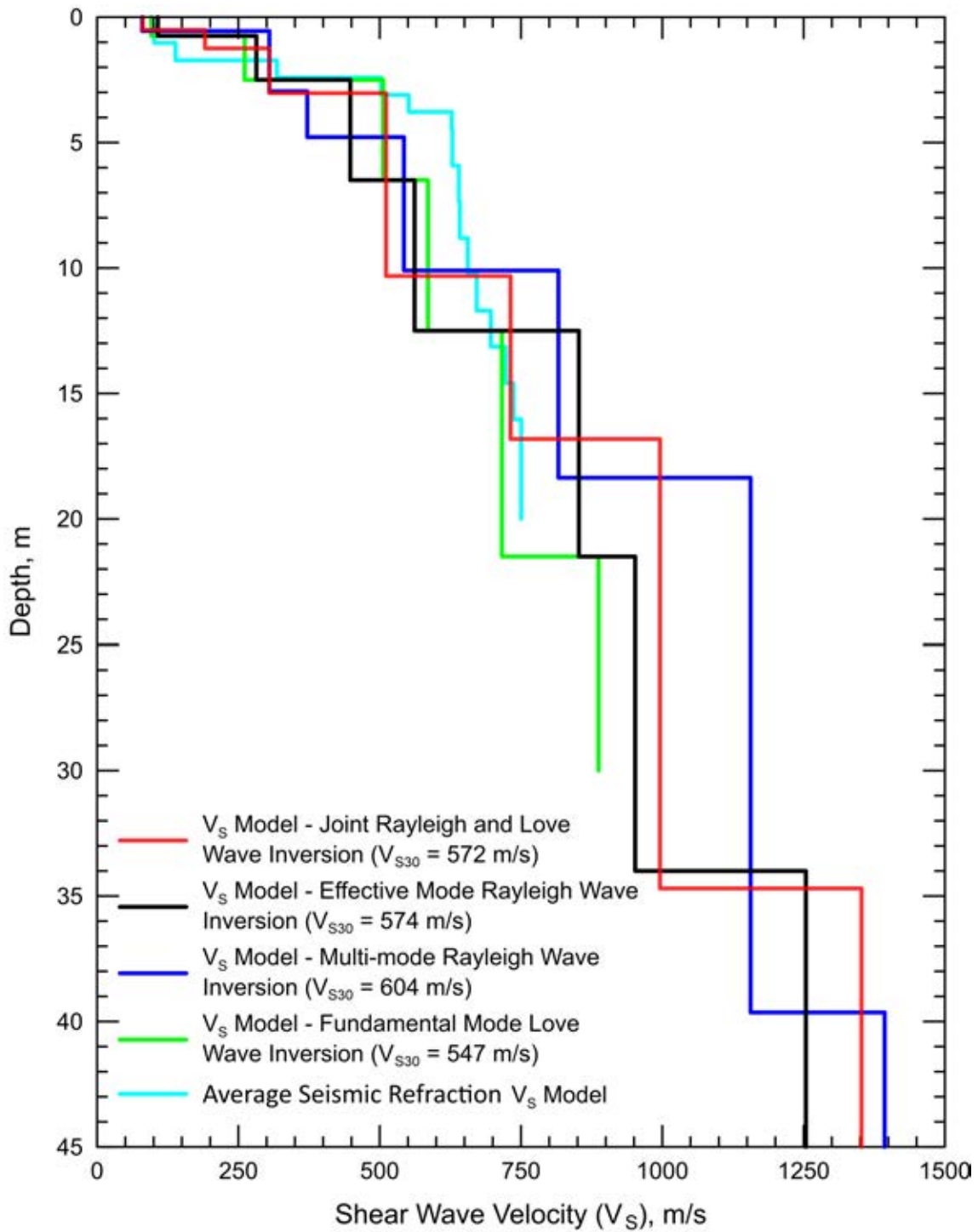


Figure 13 CE.47377 – Summary of V_s Models

Report

Geophysical Site Characterization

SMIP Station CE.47404

Station Name: Monterey – Hawthorne & Lighthouse

Location: New Monterey Fire Station #12, 582 Hawthorne St., Monterey, CA

Latitude: 36.6129

Longitude: -121.9019

V_{s30}: 825 m/s

Estimated Error in V_{s30}: ± 80 m/s

NEHRP Site Class: B

Geomatrix Code: AGA

HVSR Peak Frequency: 26.5 Hz

Site Geology: Site located in area mapped as Mesozoic granitic rock (Figure 2). Outcrop of Miocene Los Laureles Sandstone about 100 m to west. Field inspection indicates that thin layer of residual soil overlies rock.

Site Conditions: Suburban site with traffic/pedestrian noise from nearby roads. Sloping terrain in site vicinity.

Geophysical Methods Utilized: MAS_RW, array microtremor, HVSR

Geophysical Testing Arrays:

1. Array 1: 37 channel, nested triangle array utilizing 4.5 Hz vertical geophones with 4.5m sensor spacing and a 36 m maximum length of outer side of array (Figure 1).
2. Array 2: 48 channel MAS_RW array utilizing 4.5 Hz vertical geophones spaced 1 m apart for a length of 47 m, forward and reverse shot locations with multiple source offsets (1 m to 5 m at both ends of array) and multiple interior source locations (Figure 1). Energy sources consisted of a 4-lb hammer and 12-lb sledgehammer.
3. Array 3: 48 channel “L” shaped array utilizing 4.5 Hz vertical geophones spaced 3 m apart used to acquire passive surface wave data. The SE-NW and SW-NE linear segments of array have lengths of 69 and 72 m, respectively (Figure 1).
4. Two HVSR measurement locations; one in the vicinity of the center of Array 1 and the other near the fire station (Figure 1).

Table 1 Location of Geophysical Testing Arrays

Location	Latitude	Longitude
Array 1 Passive, Center of Array	36.61408	-121.90298
Array 1 Passive, Corner of Array	36.61400	-121.90277
Array 1 Passive, Corner of Array	36.61427	-121.90300
Array 1 Passive, Corner of Array	36.61397	-121.90318
Array 2 MASW, Northwest End of Array	36.61431	-121.90317
Array 2 MASW, Southeast End of Array	36.61396	-121.90286
Array 3 Passive, Northwest End of Array	36.61372	-121.90300
Array 3 Passive, Corner of Array	36.61320	-121.90255
Array 3 Passive, Southeast End of Array	36.61356	-121.90189
Seismic Station	36.6129	-121.9019
HVSR Location 1	36.61409	-121.90303
HVSR Location 2	36.61301	-121.90220

Notes: 1) WGS84 Coordinate System (decimal degrees)

S-Wave Velocity Model:

Table 2 V_s Model

Depth to Top of Layer (m)	Layer Thickness (m)	S-Wave Velocity (m/s)	Inferred P-Wave Velocity (m/s)	Assumed Poisson's Ratio	Assumed Density (g/cm ³)
0	0.5	111	207	0.300	1.70
0.5	1	269	503	0.300	1.90
1.5	3.5	566	1059	0.300	2.10
5	5	742	1387	0.300	2.20
10	10	1195	2236	0.300	2.30
20	>10	1459	2730	0.300	2.40

Notes: 1) Depth of investigation is about 30 m.
2) Bottom layer is a half space.

Observations/Discussion:

H/V Spectral Ratio

HVSR data was collected at two locations (Figure 1 and Table 1). Over 60 min of ambient vibration data were acquired at the HVSR Location 1 using a Nanometrics Trillium Compact seismograph (Trillium). A total of 30 min of ambient vibration data were acquired at the HVSR Location 2 using a MOHO Tromino ENGR (Tromino). HVSR peak frequency is about 28.5 and

26.5 Hz at Location 1 and 2, respectively (Figure 4). Such a high frequency HVSZ peak indicates that a sharp impedance contrast (e.g. bedrock) is located at very shallow depth.

Array Microtremor Data

Noise conditions at the site (multi-directional noise sources) appeared sufficient for successful application of passive surface wave techniques. The site is located on the side of a hill and we decided that the best location to acquire passive surface wave data was in a small parking lot about 150 m northwest of the seismic station. A small nested triangle array (Array 1) was utilized in the parking lot because of restricted space. A total of 50 minutes (100, 30 second seismic records) of ambient vibration data were acquired into Array 1. The ESAC technique was used to extract surface wave dispersion data from the ambient vibration data. To better characterize error, dispersion curves were generated from approximate 12.5-minute time segments of the ambient vibration data and also from the complete data set. The minimum and maximum Rayleigh wavelength extracted from Array 1 are about 18 and 71 m, respectively. Passive-source surface wave data was also acquired closer to the site using an L-shaped array (Array 3). This array failed to yield useable Rayleigh wave dispersion data, likely as a result of variable soil thickness overlying rock.

MASW Data

MASW data acquisition was conducted using a 47-m long receiver array (Array 2) as there was not sufficient space in the parking lot for a longer array. Rayleigh wave dispersion data were interpreted from 14 MAS_RW seismic records collected at 11 different source locations using 4-lb hammer and 12-lb sledgehammer energy sources. Maximum source offset was 5 m at both ends of the array. Review of MAS_RW seismic records indicated that the first higher mode Rayleigh wave was dominant over a wide frequency range. It was only possible to extract fundamental mode Rayleigh wave data at very high frequencies (wavelengths less than about 9 m). Using the 14 seismic records and variable receiver offset ranges, over 75 dispersion curves were extracted and combined for analysis. To minimize near field effects, the maximum Rayleigh wavelength data extracted from the MAS_RW data set was set equal to 1.3 times the distance between the source and midpoint of the active receiver array after inspection of the data. There is about 30 to 80 m/s of scatter in MAS_RW dispersion data, which is indicative of significant lateral velocity variability beneath the array. Fundamental mode Rayleigh wave data was extracted over the 1.5 to 9 m wavelength range and first higher mode Rayleigh wave data was extracted over the 5 to 35 m wavelength range.

Inspection of seismic refraction first arrival data indicates that weathered bedrock with P-wave velocity of over 2,000 m/s is located at a depth of about 2 m, or less.

Modeling

Rayleigh wave dispersion data from active and passive surface wave data sets are in excellent agreement over the approximate 18 to 35 m overlapping wavelength range (Figure 5). However, the dispersion data over this wavelength range appears to be first higher mode.

A representative dispersion curve was generated for each surface wave data set using a moving average, polynomial curve fitting routine. These individual representative dispersion curves were combined and a composite representative dispersion curve generated for the combined data set

for modeling. Error bars for the representative dispersion curve were estimated based on the scatter in the dispersion data. Figure 5 presents the active- and passive-source Rayleigh wave dispersion data and the associated representative dispersion curves. There is significant scatter in the dispersion data due to lateral velocity variability. The first higher mode Rayleigh wave appears to be dominant over a wide frequency/wavelength range (Figure 5).

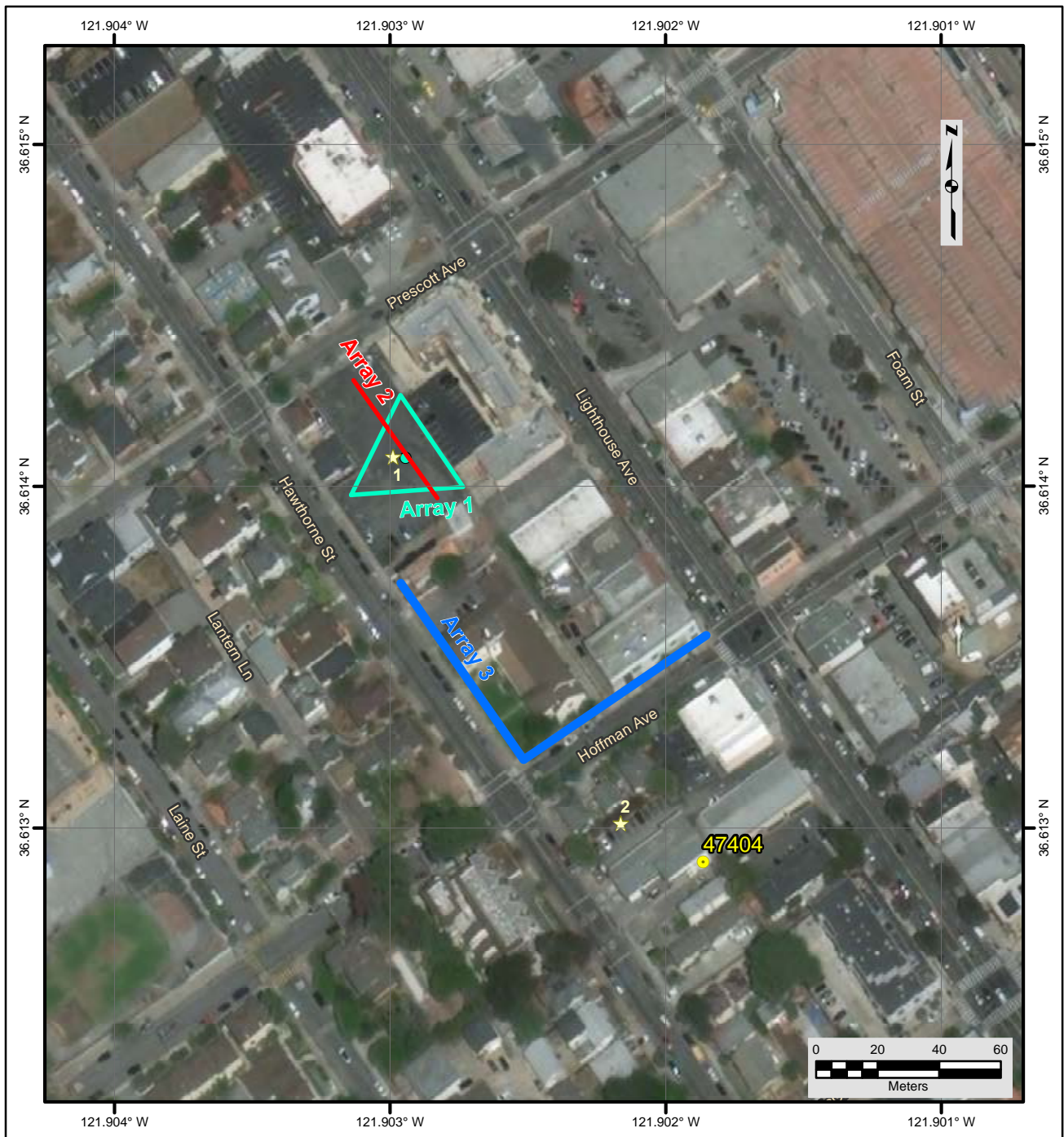
V_S models were derived by multi-mode inversion of the fundamental and first higher mode Rayleigh wave representative dispersion curves. Global search inversion routines utilizing the genetic and neighborhood algorithms were utilized to develop the V_S models. Realistic estimates of Poisson's ratio and density were used to make models as accurate as possible. Model layer thicknesses generally increased with depth to reflect the reduction in model resolution with depth. Depending upon software package utilized a single V_S model with user-defined layer thickness or ensemble of V_S models with variable layer depths were generated. Multiple model parameterizations with different layer depth and velocity search ranges were utilized to more thoroughly search the model space and better characterize non-uniqueness. Figure 6 presents an ensemble of V_S models resulting from global inversion using the Geopsy software package for one model parameterization. Generally, all V_S models presented in this example fit within the defined error for the observed dispersion data and can be considered valid.

Results

A V_S model resulting from multi-mode inversion of the Rayleigh wave dispersion data is presented in Figure 7 and Table 2. Several equivalent V_S models are also shown in Figure 7. These models are the best fitting models from global inversion using different model parameterizations. The low S-wave velocity at the surface is likely associated with residual soil. Weathered rock is encountered at a depth of about 1.5 m, which is consistent with seismic refraction observations. Surface wave depth of investigation is about 30 m based on $\lambda_{\max}/2$ to $\lambda_{\max}/2.5$.

V_{S30} is 825 m/s (NEHRP Site Class B) for the V_S models selected for site characterization. V_{S30} for the equivalent V_S models presented in Figure 7 ranges from 813 to 833 m/s (NEHRP Site Class B). The estimated error in V_{S30} , which includes expected lateral velocity variability beneath the testing arrays, is about 80 m/s. This is computed based on the sum of the following rounded to the nearest 5 m/s: an estimated error of 3% from the realistic assumed layer Poisson's ratios in the model, 1% error from the realistic assumed layer densities in the model, 2% for the variation in V_{S30} associated with non-uniqueness, and 4% to account for the scatter in the dispersion data.

If the structure housing the seismic station is founded on weathered rock then the averaged S-wave velocity between 1.5 and 31.5 m, which is 1,028 m/s, might better represent V_{S30} beneath the seismic station.



File Name: 18045_47404
Date: 5/29/2018

Legend

- CSMIP Station and Number
- ★ H/V Spectral Ratio Measurement Location
- MASW Array
- Passive Surface Wave Array
- ▭ Passive Surface Wave Triangle Array

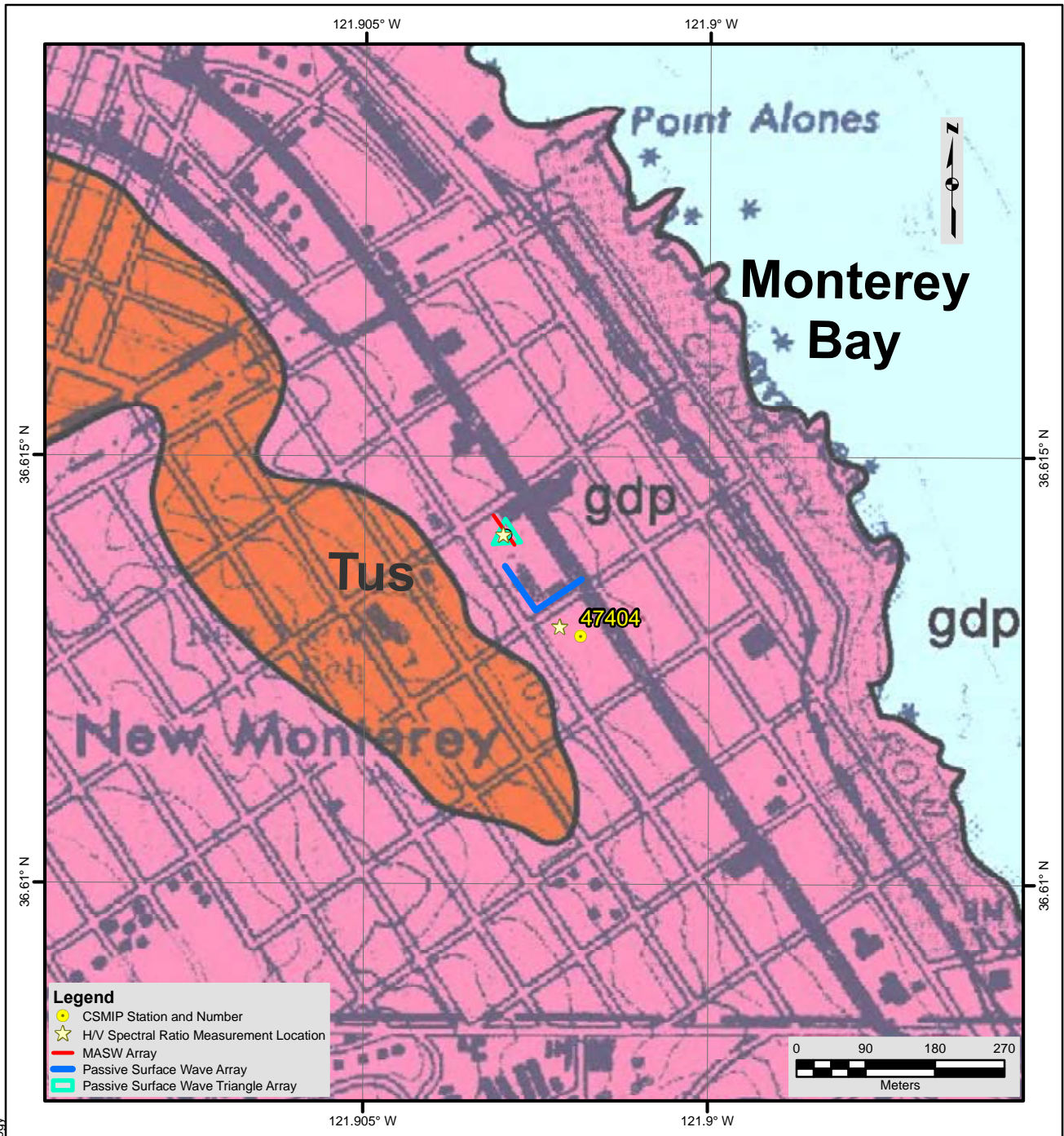
NOTES:

1. WGS 1984 Coordinate System
2. Image Source: Esri, DigitalGlobe, GeoEye, Earthstar Geographics, CNES/Airbus DS, USDA, USGS, AEX, Getmapping, Aerogrid, IGN, IGP, swisstopo, and the GIS User Community



**FIGURE 1
SITE MAP
CE • 47404**





Description of Geologic Map Units

Tus = Tertiary (Miocene) marine sandstone - Los Laureles Sandstone of Bowen, 1965
 gdp = Mesozoic granitic rocks of Salinian basement

NOTES:

1. WGS 1984 Coordinate System
2. Geologic Map of the Monterey and Seaside Quadrangles, Monterey County, California by Thomas W Dibblee, Jr., 2007

File Name: 18045_47404-Geology

Date: 5/29/2018



**FIGURE 2
 GEOLOGIC MAP
 CE • 47404**



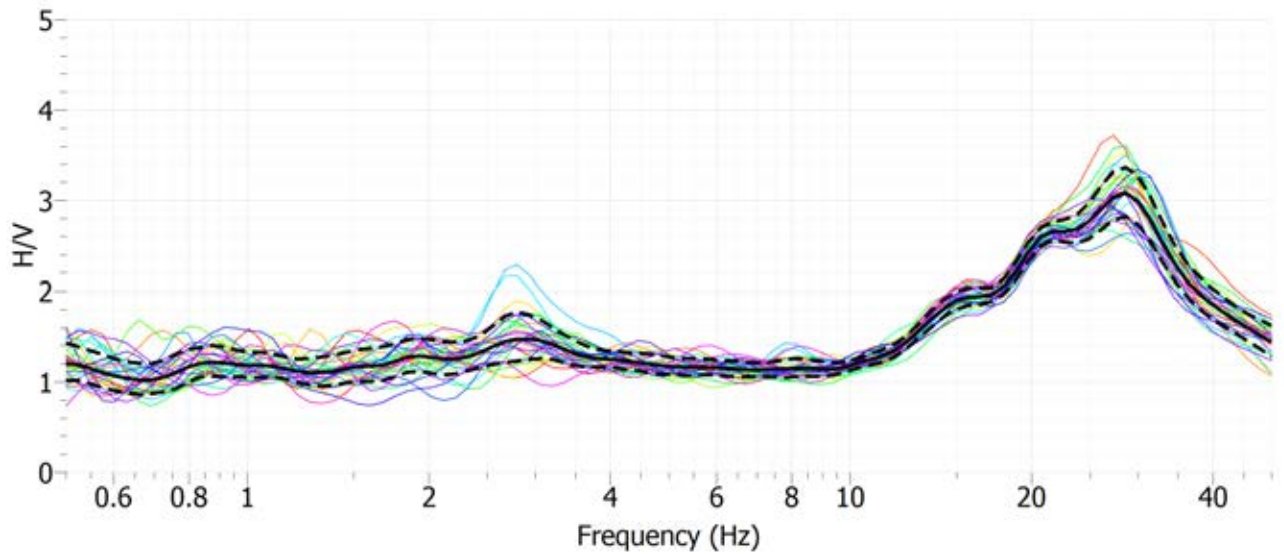


Looking northwest towards fire station housing seismic station and HVSr measurement location 2

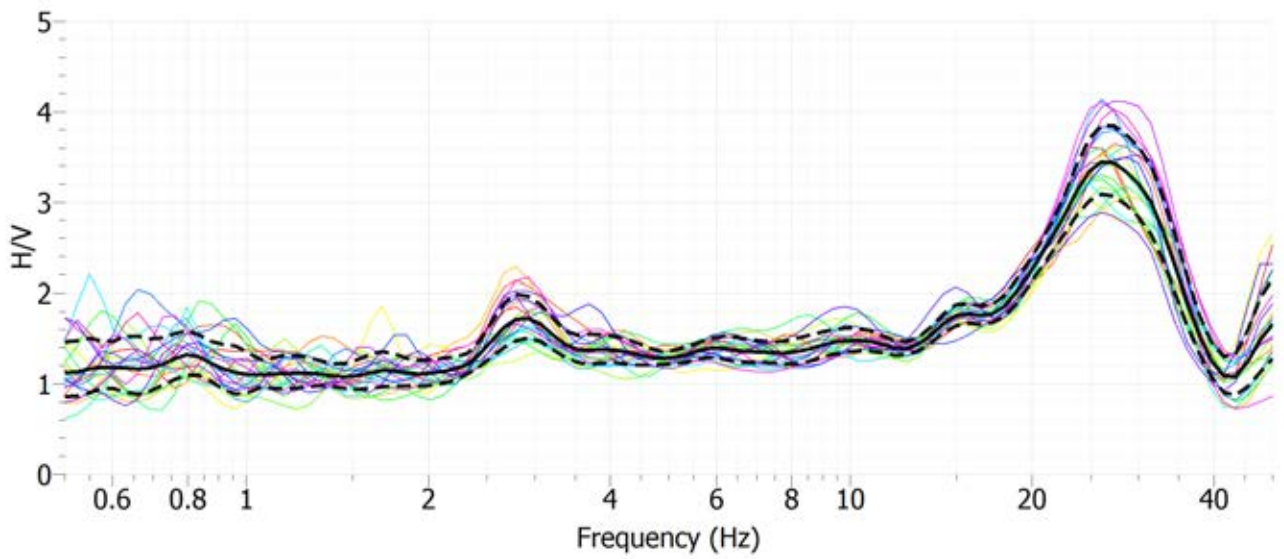


Looking northwest along MASW Array 2

Figure 3 Site CE.47404 Photographs



Site CE.47404, HVSr Location 1, Nanometrics Trillium Compact Sensor



Site CE.47404, HVSr Location 2, MOHO Tromino ENGR Sensor

Figure 4 H/V Spectral Ratio of Ambient Vibration Data – Measurement Locations 1 and 2, Site CE.47404

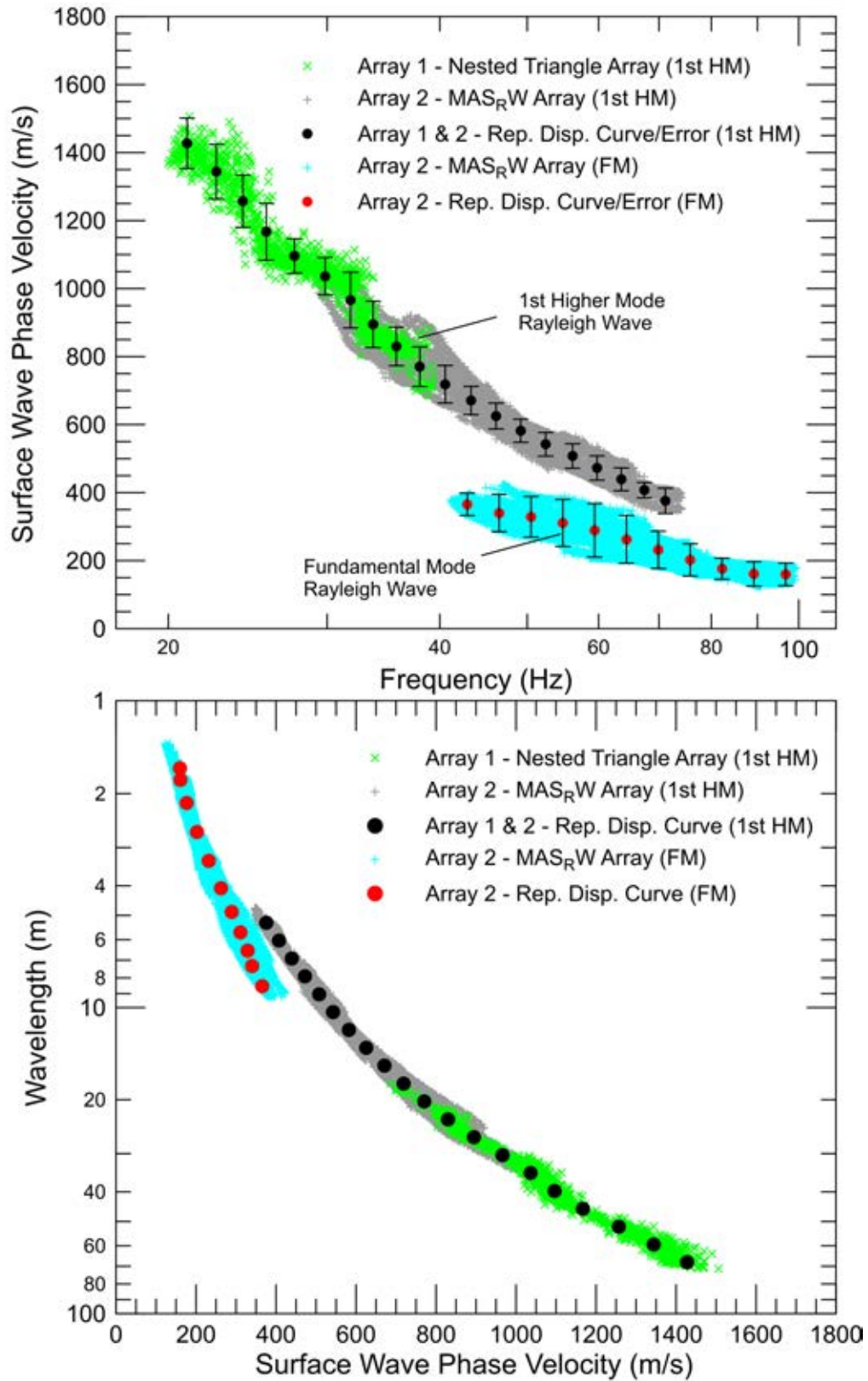


Figure 5 CE.47404 – Rayleigh wave dispersion curves derived from active- and passive-source surface wave data

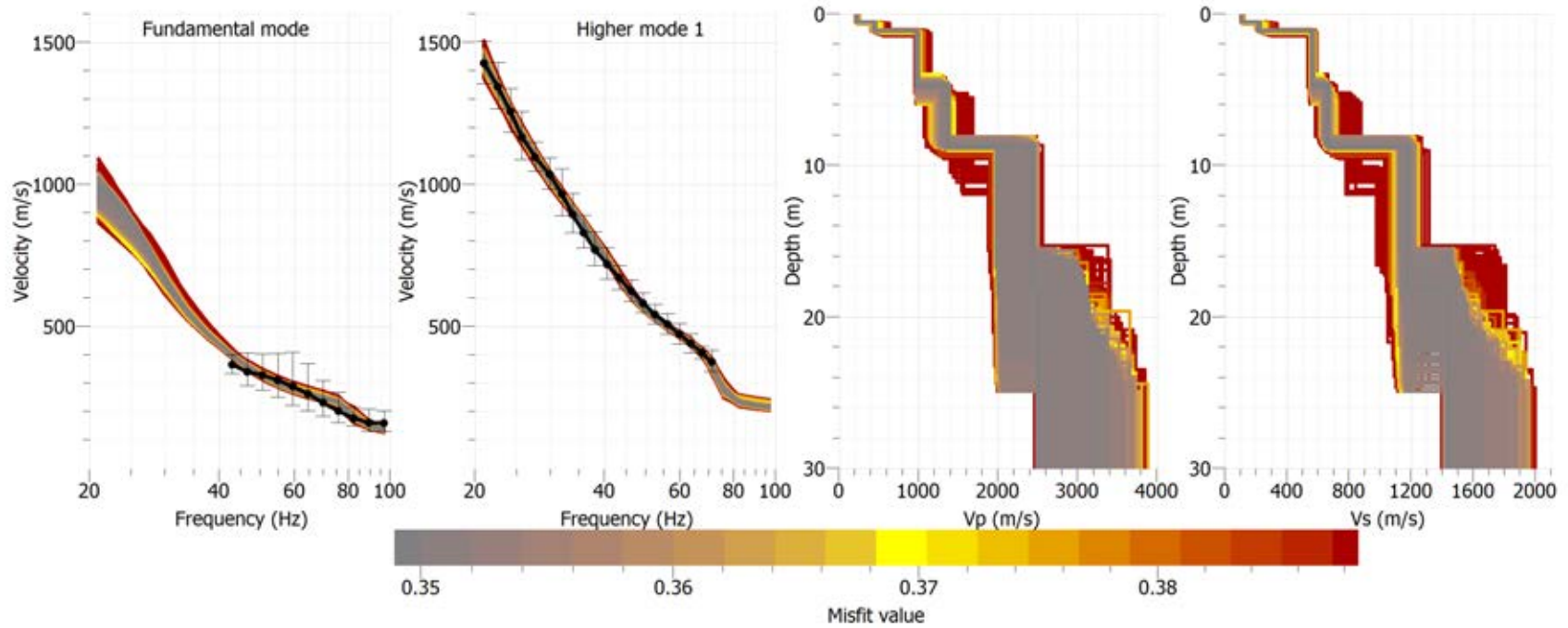


Figure 6 CE.47404 – Ensemble of V_s models resulting from global inversion of fundamental and first higher mode Rayleigh wave

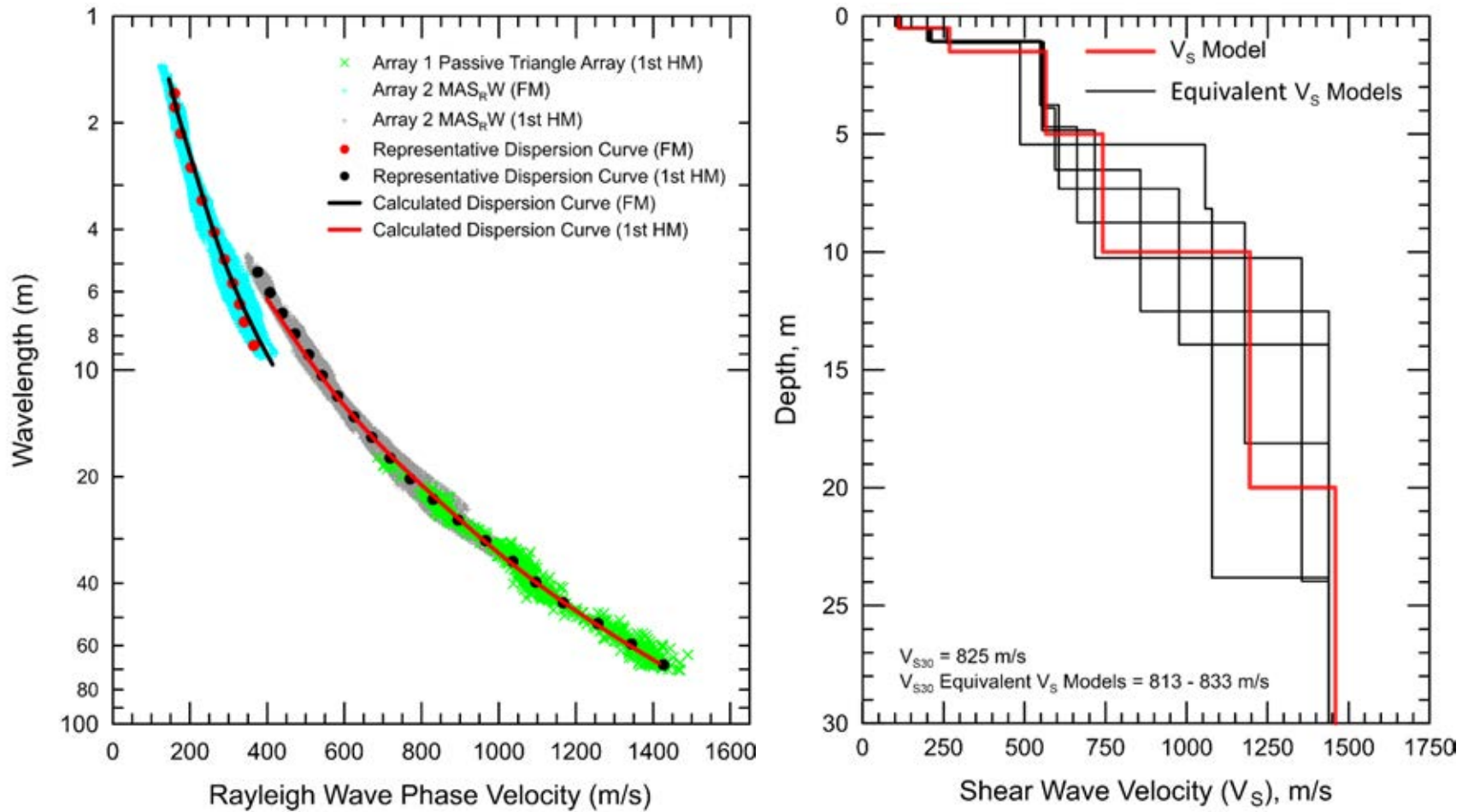


Figure 7 CE.47404 - Field, representative and calculated surface wave dispersion data (left) and associated V_s models (right)

Report Geophysical Site Characterization SMIP Station CE.47405

Station Name: Monterey – Hwy 1 & Dela Vina

Location: Monterey Fire Station #3, 401 Dela Vina Avenue, Monterey, CA

Latitude: 36.5991

Longitude: -121.8615

V_{S30}: 379 m/s

Estimated Error in V_{S30}: ± 25 m/s

NEHRP Site Class: C

Geomatrix Code: AQB/AQD

HVSR Peak Frequency: 1.05 Hz, low amplitude secondary peak at ~5 Hz

Site Geology: Site located near Monterey bay on Pleistocene alluvium; dune and drift sands (Figure 2). Site located less than 1 km from outcrops of Miocene Monterey Formation (shale) and 3 km from Mesozoic crystalline rock.

Site Conditions: Suburban site with traffic noise from nearby streets. Flat terrain in site vicinity. Hwy 1 about 200 m northwest of seismic station.

Geophysical Methods Utilized: MAS_RW, array microtremor, HVSR

Geophysical Testing Arrays:

1. Array 1: 48 channel “L” shaped array utilizing 4.5 Hz vertical geophones spaced 3 m apart used to acquire passive surface wave data (Figure 1). The W-E and S-N linear segments of array have lengths of 72 and 69 m, respectively.
2. Array 2: 48 channel MAS_RW array utilizing 4.5 Hz vertical geophones spaced 1.5 m apart for a length of 70.5 m, forward and reverse shot locations with multiple source offsets (1.5 m at the southern end and 1.5 to 10 m at the northern end) and multiple interior source locations (Figure 1). A 12-lb sledge hammer was used for all interior and off-end source locations and a 4-lb hammer was also used at selected source locations.
3. One HVSR measurement location near fire station (Figure 1).

Table 1 Location of Geophysical Testing Arrays

Location	Latitude	Longitude
Array 1 Passive, Northwest End of Array	36.59975	-121.86246
Array 1 Passive, Corner of Array	36.59930	-121.86189
Array 1 Passive, Northeast End of Array	36.59974	-121.86135
Array 2 MASW, Southwest End of Array	36.59930	-121.86189
Array 2 MASW, Northeast End of Array	36.59975	-121.86134
Seismic Station CE.47405	36.5991	-121.8615
HVSR Location 1	36.59912	-121.86122

Notes: 1) WGS84 Coordinate System (decimal degrees)

S-Wave Velocity Model:

Table 2 V_s Model

Depth to Top of Layer (m)	Layer Thickness (m)	S-Wave Velocity (m/s)	Inferred P-Wave Velocity (m/s)	Assumed Poisson's Ratio	Assumed Density (g/cm ³)
0	2	160	299	0.300	1.80
2	4	294	551	0.300	1.90
6	8	313	1600	0.480	1.90
14	18	583	1700	0.433	2.05
32	>18	695	1800	0.412	2.05

Notes: 1) Depth to saturated zone fixed at about 6-8 m based on seismic refraction data.
 2) Depth of investigation is about 50 m.
 3) Bottom layer is a half space.

Observations/Discussion:

H/V Spectral Ratio

HVSR data was collected for about a 60 minute duration at a single location near the seismic station using a Nanometrics Trillium Compact (Trillium) seismograph. The HVSR data reveals an approximate 1.05 Hz peak, which is expected to be associated with a geologic structure(s) at significantly greater depth than the expected depth of investigation of the surface wave sounding (Figure 4). There is also a possible weak secondary HVSR peak at a frequency of about 5 Hz.

Array Microtremor Data

Noise conditions at the site (multi-directional noise sources) appeared sufficient for successful application of passive surface wave techniques. A total of 45 minutes (90, 30 second seismic records) of ambient vibration data were acquired into L-shaped Array 1. The legs of the L-shaped array were only 69 and 72 m long to minimize the number of driveways that the seismic cable crossed. The ESAC technique was used to extract surface wave dispersion data from the

ambient vibration data. To better characterize error, dispersion curves were generated from approximate 11 minute time segments of the ambient vibration data and also from the complete data set. Rayleigh wave phase velocity data were very noisy at wavelengths greater than 100 m due to either geologic or ambient vibration conditions and, therefore, no attempt was made to extract dispersion data at wavelengths greater than 100 m. Based on the nature of the Rayleigh wave dispersion data at long wavelengths the possibility cannot be discounted that velocity inversions occur below 50 m depth. Additionally, Tertiary sediments expected at these depths are expected to have variable dips based on mapped outcrops in the site vicinity (Figure 2), which could result in significant lateral velocity variability. The minimum and maximum Rayleigh wavelength extracted from Array 1 are about 8 and 100 m, respectively, and there is about 50 m/s scatter in dispersion data at wavelengths greater than 60 m. The linear legs of the L-shaped array did not yield useful dispersion data.

MASW Data

MASW data acquisition was conducted using a 70.5-m long receiver array (Array 2) as shown on Figure 1. Rayleigh wave dispersion data were interpreted from 11 MAS_RW seismic records collected at 9 different source locations using 4-lb hammer and 12-lb sledgehammer energy sources. The maximum source offset was only 1.5 m at the southwest end of the array due to a road and 10 m at the northeast end of the array. Using the 11 seismic records and variable receiver offset ranges, over 75 dispersion curves were extracted and combined for analysis. To minimize near field effects, the maximum Rayleigh wavelength data extracted from the MAS_RW data set was set equal to the lesser of one times the distance between the source and midpoint of the active receiver array or 40 m. There is nominally about 20 to 30 m/s of scatter in MAS_RW dispersion data, which is likely in part due to lateral velocity variation. The minimum Rayleigh wavelength phase velocity data extracted from a 48-channel MAS_RW receiver gather was in the 7 to 10.5 m range. Reducing data from smaller hammer sources using a limited offset range receiver gather (i.e. less active geophones) allowed for extraction of surface wave dispersion data to a minimum wavelength of about 4.5 m.

Modeling

Surface wave dispersion data from active and passive surface wave data sets are in good agreement over the approximate 8 to 40 m overlapping wavelength range (Figure 5). The average phase velocity of a 40-m wavelength Rayleigh wave (V_{R40}) is 391 m/s with a coefficient of variation (COV) of 0.5 % from ESAC analysis of the ambient vibration data collected along Array 1. Representative dispersion curves were generated for each surface wave data set using a moving average, polynomial curve fitting routine. These individual representative dispersion curves were combined and a composite representative dispersion curve generated for the combined data set for modeling. Error bars for the composite representative dispersion curve were estimated based on the scatter in the dispersion data.

The composite representative dispersion curve was inverted using an iterative non-linear least squares inversion routine and fundamental mode Rayleigh wave assumption to derive V_s models. Realistic estimates of Poisson's ratio and density were used to make models as accurate as possible. High Poisson's ratio, saturated sediments were constrained at a depth of about 6 to 8 m with $V_p > 1,600$ m/s based on interactive, layer-based analysis of seismic refraction first arrival data. Poisson's ratio of the saturated sediments was set to gradually decrease with depth

as the sediments became stiffer, a common observation in borehole velocity logs. Model layer thicknesses increased with depth to reflect the reduction in model resolution with depth. Several V_S models were developed with almost identical calculated dispersion curves to demonstrate the non-uniqueness inherent in the inversion of surface wave dispersion data; especially at layer boundaries where an abrupt change in seismic velocity occurs or associated with high velocity layers or velocity inversions.

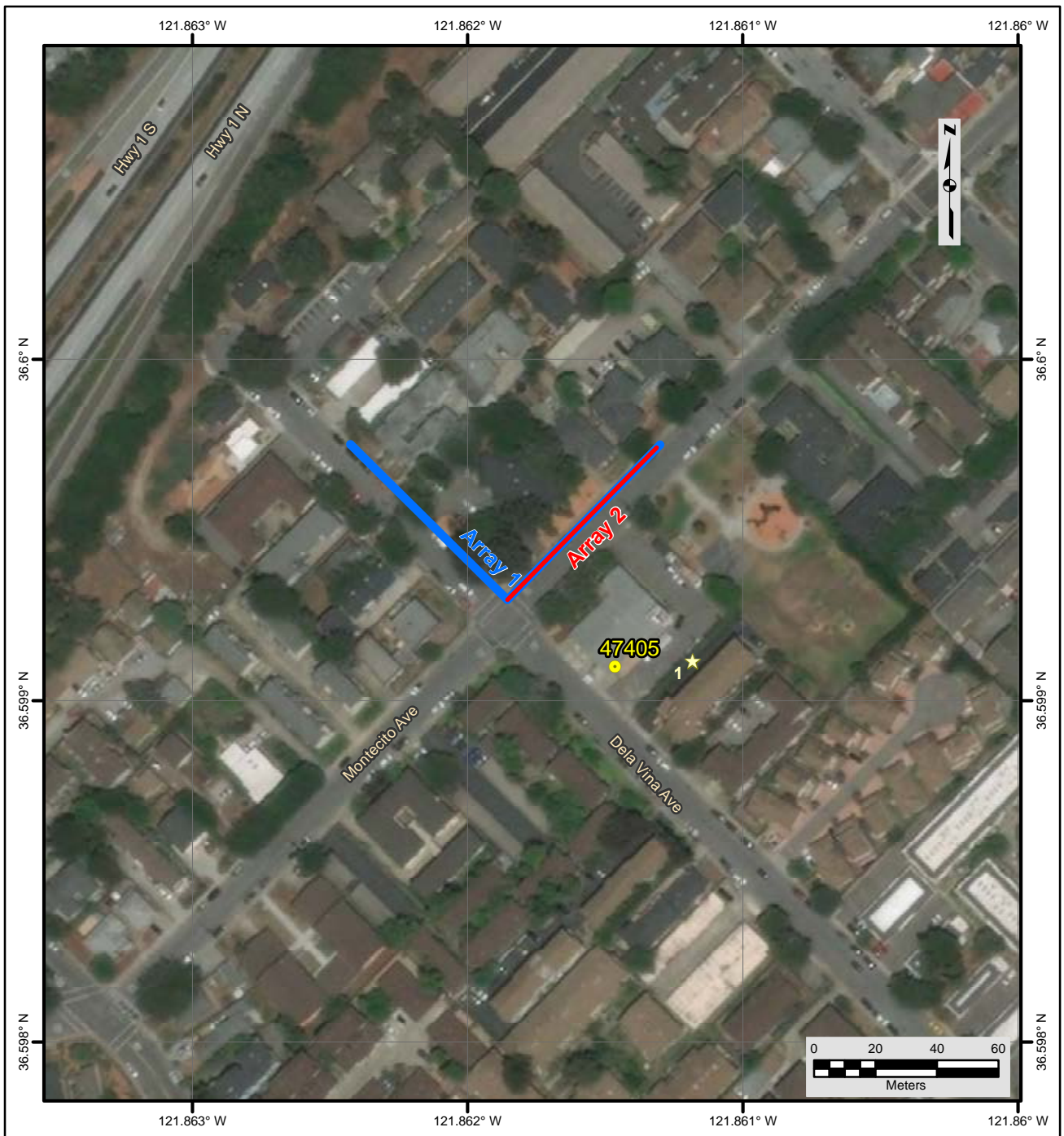
Results

V_S models are presented as Figure 6 and the V_S model selected for purpose of site characterization is presented in Table 2. V_S exceeds 500 m/s at about a depth of about 14 m which is likely the top of the Miocene Monterey Formation. Surface wave depth of investigation is about 50 m based on $\lambda_{\max}/2.5$.

V_{S30} is 379 m/s (NEHRP Site Class C). The average V_S of the upper 50 m (V_{S50}) is 461 m/s. V_{S30} is between 379 and 382 m/s for the equivalent V_S models. The estimated error in V_{S30} , which includes some effects of the lateral velocity variability beneath the testing arrays, is about 25 m/s. This is computed based on the sum of the following rounded to the nearest 5 m/s: an estimated error of 3% from the realistic assumed layer Poisson's ratios in the model, 1% error from the realistic assumed layer densities in the model, 2% for the variation in V_{S30} associated with non-uniqueness, and the 0.5 % COV in V_{R40} from the passive-source surface wave dispersion data.

Theoretical HVSR, based on the diffuse field assumption, was computed for selected V_S models using the software package *HV-Inv* Release 2.3 and reveals that the V_S models support the presence of the 5 Hz secondary peak. The 1.05 Hz primary HVSR peak is associated with deeper geologic structure, possibly crystalline basement rocks at a depth on the order of 150 m.

Interestingly, V_{S30} estimated from V_{R40} using the Brown et al., 2000 relationship ($V_{S30} \cong 1.045V_{R40}$, assuming V_{R40} represents the fundamental mode Rayleigh wave) is 409 m/s, about 8% higher than that estimated from the V_S model. In our experience, $V_{S30} \cong V_{R40}$ for sites with a shallow saturated zone, which would result in an estimated $V_{S30} = 391$ m/s, 3% higher than that estimated from the V_S model. Note that V_S models should always be used to estimate V_{S30} when possible and we are only documenting the performance of V_{S30} estimates based on V_{R40} in the event such an approach is needed in the future.



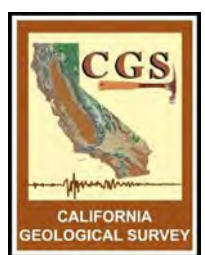
File Name: 18045_47405
Date: 5/29/2018

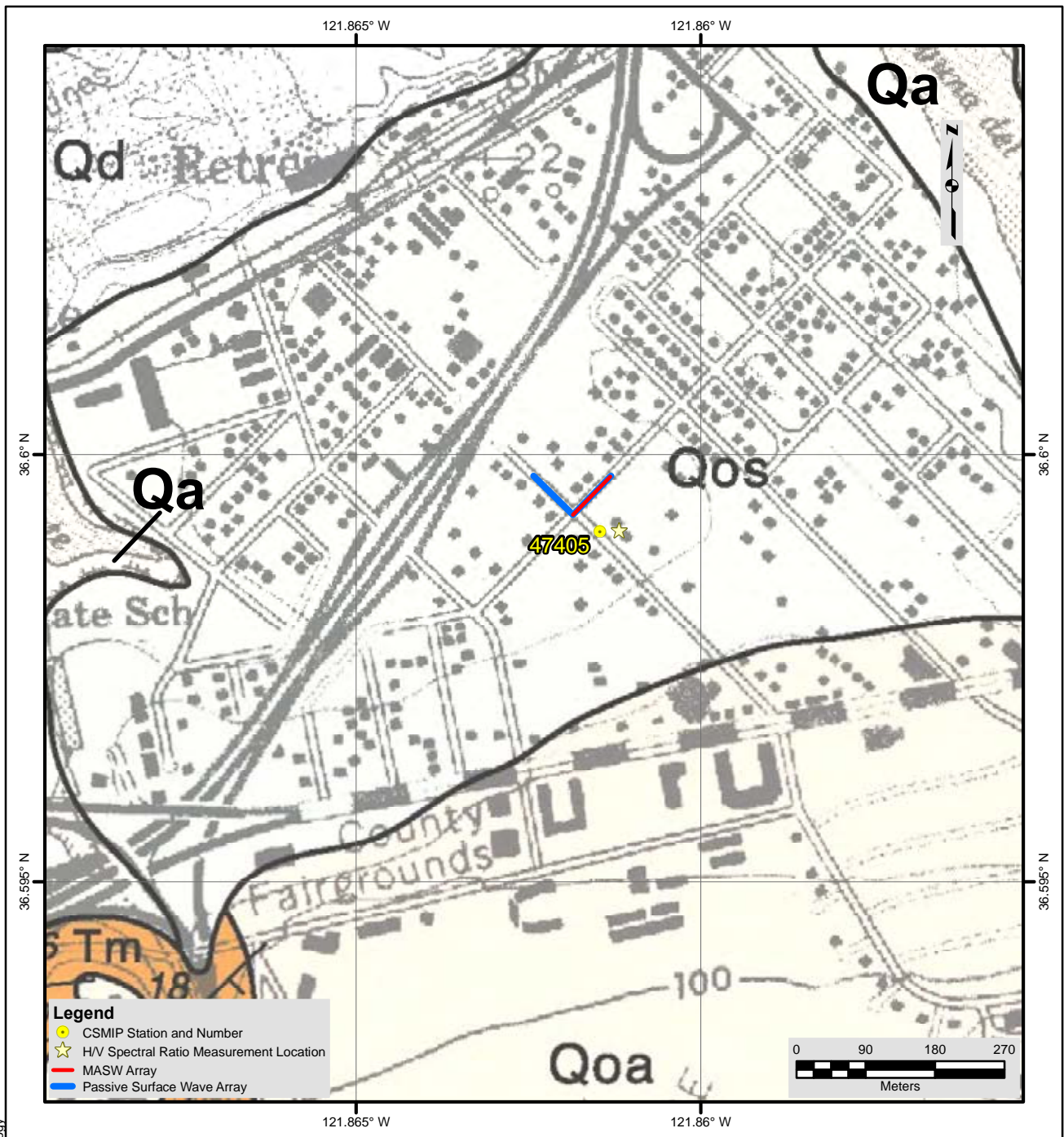
- Legend**
- CSMIP Station and Number
 - ★ H/V Spectral Ratio Measurement Location
 - MASW Array
 - Passive Surface Wave Array

- NOTES:**
1. WGS 1984 Coordinate System
 2. Image Source: Esri, DigitalGlobe, GeoEye, Earthstar Geographics, CNES/Airbus DS, USDA, USGS, AEX, Getmapping, Aerogrid, IGN, IGP, swisstopo, and the GIS User Community



**FIGURE 1
SITE MAP
CE • 47405**





Description of Geologic Map Units

Qa = Quaternary (Holocene) Alluvial gravel, sand, and silt/clay of valley areas and flood plains
 Qd = Quaternary (Holocene) Loose dune sand and drift sand
 Qoa = Quaternary (Holocene to Pleistocene) Dissected older alluvium
 Qos = Quaternary (Holocene to Pleistocene) Older stabilized dune and drift sand
 Tm = Tertiary (Miocene) Monterey Formation, Mohnian Stage, upper Miocene

NOTES:

1. WGS 1984 Coordinate System
2. Geologic Map of the Monterey and Seaside Quadrangles, Monterey County, California by Thomas W Dibblee, Jr., 2007

File Name: 18045_47405-Geology

Date: 5/29/2018



**FIGURE 2
 GEOLOGIC MAP
 CE • 47405**





Looking northwest towards fire station housing seismic station and HVSR measurement location



Looking east towards fire station, corner of L-shaped Array 1, and southeast end of MASW Array 2

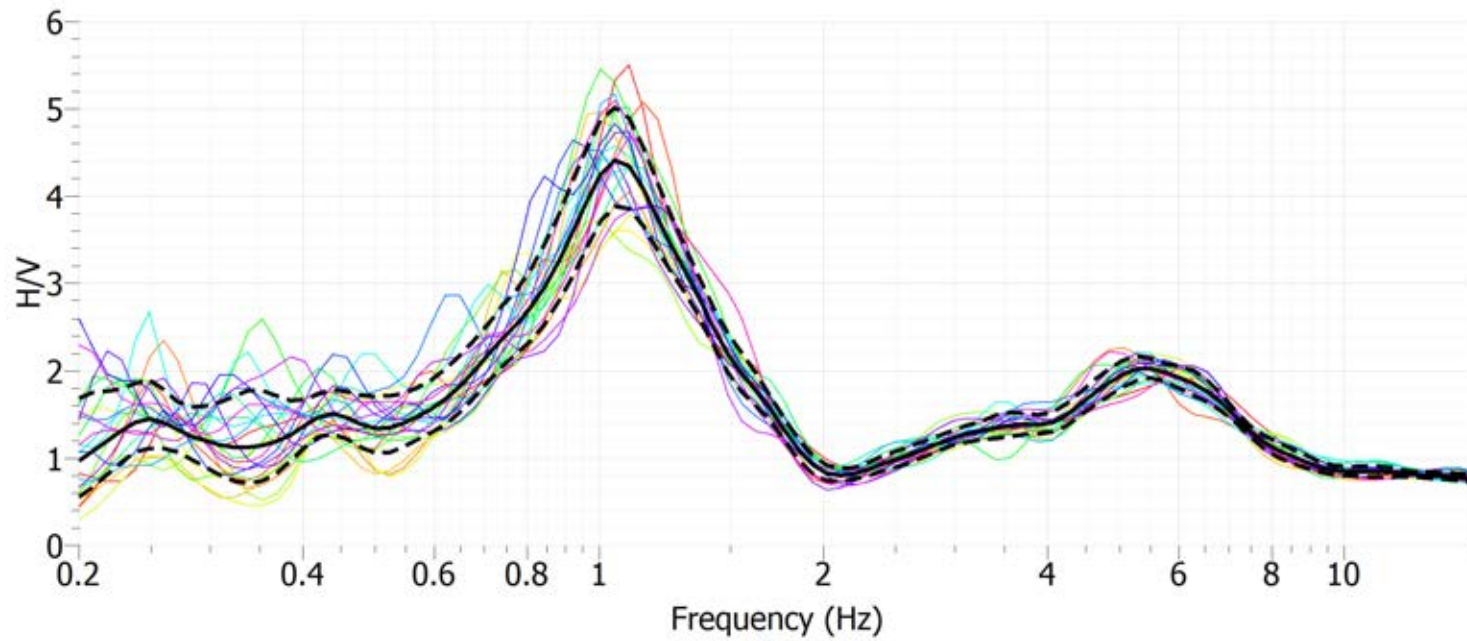


Looking southeast at center of MASW Array 2 and fire station housing seismic station



Looking northeast along leg of L-shaped Array 1

Figure 3 Site CE.47405 Photographs



Site CE.47405, HVSr Location 1, Nanometrics Trillium Compact Sensor

Figure 4 H/V Spectral Ratio of Ambient Vibration Data, Site CE.47405

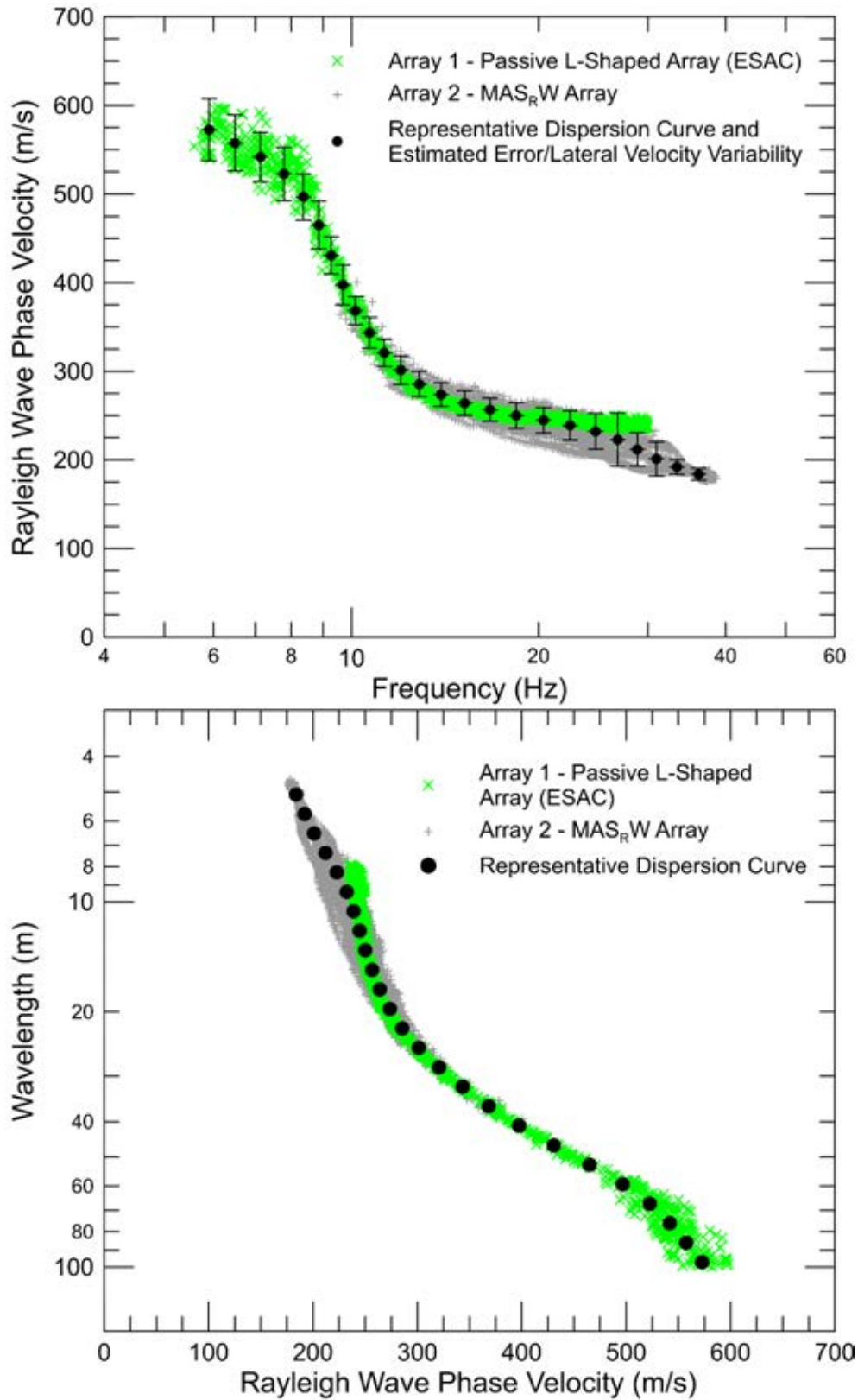


Figure 5 CE.47405 – Rayleigh wave dispersion curves derived from active- and passive-source surface wave data

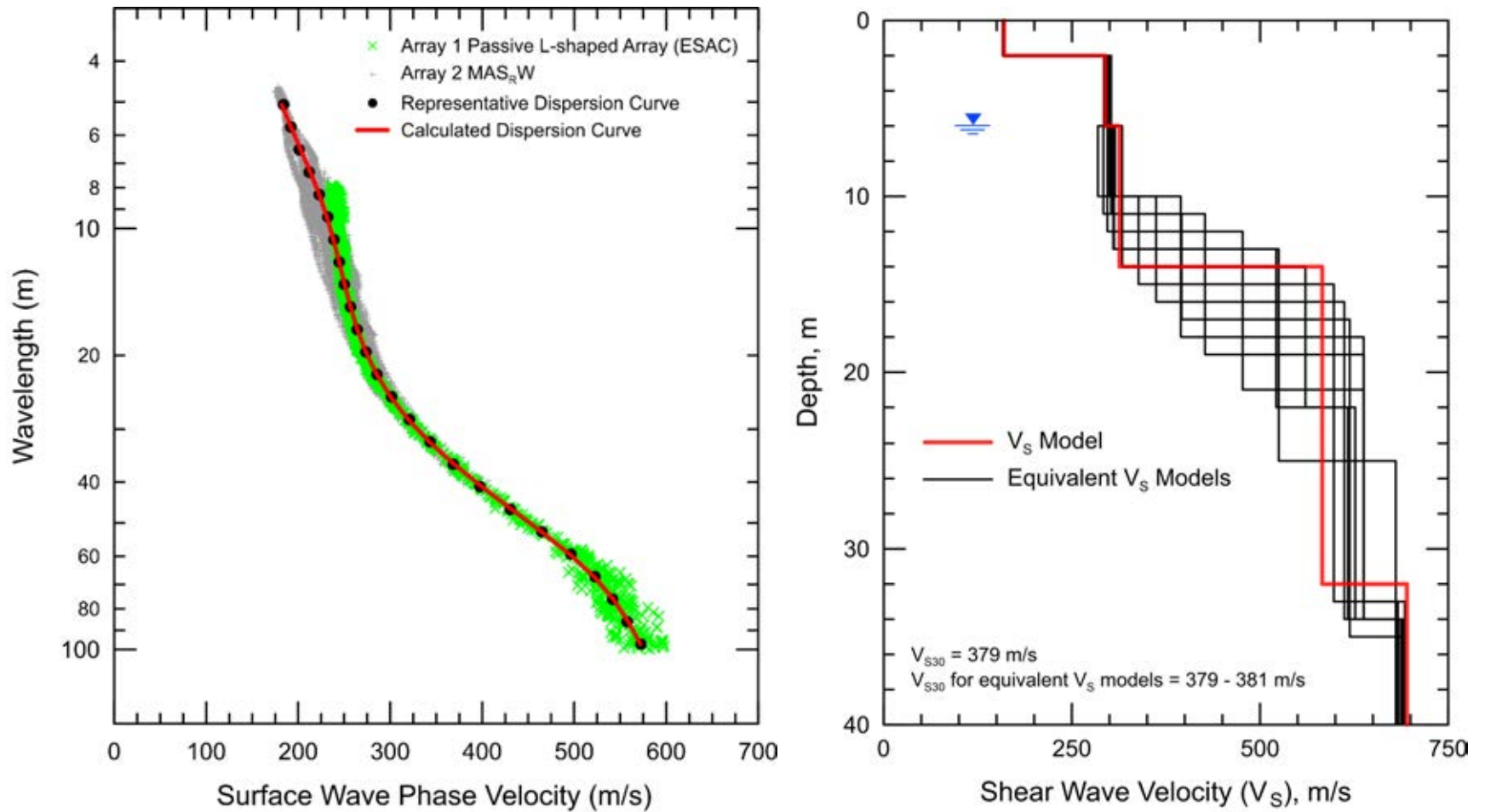


Figure 6 CE.47405 - Field, representative and calculated surface wave dispersion data (left) and associated V_S models (right)

Report

Geophysical Site Characterization

SMIP Station CE.47524

Station Name: Hollister - South and Pine

Location: Glorietta Warehouse, 711 Sally Street, Hollister, CA

Latitude: 36.8483

Longitude: -121.3973

V_{s30}: 228 m/s

Estimated Error in V_{s30}: ± 20 m/s

NEHRP Site Class: D

Geomatrix Code: IHD

HVSR Peak Frequency: ~0.2 Hz

Site Geology: Station located on Quaternary (Holocene) alluvium (Figure 2). A trace of the Calaveras fault zone is located about 225 m west of the seismic station. The nearest outcrops of Tertiary sediments and crystalline bedrock are about 1 and 5 km from the site, respectively.

Site Conditions: Suburban site with moderate traffic noise from nearby roads. Flat terrain in site vicinity.

Geophysical Methods Utilized: MAS_RW, array microtremor, HVSR

Geophysical Testing Arrays:

1. Array 1: 48 channel "L" shaped array (~60 degree angle between legs of array) utilizing 4.5 Hz vertical geophones spaced 5 m apart used to acquire passive surface wave data. The SE-NW and W-E linear segments of array have lengths of 120 and 115 m, respectively (Figure 1).
2. Array 2: 48 channel MAS_RW array utilizing 4.5 Hz vertical geophones spaced 1.5 m apart for a length of 70.5 m (Figure 1), forward and reverse shot locations with multiple source offsets (1.5 m to 30 m off both ends of the array) and multiple interior source locations. A 4-lb hammer and a 12-lb sledgehammer were used at interior and 1.5 m offset source locations and an AWD for the offset source locations.
3. One HVSR location near seismic station (Figure 1).

Table 1 Location of Geophysical Testing Arrays

Location	Latitude	Longitude
Seismic Station CE.47524	36.84830	-121.39730
Array 1 Passive, Northeast End of Array	36.84922	-121.39784
Array 1 Passive, Corner of Array	36.84827	-121.39722
Array 1 Passive, Southwest end of Array	36.84832	-121.39851
Array 2 MASW, Northwest End of Array	36.84907	-121.39775
Array 2 MASW, Southeast End of Array	36.84851	-121.39738
HVSR Location 1	36.84841	-121.39728

Notes: 1) WGS84 Coordinate System (decimal degrees)

S-Wave Velocity Model:

Table 2 V_s Model

Depth to Top of Layer (m)	Layer Thickness (m)	S-Wave Velocity (m/s)	Inferred P-Wave Velocity (m/s)	Assumed Poisson's Ratio	Assumed Density (g/cm^3)
0	1	113	225	0.333	1.60
1	1.5	130	259	0.333	1.65
2.5	2.5	161	322	0.333	1.70
5	5	206	412	0.333	1.80
10	10	252	503	0.333	1.90
20	17	317	634	0.333	1.95
37	>13	467	934	0.333	2.00

Notes: 1) Depth of investigation is about 50 m.
2) Bottom layer is a half space.

Observations/Discussion:

H/V Spectral Ratio

HVSR data were collected for at least a 60 minute duration at a single location near the seismic station using both a Nanometrics Trillium Compact (Trillium) and MOHO Tromino ENGR seismograph. The HVSR data reveals an approximate 0.2 Hz peak, which is expected to be associated with a geologic structure(s) at significantly greater depth than the expected depth of investigation of the surface wave sounding (Figure 4). The 0.2 Hz HVSR peak is more accurately resolved using the Trillium.

Array Microtremor Data

Noise conditions at the site (multi-directional noise sources) appeared sufficient for successful application of passive surface wave techniques. Over 50 minutes (108, 30 second seismic records) of ambient vibration data were acquired into Array 1, an L-shaped array with ~60 degree angle between legs of the array, as shown on Figure 1. The ESAC technique was used to extract surface wave dispersion data from the ambient vibration data. To better characterize error, dispersion curves were generated from 13.5-minute time segments of the ambient vibration data and also from the complete data set. The minimum and maximum Rayleigh wavelength extracted from Array 1 are about 23 and 122 m, respectively. No attempt was made to extract dispersion data from the less robust linear legs of the L-shaped array.

MASW Data

MASW data acquisition was conducted using a 70.5-m long receiver array (Array 2) as shown on Figure 1. Rayleigh wave dispersion data were interpreted from 19 MAS_RW seismic records collected at 15 different source locations using 4-lb hammer, 12-lb sledgehammer, and AWD energy sources. The maximum source offset was either 24.5 or 30 m from each end of the array. Using the 19 seismic records and variable receiver offset ranges, over 90 dispersion curves were extracted and combined for analysis. To minimize near field effects, the maximum Rayleigh wavelength data extracted from the MAS_RW data set was set equal to the lesser of 1.3 times the distance between the source and midpoint of the active receiver array or 65 m (expected limit of capabilities of AWD at this site). There is nominally about 20 m/s of scatter in MAS_RW dispersion data, which is likely in part due to lateral velocity variation. The minimum Rayleigh wavelength phase velocity data extracted from a 48-channel MAS_RW receiver gather was in the 2 to 4.5 m range. Reducing data from smaller hammer sources using a limited offset range receiver gather (i.e. less active geophones) allowed for extraction of surface wave dispersion data to a minimum wavelength of about 1.5 m.

Modeling

Surface wave dispersion data from active and passive surface wave data sets are in good agreement over the approximate 23 to 65 m overlapping wavelength range (Figure 5). The average phase velocity of a 40-m wavelength Rayleigh wave (V_{R40}) is 232 m/s with a coefficient of variation (COV) of 0.3 % from ESAC analysis of the ambient vibration data collected along Array 1. Average V_{R40} is 217 m/s with a coefficient of variation (COV) of 1.6 % from MASW analysis of active-source seismic data collected along Array 2. The combined data set (similar weight given to active-and passive-source data) yields an average V_{R40} of 224 m/s with a coefficient of variation (COV) of 3.6 %. Representative dispersion curves were generated for each surface wave data set using a moving average, polynomial curve fitting routine. These individual representative dispersion curves were combined and a composite representative dispersion curve generated for the combined data set for modeling. Error bars for the composite representative dispersion curve were estimated based on the scatter in the dispersion data.

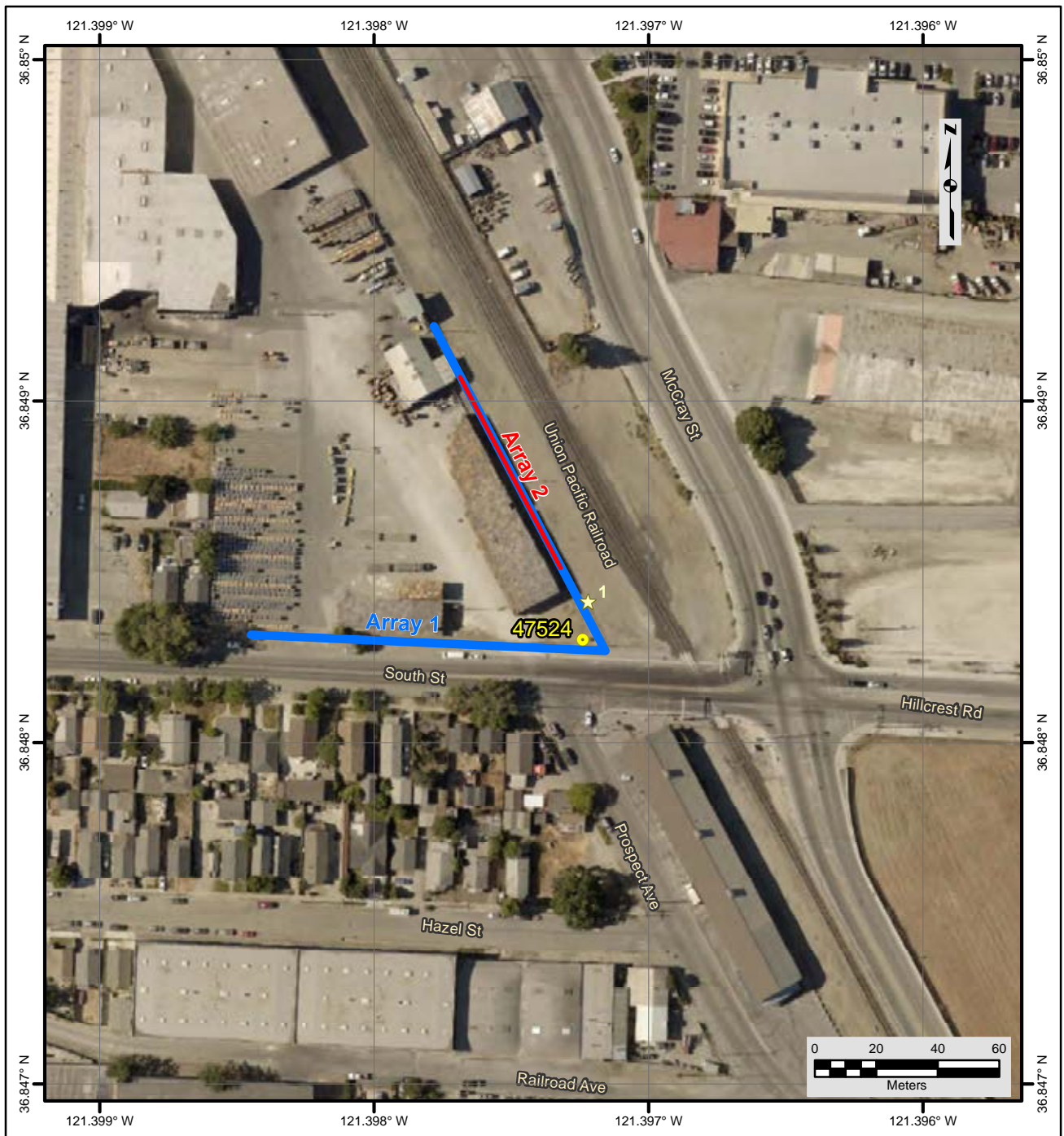
The composite representative dispersion curve was inverted using an iterative non-linear least squares inversion routine and fundamental mode Rayleigh wave assumption to derive V_s models. Realistic estimates of Poisson's ratio and density were used to make models as accurate as possible. There was no evidence of high Poisson's ratio, saturated sediments in the upper 30 to 40 m from either seismic refraction first arrival data or potential water table seismic reflectors.

Model layer thicknesses increased with depth to reflect the reduction in model resolution with depth. Several V_S models were developed with almost identical calculated dispersion curves to demonstrate the non-uniqueness inherent in the inversion of surface wave dispersion data; especially at layer boundaries where an abrupt change in seismic velocity occurs or associated with high velocity layers or velocity inversions.

Results

V_S models are presented as Figure 6. Surface wave depth of investigation is about 50 m based on $\lambda_{\max}/2.5$. The 0.2 Hz HVSR peak is associated with a geologic structure much deeper than the depth of investigation.

V_{S30} is 228 m/s (NEHRP Site Class D). The average V_S of the upper 50 m (V_{S50}) is 276 m/s. The estimated error in V_{S30} , which includes some effects of the lateral velocity variability beneath the testing arrays, is about 20 m/s. This is computed based on the sum of the following rounded to the nearest 5 m/s: an estimated error of 3% from the realistic assumed layer Poisson's ratios in the model, 1% error from the realistic assumed layer densities in the model, 2% for the variation in V_{S30} associated with non-uniqueness, and the 3.5% COV in V_{R40} from the combined active and passive-source surface wave dispersion data. V_{S30} is between 223 and 229 m/s for the equivalent V_S models demonstrating that V_{S30} does not vary much for V_S models with near identical dispersion curves. Interestingly, V_{S30} estimated from V_{R40} using the Brown et al., 2000 relationship ($V_{S30} \cong 1.045V_{R40}$, assuming V_{R40} represents the fundamental mode Rayleigh wave) is 234 m/s, only 3% higher than that estimated from the V_S model.



File Name: 18045_47524
Date: 5/29/2018

Legend

- CSMIP Station and Number
- ★ H/V Spectral Ratio Measurement Location
- MASW Array
- Passive Surface Wave Array

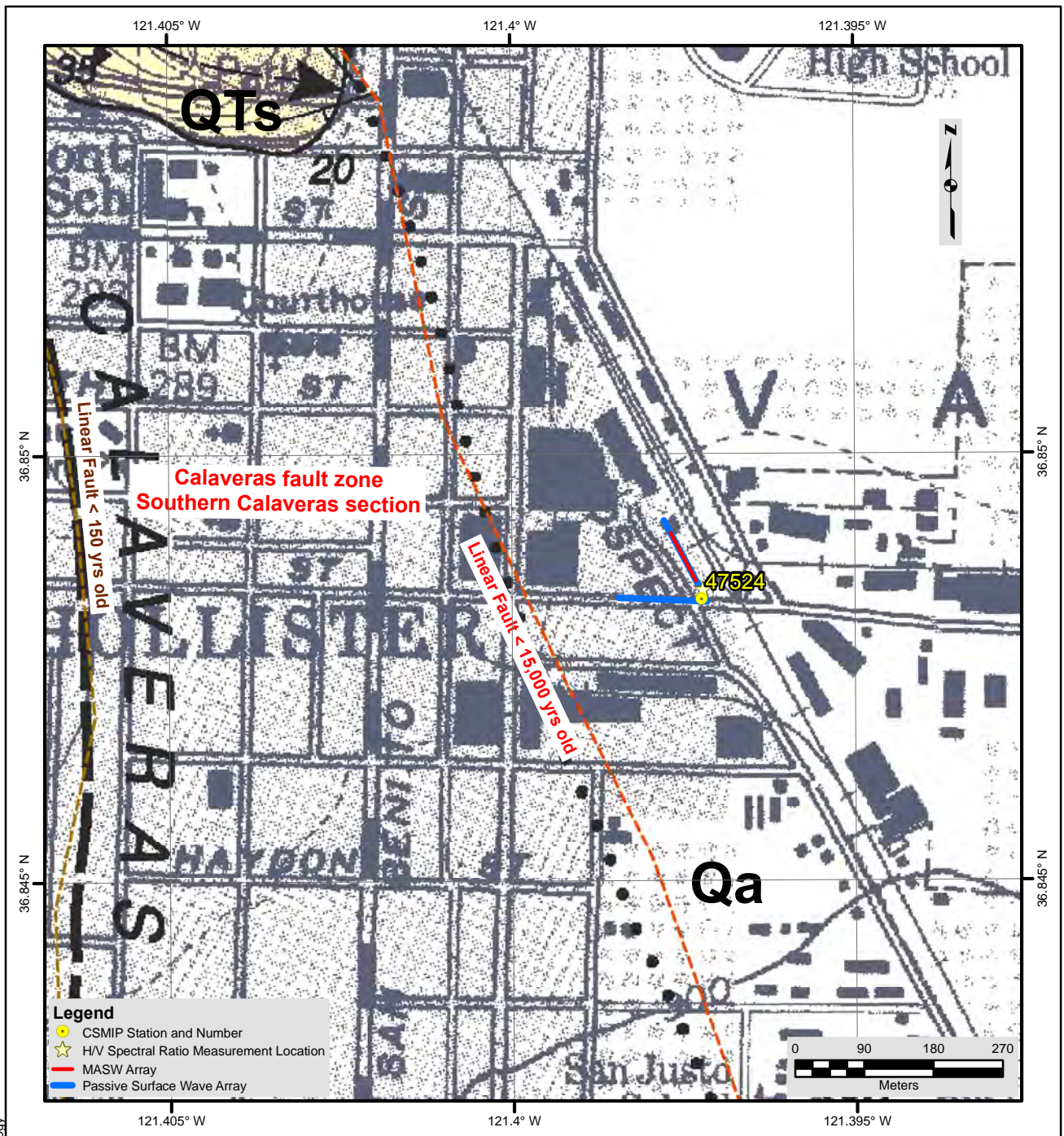
NOTES:

1. WGS 1984 Coordinate System
2. Image Source: Esri, DigitalGlobe, GeoEye, Earthstar Geographics, CNES/Airbus DS, USDA, USGS, AEX, Getmapping, Aerogrid, IGN, IGP, swisstopo, and the GIS User Community



**FIGURE 1
SITE MAP
CE • 47524**





Description of Geologic Map Units

Qa = Quaternary (Holocene) Alluvial pebble gravel, sand and clay of valley areas
 QTs = Quaternary (Pleistocene to Pliocene) Santa Clara Formation, exposed near Calaveras fault zone

NOTES:

1. WGS 1984 Coordinate System
2. Geologic Map of the Hollister Quadrangle, Monterey & San Benito Counties, California by Thomas W Dibblee, Jr., 2006

File Name: 18045_47524-Geology
Date: 5/29/2018



**FIGURE 2
 GEOLOGIC MAP
 CE • 47524**





Looking northwest at Seismic Station CE.47524 and corner of Array 1



Looking northwest along SE-NW leg of Array 1 and towards HVSR measurement location 1

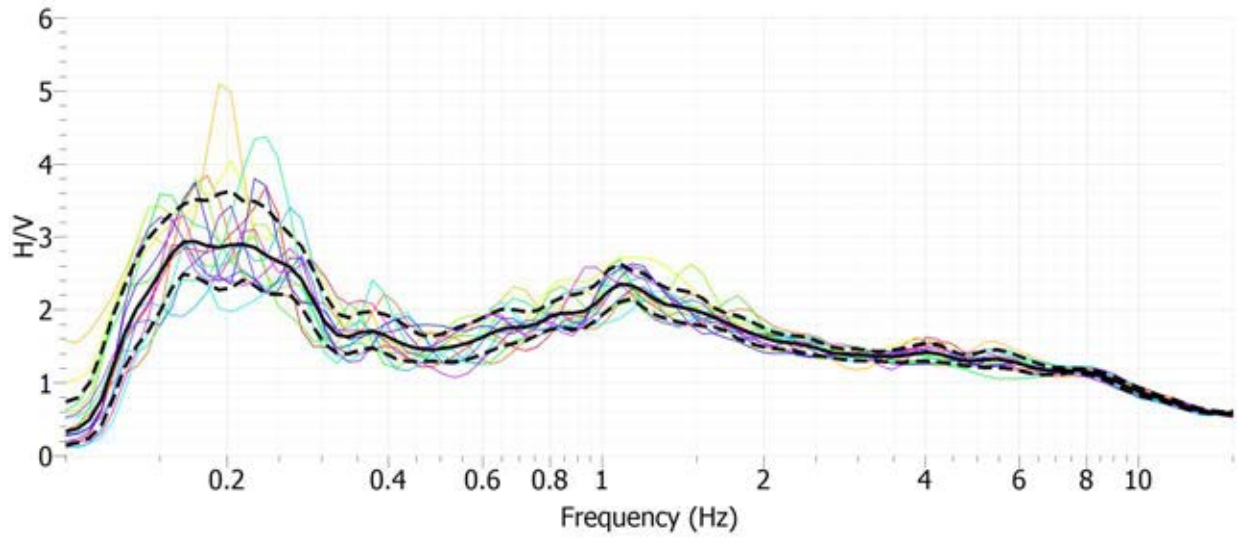


Looking down W-E leg of microtremor Array 1

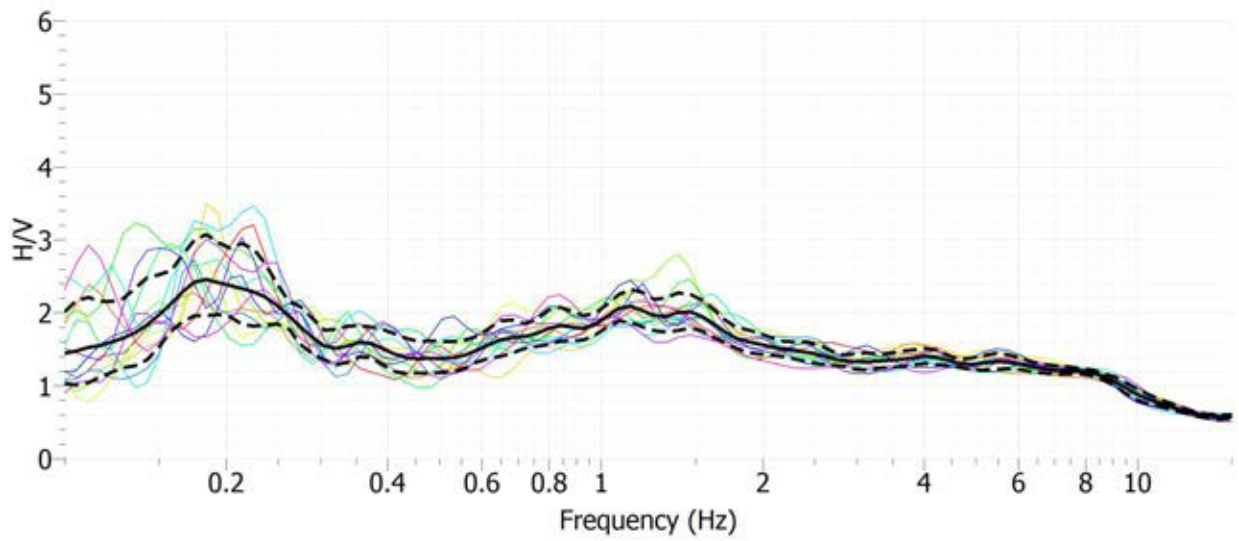


Data acquisition on microtremor Array 1

Figure 3 Site CE.47524 Photographs



Site CE.47524, HVSr Location 1, Nanometrics Trillium Compact Sensor



Site CE.47524, HVSr Location 1, MOHO Tromino ENGR Sensor

Figure 4 H/V Spectral Ratio of Ambient Vibration Data – Measurement Location 1, Site CE.47524

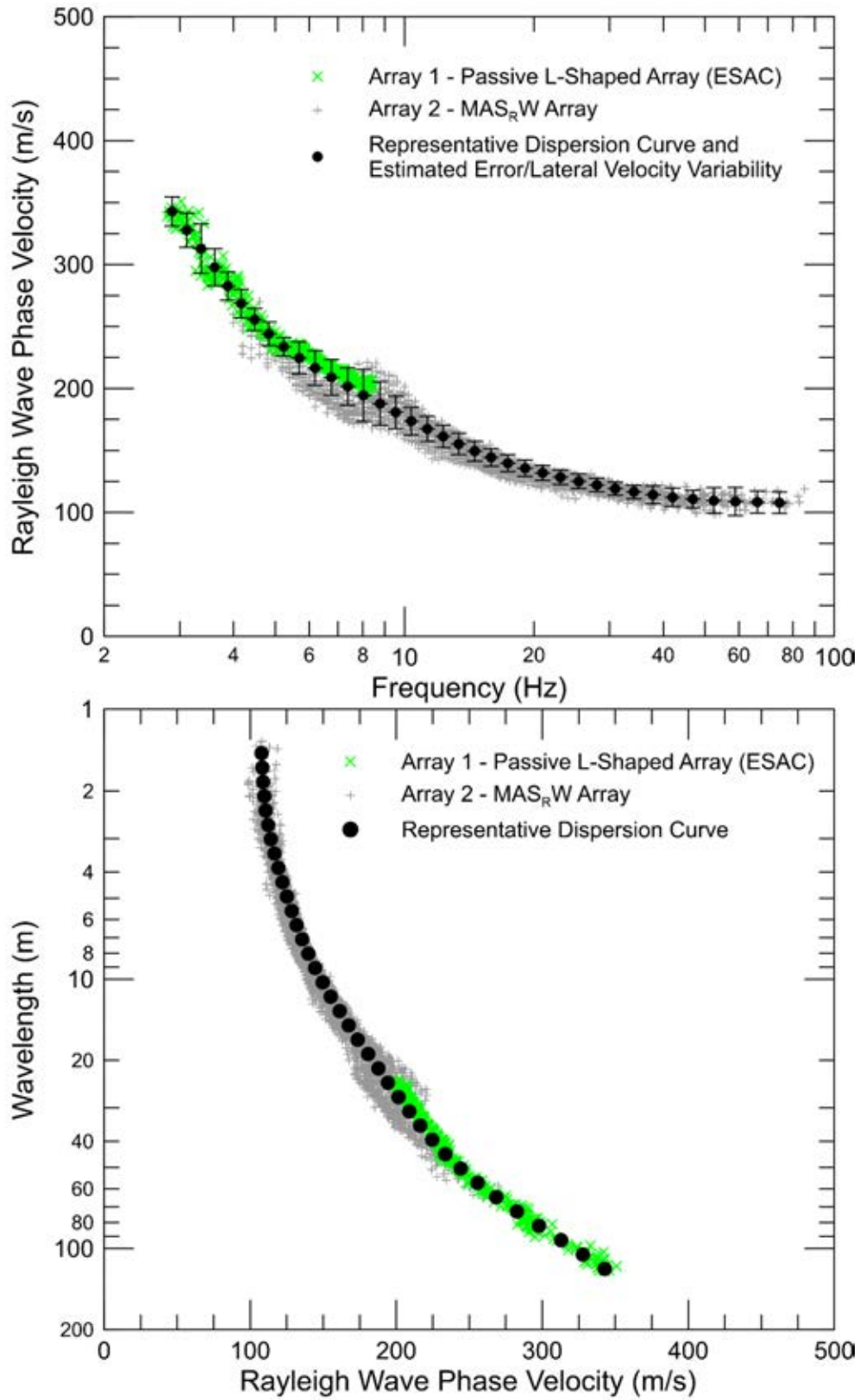


Figure 5 CE.47524 – Rayleigh wave dispersion curves derived from active- and passive-source surface wave data

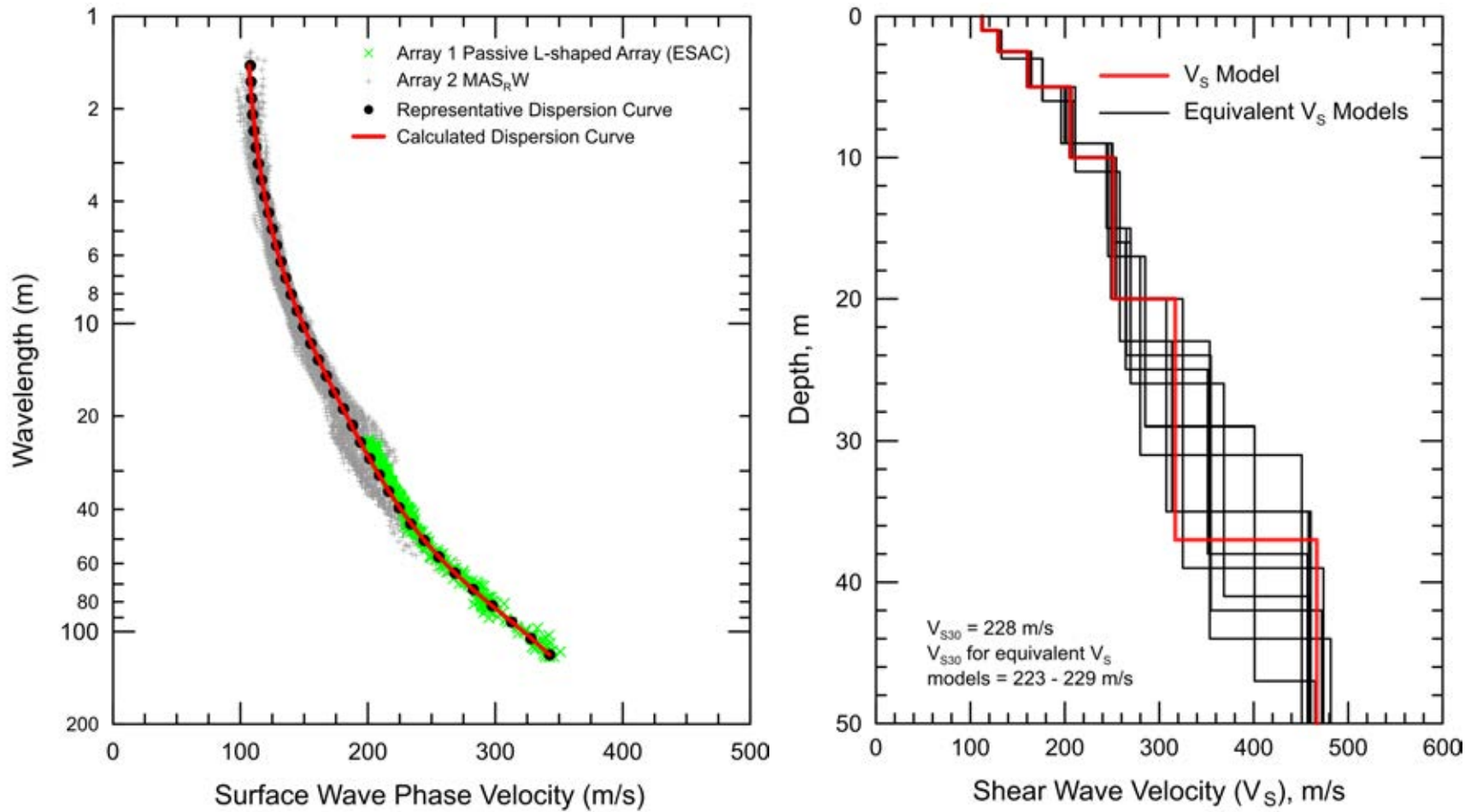


Figure 6 CE.47524 - Field, representative and calculated surface wave dispersion data (left) and associated V_S models (right)

Report

Geophysical Site Characterization

SMIP Station CE.47567

Station Name: Moss Landing – Hwy 1 & Dolan Road

Location: PG&E Moss Landing Substation, Dolan Road, Moss Landing, California

Latitude: 36.8076

Longitude: -121.7789

V_{s30}: 288 m/s

Estimated Error in V_{s30}: ± 20 m/s

NEHRP Site Class: D

Geomatrix Code: AHD

HVSR Peak Frequency: ~0.2 Hz (not well defined)

Site Geology: Site located on Holocene alluvium (Eolian deposits overlying fluvial deposits) and is adjacent to Elkhorn Slough to the north and Monterey Bay to the west (Figure 2). The San Andreas Fault is about 20 km northeast of the site.

Site Conditions: Rural site with high-frequency ambient vibrations from nearby roads and power plant and lower frequency ambient vibrations from Monterey Bay and Elkhorn Slough. Flat terrain in site vicinity.

Geophysical Methods Utilized: MAS_{RW}, array microtremor, HVSR

Geophysical Testing Arrays:

1. Array 1: 37 channel nested triangle array utilizing 4.5 Hz vertical geophones spaced at 6 m intervals along three nested triangles. The maximum receiver spacing (length of outer side of the array) is 48 m (Figure 1).
2. Array 2: 48 channel MAS_{RW} array utilizing 4.5 Hz vertical geophones spaced 1.5 m apart for a length of 70.5 m, forward and reverse shot locations with multiple source offsets (1.5 m and 10 m on the low end and 1.5 m off the high end of the array) and multiple interior source locations. A 2.5-lb hammer was used at 1.5 m offset source locations and center source locations. A 12-lb sledgehammer hammers was used at the 1.5 m offset source locations and all interior source locations and a 20-lb sledgehammer used for all offset source locations (Figure 1).
3. One HVSR location near the center of Arrays 1 and 2 (Figure 1).

Table 1 Location of Geophysical Testing Arrays

Location	Latitude	Longitude
Seismic Station CE.47567	36.80760	-121.77890
Array 1 Passive, Center of Triangle Array	36.80722	-121.77868
Array 1 Passive, Corner of Triangle Array	36.80730	-121.77897
Array 1 Passive, Corner of Triangle Array	36.80698	-121.77862
Array 1 Passive, Corner of Triangle Array	36.80739	-121.77845
Array 2 MASW, Northwest End of Array	36.80751	-121.77891
Array 2 MASW, Southeast End of Array	36.80696	-121.77852
HVSR Location 1	36.80723	-121.77869

Notes: 1) WGS84 Coordinate System (decimal degrees)

S-Wave Velocity Model:

Table 2 V_s Model

Depth to Top of Layer (m)	Layer Thickness (m)	S-Wave Velocity (m/s)	Inferred P-Wave Velocity (m/s)	Assumed Poisson's Ratio	Assumed Density (g/cm^3)
0	1	211	395	0.300	1.80
1	1.5	264	494	0.300	1.85
2.5	2.5	306	572	0.300	1.90
5	7	280	524	0.300	1.85
12	12	290	1600	0.483	1.90
24	13.5	312	1650	0.481	1.90
37.5	>12.5	411	1700	0.469	2.00

Notes: 1) Depth to saturated zone fixed at about 12 m based on seismic refraction data.
 2) Depth of investigation is about 50 m.
 3) Bottom layer is a half space.

Observations/Discussion:

H/V Spectral Ratio

HVSR data were collected using both Nanometrics Trillium Compact (Trillium) and MOHO Tromino ENGR (Tromino) seismographs. The HVSR data from the Trillium reveals a potential ~0.2 Hz peak (Figure 4), which would be associated with a geologic structure(s) at a depth much greater than the expected depth of investigation of the surface wave sounding. The Tromino does not detect this HVSR peak because the instrument is not designed to reliably detect HVSR peaks associated with deep geologic structures, such as this. Both the Trillium and Tromino also detect a weak 1.2 Hz HVSR peak (Figure 4). Only the S-N horizontal component of the ambient vibration data contribute to the peak and it is not clear if this peak has a geologic or anthropologic source.

Array Microtremor Data

Noise conditions at the site (multi-directional noise sources) appeared sufficient for successful application of passive surface wave techniques. A nested triangle array (Array 1) was utilized at this site because of limited site access and possible directional noise bias due to presence of a power plant next to the site. A nested triangle array has better azimuthal coverage (three azimuths for every sensor spacing) than a L-shaped array (two azimuths in the leg directions and one azimuth between receivers on different legs) and should, therefore, perform better in a variety of noise conditions. Over 60 minutes (129, 30 second seismic records) of ambient vibration data were acquired into Array 1. The ESAC technique was used to extract surface wave dispersion data from the ambient vibration data. To better characterize error, dispersion curves were generated from approximate 15-minute time segments of the ambient vibration data and also from the complete data set. The minimum and maximum Rayleigh wavelength extracted from Array 1 were about 16 and 108 m, respectively.

MASW Data

MASW data acquisition was conducted using a 70.5 m long receiver array (Array 2). Rayleigh wave dispersion data were interpreted from 13 MAS_RW seismic records collected at 8 different source locations using 2.5-lb hammer and 12- and 20-lb sledgehammer energy sources. Maximum source offset was 1.5 m at the northwest end of the array and 10 m at the southeast end of the array. Using the 13 seismic records and variable receiver offset ranges, over 60 dispersion curves were extracted and combined for analysis. To minimize near field effects, the maximum Rayleigh wavelength data extracted from the MAS_RW data set was set equal to one times the distance between the source and midpoint of the active receiver array. There is nominally about 20 to 30 m/s of scatter in MAS_RW dispersion data, which is likely in part due to lateral velocity variation. The minimum Rayleigh wavelength phase velocity data extracted from a 48-channel MAS_RW receiver gather was about 4 m. Reducing data from smaller hammer sources using a limited offset range receiver gather (i.e. less active geophones) allowed for extraction of surface wave dispersion data to a minimum wavelength of about 2 m.

Modeling

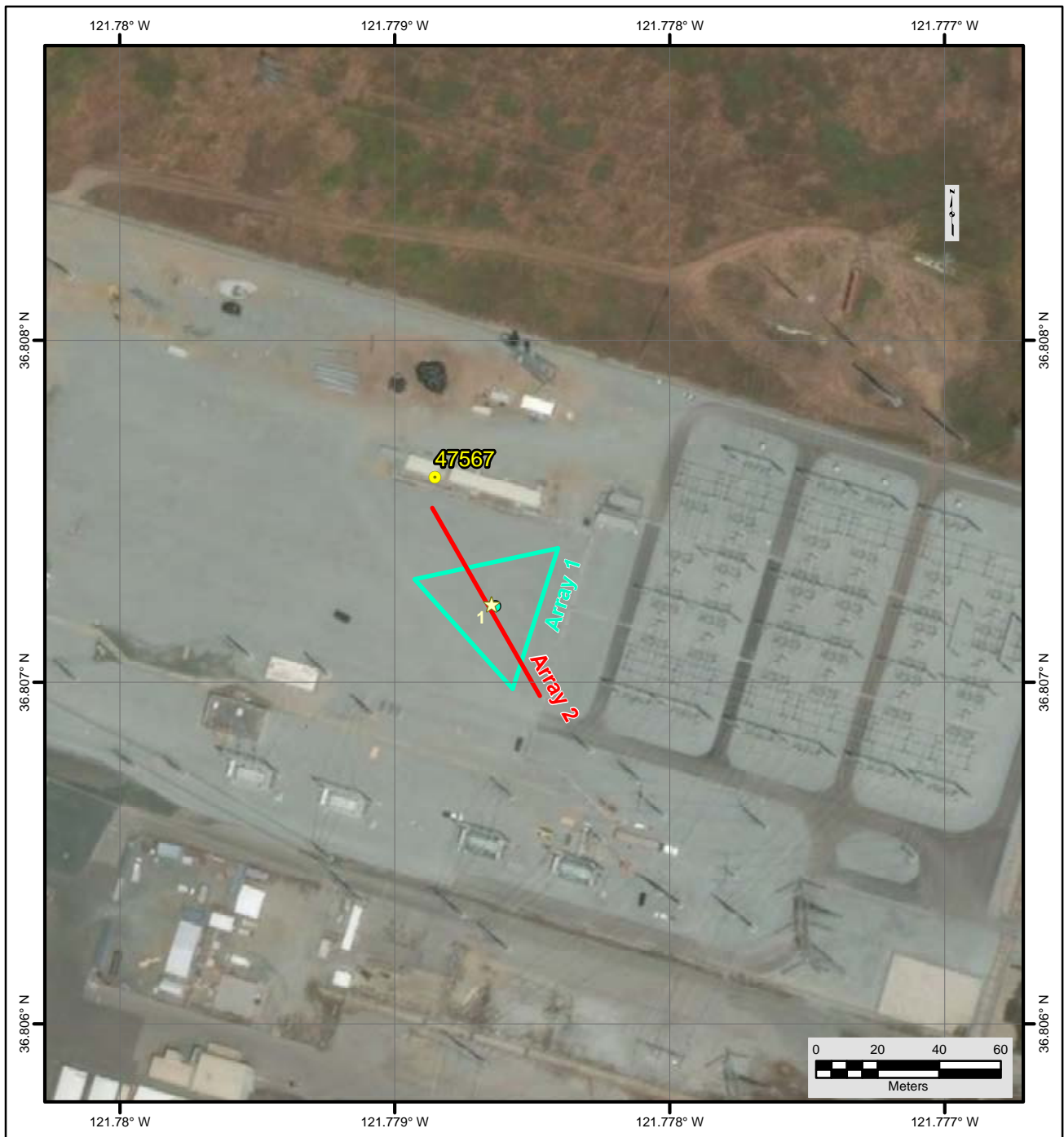
Surface wave dispersion data from active and passive surface wave data sets are in excellent agreement over the approximate 16 to 40 m overlapping wavelength range (Figure 5). The phase velocity of a 40-m wavelength Rayleigh wave (V_{R40}) is 262 m/s with a coefficient of variation (COV) of 0.5 % from ESAC analysis of the ambient vibration data collected along Array 1. Representative dispersion curves were generated for each surface wave data set using a moving average, polynomial curve fitting routine. These individual representative dispersion curves were combined and a composite representative dispersion curve generated for the combined data set for modeling. Error bars for the composite representative dispersion curve were estimated based on the scatter in the dispersion data.

The composite representative dispersion curve was inverted using an iterative non-linear least squares inversion routine and fundamental mode Rayleigh wave assumption to derive V_s models. Realistic estimates of Poisson's ratio and density were used to make models as accurate as possible. High Poisson's ratio, saturated sediments were constrained at a depth of about 12 m with $V_p > 1,600$ m/s based on interactive, layer-based analysis of seismic refraction first arrival

data. Poisson's ratio of the saturated sediments was set to gradually decrease with depth as the sediments became stiffer, a common observation in borehole velocity logs. Model layer thicknesses increased with depth to reflect the reduction in model resolution with depth. Several V_S models were developed with almost identical calculated dispersion curves to demonstrate the non-uniqueness inherent in the inversion of surface wave dispersion data, especially at layer boundaries where an abrupt change in seismic velocity occurs or associated with high velocity layers or velocity inversions.

Results

V_S models are presented as Figure 6. Surface wave depth of investigation is about 50 m based on $\lambda_{\max}/2$. V_{S30} is 288 m/s (NEHRP Site Class D). The average V_S of the upper 50 m (V_{S50}) is 315 m/s. The estimated error in V_{S30} , which includes some effects of the lateral velocity variability beneath the testing arrays, is about 20 m/s. This is computed based on the sum of the following rounded to the nearest 5 m/s: an estimated error of 3% from the realistic assumed layer Poisson's ratios in the model, 1% error from the realistic assumed layer densities in the model, 2% for the variation in V_{S30} associated with non-uniqueness, and the 0.5 % COV in V_{R40} from the passive-source surface wave dispersion data. V_{S30} is between 282 and 289 m/s for the equivalent V_S models, demonstrating that non-uniqueness does not have a large impact on estimated V_{S30} . Interestingly, V_{S30} estimated from V_{R40} using the Brown et al., 2000 relationship ($V_{S30} \cong 1.045V_{R40}$, assuming V_{R40} represents the fundamental mode Rayleigh wave) is 274 m/s, only 5% different than that estimated from the V_S model.



File Name: 18045_47567
Date: 5/29/2018

Legend

- CSMIP Station and Number
- ★ H/V Spectral Ratio Measurement Location
- MASW Array
- ▢ Passive Surface Wave Triangle Array

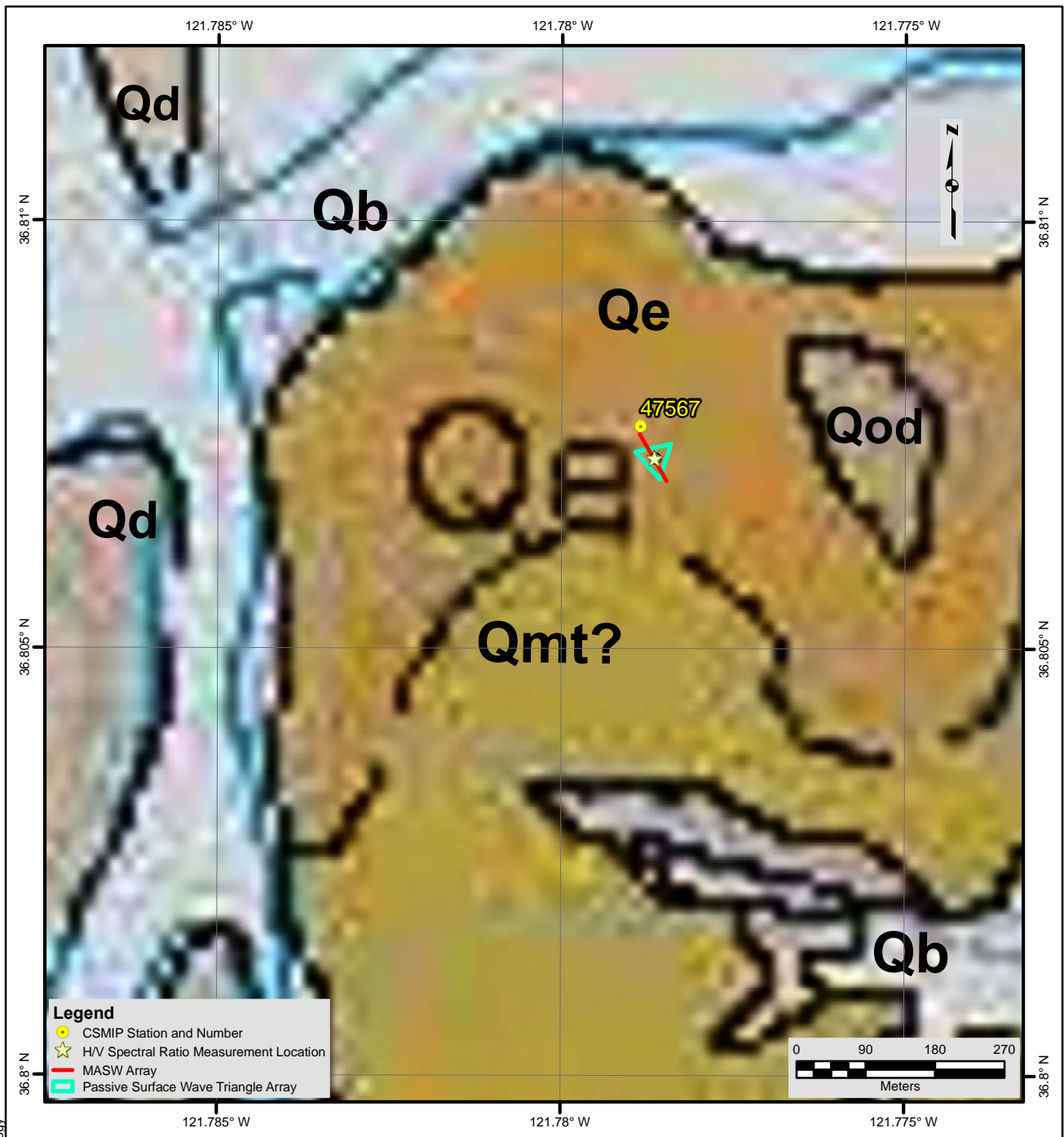
NOTES:

1. WGS 1984 Coordinate System
2. Image Source: Esri, DigitalGlobe, GeoEye, Earthstar Geographics, CNES/Airbus DS, USDA, USGS, AEX, Getmapping, Aerogrid, IGN, IGP, swisstopo, and the GIS User Community



**FIGURE 1
SITE MAP
CE • 47567**





Description of Geologic Map Units

Qb = Quaternary (Holocene) Basin deposits
 Qd = Quaternary (Holocene) Dune sand
 Qe = Quaternary (Holocene) Eolian sand
 Qod = Quaternary (Pleistocene) Older dune sand
 Qmt? Quaternary (Pleistocene) Marine terrace deposits

NOTES:

1. WGS 1984 Coordinate System
2. Geologic Map of the Monterey 30'x60' Quadrangle and Adjacent Areas, California Compiled by David L. Wagner, H. Gary Greene, George J. Saucedo, and Cynthia L. Pridmore, 2002

File Name: 18045_47567-Geology

Date: 5/29/2018



**FIGURE 2
 GEOLOGIC MAP
 CE • 47567**





Looking northwest at microtremor Array 1 towards structure housing seismic station



HVSR measurements

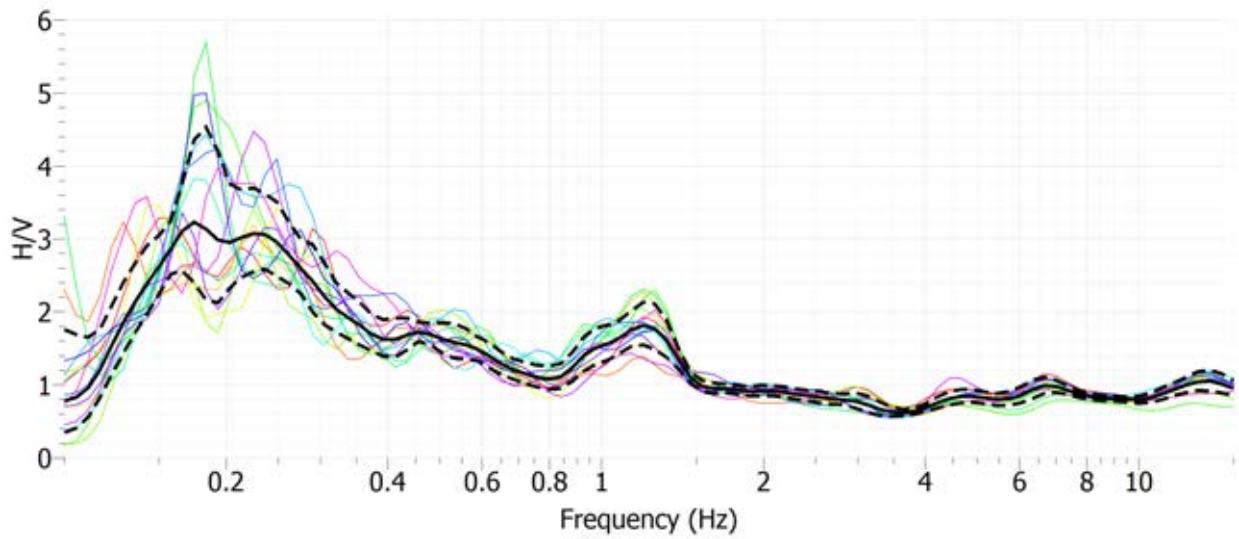


Looking northwest along MASW Array 2

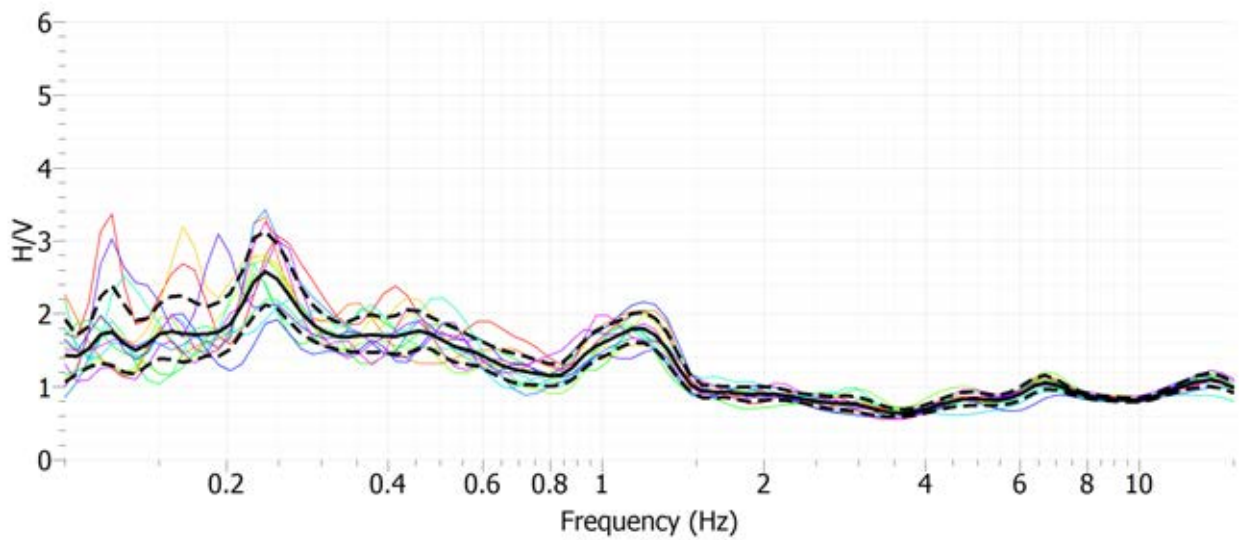


Looking southwest at microtremor Array 1

Figure 3 Site CE.47567 Photographs



Site CE.47567, HVSr Location 1, Nanometrics Trillium Compact Sensor



Site CE.47567, HVSr Location 1, MOHO Tromino ENGR Sensor

Figure 4 H/V Spectral Ratio of Ambient Vibration Data, Site CE.47567

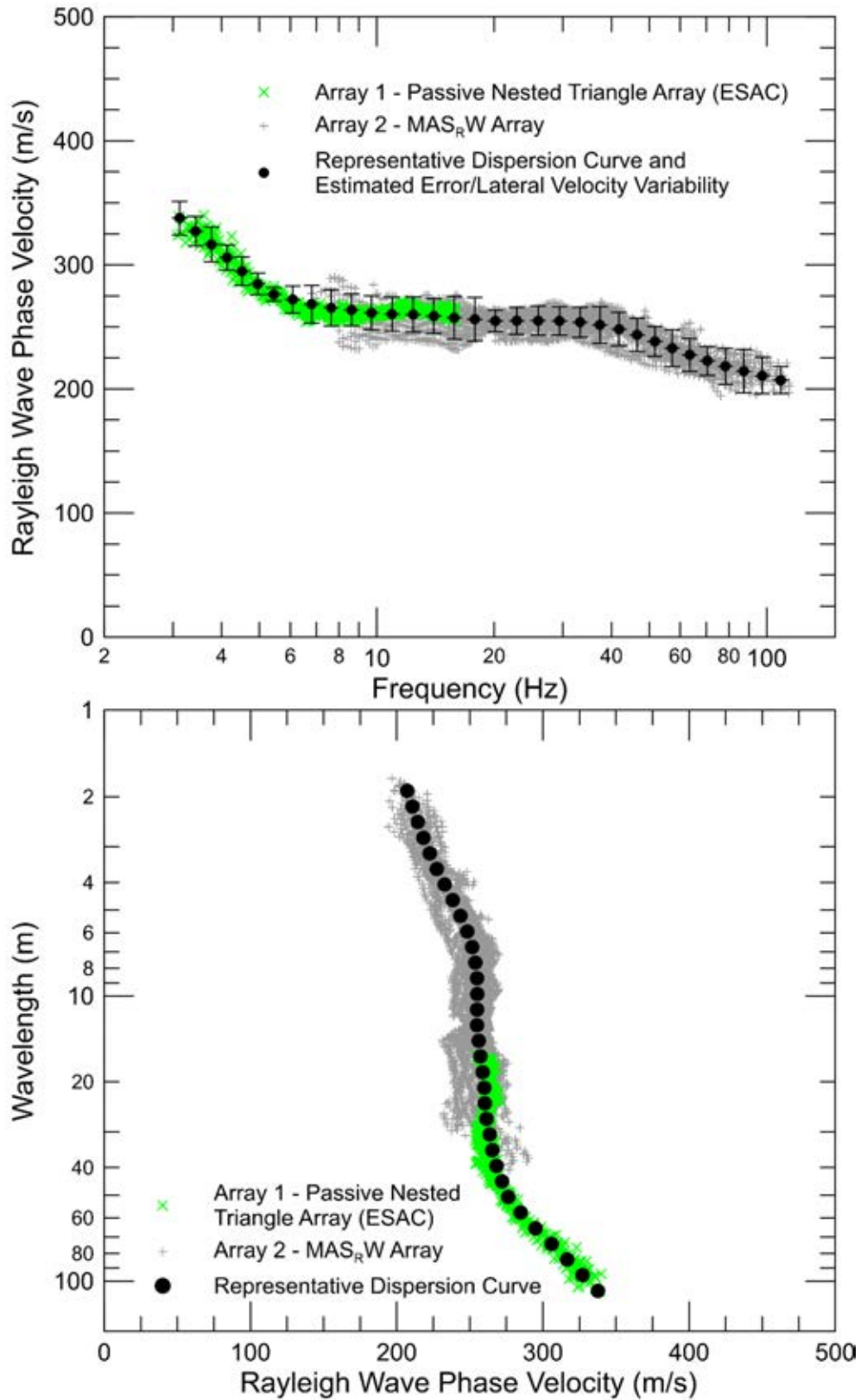


Figure 5 CE.47567 – Rayleigh wave dispersion curves derived from active- and passive-source surface wave data

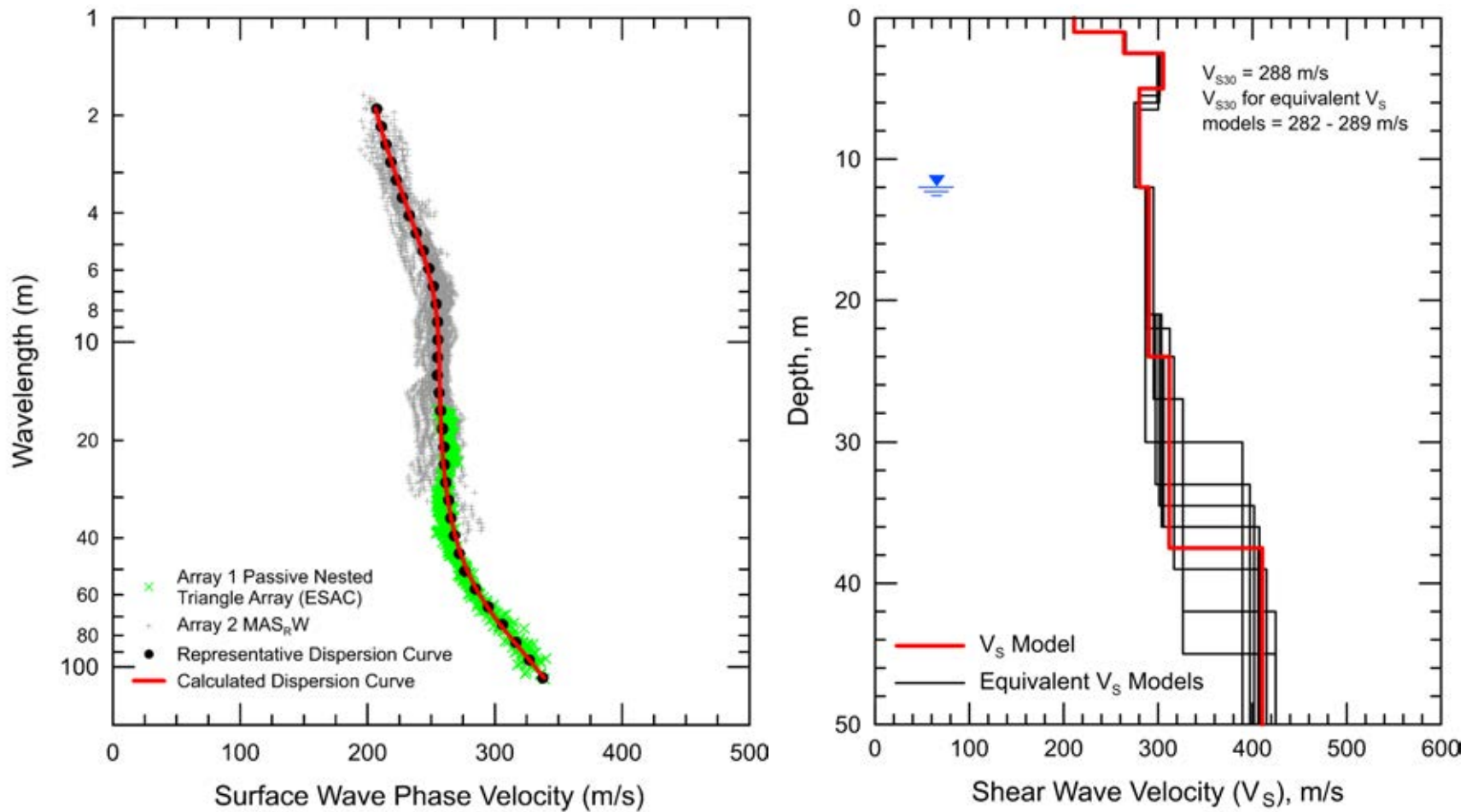


Figure 6 CE.47567 - Field, representative and calculated surface wave dispersion data (left) and associated V_s models (right)

Report

Geophysical Site Characterization

SMIP Station CE.47762

Station Name: Salinas - County Hospital Grounds

Location: Natividad Medical Center, 1441 Constitution Blvd., Salinas, California

Latitude: 36.6973

Longitude: -121.6342

V_{s30}: 237 m/s

Estimated Error in V_{s30}: ± 15 m/s

NEHRP Site Class: D

Geomatrix Code: IQD/IHD

HVSR Peak Frequency: 0.31 Hz, possible weak secondary peak at 1.1 Hz

Site Geology: Station located on older alluvium (Pleistocene to Holocene) more than 5 km from outcrops of Mesozoic granodiorite and metasedimentary rocks (Figure 2).

Site Conditions: Suburban site with moderate traffic noise from nearby roads. Relatively flat terrain in site vicinity.

Geophysical Methods Utilized: MAS_RW, array microtremor, HVSR

Geophysical Testing Arrays:

1. Array 1: 48 channel L-shaped array utilizing 4.5 Hz vertical geophones spaced 3 m apart used to acquire passive surface wave data. The SW-NE and NW-SE linear segments of array have lengths of 72 and 69 m, respectively (Figure 1).
2. Array 2: 48 channel MAS_RW array utilizing 4.5 Hz vertical geophones spaced 1.5 m apart for a length of 70.5 m, forward and reverse shot locations with multiple source offsets (1.5 m and 5 m from each end of the array) and multiple interior source locations. A 4-lb hammer was used for the near-offset and center source location. A 12-lb sledgehammer was used for the near-offset and all interior source locations. A 20-lb sledgehammer was used for all offset source locations (Figure 1).
3. One HVSR location, near seismic station (Figure 1).

Table 1 Location of Geophysical Testing Arrays

Location	Latitude	Longitude
Seismic Station CE.47762	36.69730	-121.63420
Array 1 Passive, Northwest End of Array	36.69792	-121.63462
Array 1 Passive, Corner of Array	36.69734	-121.63499
Array 1 Passive, Southeast end of Array	36.69706	-121.63430
Array 2 MASW, Northwest End of Array	36.69736	-121.63503
Array 2 MASW, Southeast End of Array	36.69707	-121.63433
HVSR Location 1	36.69729	-121.63420

Notes: 1) WGS84 Coordinate System (decimal degrees)

S-Wave Velocity Model:

Table 2 V_s Model

Depth to Top of Layer (m)	Layer Thickness (m)	S-Wave Velocity (m/s)	Inferred P-Wave Velocity (m/s)	Assumed Poisson's Ratio	Assumed Density (g/cm ³)
0	2.5	190	356	0.300	1.80
2.5	5	221	414	0.300	1.85
7.5	7.5	229	1600	0.490	1.90
15	12	249	1600	0.488	1.90
27	15.5	299	1600	0.482	1.90
42.5	17.5	346	1700	0.478	1.95
60	>10	629	1800	0.430	2.05

Notes: 1) Depth to saturated zone fixed at about 7.5 m based on seismic refraction data.
 2) Depth of investigation is about 70 m.
 3) Bottom layer is a half space.

Observations/Discussion:

H/V Spectral Ratio

HVSR data collected using both Nanometrics Trillium Compact (Trillium) and MOHO Tromino ENGR (Tromino) seismographs. The HVSR data from the Trillium reveals a 0.31 Hz peak, which is likely associated with a geologic structure(s) at a depth much greater than the expected depth of investigation of the surface wave sounding. The Tromino does not detect this HVSR peak, which is not unexpected as the Tromino is not designed to reliably detect HVSR peaks associated with deep geologic structures. Both the Trillium and Tromino also detect a weak 1.1 Hz HVSR peak, which may be associated with a shallower geologic structure.

Array Microtremor Data

Noise conditions at the site (multi-directional noise sources) appeared sufficient for successful application of passive surface wave techniques. Close to 60 minutes (115, 30 second seismic records) of ambient vibration data were acquired with an L-shaped array (Array 1). The legs of the L-shaped array were only 69 and 72 m long due to limited space. The ESAC technique was used to extract surface wave dispersion data from the ambient vibration data. To better characterize error, dispersion curves were generated from approximate 15 minute time segments of the ambient vibration data and also from the complete data set. The minimum and maximum Rayleigh wavelength extracted from Array 1 are about 16 and 175 m, respectively. No attempt was made to extract surface wave dispersion data from the linear legs of the L-shaped array because 2D arrays will yield more reliable dispersion data than linear arrays.

MASW Data

MASW data acquisition was conducted using a 70.5 m long receiver array (Array 2). Rayleigh wave dispersion data were interpreted from 14 MAS_RW seismic records collected at 9 different source locations using 4-lb hammer, and 12- and 20-lb sledgehammer energy sources. Due to limited space, the maximum source offset was 5 m from each end of the array. Using the 14 seismic records and variable receiver offset ranges, over 60 dispersion curves were extracted and combined for analysis. To minimize near field effects, the maximum Rayleigh wavelength data extracted from the MAS_RW data set was set equal to one times the distance between the source and midpoint of the active receiver array. There is nominally about 30 m/s of scatter in MAS_RW dispersion data, which is likely in part due to lateral velocity variation. The minimum Rayleigh wavelength phase velocity data extracted from a 48-channel MAS_RW receiver gather was about 6 m. Reducing data from smaller hammer sources using a limited offset range receiver gather (i.e. less active geophones) allowed for extraction of surface wave dispersion data to a minimum wavelength of about 2.5 m.

Modeling

Surface wave dispersion data from active and passive surface wave data sets are in excellent agreement over the approximate 16 to 40 m overlapping wavelength range (Figure 5). The phase velocity of a 40 m wavelength Rayleigh wave (V_{R40}) is 225 m/s with a coefficient of variation (COV) of 1% from ESAC analysis of the ambient vibration data collected along Array 1. Representative dispersion curves were generated for each surface wave data set using a moving average, polynomial curve fitting routine. These individual representative dispersion curves were combined and a composite representative dispersion curve was generated for the combined data set for modeling. Error bars for the composite representative dispersion curve were estimated based on the scatter in the dispersion data.

The composite representative dispersion curve was inverted using an iterative non-linear least squares inversion routine and fundamental mode Rayleigh wave assumption to derive V_S models. Realistic estimates of Poisson's ratio and density were used to make models as accurate as possible. High Poisson's ratio, saturated sediments were constrained at a depth of about 7.5 m with $V_P > 1,600$ m/s based on interactive, layer-based analysis of seismic refraction first arrival data. Poisson's ratio of the saturated sediments was set to gradually decrease with depth as the sediments became stiffer, a common observation in borehole velocity logs. Model layer thicknesses increased with depth to reflect the reduction in model resolution with depth. Several

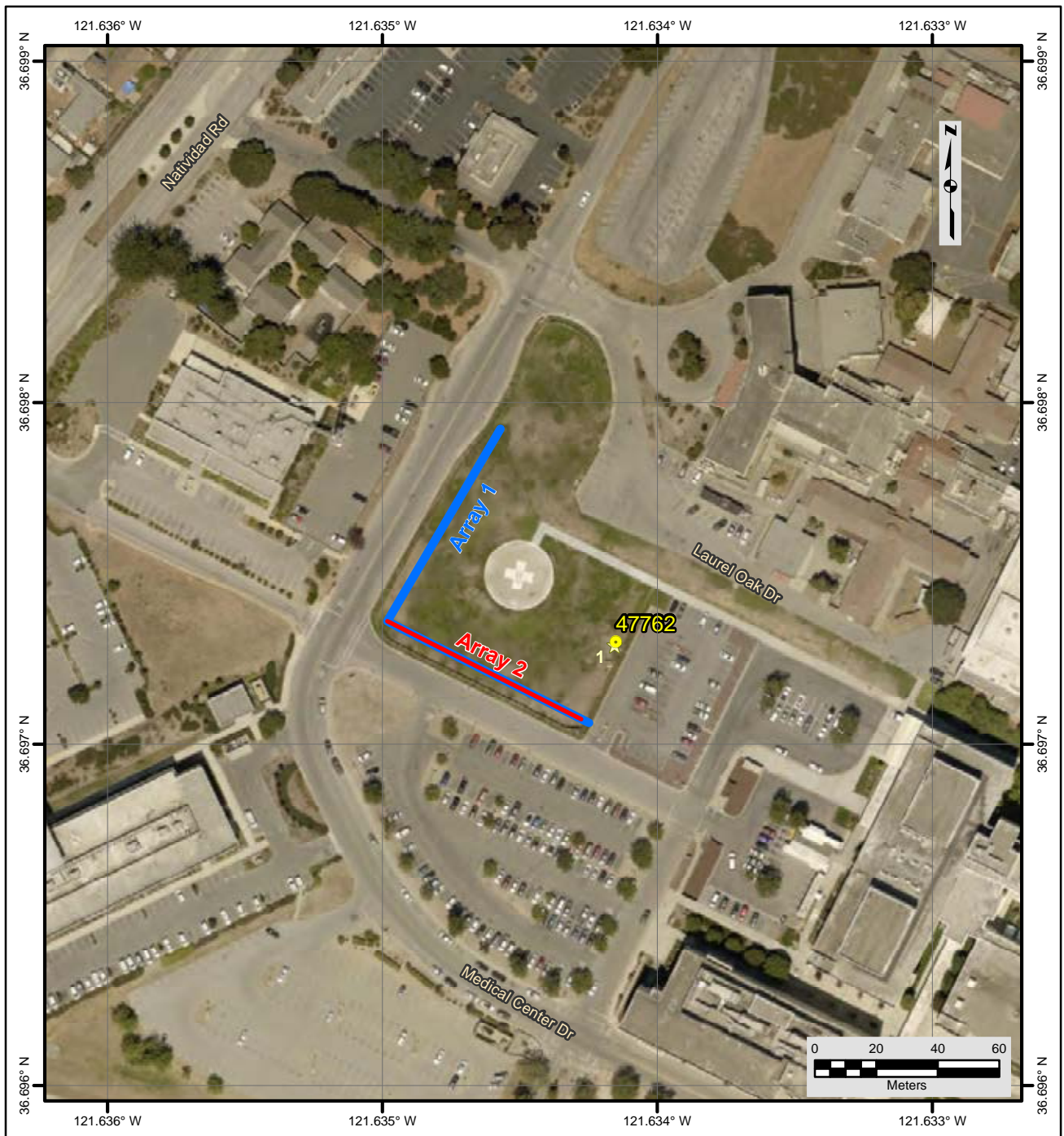
V_S models were developed with almost identical calculated dispersion curves to demonstrate the non-uniqueness inherent in the inversion of surface wave dispersion data; especially at layer boundaries where an abrupt change in seismic velocity occurs or associated with high velocity layers or velocity inversions.

Theoretical HVSR, based on the diffuse field assumption, was computed for all V_S models using the software package *HV-Inv* Release 2.3 and the assumption that the noise field consists of only Rayleigh waves.

Results

V_S models are presented as Figure 6. Surface wave depth of investigation is about 70 m based on $\lambda_{\max}/2.5$. The HVSR peak frequency computed from the V_S models is in good agreement with observed HVSR data (secondary peak at about 1.2 Hz) with the assumption that the noise field consists primarily of Rayleigh waves over the pertinent frequency range (Figure 7).

V_{S30} is 237 m/s (NEHRP Site Class D). The average V_S of the upper 70 m (V_{S70}) is 298 m/s. The estimated error in V_{S30} , which includes some effects of the lateral velocity variability beneath the testing arrays, is about 15 m/s. This is computed based on the sum of the following rounded to the nearest 5 m/s: an estimated error of 3% from the realistic assumed layer Poisson's ratios in the model, 1% error from the realistic assumed layer densities in the model, 2% for the variation in V_{S30} associated with non-uniqueness, and the 1% COV in V_{R40} from the passive-source surface wave dispersion data. V_{S30} is between 236 and 238 m/s for the equivalent V_S models. There is only a small variation in V_{S30} between equivalent models because non-uniqueness was only evaluated for a model layer between 50 and 75 m depth and not for layers in the upper 30 m. Interestingly, V_{S30} estimated from V_{R40} using the Brown et al., 2000 relationship ($V_{S30} \cong 1.045V_{R40}$, assuming V_{R40} represents the fundamental mode Rayleigh wave) is 235 m/s, only 1 % different than that estimated from the V_S model.



File Name: 18045_47762
Date: 6/7/2018

Legend

- CSMIP Station and Number
- H/V Spectral Ratio Measurement Location
- MASW Array
- Passive Surface Wave Array

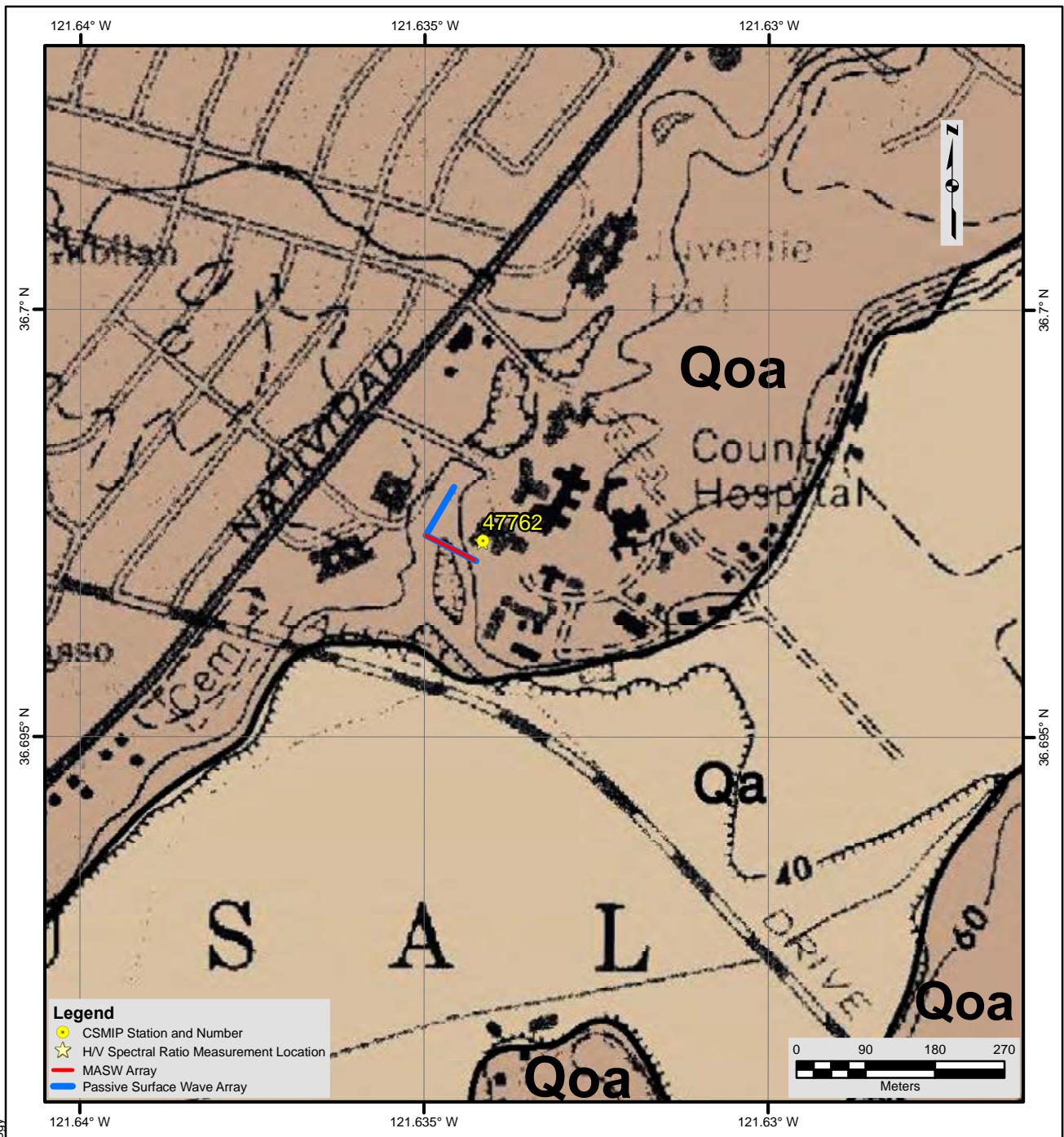
NOTES:

1. WGS 1984 Coordinate System
2. Image Source: Esri, DigitalGlobe, GeoEye, Earthstar Geographics, CNES/Airbus DS, USDA, USGS, AEX, Getmapping, Aerogrid, IGN, IGP, swisstopo, and the GIS User Community



**FIGURE 1
SITE MAP
CE • 47762**





Description of Geologic Map Units

Qa = Quaternary (Holocene) Alluvial gravel, sand, and silt/clay of valley areas and flood plains
 Qoa = Quaternary (Holocene - Pliocene) Dissected older alluvium

NOTES:
 1. WGS 1984 Coordinate System
 2. Geologic Map of the Marina and Salinas Quadrangles, Monterey County, California by Thomas W Dibblee, Jr., 2007

File Name: 18045_47762-Geology
Date: 5/29/2018



**FIGURE 2
 GEOLOGIC MAP
 CE • 47762**





Looking east at HVSr measurement location and seismic station CE.47762



Looking northeast towards seismic station from southeast corner of Arrays 1 and 2

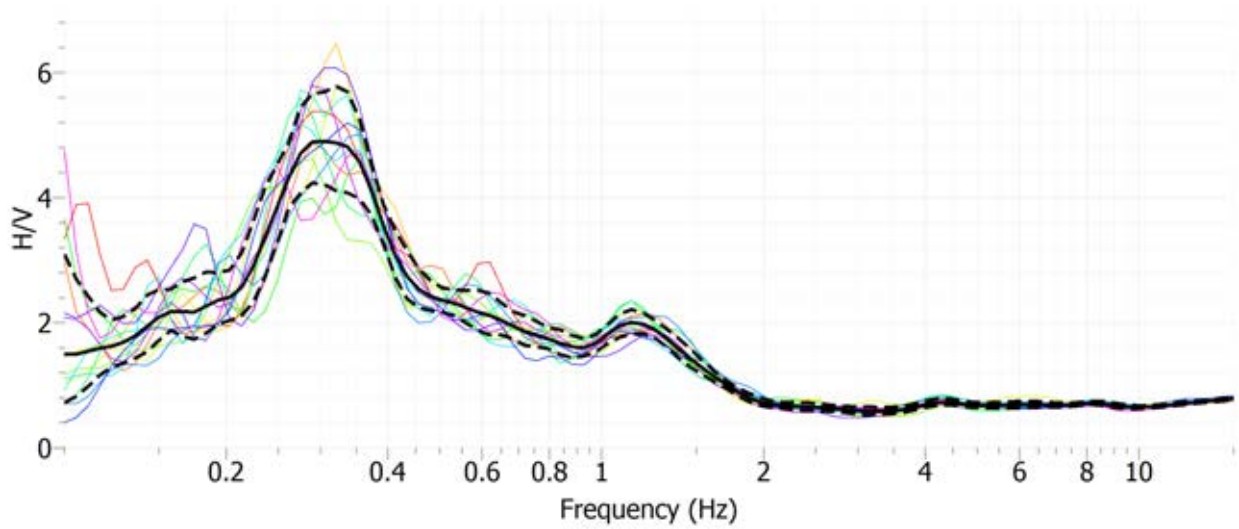


Looking southeast along MASW Array 2

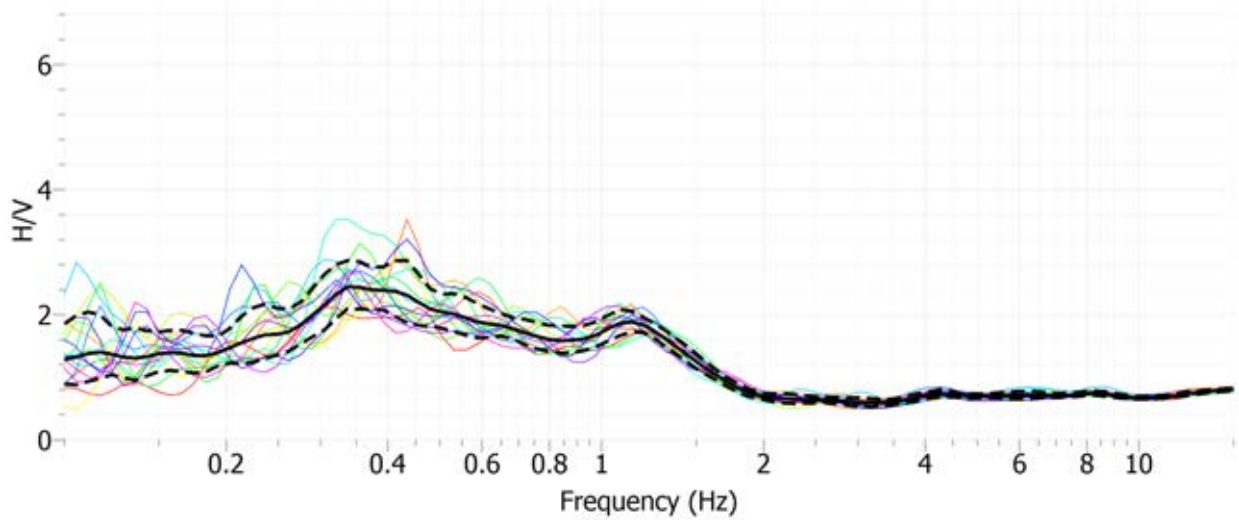


Looking east at seismic acquisition system from west corner of microtremor Array 1

Figure 3 Site CE.47762 Photographs



Site CE.47762, HVSR Location 1, Nanometrics Trillium Compact Sensor



Site CE.47762, HVSR Location 1, MOHO Tromino ENGR Sensor

Figure 4 H/V Spectral Ratio of Ambient Vibration Data, Site CE.47762

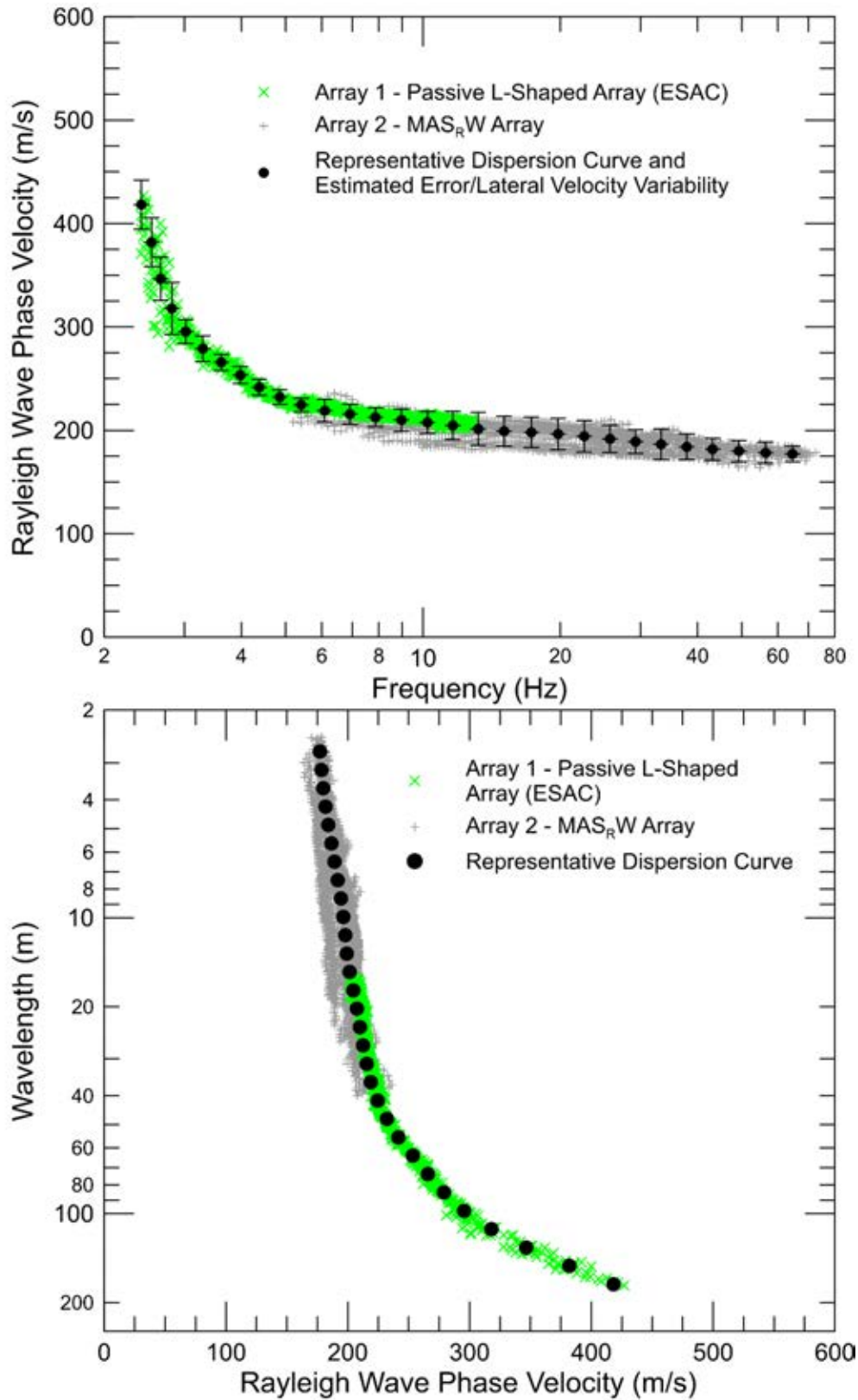


Figure 5 CE.47762 – Rayleigh wave dispersion curves derived from active- and passive-source surface wave data

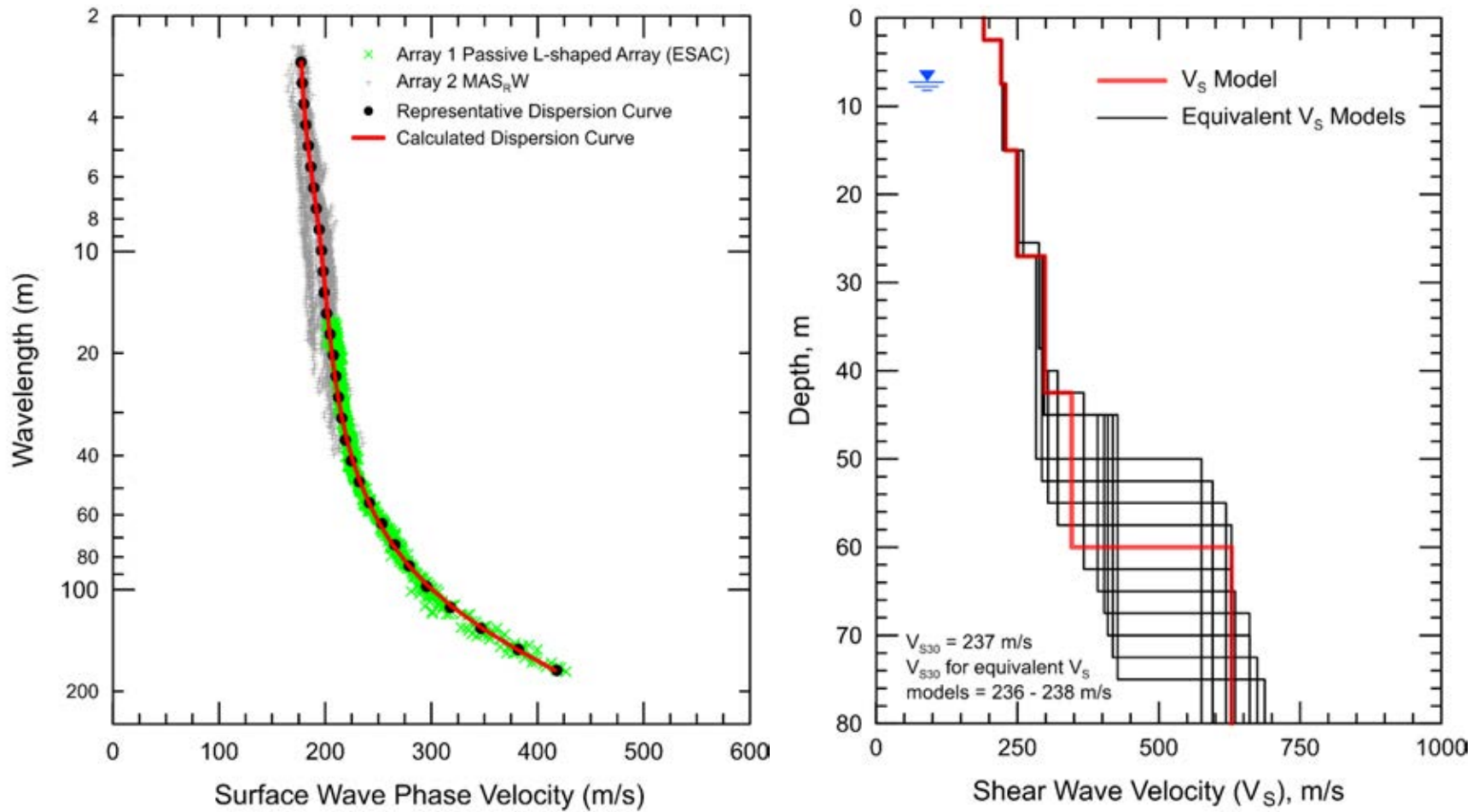


Figure 6 CE.47762 - Field, representative and calculated surface wave dispersion data (left) and associated V_s models (right)

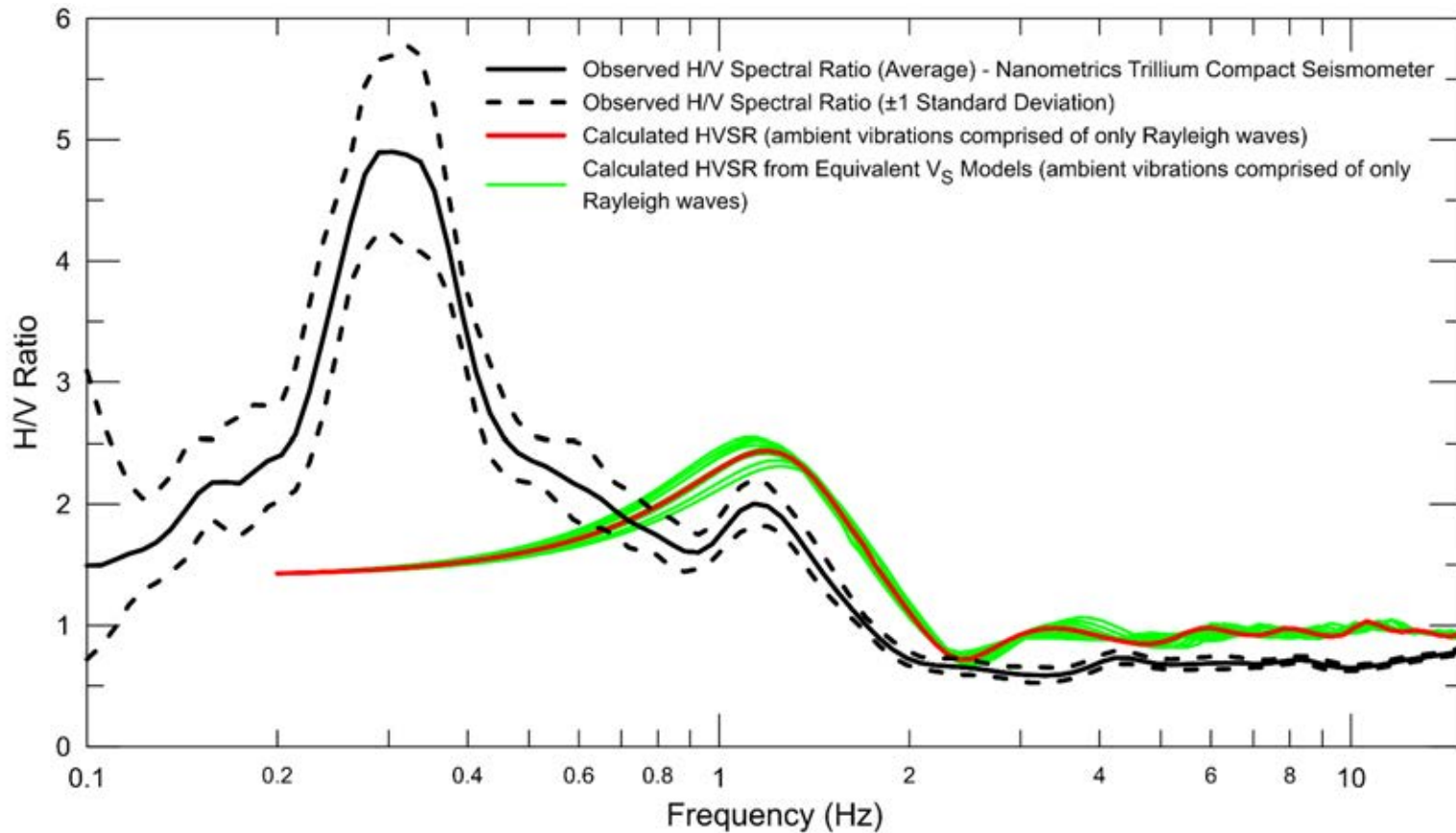


Figure 7 CE.47762 – Calculated HVSR response for V_S models based on diffuse field assumption. The 0.3 Hz HVSR peak is associated with a geologic structure at a depth much greater than the depth of investigation. The V_S models support the presence of the 1.2 Hz HVSR peak.

Report Geophysical Site Characterization SMIP Station CE.48906

Station Name: Santa Cruz - County Office Bldg Grounds

Location: Santa Cruz County Superior Court, 701 Ocean Street, Santa Cruz, CA

Latitude: 36.9781

Longitude: -122.0211

V_{s30}: 297 m/s

Estimated Error in V_{s30}: ± 25 m/s

NEHRP Site Class: D

Geomatrix Code: IHC/IHB

HVSR Peak Frequency: Broad peak/multiple peaks between 1.5 and 4 Hz

Site Geology: Site located on Holocene alluvium near San Lorenzo River and 2 km from Ben Lomond fault zone (Figure 2). Outcrops of Pliocene/Miocene Purisima and Santa Cruz Formations within 300 m of the site. Outcrops of crystalline bedrock within 2 to 3 km of site. Site likely located on moderately thick layer of alluvium overlying Pliocene sedimentary rocks.

Site Conditions: Suburban site with traffic noise from nearby roads. Flat terrain in site vicinity.

Geophysical Methods Utilized: MAS_RW, array microtremor, HVSR

Geophysical Testing Arrays:

1. Array 1: 37 channel nested triangle array utilizing 4.5 Hz vertical geophones spaced at 6 m intervals along three nested triangles. The maximum receiver spacing (length of outer side of the array) is 48 m (Figure 1).
2. Array 2: 48 channel MAS_RW array utilizing 4.5 Hz vertical geophones spaced 1 m apart for a length of 47 m, forward and reverse shot locations with multiple source offsets (1 m to 15 m at both ends of array) and multiple interior source locations. A 4-lb hammer was used at 1 m offset source locations and center source locations. A 12-lb sledgehammer hammers was used at the 1 m offset source locations and all interior source locations and a 20-lb sledgehammer used for all far-offset source locations (Figure 1).
3. Three (3) HVSR locations, one near seismic sensor and eastern corner of Array 1 and the other two at the other corners of Array 1 (Figure 1).

Table 1 Location of Geophysical Testing Arrays

Location	Latitude	Longitude
Seismic Station CE.48906	36.97810	-122.02110
Array 1 Passive, Center of Triangle Array	36.978105	-122.021502
Array 1 Passive, Corner of Triangle Array	36.97827	-122.02174
Array 1 Passive, Corner of Triangle Array	36.97786	-122.02156
Array 1 Passive, Corner of Triangle Array	36.97819	-122.02120
Array 2 MASW, South end of Array	36.97791	-122.021357
Array 2 MASW, North end of Array	36.97831	-122.02153
HVSR Location 1	36.97807	-122.02117
HVSR Location 2	36.97827	-122.02174
HVSR Location 3	36.97786	-122.02156

Notes: 1) WGS84 Coordinate System (decimal degrees)

S-Wave Velocity Model:

Table 2 V_s Model

Depth to Top of Layer (m)	Layer Thickness (m)	S-Wave Velocity (m/s)	Inferred P-Wave Velocity (m/s)	Assumed Poisson's Ratio	Assumed Density (g/cm ³)
0	1	176	328	0.298	1.80
1	3	154	288	0.300	1.75
4	3	174	1524	0.493	1.80
7	3	204	1553	0.491	1.90
10	10	443	1793	0.467	2.00
20	15	467	1816	0.465	2.00
35	>15	690	2039	0.435	2.10

Notes: 1) Depth to saturated zone fixed at about 4 m based on seismic refraction data.
 2) Depth of investigation is about 50 m.
 3) Bottom layer is a half space.

Observations/Discussion:

H/V Spectral Ratio

HVSR data collected using both Nanometrics Trillium Compact (Trillium) and MOHO Tromino ENGR (Tromino) seismographs. Both the Trillium and Tromino were utilized at HVSR Location 1 (~ 1-hour recording duration) with almost identical results and, therefore, only the Tromino (20-minute recording duration) was utilized at HVSR Locations 2 and 3. The site has a complex HVSR response (Figure 4 and 5) with a broad peak or multiple peaks between about 1.5 and 4 Hz. There are some differences in both the HVSR peak frequency and amplitude between

the three measurement locations indicating that there is some lateral variability in velocity structure beneath the site. A small reduction in near surface S-wave velocity could explain the increase in amplitude and decrease in the frequency of the highest frequency HVSR peak at measurement location 2. It is probable that multiple subsurface geologic units contribute to the HVSR peak.

Array Microtremor Data

Noise conditions at the site (multi-directional noise sources) appeared sufficient for successful application of passive surface wave techniques. A nested triangle array (Array 1) was utilized at this site to avoid blocking driveways in the parking lot with an L-shaped array. A nested triangle array has better azimuthal coverage (three azimuths for every sensor spacing) than a L-shaped array (two azimuths in the leg directions and one azimuth between receivers on different legs) and should, therefore, perform better in a variety of noise conditions. Sixty (60) minutes (120, 30 second seismic records) of ambient vibration data were acquired into Array 1. The ESAC technique was used to extract surface wave dispersion data from the ambient vibration data. To better characterize error, dispersion curves were generated from approximate 15-minute time segments of the ambient vibration data and also from the complete data set. The minimum and maximum Rayleigh wavelength extracted from Array 1 were about 6 and 125 m, respectively.

MASW Data

MASW data acquisition was conducted using a 47 m long receiver array (Array 2) as a longer array would have blocked access to the parking lot where the testing was conducted. Rayleigh wave dispersion data were interpreted from 16 MAS_RW seismic records collected at 13 different source locations using 4-lb hammer and 12- and 20-lb sledgehammer energy sources. Maximum source offset was 15 m at both ends of the array. Using the 16 seismic records and variable receiver offset ranges, over 75 dispersion curves were extracted and combined for analysis. To minimize near field effects, the maximum Rayleigh wavelength data extracted from the MAS_RW data set was set equal to 1.3 times the distance between the source and midpoint of the active receiver array after inspection of the data. The maximum wavelength Rayleigh wave was not permitted to exceed 40 m which occurred at a frequency near 7.5 Hz (expected low frequency limit of 20 lb sledgehammer). There is nominally about 15 to 30 m/s of scatter in MAS_RW dispersion data, which is likely in part due to lateral velocity variation. The minimum Rayleigh wavelength phase velocity data extracted from a 48-channel MAS_RW receiver gather was approximately 2 to 6 m. Reducing data from smaller hammer sources using a limited offset range receiver gather (i.e. less active geophones) allowed for extraction of surface wave dispersion data to a minimum wavelength of about 1.5 m.

Modeling

Surface wave dispersion data from active and passive surface wave data sets are in excellent agreement over the approximate 6 to 40 m overlapping wavelength range (Figure 5). The phase velocity of a 40 m wavelength Rayleigh wave (V_{R40}) is 315 m/s with a coefficient of variation (COV) of 0.5 % from ESAC analysis of the ambient vibration data collected along Array 1. Representative dispersion curves were generated for each surface wave data set using a moving average, polynomial curve fitting routine. These individual representative dispersion curves were combined and a composite representative dispersion curve generated for the combined data

set for modeling. Error bars for the composite representative dispersion curve were estimated based on the scatter in the dispersion data.

Preliminary modeling of the Rayleigh wave dispersion data indicated that the fundamental mode assumption may not be valid at this site. Therefore, the composite representative dispersion curve was inverted using both a genetic algorithm (global search) and iterative non-linear least squares (local search) inversion routines and the effective mode Rayleigh wave assumption to derive V_S models. Realistic estimates of Poisson's ratio and density were used to make models as accurate as possible. High Poisson's ratio, saturated sediments were constrained at a depth of about 4 m with $V_P > 1,600$ m/s based on interactive, layer-based analysis of seismic refraction first arrival data. Poisson's ratio of the saturated sediments was set to gradually decrease with depth as the sediments became stiffer, a common observation in borehole velocity logs. Model layer thicknesses increased with depth to reflect the reduction in model resolution with depth. Several V_S models were developed with almost identical calculated dispersion curves to demonstrate the non-uniqueness inherent in the inversion of surface wave dispersion data; especially at layer boundaries where an abrupt change in seismic velocity occurs or associated with high velocity layers or velocity inversions.

Theoretical HVSR, based on the diffuse field assumption, was computed for all V_S models using the software package *HV-Inv* Release 2.3 and the assumption that the noise field consists of only Rayleigh waves.

Results

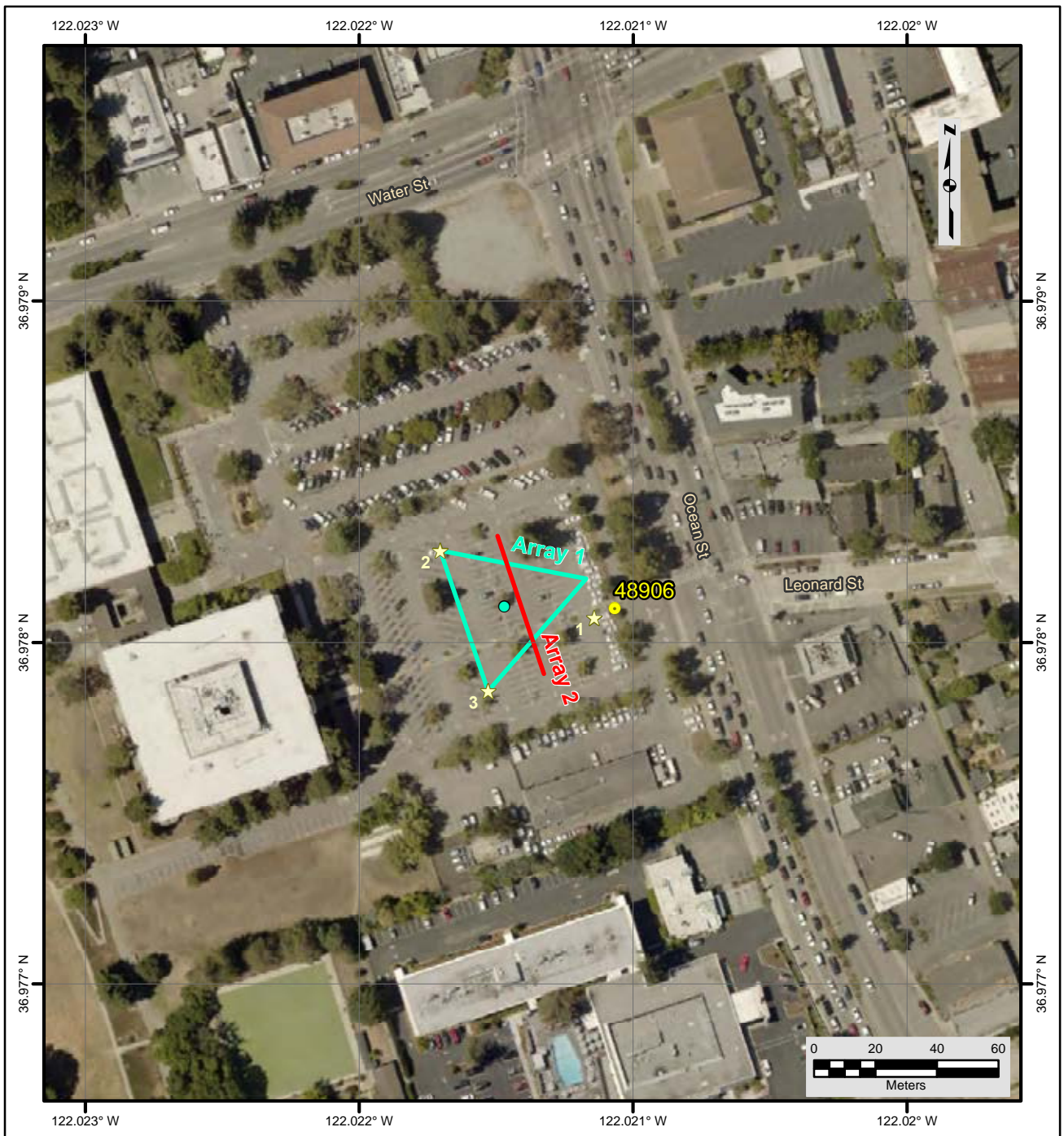
V_S models are presented as Figure 6 and the V_S model selected for purpose of site characterization is presented in Table 2. V_S exceeds 400 m/s at a depth of about 10 m, which is likely the top of Tertiary sediments. Surface wave depth of investigation is about 50 m based on $\lambda_{\max}/2.5$. The HVSR peak frequency computed from the V_S models is in acceptable agreement with the highest frequency component of the observed HVSR data (Figure 7).

V_{S30} is 297 m/s (NEHRP Site Class D). The average V_S of the upper 50 m (V_{S50}) is 374 m/s. V_{S30} is between 287 and 301 m/s for the equivalent V_S models, slightly more than typically observed due to both an abrupt increase in velocity at relatively shallow depth and larger errors between observed and calculated effective mode dispersion curves from the V_S models. The estimated error in V_{S30} , which includes some effects of the lateral velocity variability beneath the testing arrays, is about 25 m/s. This is computed based on the sum of the following rounded to the nearest 5 m/s: an estimated error of 3% from the realistic assumed layer Poisson's ratios in the model, 1% error from the realistic assumed layer densities in the model, 4% for the variation in V_{S30} associated with non-uniqueness, and the 0.5 % COV in V_{R40} from the passive-source surface wave dispersion data.

Interestingly, V_{S30} estimated from V_{R40} using the Brown et al., 2000 relationship ($V_{S30} \cong 1.045V_{R40}$, assuming V_{R40} represents the fundamental mode Rayleigh wave) is 329 m/s, about 10 % higher than that estimated from the V_S model. In our experience, $V_{S30} \cong V_{R40}$ for sites with a shallow saturated zone, which would result in an estimated $V_{S30} = 315$ m/s, 5% higher than that estimated from the V_S model. Although the Rayleigh wave dispersion data was modeled using the effective mode approximation, the dispersion curve at 40 m wavelength is fundamental mode

(Figure 6) and; therefore, the V_{R40} relationship for estimating V_{S30} is still valid. Note that V_S models should always be used to estimate V_{S30} when possible and we are only documenting the performance of V_{S30} estimates based on V_{R40} in the event such an approach is needed in the future.

The V_S models presented as Figure 6 and Table 2 only explain the highest frequency component of the observed HVSR peaks (Figure 7). Figure 8 presents an example V_S model with another increase in V_S at approximately 80 m depth (below depth of investigation of surface wave sounding) to demonstrate that a deeper geologic structure gives rise to the lower frequency component of the observed HVSR response.



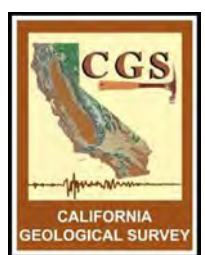
File Name: 18045_48906
Date: 5/29/2018

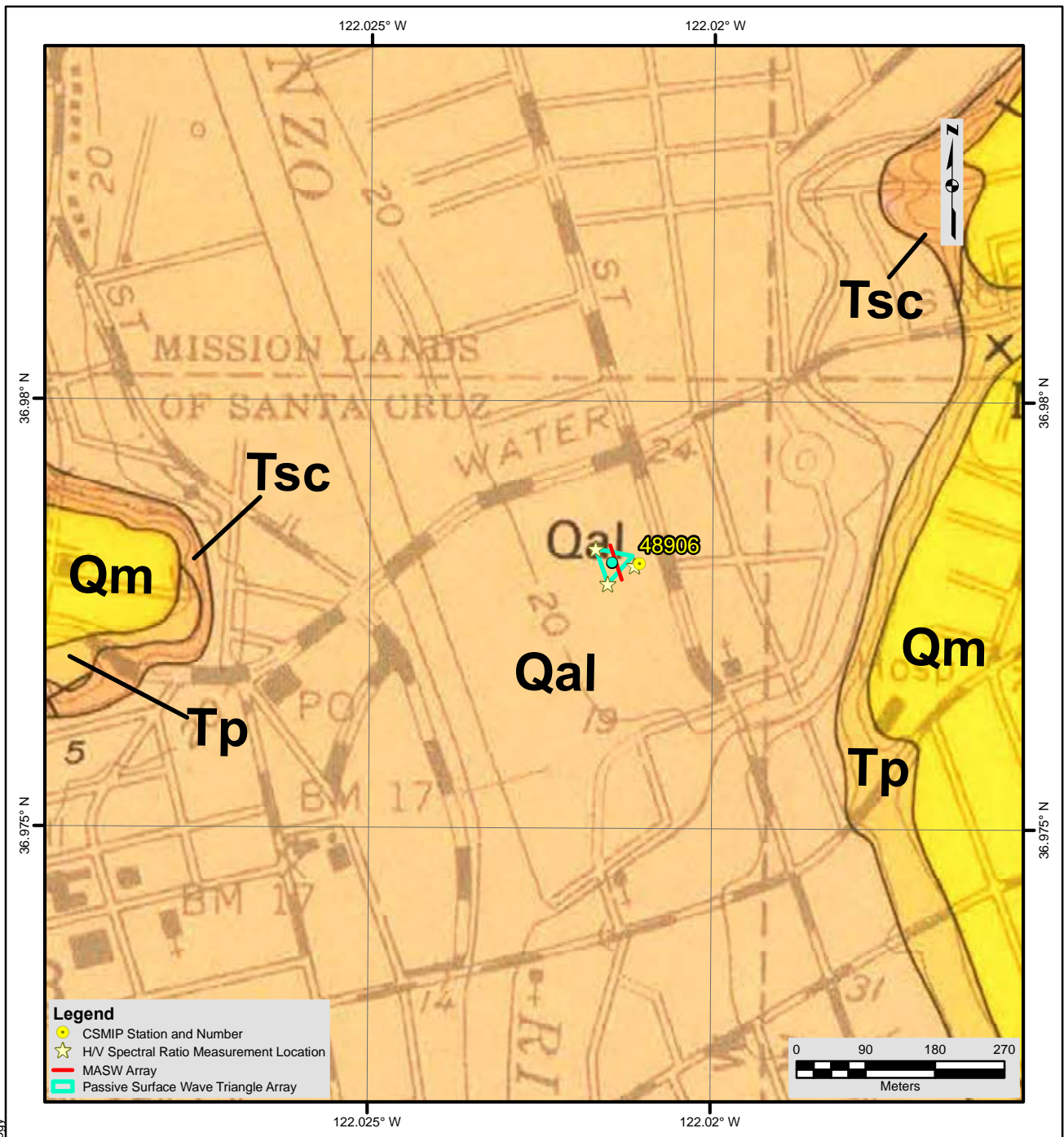
- Legend**
- ★ CSMIP Station and Number
 - ★ H/V Spectral Ratio Measurement Location
 - MASW Array
 - Passive Surface Wave Triangle Array

- NOTES:**
1. WGS 1984 Coordinate System
 2. Image Source: Esri, DigitalGlobe, GeoEye, Earthstar Geographics, CNES/Airbus DS, USDA, USGS, AEX, Getmapping, Aerogrid, IGN, IGP, swisstopo, and the GIS User Community



**FIGURE 1
SITE MAP
CE • 48906**





Description of Geologic Map Units

Qal = Quaternary (Holocene) Alluvium
 Qm = Quaternary (Pleistocene) Marine Terrace Deposit
 Tp = Tertiary (Upper Miocene and Pliocene) Purisima Formation
 Tsc = Tertiary (Upper Miocene) Santa Cruz Mudstone

NOTES:

1. WGS 1984 Coordinate System
2. Geologic Map and Sections of the Felton-Santa Cruz Area, Santa Cruz County, California by USGS 1954, 1955, 1960-69

File Name: 18045_48906-Geology

Date: 5/29/2018



**FIGURE 2
 GEOLOGIC MAP
 CE • 48906**





Seismic Station CE.48906



Looking towards HVSr measurement location 1 and seismic station

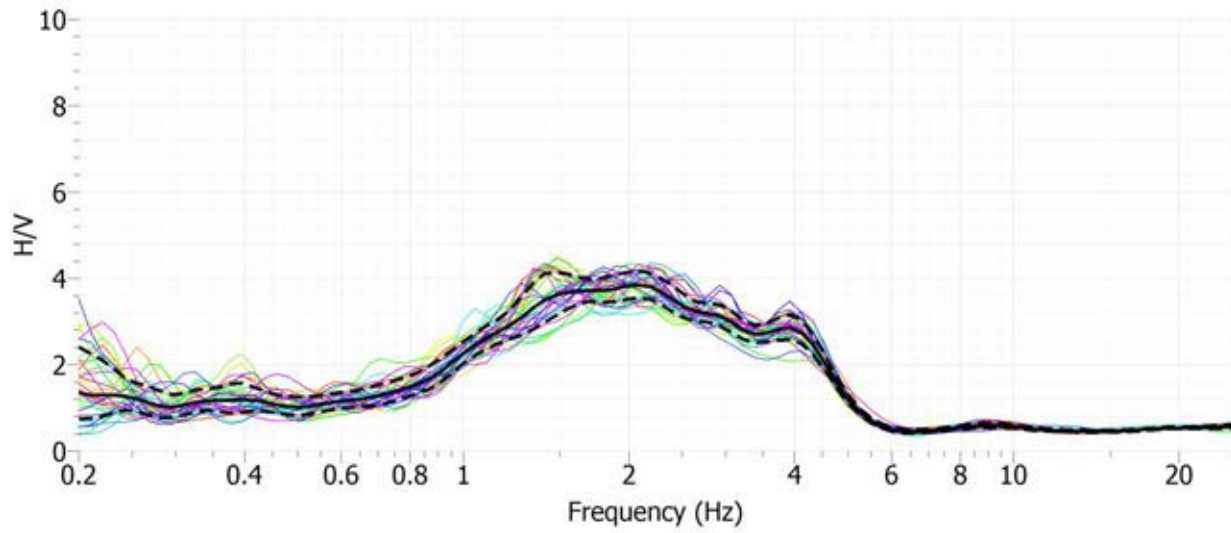


Looking southwest at microtremor Array 1

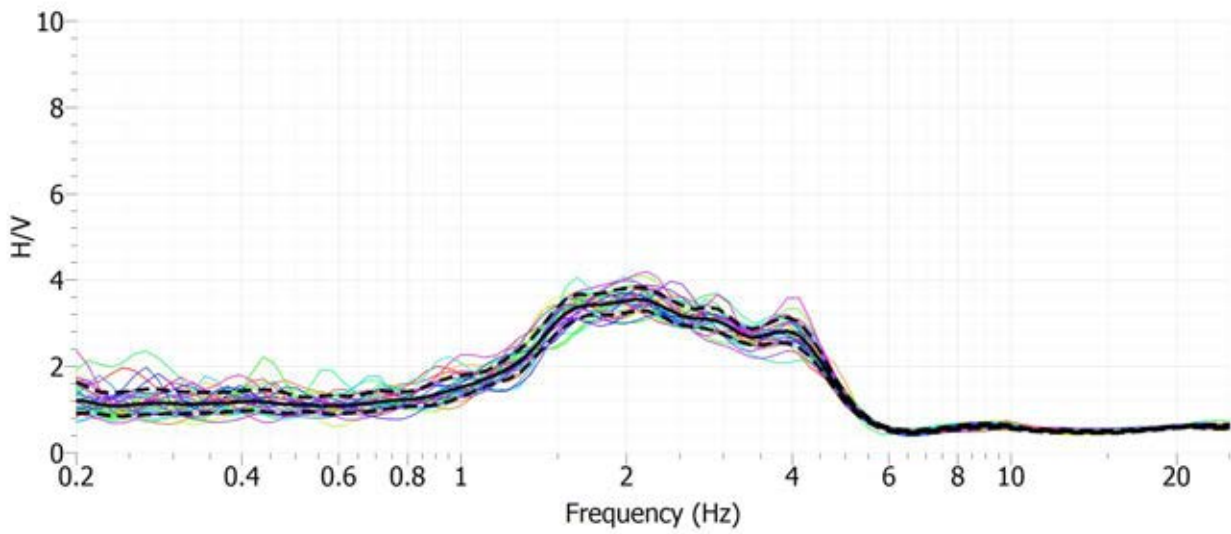


Looking northwest along MASW Array 2

Figure 3 Site CE.48906 Photographs

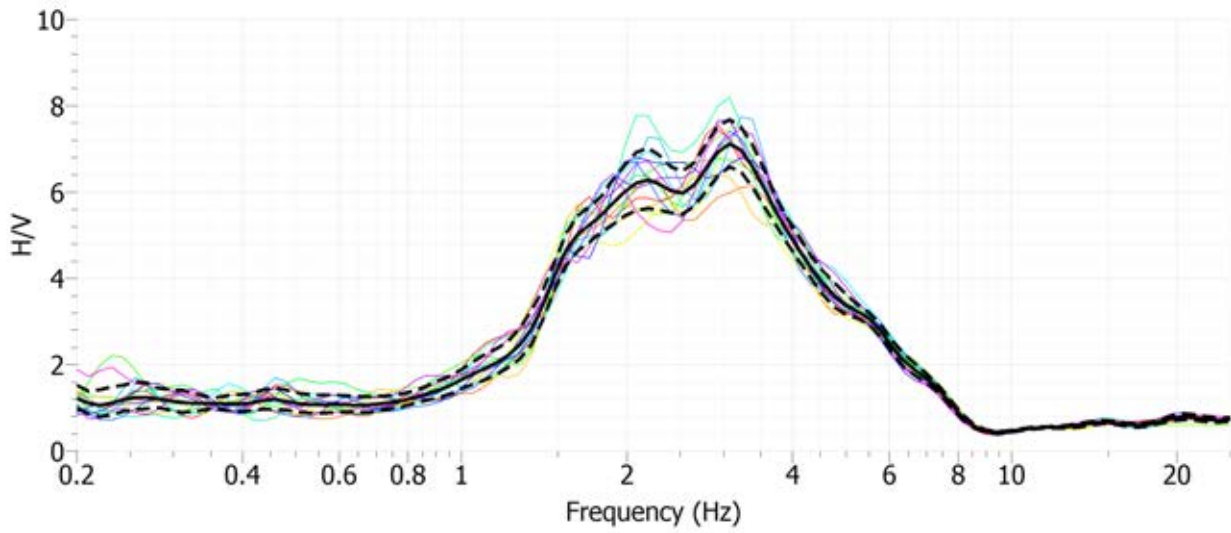


Site CE.48906, HVSR Location 1, Nanometrics Trillium Compact Sensor

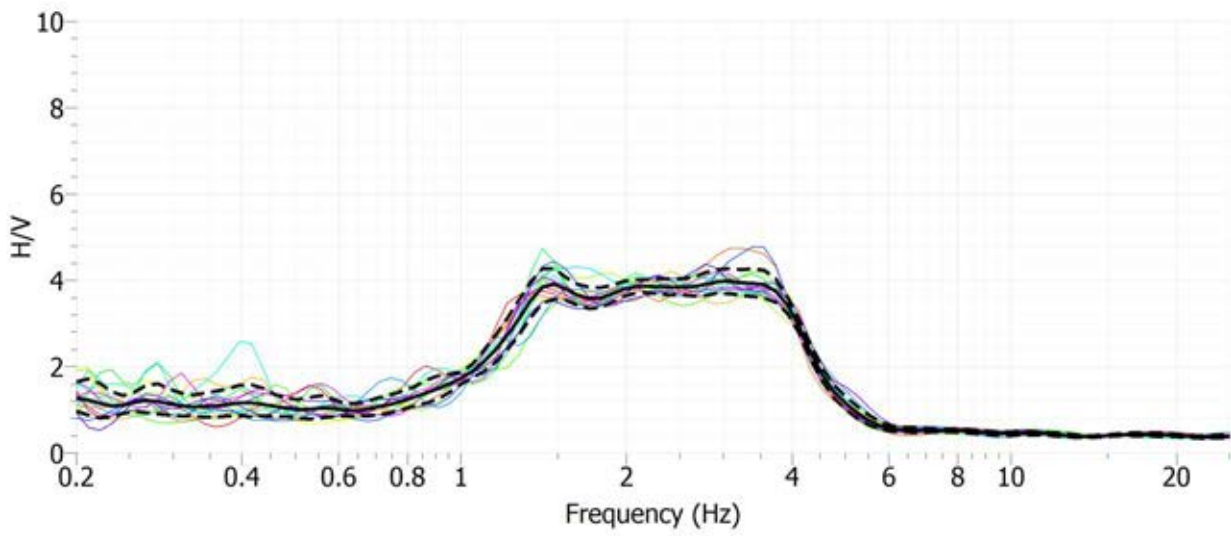


Site CE.48906, HVSR Location 1, MOHO Tromino ENGR Sensor

Figure 4 H/V Spectral Ratio of Ambient Vibration Data – Measurement Location 1, Site CE.48906



Site CE.48906, HVSr Location 2, MOHO Tromino ENGR Sensor



Site CE.48906, HVSr Location 3, MOHO Tromino ENGR Sensor

Figure 5 H/V Spectral Ratio of Ambient Vibration Data – Measurement Locations 2 and 3, Site CE.48906

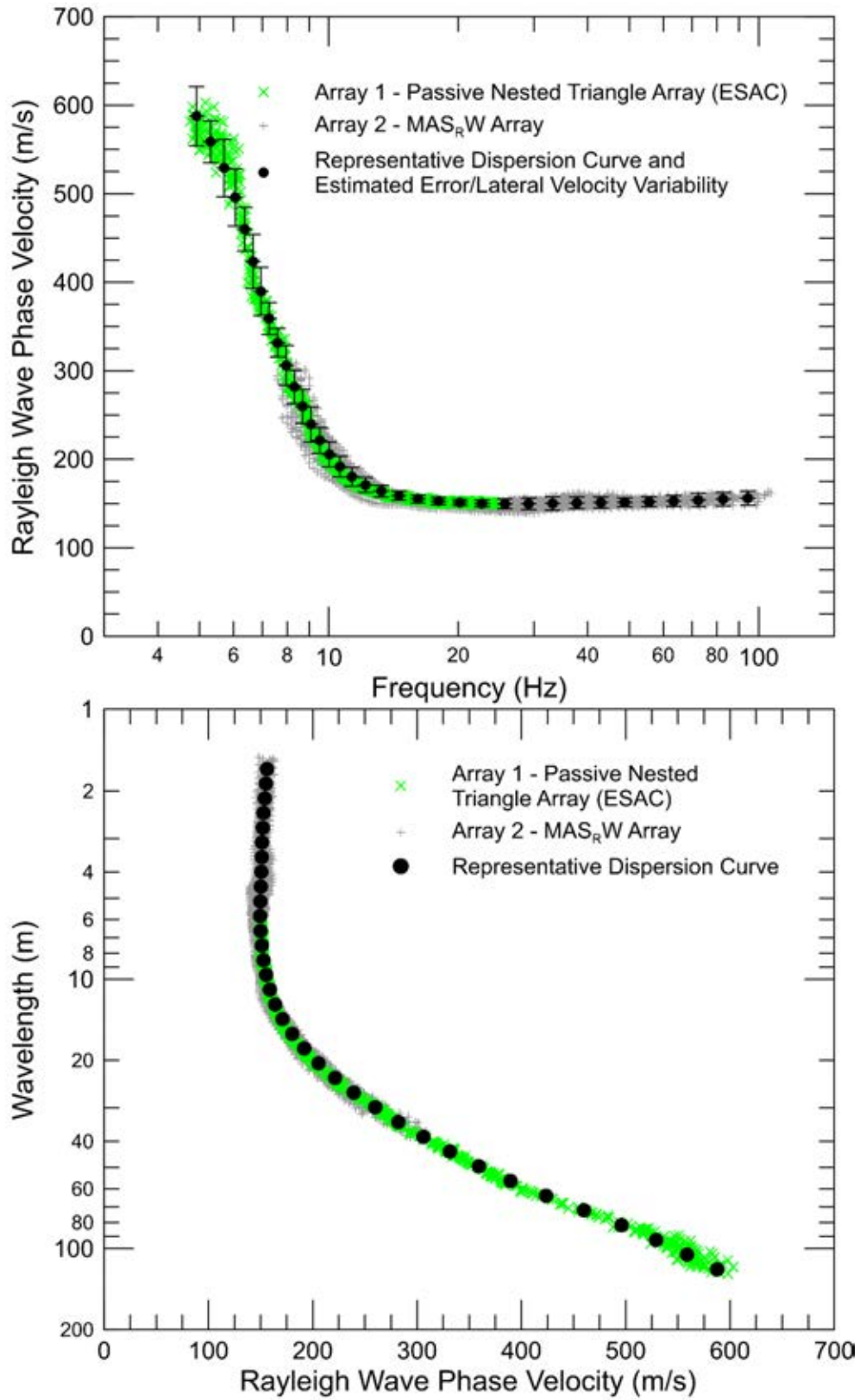


Figure 6 CE.48906 – Rayleigh wave dispersion curves derived from active- and passive-source surface wave data

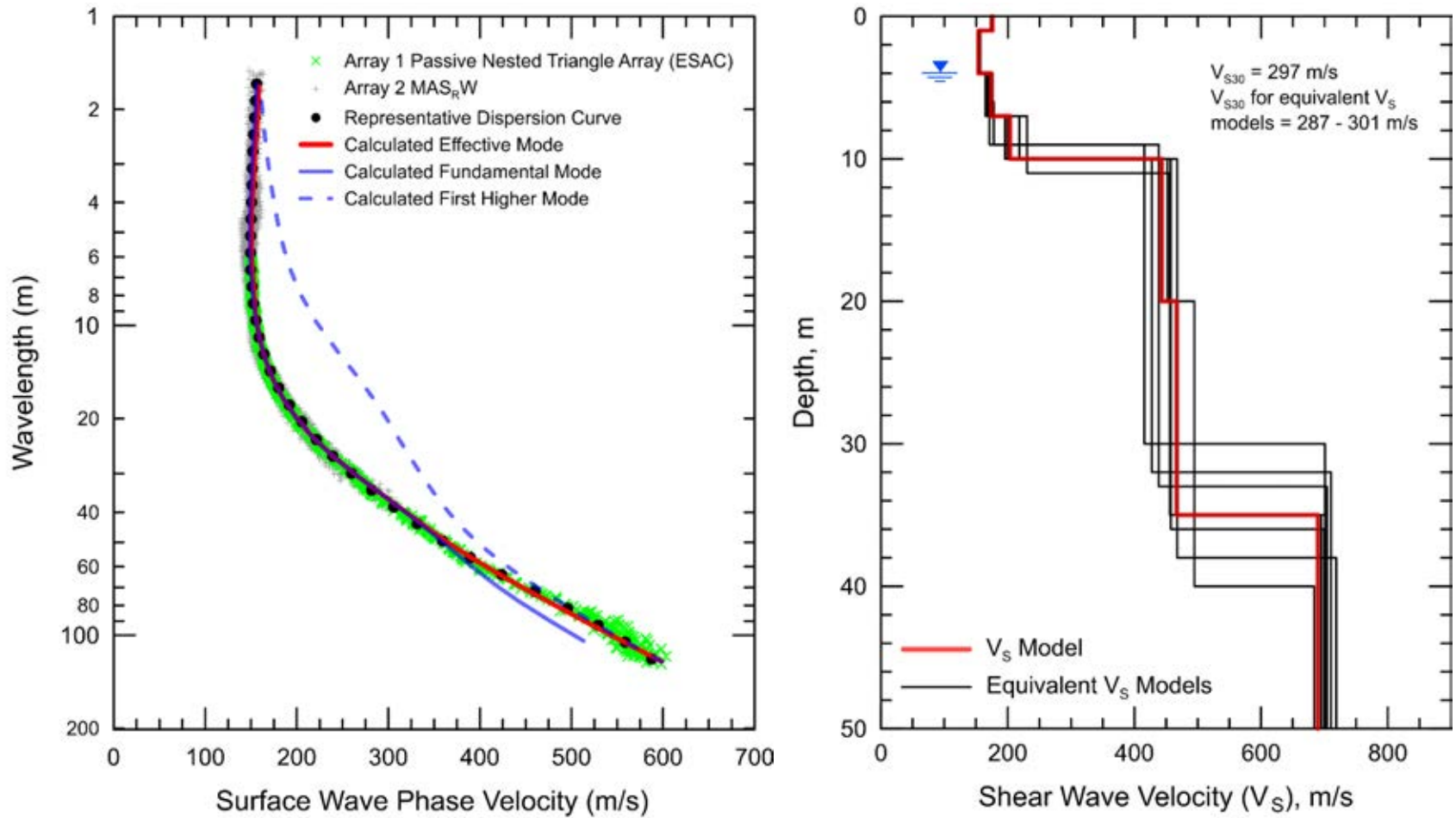
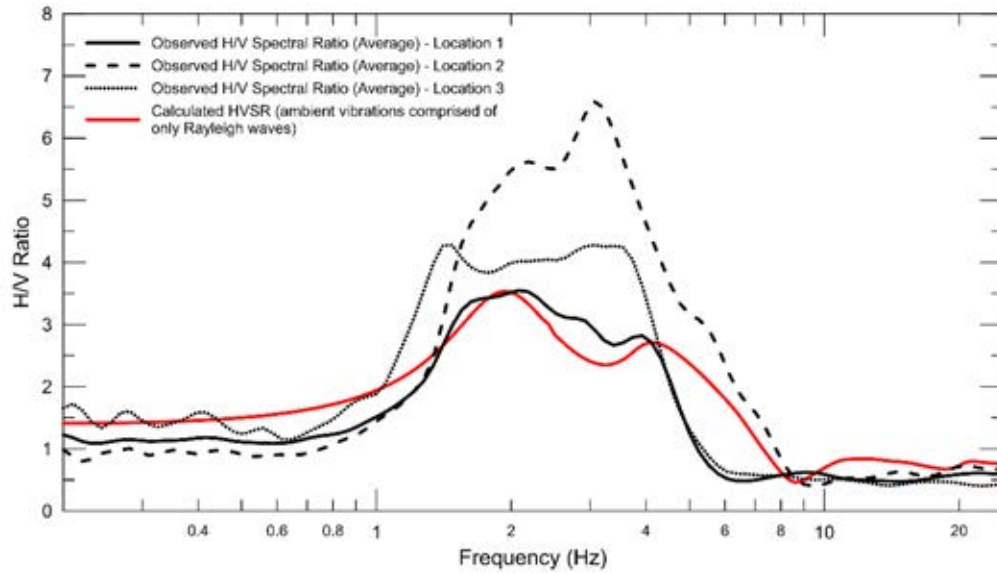
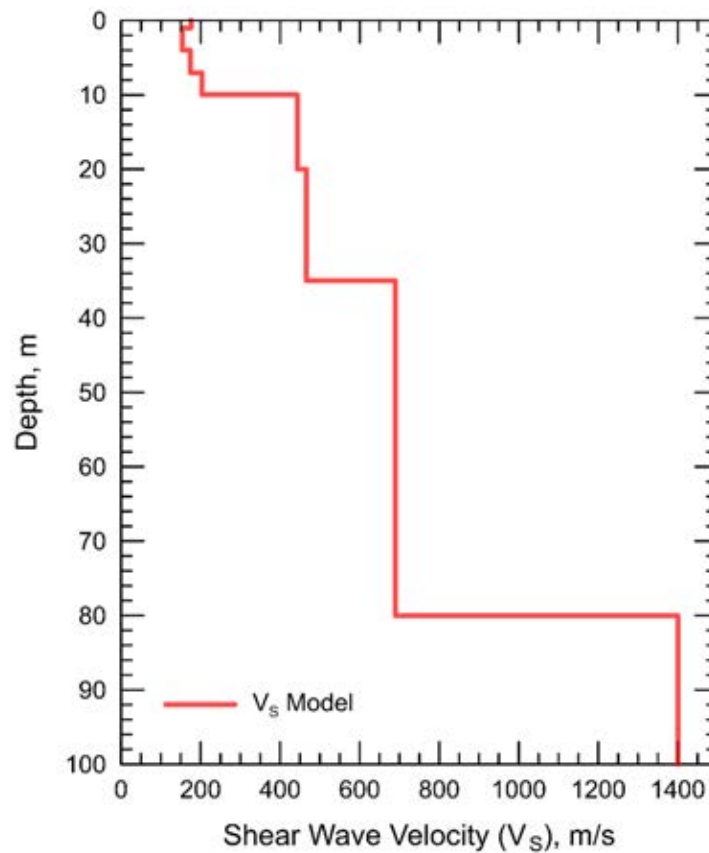


Figure 7 CE.48906 - Field, representative and calculated surface wave dispersion data (left) and associated V_s models (right)



Site CE.48906, Calculated HVSR Response (Rayleigh Wave Noise Field) for V_S Model Shown Below



V_S Model Modified to Better Fit Observed HVSR Data

Figure 8 V_S Model Extended to 80 m Depth to Fit Low Frequency HVSR Peak, Site CE.48906

Report

Geophysical Site Characterization

SMIP Station CE.57203

Station Name: Gilroy – Hwy 101 & Cohansey

Location: St. Louise Regional Hospital, 9400 No Name Uno, Gilroy, California

Latitude: 37.0355

Longitude: -121.5714

V_{s30}: 323 m/s

Estimated Error in V_{s30}: ± 30 m/s

NEHRP Site Class: D

Geomatrix Code: IHD

HVSR Peak Frequency: 0.5 Hz, possible secondary peak at about 0.7 Hz

Site Geology: Site located on Holocene alluvium (Figure 2) over 4 km from nearest outcrop of Franciscan complex greenstone. Site likely on deep basin of valley sediments over bedrock. Calaveras Fault Zone located about 5 km east of the site.

Site Conditions: Suburban site with traffic noise from nearby roads, specifically Hwy 101 to west. Flat terrain in site vicinity.

Geophysical Methods Utilized: MAS_RW, array microtremor, HVSR

Geophysical Testing Arrays:

1. Array 1: 48 channel “L” shaped array utilizing 4.5 Hz vertical geophones spaced 4.5 m apart for lengths of 90 m and 121.5 m on the SE to NW and SW to NE legs, respectively, used to acquire passive surface wave data (Figure 1).
2. Array 2: 48 channel MAS_RW array utilizing 4.5 Hz vertical geophones spaced 1.5 m apart for a length of 70.5 m (Figure 1), forward and reverse shot locations with multiple source offsets (1.5 m to 27.5 m on the high end and 30 m on the low end of the array) and multiple interior source locations. The 4-lb hammer and 12-lb sledgehammer were used at 1.5 m offset source locations and interior source locations and the AWD was used for all offset source locations.
3. One HVSR location, near seismic station (Figure 1).

Table 1 Location of Geophysical Testing Arrays

Location	Latitude	Longitude
Seismic Station	37.0355	-121.5714
Array 1 Passive, Northwest end of Array	37.03575	-121.57310
Array 1 Passive, Corner of Array	37.03501	-121.57269
Array 1 Passive, Southeast end of Array	37.03546	-121.57144
Array 2 MASW, Southwest end of Array	37.03512	-121.57238
Array 2 MASW, Northeast end of Array	37.03538	-121.57165
HVSR Location 1	37.03547	-121.57140

Notes: 1) WGS84 Coordinate System (decimal degrees)

S-Wave Velocity Model:

Table 2 V_s Model

Depth to Top of Layer (m)	Layer Thickness (m)	S-Wave Velocity (m/s)	Inferred P-Wave Velocity (m/s)	Assumed Poisson's Ratio	Assumed Density (g/cm ³)
0	1	180	337	0.300	1.80
1	2	251	470	0.300	1.90
3	3.5	293	548	0.300	1.95
6.5	7.5	400	749	0.300	2.00
14	11	316	1600	0.480	1.95
25	15	362	1650	0.475	2.00
40	25	406	1650	0.468	2.00
65	>15	571	1750	0.441	2.05

Notes: 1) Depth to groundwater constrained at 14 m depth based on seismic refraction data.
 2) Depth of investigation is about 80 m.
 3) Bottom layer is a half space.

Observations/Discussion:

H/V Spectral Ratio

HVSR data was collected for at least a 60-minute duration at a single location near the seismic station using both a Nanometrics Trillium Compact (Trillium) and MOHO Tromino ENGR seismograph. The HVSR data from the Trillium reveals a 0.5 Hz peak and a possible secondary peak at 0.7 Hz (Figure 4). These peaks are likely associated with geologic structures at a depth greater than the expected depth of investigation of the surface wave sounding. The Tromino does not detect these HVSR peaks, which is expected because the instrument is not designed to reliably detect HVSR peaks associated with deep geologic structures.

Array Microtremor Data

Noise conditions at the site (multi-directional noise sources) appeared sufficient for successful application of passive surface wave techniques. About 60 minutes (121, 30 second seismic records) of ambient vibration data were acquired into L-shaped Array 1 (Figure 1). The ESAC technique was used to extract surface wave dispersion data from the ambient vibration data. To better characterize error, dispersion curves were generated from 15-minute time segments of the ambient vibration data and the complete data set. The minimum and maximum Rayleigh wavelength extracted from Array 1 are about 16 and 160 m, respectively.

MASW Data

MASW data acquisition was conducted using a 70.5-m long receiver array (Array 2) as shown on Figure 1. Rayleigh wave dispersion data were interpreted from 20 MAS_RW seismic records collected at 15 different source locations using 4-lb hammer, 12-lb sledgehammer and AWD energy sources. The maximum source offset was either 27.5 or 30 m from each end of the array. Using the 20 seismic records and variable receiver offset ranges, over 90 dispersion curves were extracted and combined for analysis. To minimize near field effects, the maximum Rayleigh wavelength data extracted from the MAS_RW data set was set equal to the lesser of one times the distance between the source and midpoint of the active receiver array or 50 m (high noise site due to nearby Hwy 101). It was very difficult to extract fundamental mode Rayleigh wave data at wavelengths less than 10 m due to dominant higher mode energy at high frequencies. Typically, a multi-mode modeling approach would be utilized with such a data set; however, the higher mode propagation also appeared complex. With significant effort, apparent fundamental mode Rayleigh wave data was extracted at smaller wavelengths. Love wave or radial component Rayleigh wave data might have been useful at this site but were not acquired. There is nominally about 30 m/s of scatter in MAS_RW dispersion data, which is likely in part due to lateral velocity variation. The minimum Rayleigh wavelength phase velocity data extracted from a 48-channel MAS_RW receiver gather was in the 9 to 19 m range. Reducing data from smaller hammer sources using a limited offset range receiver gather (i.e. less active geophones) allowed for extraction of surface wave dispersion data to a minimum wavelength of about 2.5 m.

Modeling

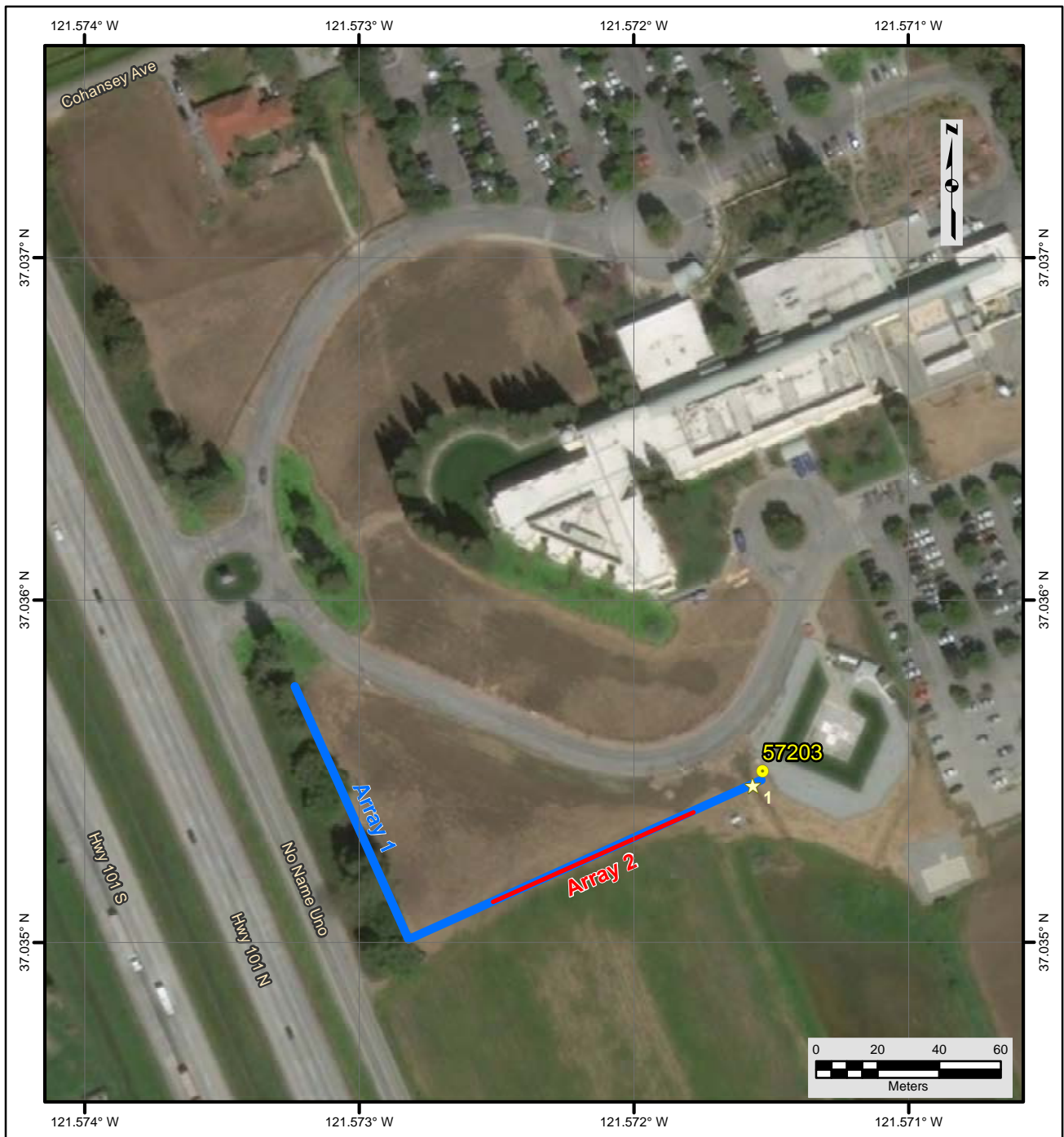
Surface wave dispersion data from active and passive surface wave data sets are in good agreement over the approximate 16 to 50 m overlapping wavelength range (Figure 5). The average phase velocity of a 40-m wavelength Rayleigh wave (V_{R40}) is 303 m/s with a coefficient of variation (COV) of 0.5% from ESAC analysis of the ambient vibration data collected along Array 1. Average V_{R40} is 304 m/s with a coefficient of variation (COV) of 3.3 % from MASW analysis of active-source seismic data collected along Array 2. The combined data set (similar weight given to active-and passive-source data) yields an average V_{R40} of 303 m/s with a coefficient of variation (COV) of 2.9 %. Representative dispersion curves were generated for each surface wave data set using a moving average, polynomial curve fitting routine. These individual representative dispersion curves were combined and a composite representative dispersion curve was generated for the combined data set for modeling. Error bars for the composite representative dispersion curve were estimated based on the scatter in the dispersion data.

The composite representative dispersion curve was inverted using an iterative non-linear least squares inversion routine and fundamental mode Rayleigh wave assumption to derive V_S models. Realistic estimates of Poisson's ratio and density were used to make models as accurate as possible. High Poisson's ratio, saturated sediments were constrained at a depth of about 13 to 17 m with $V_P > 1,600$ m/s based on interactive, layer-based analysis of seismic refraction first arrival data. Poisson's ratio of the saturated sediments was set to gradually decrease with depth as the sediments became stiffer, a common observation in borehole velocity logs. Model layer thicknesses increased with depth to reflect the reduction in model resolution with depth. Several V_S models were developed with almost identical calculated dispersion curves to demonstrate the non-uniqueness inherent in the inversion of surface wave dispersion data; especially at layer boundaries where an abrupt change in seismic velocity occurs or associated with high velocity layers or velocity inversions. The V_S models for this site have a velocity inversion; whereby, there is significant non-uniqueness associated with the thickness and velocity of the low velocity layer and overlying high velocity layer. Additionally, there is significant non-uniqueness associated with the velocity and depth of the half space. A total of 15 V_S models were developed to demonstrate the non-uniqueness but a better modeling approach would have been to use a global inversion routine to develop an ensemble of several hundred models that fit the observed dispersion data.

Results

V_S models are presented as Figure 6. Surface wave depth of investigation is about 80 m based on $\lambda_{max}/2$. The 0.5 and 0.7 Hz HVSR peaks are associated with geologic structures deeper than the depth of investigation.

V_{S30} is 323 m/s (NEHRP Site Class D). The average V_S of the upper 80 m (V_{S80}) is 384 m/s. The estimated error in V_{S30} , which includes some effects of the lateral velocity variability beneath the testing arrays, is about 30 m/s. This is computed based on the sum of the following rounded to the nearest 5 m/s: an estimated error of 3% from the realistic assumed layer Poisson's ratios in the model, 1% error from the realistic assumed layer densities in the model, 2% for the variation in V_{S30} associated with non-uniqueness, and the 3% COV in V_{R40} from the active and passive-source surface wave dispersion data. V_{S30} is between 319 and 324 m/s for the equivalent V_S models. Interestingly, V_{S30} estimated from V_{R40} using the Brown et al., 2000 relationship ($V_{S30} \cong 1.045V_{R40}$, assuming V_{R40} represents the fundamental mode Rayleigh wave) is 317 m/s, only 2% different from that estimated from the V_S model.



File Name: 18045_57203
Date: 5/29/2018

Legend

- CSMIP Station and Number
- ★ H/V Spectral Ratio Measurement Location
- MASW Array
- Passive Surface Wave Array

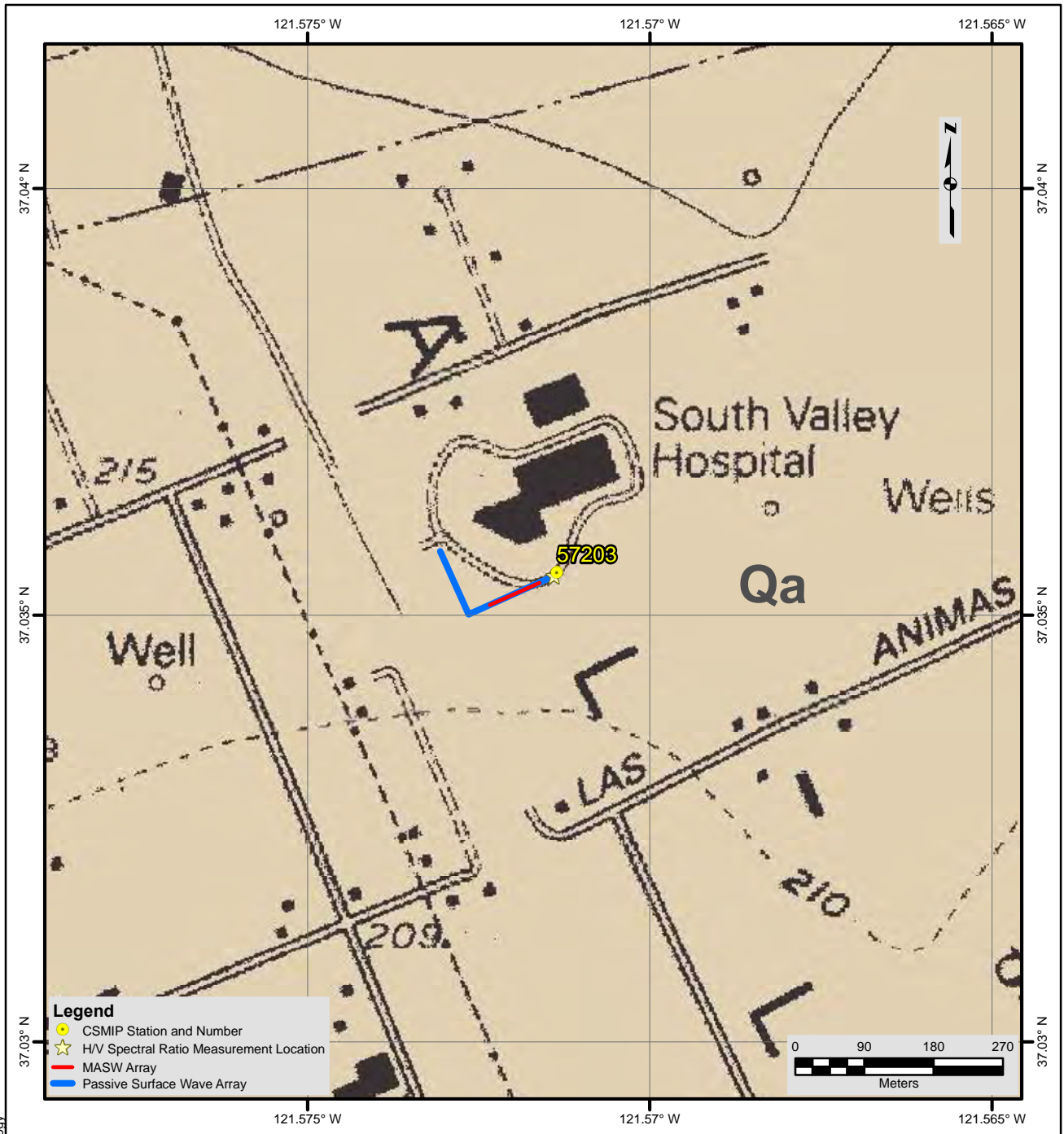
NOTES:

1. WGS 1984 Coordinate System
2. Image Source: Esri, DigitalGlobe, GeoEye, Earthstar Geographics, CNES/Airbus DS, USDA, USGS, AEX, Getmapping, Aerogrid, IGN, IGP, swisstopo, and the GIS User Community



**FIGURE 1
SITE MAP
CE-57203**





Description of Geologic Map Units

Qa = Quaternary (Holocene) Alluvial Gravel, Sand and Clay soil of valley areas

NOTES:

1. WGS 1984 Coordinate System
2. Geologic Map of the Gilroy Quadrangle, Santa Clara County, California by Thomas W Dibblee, Jr., 2005

File Name: 18045_57203-Geology
Date: 5/29/2018



**FIGURE 2
GEOLOGIC MAP
CE • 57203**





Looking northeast at Seismic Station CE.57203, northeast end of Array 1, and HVSR measurement location 1



HVSR measurement location 1

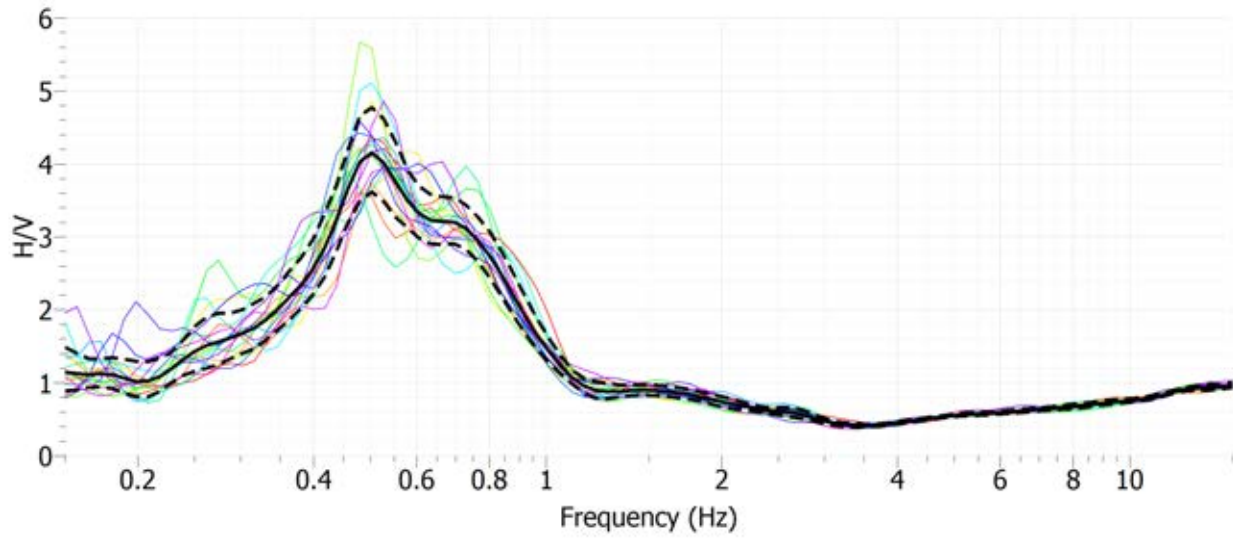


Looking northeast along MASW Array 2

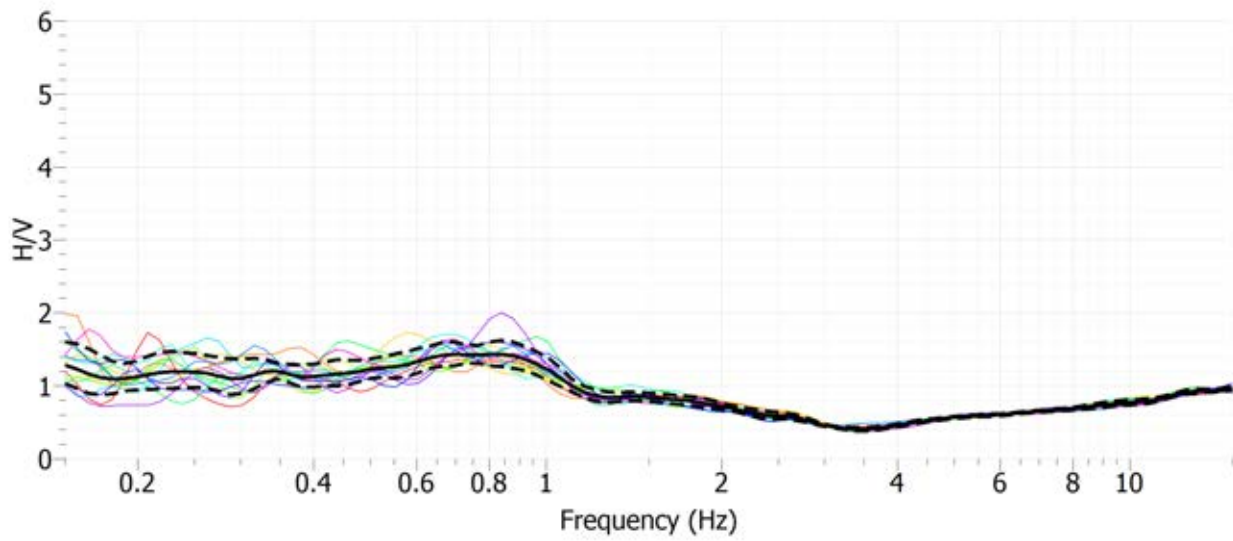


Looking northeast along SW-NE leg of microtremor Array 1

Figure 3 Site CE.57203 Photographs



Site CE.57203, HVSr Location 1, Nanometrics Trillium Compact Sensor



Site CE.57203, HVSr Location 1, MOHO Tromino ENGR Sensor

Figure 4 H/V Spectral Ratio of Ambient Vibration Data – Measurement Location 1, Site CE.57203

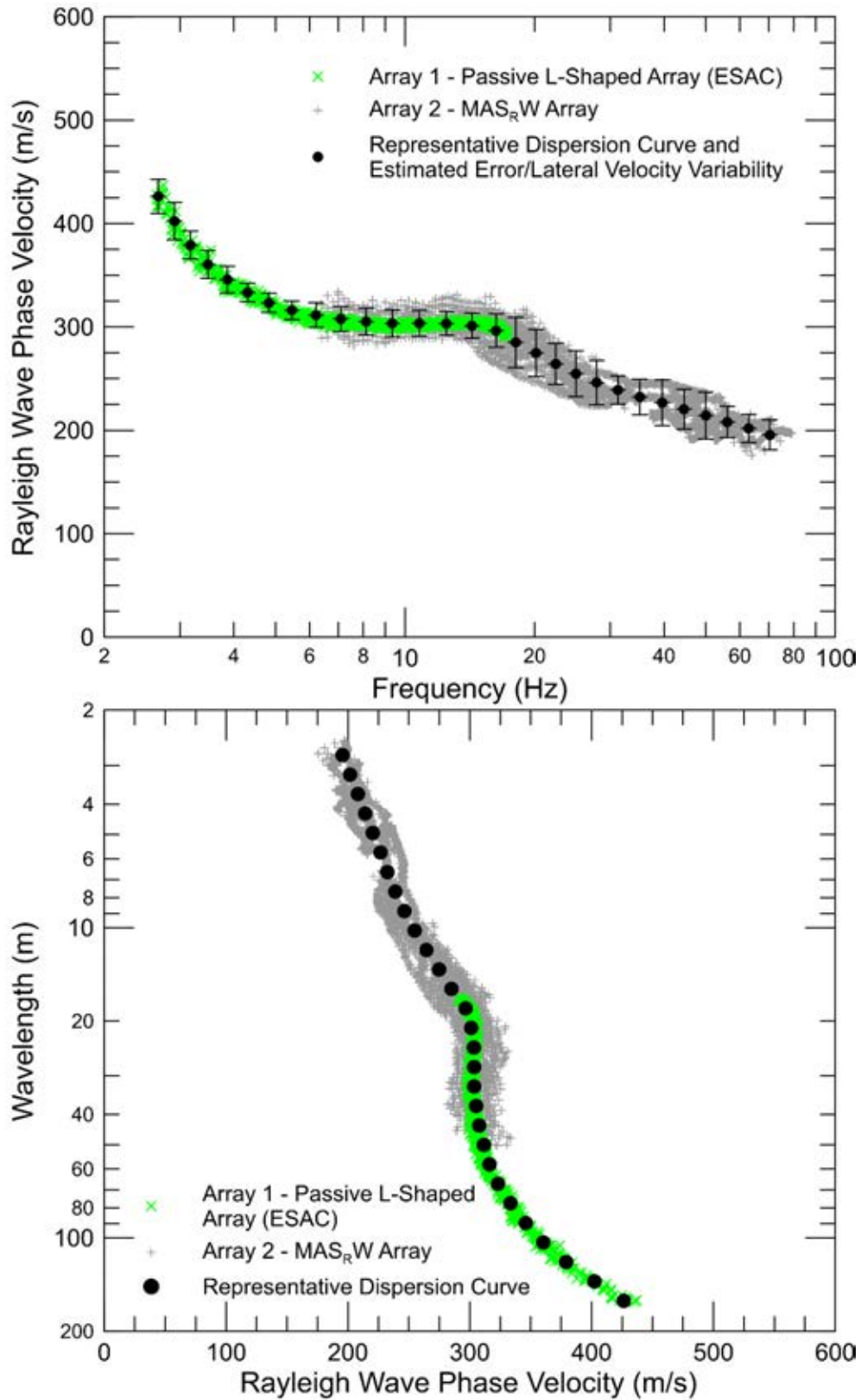


Figure 5 CE.57203 – Rayleigh wave dispersion curves derived from active- and passive-source surface wave data

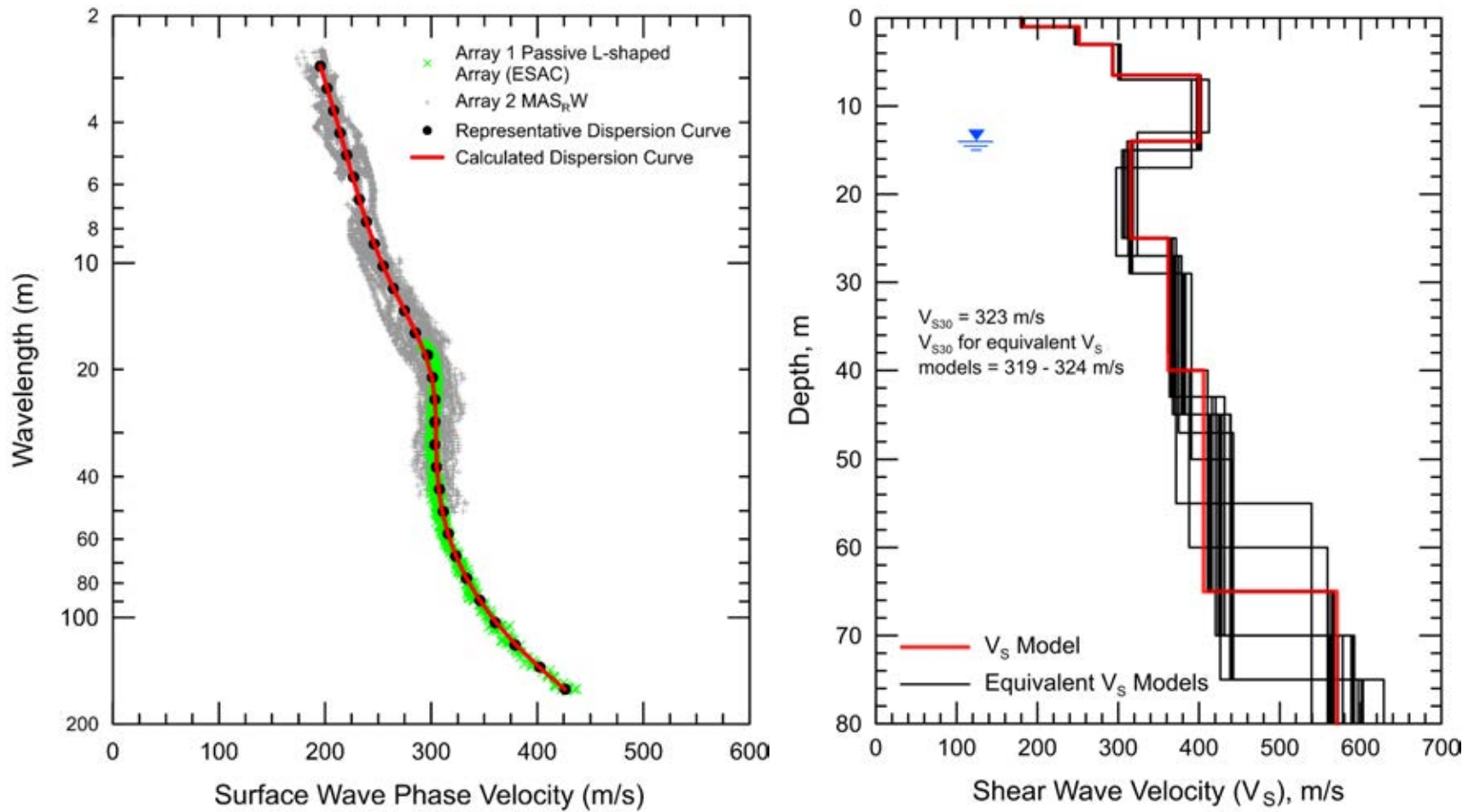


Figure 6 CE.57203 - Field, representative and calculated surface wave dispersion data (left) and associated V_s models (right)

Report Geophysical Site Characterization SMIP Station CE.57218

Station Name: San Jose – Hwy 101 & Metcaff Rd

Location: PG&E Metcalf Transmission Substation, 150 Metcalf Rd., San Jose, California

Latitude: 37.22410

Longitude: --121.74166

V_{s30}: 445 m/s

Estimated Error in V_{s30}: ± 25 m/s

NEHRP Site Class: C

Geomatrix Code: AHB

HVSR Peak Frequency: Highly variable from no peaks to possible weak peak at 1.6 Hz and multiple weak peaks between 4.5 and 16 Hz.

Site Geology: Site located near Coyote Creek channel on Holocene alluvium; gravel, sand, and clays (Figure 2). Site located less than 300 m from Coyote Creek fault and 1 km from Metcalf fault. Outcrops of Jurassic/Cretaceous serpentinite (coast ophiolite complex) outcrops located about 180 m southeast, 300 m northeast and 1 km southwest of seismic station (Figure 2).

Site Conditions: Rural site with traffic noise from nearby Hwy 101. Flat terrain in immediate site vicinity.

Geophysical Methods Utilized: MAS_RW, MAS_LW, array microtremor, HVSR

Geophysical Testing Arrays:

1. Array 1: 48 channel “L” shaped array utilizing 4.5 Hz vertical geophones spaced 6 m apart used to acquire passive surface wave data. The W-E and S-N linear segments of array have lengths of 144 and 138 m, respectively (Figure 1).
2. Array 2: 48 channel MAS_LW array utilizing 4.5 Hz horizontal geophones spaced 2 m apart for a length of 94 m, forward and reverse shot locations with multiple source offsets (2 to 30 m at both ends of array) and multiple interior source locations. Portable aluminum shear wave source with 12- and 20-lb sledgehammers used as the energy source(Figure 1).
3. Array 2: 48 channel MAS_RW array utilizing 4.5 Hz vertical geophones spaced 2 m apart for a length of 94 m, forward and reverse shot locations with multiple source offsets (2 m to 30 m at both ends of array) and multiple interior source locations. Energy sources consisted of a 4-lb hammer, 12-lb sledgehammer and accelerated weight drop (AWD). Same location as MAS_LW array.

4. Array 3: 48 channel MAS_LW array utilizing 4.5 Hz horizontal geophones spaced 2 m apart for a length of 94 m, forward and reverse shot locations with multiple source offsets (2 to 24 m or 30 m at either end of array) and multiple interior source locations. Primary energy source was a portable aluminum shear wave source with 12 and 20-lb sledgehammers (Figure 1).
5. Five HVSR measurement locations along Array 1(Figure 1).

Table 1 Location of Geophysical Testing Arrays

Location	Latitude	Longitude
Seismic Station (relocated)	37.22410	-121.74166
Array 1 Passive, Northwest of Array	37.22335	-121.74281
Array 1 Passive, Corner of Array	37.22273	-121.74138
Array 1 Passive, Northeast of Array	37.22356	-121.74022
Array 2 MASW, Northwest end of Array	37.22326	-121.74260
Array 2 MASW, Southeast end of Array	37.22286	-121.74167
Array 3 MASW, Northwest end of Array	37.22455	-121.74252
Array 3 MASW, Southeast end of Array	37.22393	-121.74178
HVSR Location 1	37.22335	-121.74281
HVSR Location 2	37.22306	-121.74214
HVSR Location 3	37.22273	-121.74137
HVSR Location 4	37.22315	-121.74080
HVSR Location 5	37.22357	-121.74027

- Notes: 1) WGS84 Coordinate System (decimal degrees)
 2) Location of seismic station moved to reflect actual approximate location.

S-Wave Velocity Model:

Table 2 Array 2 - V_S Model (Inversion of Love Wave Dispersion Data)

Depth to Top of Layer (m)	Layer Thickness (m)	S-Wave Velocity (m/s)	Assumed Density (g/cm ³)
0	1	141	1.70
1	5	209	1.80
6	5	438	1.90
11	6	530	2.00
17	7	612	2.05
24	>6	681	2.10

- Notes: 1) Depth of investigation is about 30 m.
 2) Bottom layer is a half space.

Table 3 Array 3 - V_s Model (Inversion of Love Wave Dispersion Data)

Depth to Top of Layer (m)	Layer Thickness (m)	S-Wave Velocity (m/s)	Assumed Density (g/cm ³)
0	1.5	173	1.75
1.5	2.5	250	1.90
4	4	351	1.95
8	6	449	2.00
14	9	608	2.05
23	>7	769	2.10

Notes: 1) Depth of investigation is about 30 m.
2) Bottom layer is a half space.

Observations/Discussion:

H/V Spectral Ratio

HVSR data was collected for over 2 hours at one location (HVSR location 2) using a Nanometrics Trillium Compact seismograph as shown in Figure 1 and Table 1. HVSR data was collected for 20 minutes at four additional locations (HVSR locations 1, 3, 4, and 5) using a MOHO Tromino ENGR (Tromino) seismograph as shown in Figure 1 and Table 1. About 30 min of ambient vibration data were acquired at each HVSR Location. HVSR data is highly variable. HVSR locations 4 and 5 near an outcrop of Mesozoic Coast Range Ophiolite have no clear peaks. HVSR locations 1 to 3 have a possible weak HVSR peak in the 1.5 to 1.6 Hz range and multiple, weak, high frequency peaks between 4.5 and 16 Hz (Figures 4 and 5).

Array Microtremor Data

Array microtremor data was acquired along L-shaped Array 1 (Figure 1). Over 1.5 hours of ambient vibration data (189, 30-second seismic records) were acquired into this array. Due to probable, significant lateral velocity variation, based on an outcrop of Coast Range Ophiolite near one leg of the array, and complex Rayleigh wave propagation, this array did not yield usable Rayleigh wave dispersion data and was not used for site characterization.

MASW Data

Rayleigh and Love wave MASW data acquisition was originally conducted along a 94-m long receiver array (Array 2). Due to suspected lateral variability at the site, arrangements were made to test on the PG&E substation, closer to the seismic station. Due to weather, there was only sufficient time to acquire Love wave MASW data along a 94-m long receiver array (Array 3).

Rayleigh wave dispersion data were interpreted from 14 MAS_RW seismic records collected at 9 different source locations along Array 2 using 4-lb hammer, 12-lb sledgehammer, and AWD energy sources. Maximum source offset was 1.5 m at the northwest end of the array and 10 m at the southeast end of the array. Review of Rayleigh wave (MAS_RW) data indicated that the first higher mode may be dominant at low frequencies and it was not possible to extract reliable

dispersion data at wavelengths greater than 15 m. Because of the complex Rayleigh wave propagation, it was not possible to develop an acceptable Rayleigh wave dispersion curve over sufficient wavelength range for modeling.

Love wave dispersion data were interpreted from 9 MAS_LW seismic records collected at 9 different source locations along Array 2. Using the 9 seismic records and variable receiver offset ranges, over 60 dispersion curves were extracted from the Love wave seismic records and combined for analysis. To minimize near field effects, the maximum wavelength Love wave extracted from the MAS_LW data set was set equal to the lesser of 1.3 times the distance between the source and midpoint of the active receiver array or 80 m. There is nominally about 30 m/s of scatter in MAS_LW dispersion data, which is likely in part due to lateral velocity variation. The minimum wavelength Love wave phase velocity data extracted from a 48-channel MAS_LW receiver gather is in the 4 to 12 m range. Reducing data from smaller hammer sources using a limited offset range receiver gather (i.e. less active geophones) allowed for extraction of surface wave dispersion data to a minimum wavelength of about 1.7 m.

Love wave dispersion data were interpreted from 14 MAS_LW seismic records collected at 11 different source locations along Array 3. Using the 14 seismic records and variable receiver offset ranges, over 60 dispersion curves were extracted from the Love wave seismic records and combined for analysis. To minimize near field effects, the maximum wavelength Love wave extracted from the MAS_LW data set was set equal to the lesser of 1.3 times the distance between the source and midpoint of the active receiver array or 80 m. There is nominally about 40 to 50 m/s of scatter in MAS_LW dispersion data, which is likely in part due to lateral velocity variation. The Love wave dispersion data from Array 3 is generally noisier than that from Array 2 as data was acquired along this array during intermittent rain showers, whereby the wet ground and presence of transmission lines induced significant 60 Hz noise in the seismic records. The minimum wavelength Love wave phase velocity data extracted from a 48-channel MAS_LW receiver gather is in the 9 to 24 m range. Reducing data from smaller hammer sources using a limited offset range receiver gather (i.e. less active geophones) allowed for extraction of surface wave dispersion data to a minimum wavelength of about 4 m.

Surface Wave Modeling

The phase velocity of 50 and 55 m wavelength Love waves (V_{L50} and V_{L55}) average 380 and 402 m/s with a coefficients of variation (COV) of 2.6 and 2.2%, respectively, from 20 and 14 dispersion curves reduced from MAS_LW data collected along Array 2. V_{L50} and V_{L55} average 419 and 437 m/s with a coefficients of variation (COV) of 2.8 and 3.0%, respectively, from 22 and 20 dispersion curves reduced from MAS_LW data collected along Array 3.

Representative dispersion curves were generated for surface wave data set using a moving average, polynomial curve fitting routine. Error bars for the representative dispersion curve were estimated based on the scatter in the dispersion data. Figure 6 presents the Love wave dispersion data and representative dispersion curves for Arrays 2 and 3.

The representative dispersion curves were inverted using an iterative non-linear least squares (local search) inversion routine with the fundamental mode Love wave assumption to derive V_s models. Realistic estimates of density were used to make models as accurate as possible.

Poisson's ratio does not affect Love wave propagation. Model layer thicknesses generally increased with depth to reflect the reduction in model resolution with depth. Multiple V_S models were developed with almost identical calculated dispersion curves to demonstrate the non-uniqueness inherent in the inversion of surface wave dispersion data; especially at layer boundaries where an abrupt change in seismic velocity occurs or associated with high velocity layers or velocity inversions.

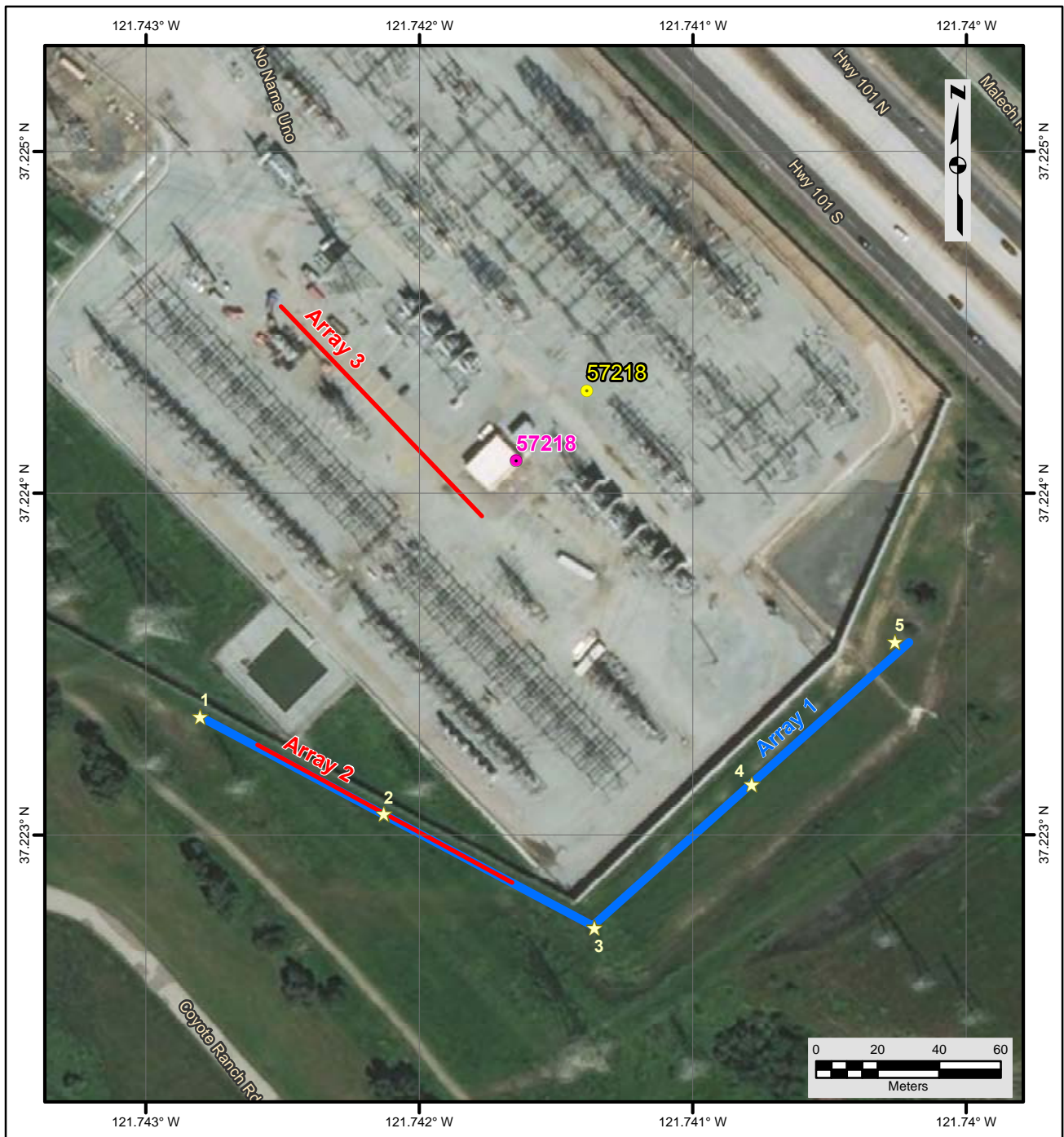
Results

V_S models from inversion of the Love wave dispersion data collected along Arrays 2 and 3 are presented as Figures 7 and 8, respectively. The V_S models selected for purpose of site characterization are presented in Tables 2 and 3, respectively. Surface wave depth of investigation is about 30 m based on $\lambda_{\max}/2.5$. Array 2 yielded better quality Love wave dispersion data; however, Array 3 should be used for site characterization as it is located closer to the seismic station.

V_{S30} from the V_S model developed from the Love wave data collected along Array 2 is 405 m/s (NEHRP Site Class C). The estimated error in V_{S30} , which includes some effects of the lateral velocity variability beneath the testing arrays, is about 25 m/s. This is computed based on the sum of the following rounded to the nearest 5 m/s: 1% error from the realistic assumed layer densities in the model, 2% for the variation in V_{S30} associated with non-uniqueness, and the 2.5% COV in V_{L50}/V_{L55} from the Love wave dispersion data.

V_{S30} from the V_S model developed from the Love wave data collected along Array 3 is 445 m/s (NEHRP Site Class C). The estimated error in V_{S30} , which includes some effects of the lateral velocity variability beneath the testing arrays, is about 25 m/s. This is computed based on the sum of the following rounded to the nearest 5 m/s: 1% error from the realistic assumed layer densities in the model, 2% for the variation in V_{S30} associated with non-uniqueness, and the 3% COV in V_{L50}/V_{L55} from the Love wave dispersion data.

A formal empirical relationship between Love wave phase velocity and V_{S30} has not been developed; however, we often find that V_{S30} is between V_{L50} and V_{L55} . At this site V_{L50} and V_{L55} are 380 and 402 m/s for Array 2 and 419 and 437 m/s for Array 3 with V_{L55} being closest to V_{S30} calculated from the velocity models. Such empirical relationships should not be used for site characterization; however, we use the scatter in V_{L50}/V_{L55} to estimate lateral velocity variability and/or error in the velocity models.



File Name: 18045_57218
Date: 5/29/2018

Legend

- Corrected CSMIP Station
- CSMIP Station and Number
- ★ H/V Spectral Ratio Measurement Location
- MASW Array
- Passive Surface Wave Array

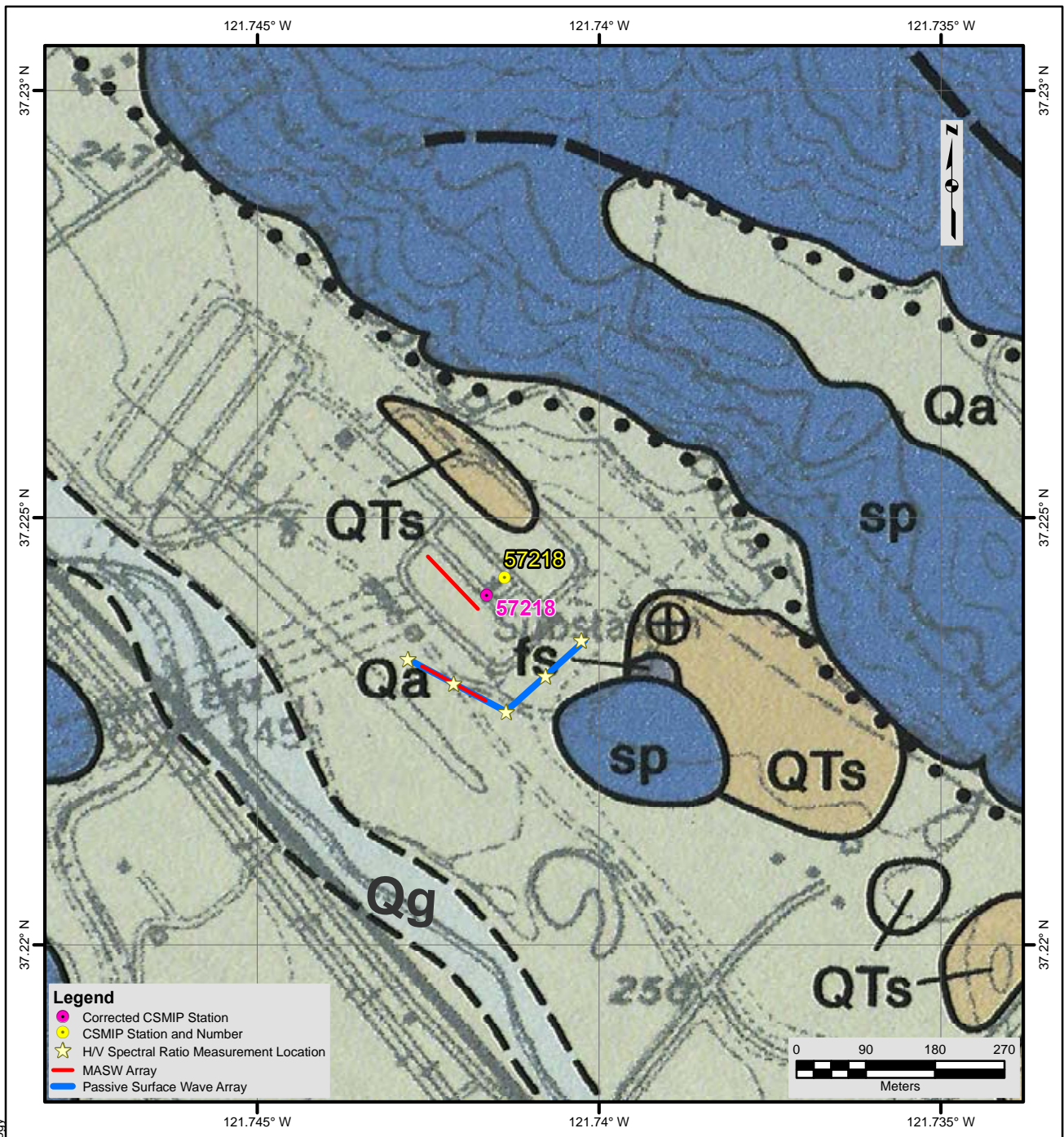
NOTES:

1. WGS 1984 Coordinate System
2. Image Source: Esri, DigitalGlobe, GeoEye, Earthstar Geographics, CNES/Airbus DS, USDA, USGS, AEX, Getmapping, Aerogrid, IGN, IGP, swisstopo, and the GIS User Community



**FIGURE 1
SITE MAP
CE • 57218**





Description of Geologic Map Units

Qa = Quaternary (Holocene) Alluvial gravel, sand, and clay of valleys
 Qg = Quaternary (Holocene) Sand and Gravel of Coyote Creek channel
 QTs = Quaternary (Pleistocene) Santa Clara Formation
 sp = Mesozoic (Jurassic and Cretaceous) Coast Range Ophiolite Complex
 fs = Mesozoic (Jurassic and Cretaceous) Franciscan Assemblage

NOTES:

1. WGS 1984 Coordinate System
2. Geologic Map of the Morgan Hill Quadrangle, Santa Clara County, California by Thomas W Dibblee, Jr., 2005

File Name: 18045_57218-Geology

Date: 5/29/2018



**FIGURE 2
 GEOLOGIC MAP
 CE • 57218**





Seismic Station CE.57218



Looking southeast along MASW Array 3 towards building housing seismic station

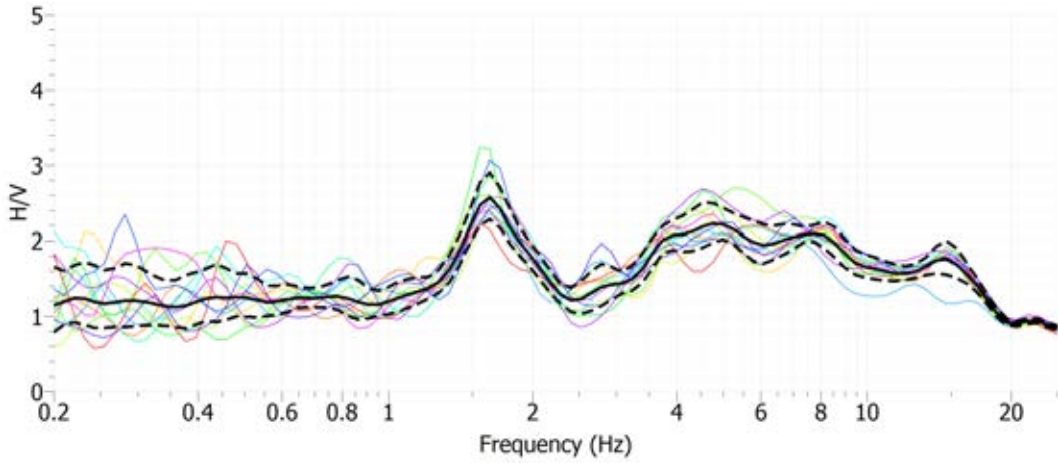


HVSr measurement location 2

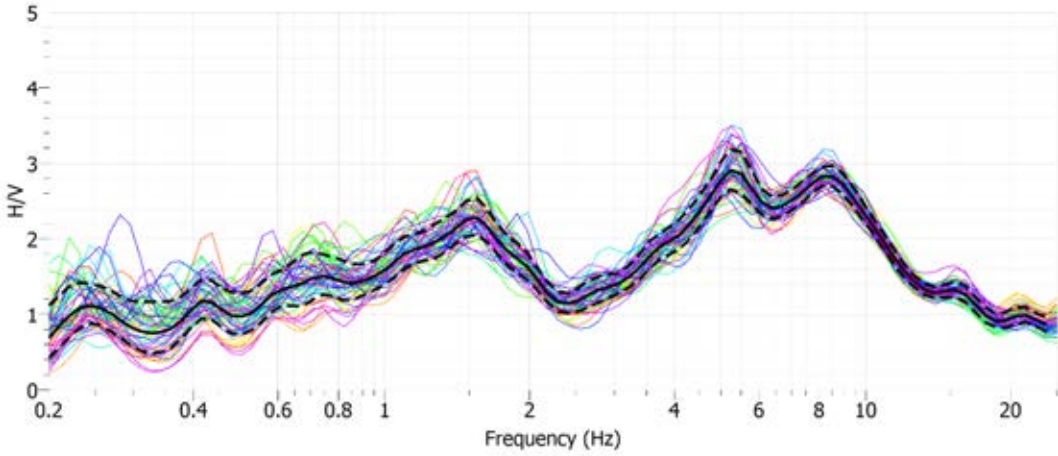


Love wave data acquisition on MASW Array 2

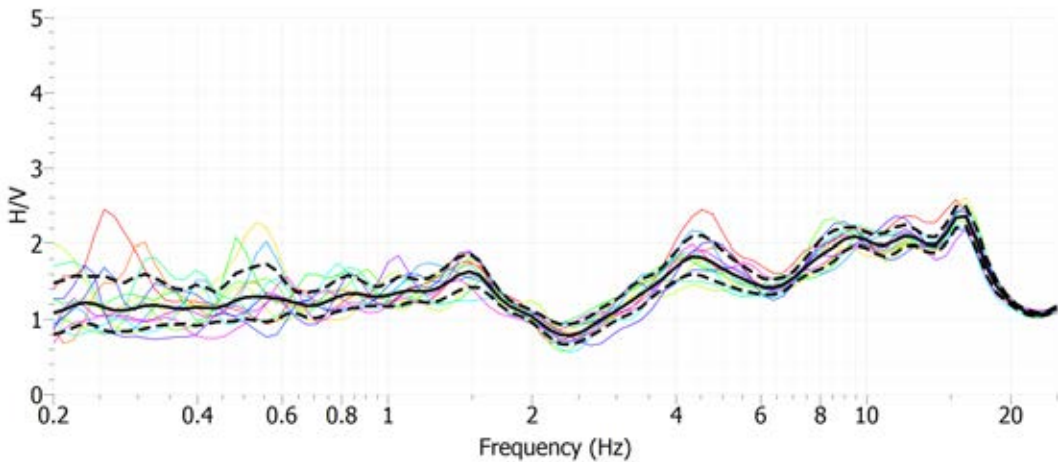
Figure 3 Site CE.57218 Photographs



Site CE.57218, HVSr Location 1, MOHO Tromino ENGR Sensor

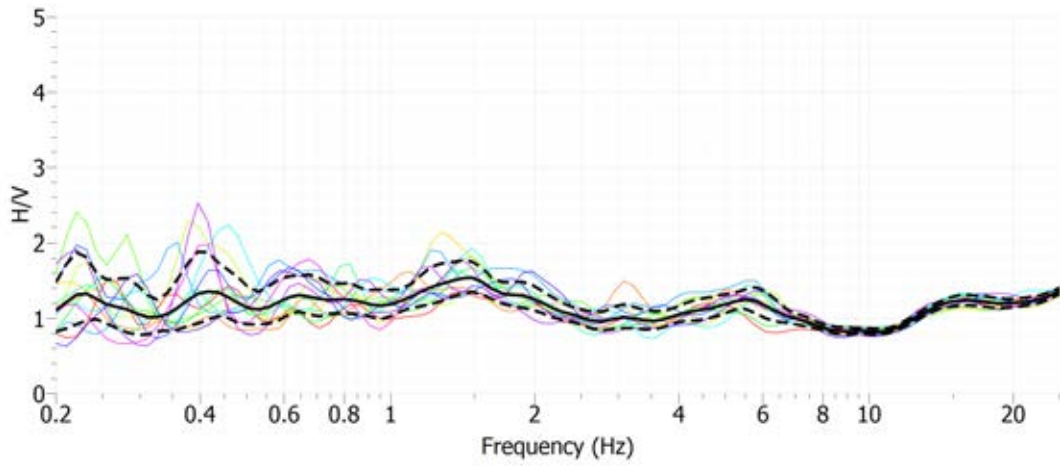


Site CE.57218, HVSr Location 2, Nanometrics Trillium Compact Sensor

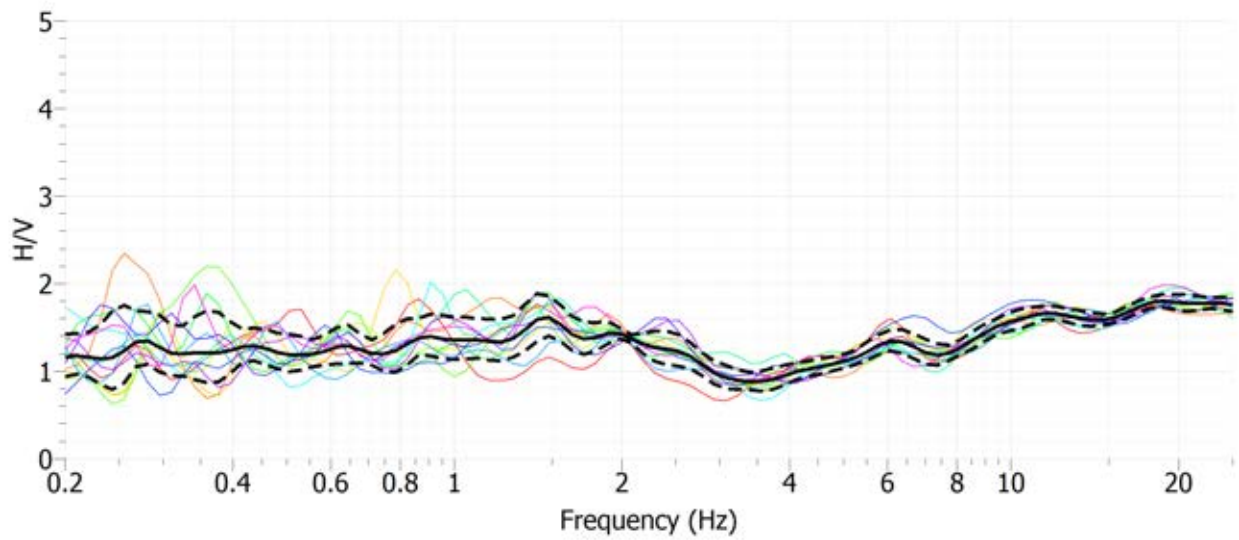


Site CE.57218, HVSr Location 3, MOHO Tromino ENGR Sensor

Figure 4 H/V Spectral Ratio of Ambient Vibration Data – Site CE.57218



Site CE.57218, HVSr Location 4, MOHO Tromino ENGR Sensor



Site CE.57218, HVSr Location 5, MOHO Tromino ENGR Sensor

Figure 5 H/V Spectral Ratio of Ambient Vibration Data – Site CE.57218

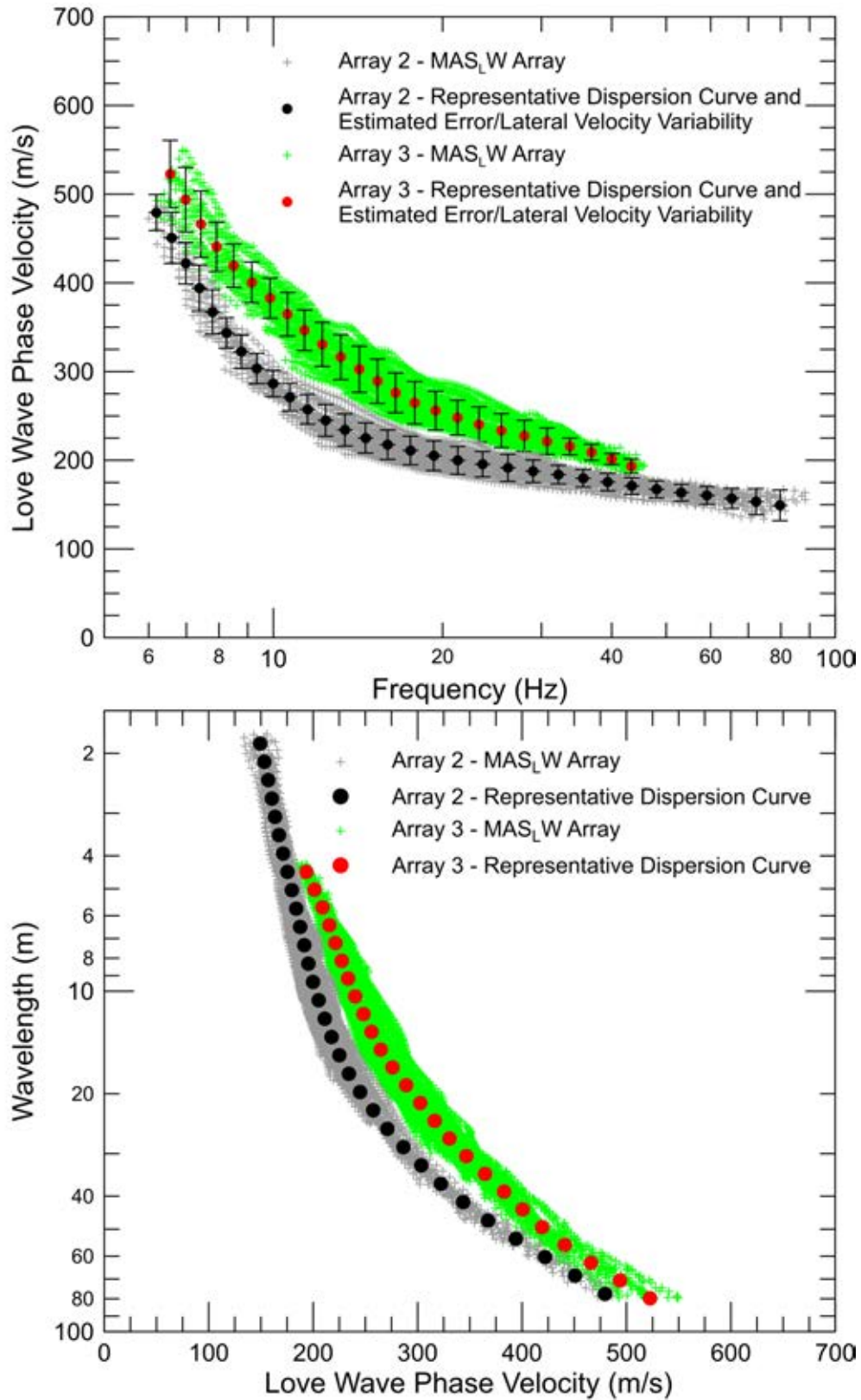


Figure 6 CE.57218 – Love wave dispersion curves derived from active-source surface wave data collected along Arrays 2 and 3

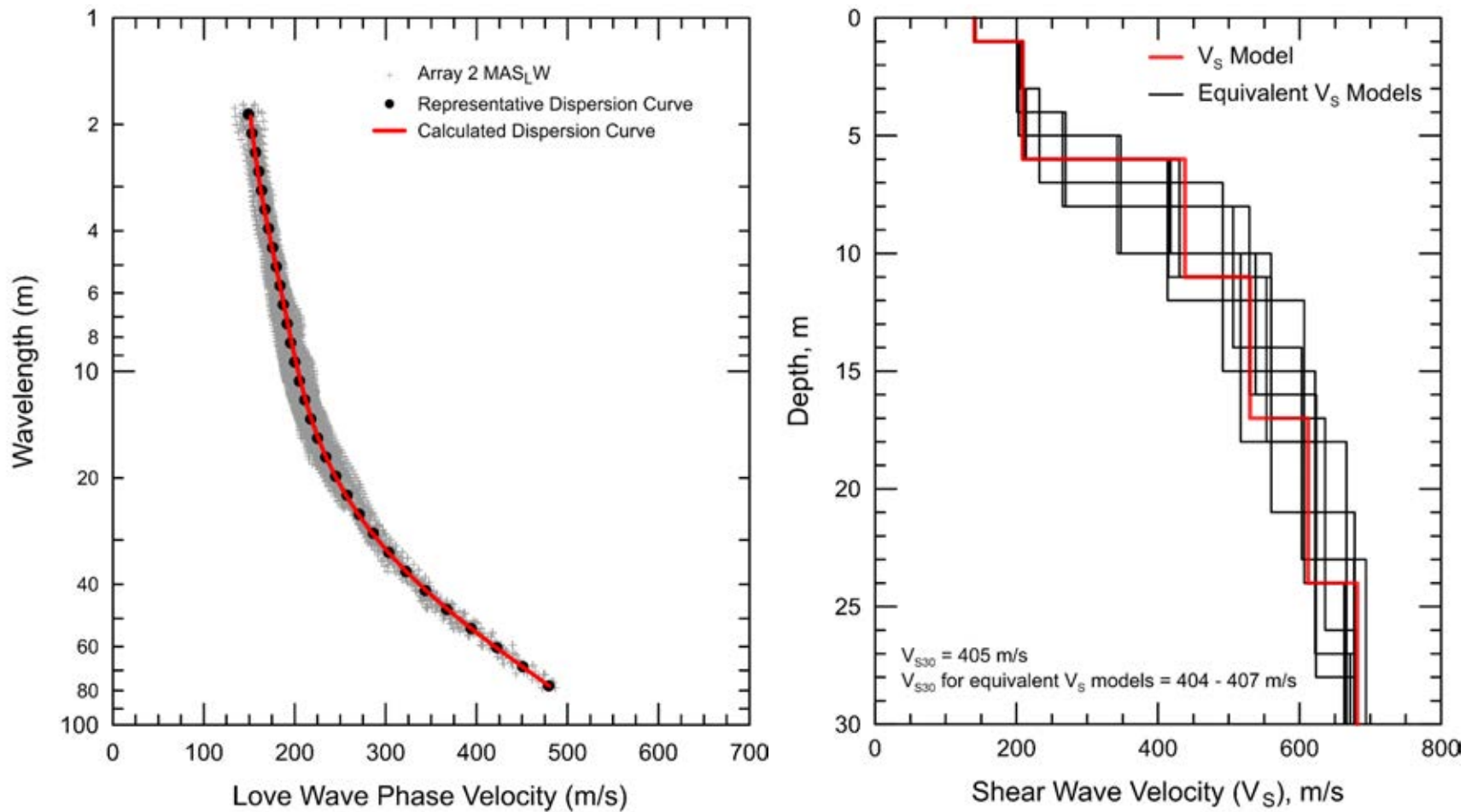


Figure 7 CE.57218 - Field, representative and calculated Love wave dispersion data (left) and associated V_S models (right) for Array 2

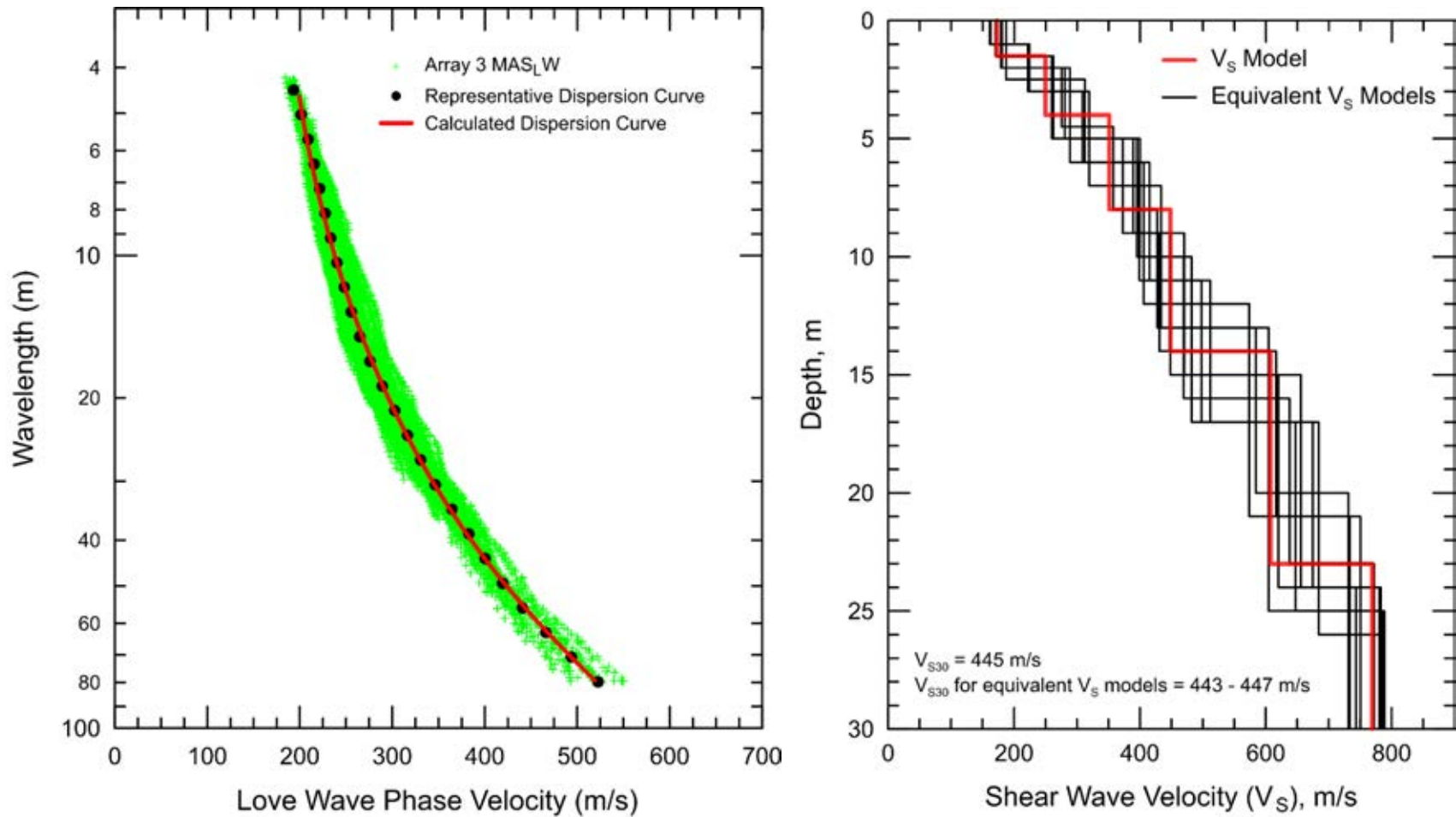


Figure 8 CE.57218 - Field, representative and calculated Love wave dispersion data (left) and associated V_S models (right) for Array 3

Report Geophysical Site Characterization SMIP Station CE.57370

Station Name: San Jose – San Felipe & Villages Pkwy

Location: San Jose Fire Station #11, 2840 Villages Parkway, San Jose, CA

Latitude: 37.2903

Longitude: -121.7640

V_{S30}: 436 m/s

Estimated Error in V_{S30}: ± 30 m/s

NEHRP Site Class: C

Geomatrix Code: APB/APC

HVSR Peak Frequency: 0.6 Hz

Site Geology: Site located near Thompson Creek on Pliocene Santa Clara Formation; valley sediments, gravels and conglomerates. Site located about 1 km from Silver Creek Fault and the Cretaceous Knoxville formation shale/coast ophiolite complex outcrops.

Site Conditions: Suburban site with traffic noise from nearby roads. Gently sloping terrain in site vicinity.

Geophysical Methods Utilized: MAS_RW, array microtremor, HVSR

Geophysical Testing Arrays:

1. Array 1: 48 channel L-shaped array utilizing 4.5 Hz vertical geophones spaced 3 m apart used to acquire passive surface wave data. The S-N and W-E linear segments of array have lengths of 39 and 102 m, respectively (Figure 1).
2. Array 2: 48 channel MAS_RW array utilizing 4.5 Hz vertical geophones spaced 1 m apart for a length of 47 m, forward and reverse shot locations with multiple source offsets (1 m to 12 m at both ends of array) and multiple interior source locations. Energy sources consisted of a 4-lb hammer and 12-lb sledgehammer.
3. One HVSR measurement location; near seismic station.

Table 1 Location of Geophysical Testing Arrays

Location	Latitude	Longitude
Seismic Station	37.2903	-121.7640
Array 1 Passive, Southwest of Array	37.29007	-121.76376
Array 1 Passive, Corner of Array	37.29039	-121.76358
Array 1 Passive, Northeast of Array	37.29012	-121.76249
Array 2 MASW, West end of Array	37.29029	-121.76331
Array 2 MASW, East end of Array	37.29019	-121.76279
HVSR Location 1	37.29032	-121.76414

Notes: 1) WGS84 Coordinate System (decimal degrees)

S-Wave Velocity Model:

Table 2 V_s Model

Depth to Top of Layer (m)	Layer Thickness (m)	S-Wave Velocity (m/s)	Inferred P-Wave Velocity (m/s)	Assumed Poisson's Ratio	Assumed Density (g/cm^3)
0	1.5	168	336	0.333	1.75
1.5	2	305	611	0.333	1.95
3.5	3.5	394	788	0.333	2.00
7	10	492	984	0.333	2.03
17	20	541	1082	0.333	2.05
37	>13	566	1131	0.333	2.05

Notes: 1) Depth of investigation is about 50 m.
2) Bottom layer is a half space.

Observations/Discussion:

H/V Spectral Ratio

HVSR data was collected for a 60-minute duration using a Nanometrics Trillium Compact (Trillium) seismograph. The HVSR data reveals a 0.6 Hz peak, which is likely associated with a geologic structure(s) at a depth much greater than the expected depth of investigation of the surface wave sounding (Figure 4).

Array Microtremor Data

Noise conditions at the site (multi-directional noise sources) appeared sufficient for successful application of passive surface wave techniques. A total of 50 minutes (100, 30 second seismic records) of ambient vibration data were acquired into an L-shaped array (Array 1) as shown on Figure 1. The legs of the L-shaped array were only 39 and 102 m long due to limited space. The ESAC technique was used to extract surface wave dispersion data from the ambient vibration data. To better characterize error, dispersion curves were generated from 12.5-minute time

segments of the ambient vibration data and also from the complete data set. The minimum and maximum Rayleigh wavelength extracted from Array 1 are about 13 and 135 m, respectively. Surface wave dispersion data was also extracted from the 102-m long E-W linear leg of the L-shaped array using the ESAC and ReMi™ techniques. The resulting two dispersion curves from the linear array are not in good agreement with each other or the L-shaped array and were not utilized for site characterization.

MASW Data

MASW data acquisition was conducted using a 47-m long receiver array (Array 2) as shown on Figure 1. There was not sufficient space for a longer array without placing the array on a concrete side walk. Rayleigh wave dispersion data were interpreted from 12 MAS_RW seismic records collected at 10 different source locations using 4-lb hammer and 12-lb sledgehammer energy sources. Larger sledgehammer energy sources were not utilized to minimize noise as measurements were made near houses in the evening. Due to limited space, the maximum source offset was 12 m from each end of the array. Using the 12 seismic records and variable receiver offset ranges, over 60 dispersion curves were extracted and combined for analysis. It was difficult to extract a fundamental mode dispersion curve over a wide frequency range because higher mode Rayleigh waves were often dominant at high frequencies. To minimize near field effects, the maximum Rayleigh wavelength data extracted from the MAS_RW data set was set equal to the lesser of one times the distance between the source and midpoint of the active receiver array or 35 m (expected limit of capabilities of 12-lb hammer at this site). There is nominally about 30 to 40 m/s of scatter in MAS_RW dispersion data, which is likely in part due to lateral velocity variation. The minimum Rayleigh wavelength phase velocity data extracted from a 48-channel MAS_RW receiver gather was in the 6 to 7 m range. Reducing data from smaller hammer sources using a limited offset range receiver gather (i.e. less active geophones) allowed for extraction of surface wave dispersion data to a minimum wavelength of about 3 m.

Modeling

Surface wave dispersion data from active and passive surface wave data sets are in excellent agreement over the approximate 15 to 35 m overlapping wavelength range (Figure 5). The phase velocity of a 40-m wavelength Rayleigh wave (V_{R40}) is 434 m/s with a coefficient of variation (COV) of 1 % from ESAC analysis of the ambient vibration data collected along Array 1. Representative dispersion curves were generated for each surface wave data set using a moving average, polynomial curve fitting routine. These individual representative dispersion curves were combined and a composite representative dispersion curve generated for the combined data set for modeling. Error bars for the composite representative dispersion curve were estimated based on the scatter in the dispersion data.

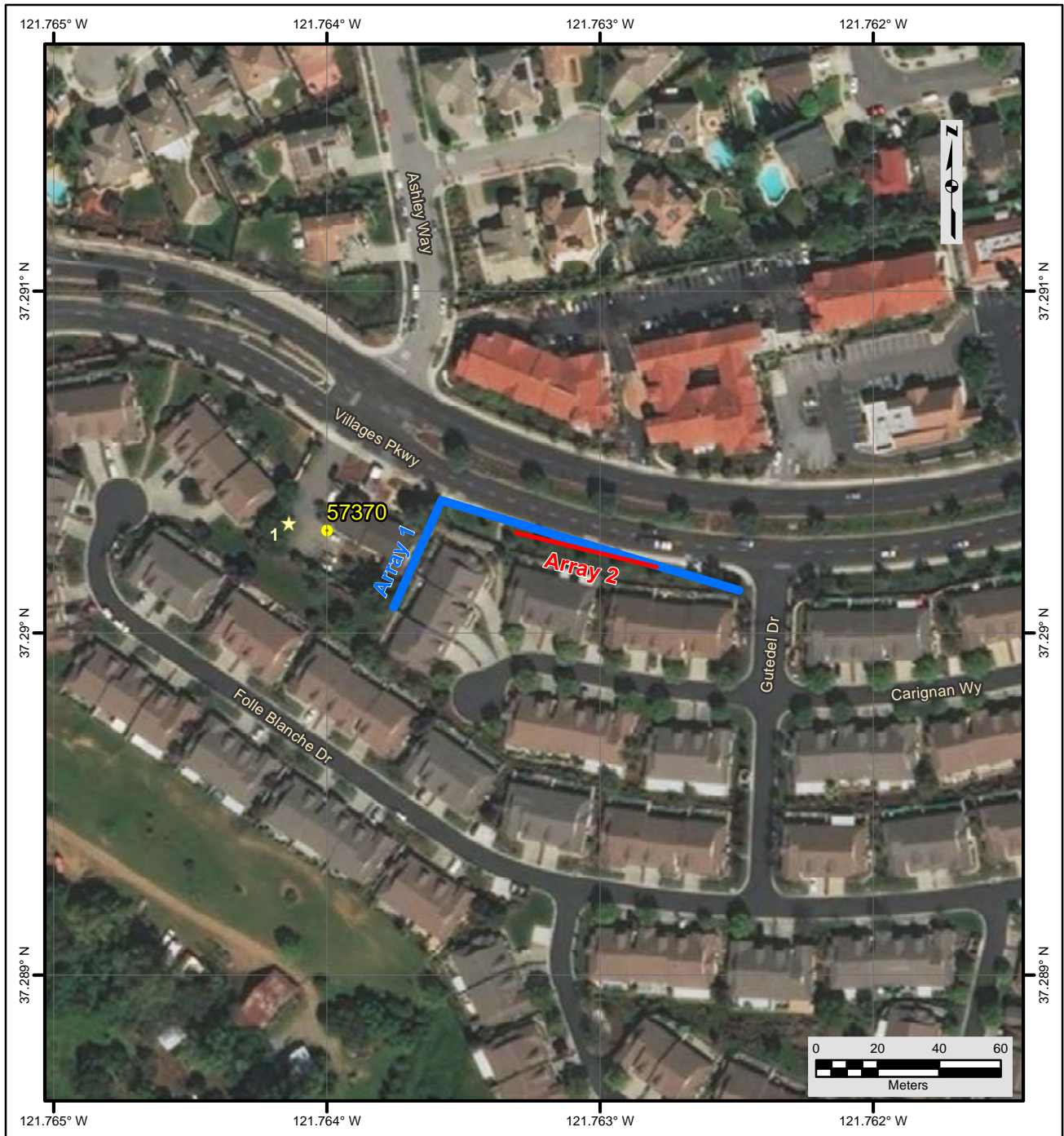
The composite representative dispersion curve was inverted using an iterative non-linear least squares inversion routine and fundamental mode Rayleigh wave assumption to derive V_S models. Realistic estimates of Poisson's ratio and density were used to make models as accurate as possible. There was no evidence of high Poisson's ratio, saturated sediments in the upper 15 m from seismic refraction first arrival data. Model layer thicknesses increased with depth to reflect the reduction in model resolution with depth. Several V_S models were developed with almost identical calculated dispersion curves to demonstrate the non-uniqueness inherent in the

inversion of surface wave dispersion data; especially at layer boundaries where an abrupt change in seismic velocity occurs or associated with high velocity layers or velocity inversions.

Results

V_S models are presented as Figure 6. Surface wave depth of investigation is about 50 m based on $\lambda_{\max}/2.5$. The 0.6 Hz HVSR peak is associated with a geologic structure much deeper than the depth of investigation.

V_{S30} is 436 m/s (NEHRP Site Class C). The average V_S of the upper 50 m (V_{S50}) is 478 m/s. The estimated error in V_{S30} , which includes some effects of the lateral velocity variability beneath the testing arrays, is about 30 m/s. This is computed based on the sum of the following rounded to the nearest 5 m/s: an estimated error of 3% from the realistic assumed layer Poisson's ratios in the model, 1% error from the realistic assumed layer densities in the model, 2% for the variation in V_{S30} associated with non-uniqueness, and the 1% COV in V_{R40} from the passive-source surface wave dispersion data. V_{S30} is between 233 and 237 m/s for the equivalent V_S models demonstrating that V_{S30} does not vary much for V_S models with near identical dispersion curves. Interestingly, V_{S30} estimated from V_{R40} using the Brown et al., 2000 relationship ($V_{S30} \cong 1.045V_{R40}$, assuming V_{R40} represents the fundamental mode Rayleigh wave) is 454 m/s, only 4 % higher than that estimated from the V_S model.



File Name: 18045_57370
Date: 5/29/2018

Legend

- CSMIP Station and Number
- ★ H/V Spectral Ratio Measurement Location
- MASW Array
- Passive Surface Wave Array

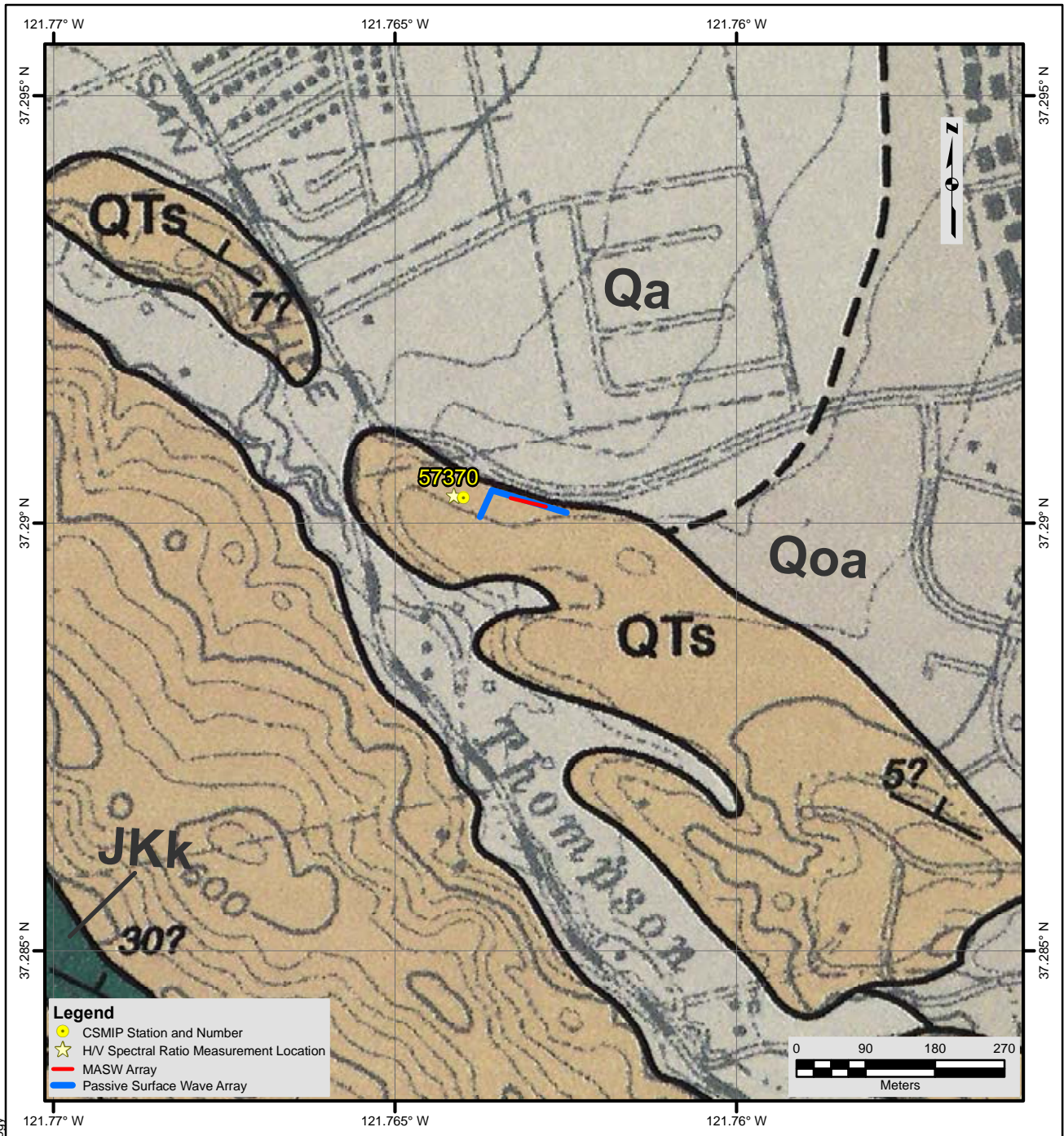
NOTES:

1. WGS 1984 Coordinate System
2. Image Source: Esri, DigitalGlobe, GeoEye, Earthstar Geographics, CNES/Airbus DS, USDA, USGS, AEX, Getmapping, Aerogrid, IGN, IGP, swisstopo, and the GIS User Community



**FIGURE 1
SITE MAP
CE • 57370**





Description of Geologic Map Units

Qa = Quaternary (Holocene) Alluvial Gravel, Sand and Clay soil of valley areas
 Qoa = Quaternary (Pleistocene) Dissected alluvial gravel and sand
 QTs = Quaternary (Pliocene) Santa Clara Formation
 JKK = Mesozoic (Jurassic and Cretaceous) Knoxville Formation

NOTES:

1. WGS 1984 Coordinate System
2. Geologic Map of the San Jose East Quadrangle, Santa Clara County, California by Thomas W Dibblee, Jr., 2005

File Name: 18045_57370-Geology
Date: 5/29/2018



**FIGURE 2
 GEOLOGIC MAP
 CE • 57370**





Looking east towards fire station housing seismic station and HVSr measurement location



Looking south towards fire station and corner of L-shaped Array 1

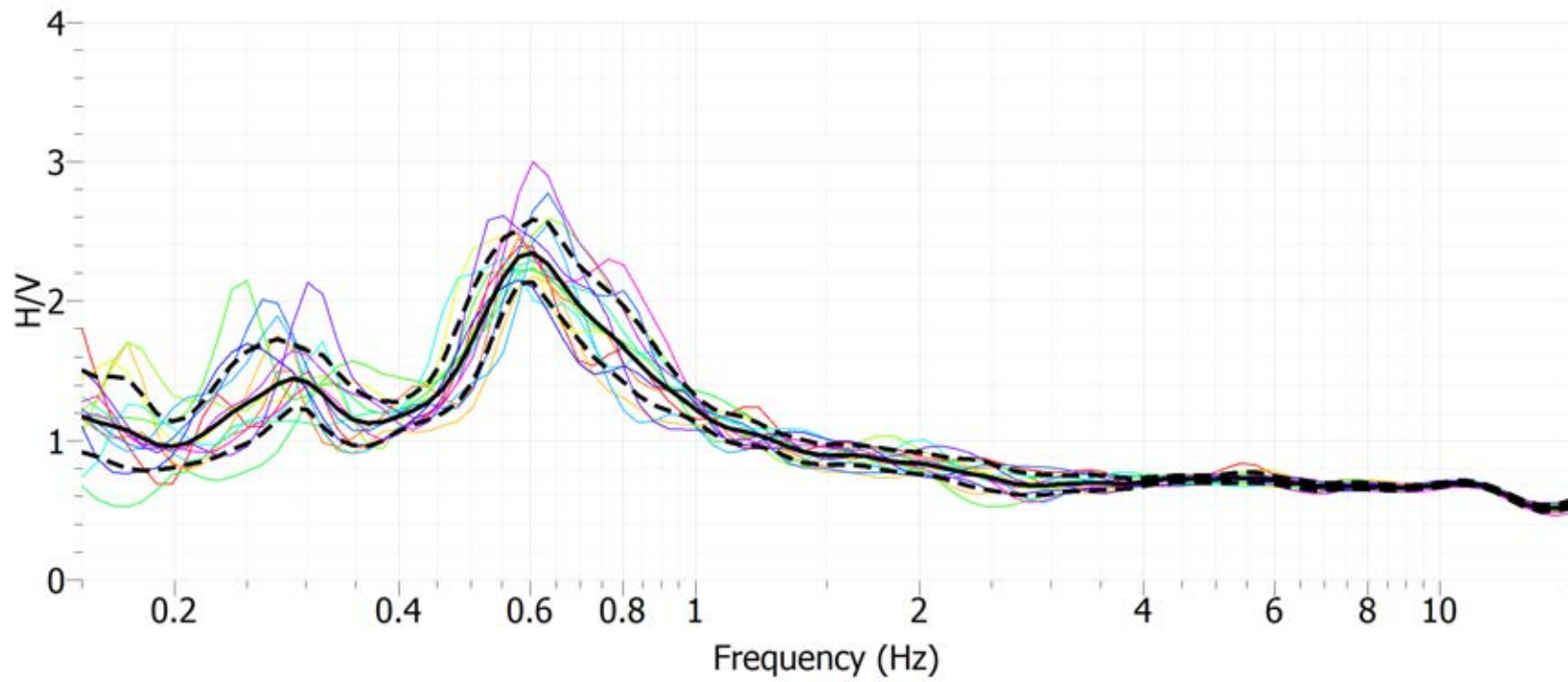


Looking east along leg of L-shaped Array 1



Looking west along MASW Array 2

Figure 3 Site CE.57370 Photographs



Site CE.57370, HVSR Location 1, Nanometrics Trillium Compact Sensor

Figure 4 H/V Spectral Ratio of Ambient Vibration Data, Site CE.57370

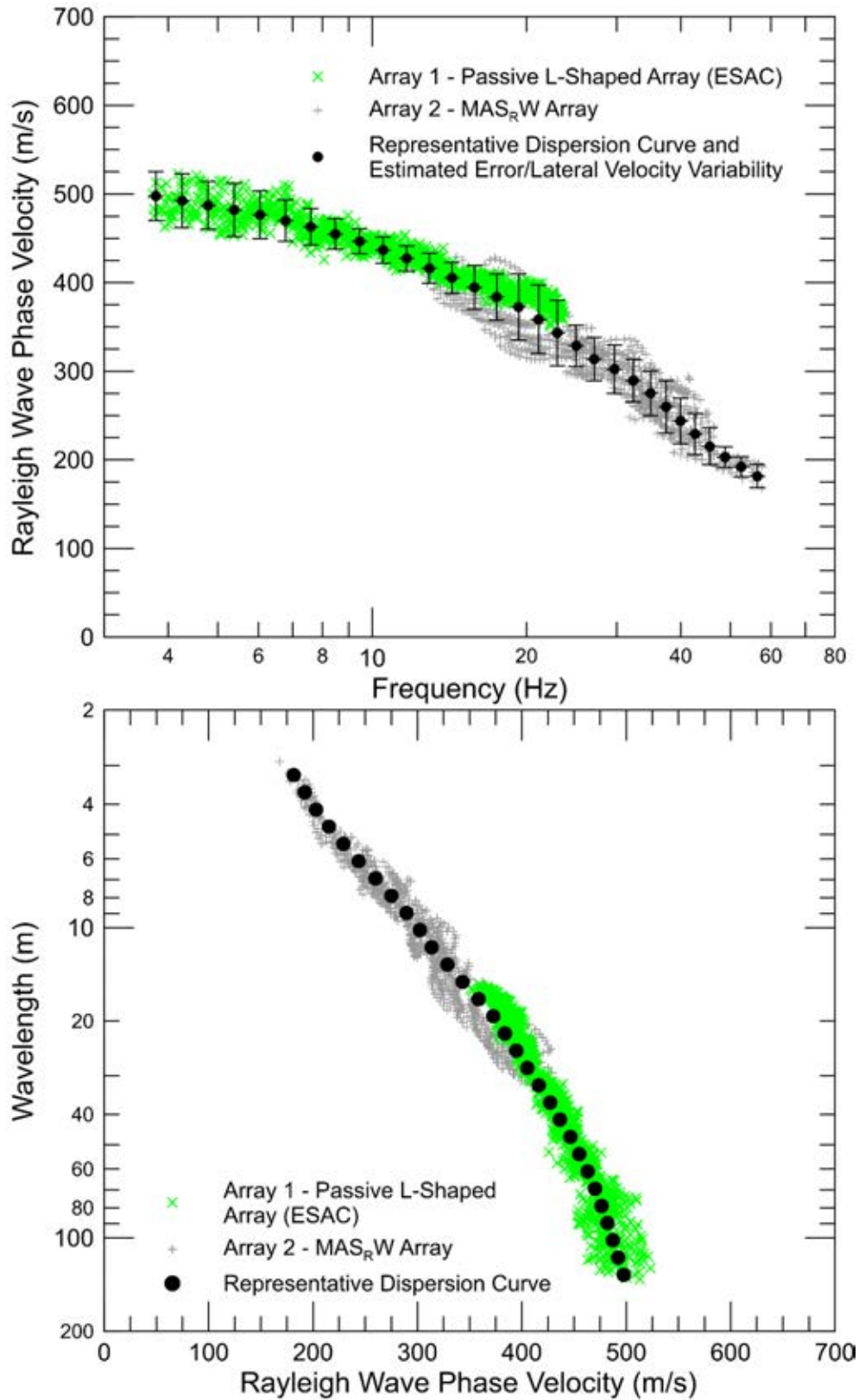


Figure 5 CE.57370 – Rayleigh wave dispersion curves derived from active- and passive-source surface wave data

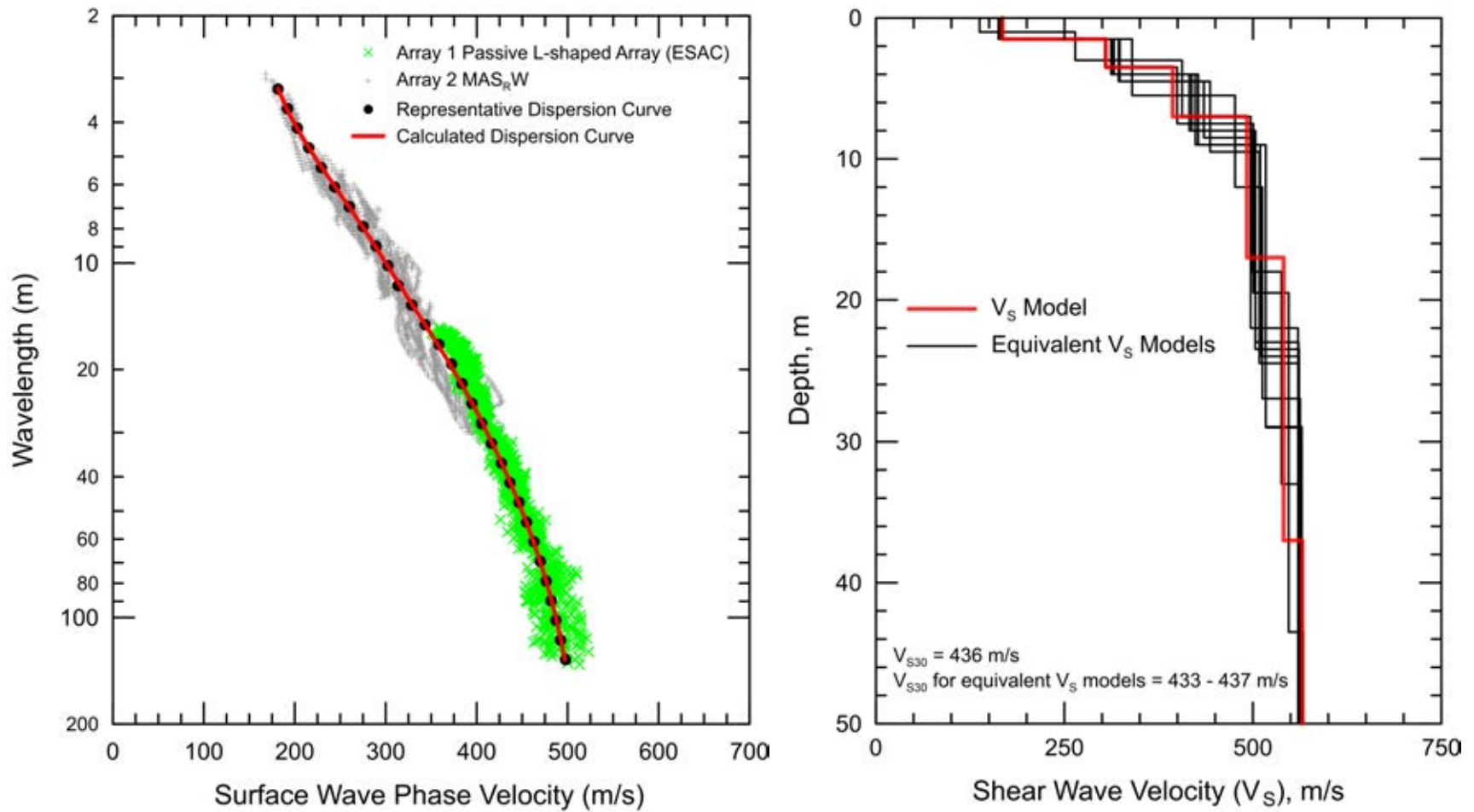


Figure 6 CE.57370 - Field, representative and calculated surface wave dispersion data (left) and associated V_S models (right)

Report

Geophysical Site Characterization

SMIP Station CE.57371

Station Name: San Jose – Monterey Hwy & Skyway Dr.

Location: San Jose Fire Department Station #18, 4430 South Monterey Hwy., San Jose, California

Latitude: 37.2730

Longitude: -121.8289

V_{s30}: 282 m/s

Estimated Error in V_{s30}: ± 25 m/s

NEHRP Site Class: D

Geomatrix Code: AHD

HVSR Peak Frequency: 2 – 2.8 Hz

Site Geology: Site located on Holocene alluvium near Coyote Creek and on coast range thrust fault zone. Outcrop of Cretaceous coast range ophiolite complex serpentinite and Franciscan less than ¼ km from station location. The inferred location of an unnamed fault is in close proximity to the seismic station.

Site Conditions: Suburban site with traffic noise from nearby roads. Relatively flat terrain in site vicinity.

Geophysical Methods Utilized: MAS_RW, array microtremor, HVSR

Geophysical Testing Arrays:

1. Array 1: 48 channel “L” shaped array utilizing 4.5 Hz vertical geophones spaced 3 m apart on the NW to SE leg and 4.5 m apart on the SW to NE leg for lengths of 72 m and 103.5 m, respectively, used to acquire passive surface wave data (Figure 1).
2. Array 2: 48 channel MAS_RW array utilizing 4.5 Hz vertical geophones spaced 1.5 m apart for a length of 70.5 m, forward and reverse shot locations with multiple source offsets (1.5 m to 6 m on the low end of the array and 1.5 m on the high end) and multiple interior source locations (Figure 1). A 4-lb hammer was used at 1.5 m offset source locations and center shot location. A 12-lb sledge hammer was used at 1.5 m offset source locations and all interior source locations and a 20-lb sledgehammer was used for all offset source locations.
3. Two HVSR locations, one near the fire station housing the seismic station and the other at the northeast end of Array 1 (Figure 1).

Table 1 Location of Geophysical Testing Arrays

Location	Latitude	Longitude
Seismic Station	37.2730	-121.8289
Array 1 Passive, Northwest of Array	37.27354	-121.82911
Array 1 Passive, Corner of Array	37.27311	-121.82849
Array 1 Passive, Northeast of Array	37.27383	-121.82774
Array 2 MASW, Northwest End of Array	37.27343	-121.82924
Array 2 MASW, Southeast End of Array	37.27302	-121.82863
HVSR Location 1	37.27332	-121.82924
HVSR Location 2	37.27391	-121.82781

Notes: 1) WGS84 Coordinate System (decimal degrees)

S-Wave Velocity Model:

Table 2 V_s Model

Depth to Top of Layer (m)	Layer Thickness (m)	S-Wave Velocity (m/s)	Inferred P-Wave Velocity (m/s)	Assumed Poisson's Ratio	Assumed Density (g/cm^3)
0	2.5	191	382	0.333	1.80
2.5	4.5	252	503	0.333	1.90
7	7	253	506	0.333	1.90
14	11	282	564	0.333	1.95
25	15	563	1126	0.333	2.05
40	>10	827	1654	0.333	2.15

Notes: 1) Depth of investigation is about 50 m.
2) Bottom layer is a half space.

Table 3 Modified V_s Model Based on HVSR Peak Frequency Near Seismic Station

Depth to Top of Layer (m)	Layer Thickness (m)	S-Wave Velocity (m/s)	Inferred P-Wave Velocity (m/s)	Assumed Poisson's Ratio	Assumed Density (g/cm^3)
0	2.5	191	382	0.333	1.80
2.5	4.5	252	503	0.333	1.90
7	7	253	506	0.333	1.90
14	18	282	564	0.333	1.95
32	15	563	1126	0.333	2.05
47	>4	827	1654	0.333	2.15

Notes: 1) Depth of investigation is about 50 m.
2) Bottom layer is a half space.

Observations/Discussion:

H/V Spectral Ratio

HVSR data collected using both Nanometrics Trillium Compact (Trillium) and MOHO Tromino ENGR (Tromino) seismographs. Both the Trillium and Tromino were utilized at HVSR Location 1 (~ 1-hour recording duration) with almost identical results at frequencies greater than 1.5 Hz (Figure 4) and, therefore, only the Tromino (30-minute recording duration) was utilized at HVSR Location 2. It is probable that multiple subsurface geologic units contribute to the HVSR peak. HVSR peak frequency is about 2.05 Hz at Location 1 and 2.8 Hz at Location 2 (Figure 4). The top of the Coast Range Ophiolite Complex may be the source of the HVSR peak. The different peak frequencies at Locations 1 and 2 indicate that top of this geologic unit may be gradually deepening to the southwest.

Array Microtremor Data

Noise conditions at the site (multi-directional noise sources) appeared sufficient for successful application of passive surface wave techniques. Over 90 minutes (188, 30 second seismic records) of ambient vibration data were acquired into an L-shaped array (Array 1) as shown on Figure 1. The legs of the L-shaped array were only 72 and 103.5 m long due to limited space. The ESAC technique was used to extract surface wave dispersion data from the ambient vibration data. To better characterize error, dispersion curves were generated from nominal 15-minute time segments of the ambient vibration data and also from the complete data set. The minimum and maximum Rayleigh wavelength extracted from Array 1 are about 12 and 130 m, respectively. Although not presented or utilized for site characterization, surface wave dispersion data was also extracted from the linear legs of the L-shaped array using the ESAC and ReMi™ techniques. The resulting four dispersion curves were in acceptable with one other and that from the L-shaped array.

MASW Data

MASW data acquisition was conducted using a 70.5 m long receiver array (Array 2); however, there was only space for a 6-m source offset at one end of the array and 1.5 m source offset at the other end. Rayleigh wave dispersion data were interpreted from 13 MAS_RW seismic records collected at 8 different source locations using 4-lb hammer and 12- and 20-lb sledgehammer energy sources. Using the 13 seismic records and variable receiver offset ranges, over 60 dispersion curves were extracted and combined for analysis. To minimize near field effects, the maximum Rayleigh wavelength data extracted from the MAS_RW data set was set equal to the lesser of 45 m and one times the distance between the source and midpoint of the active receiver array. There is nominally about 25 to 40 m/s of scatter in MAS_RW dispersion data, which is likely in part due to lateral velocity variation. The minimum Rayleigh wavelength phase velocity data extracted from a 48-channel MAS_RW receiver gather was about 3.5 to 5.5 m. Reducing data from smaller hammer sources using a limited offset range receiver gather (i.e. less active geophones) allowed for extraction of surface wave dispersion data to a minimum wavelength of less than 2 m.

Modeling

Surface wave dispersion data from active and passive surface wave data sets are in excellent agreement over the approximate 12 to 45 m overlapping wavelength range (Figure 5). The average phase velocity of a 40-m wavelength Rayleigh wave (V_{R40}) is 256 m/s with a coefficient of variation (COV) of 0.6 % from ESAC analysis of the ambient vibration data collected along Array 1. Average V_{R40} is 263 m/s with a coefficient of variation (COV) of 2.7 % from MASW analysis of active-source seismic data collected along Array 2. The combined data set (similar weight given to active-and passive-source data) yields an average V_{R40} of 259 m/s with a coefficient of variation (COV) of 2.3 %. Representative dispersion curves were generated for each surface wave data set using a moving average, polynomial curve fitting routine. These individual representative dispersion curves were combined and a composite representative dispersion curve generated for the combined data set for modeling. Error bars for the composite representative dispersion curve were estimated based on the scatter in the dispersion data.

The composite representative dispersion curve was inverted using an iterative non-linear least squares inversion routine and the fundamental mode Rayleigh wave assumption to derive V_S models. Realistic estimates of Poisson's ratio and density were used to make models as accurate as possible. There was no evidence of high Poisson's ratio, saturated sediments in the upper 15 m from seismic refraction first arrival data. Model layer thicknesses increased with depth to reflect the reduction in model resolution with depth. Several V_S models were developed with almost identical calculated dispersion curves to demonstrate the non-uniqueness inherent in the inversion of surface wave dispersion data; especially at layer boundaries where an abrupt change in seismic velocity occurs or associated with high velocity layers or velocity inversions.

Theoretical HVSR, based on the diffuse field assumption, was computed for all V_S models using the software package *HV-Inv* Release 2.3 and the assumption that the noise field consists of both Rayleigh and Love waves and only Rayleigh waves.

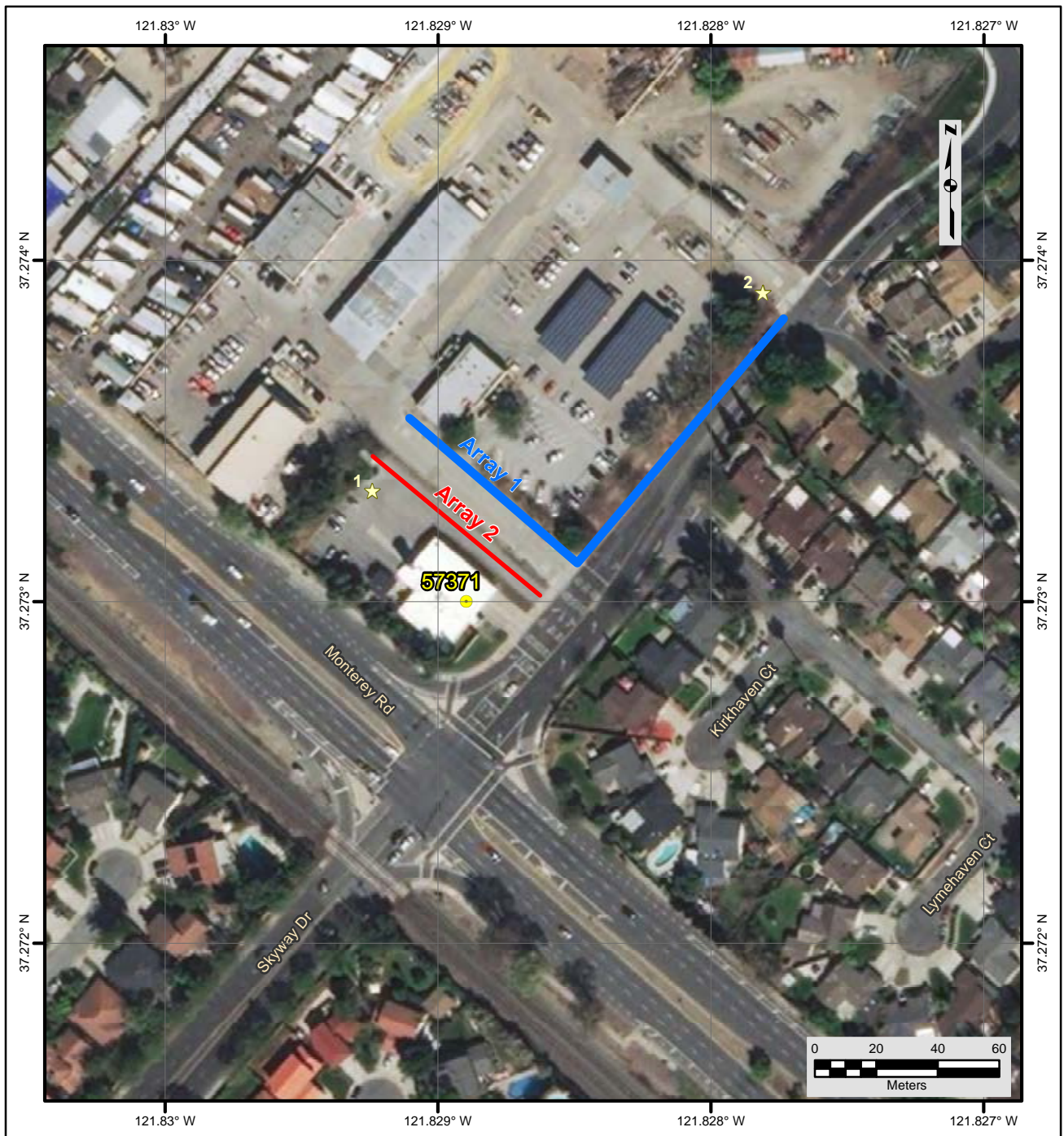
Results

V_S models are presented as Figure 6 and the V_S model selected for purpose of site characterization is presented in Table 2. V_S exceeds 560 m/s at about a depth of about 25-m at which is likely the top of the Coast Range Ophiolite Complex. Surface wave depth of investigation is about 50 m based on $\lambda_{max}/2.5$. HVSR peaks at locations 1 and 2, which are located at the southwest and northeast corners of the area investigated are about 2.05 and 2.8 Hz respectively. The HVSR peak frequency computed from the V_S models is about 2.5 Hz, between the observed HVSR peaks as would be expected (Figure 7).

V_{S30} is 282 m/s (NEHRP Site Class D). The average V_S of the upper 50 m (V_{S50}) is 367 m/s. V_{S30} is between 276 and 284 m/s for the equivalent V_S models, demonstrating that V_{S30} does not vary much for V_S models with near identical dispersion curves. The estimated error in V_{S30} , which includes some effects of the lateral velocity variability beneath the testing arrays, is about 25 m/s. This is computed based on the sum of the following rounded to the nearest 5 m/s: an estimated error of 3% from the realistic assumed layer Poisson's ratios in the model, 1% error from the realistic assumed layer densities in the model, 2% for the variation in V_{S30} associated with non-uniqueness, and the 2.5% COV in V_{R40} from the combined active- and passive-source surface wave dispersion data.

Interestingly, V_{S30} estimated from V_{R40} using the Brown et al., 2000 relationship ($V_{S30} \cong 1.045V_{R40}$, assuming V_{R40} represents the fundamental mode Rayleigh wave) is 271 m/s, about 4% lower than that estimated from the V_S model. Note that V_S models should always be used to estimate V_{S30} when possible and we are only documenting the performance of V_{S30} estimates based on V_{R40} in the event such an approach is needed in the future.

HVSR Location 1, with a peak frequency of about 2.05 Hz is closest to the seismic station; therefore, the depth to the soft rock unit was adjusted from 25 to 32 m such that calculated HVSR peak frequency was closer to the observed peak frequency near the seismic station (Figure 8 and Table 3). V_{S30} for this model is 260 m/s which is 8% lower than that presented above. However, V_{S30} for the modified V_S model is within the error presented above for V_{S30} and only 4% lower than a V_{R40} based V_{S30} estimate.



File Name: 18045_57371
Date: 5/29/2018

Legend

- CSMIP Station and Number
- ★ H/V Spectral Ratio Measurement Location
- MASW Array
- Passive Surface Wave Array

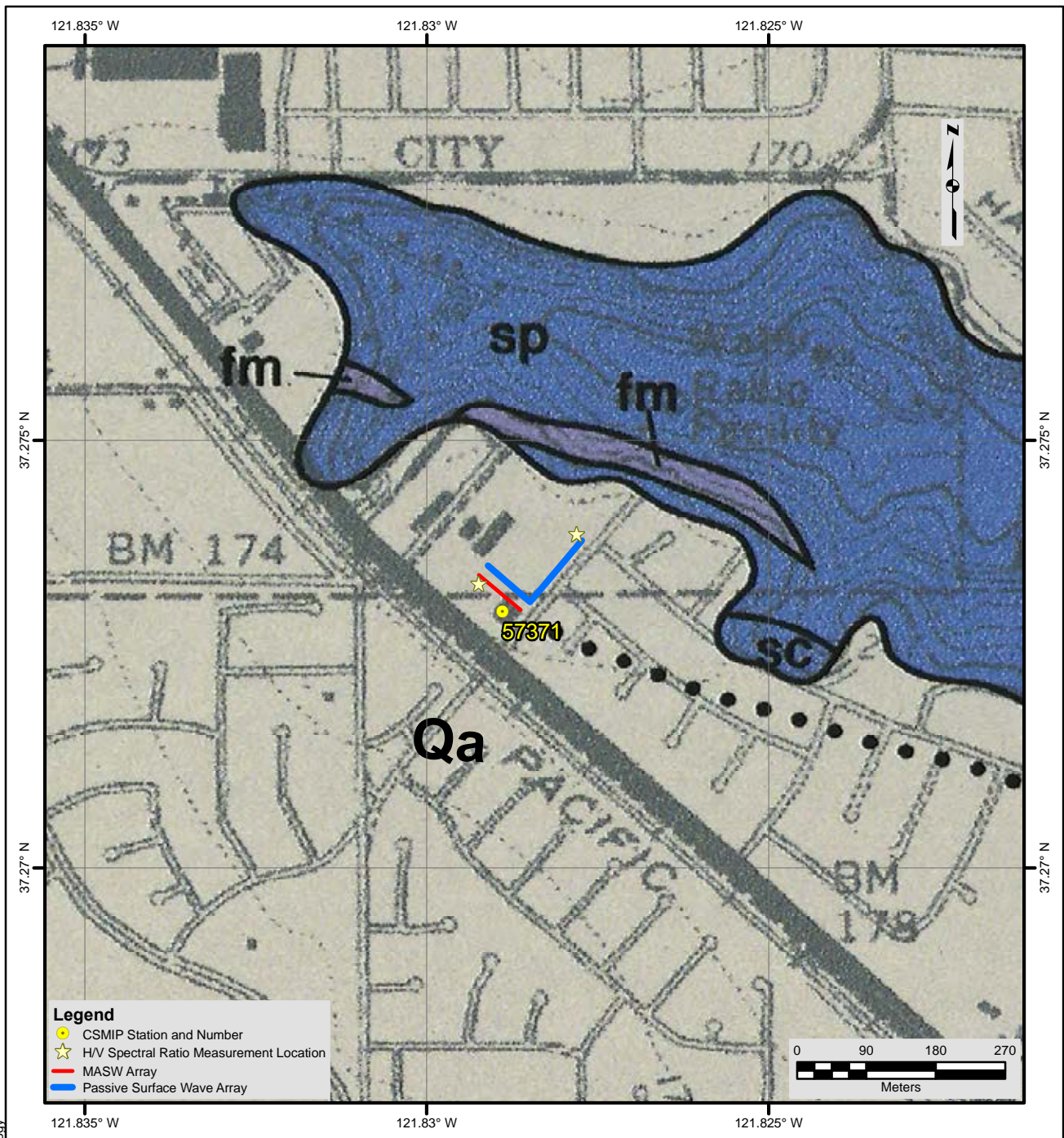
NOTES:

1. WGS 1984 Coordinate System
2. Image Source: Esri, DigitalGlobe, GeoEye, Earthstar Geographics, CNES/Airbus DS, USDA, USGS, AEX, Getmapping, Aerogrid, IGN, IGP, swisstopo, and the GIS User Community



**FIGURE 1
SITE MAP
CE • 57371**





Description of Geologic Map Units

Qa = Quaternary (Holocene) Alluvial gravel, sand, and clay soil of valley areas
 sp = Mesozoic (Jurassic and Cretaceous) Coast Range Ophiolite Complex: Serpentinite hydrothermally metamorphosed from ultramafic igneous rocks
 sc = Mesozoic (Jurassic and Cretaceous) Coast Range Ophiolite Complex: Serpentinite altered to ferruginous silica-carbonate rock
 fm = Mesozoic (Jurassic and Cretaceous) Franciscan Assemblage

NOTES:

1. WGS 1984 Coordinate System
2. Geologic Map of the San Jose East Quadrangle, Santa Clara County, California by Thomas W Dibblee, Jr., 2005

File Name: 18045_57371-Geology
Date: 5/29/2018



**FIGURE 2
GEOLOGIC MAP
CE • 57371**





Looking southeast towards fire station housing seismic station and MASW Array 2



HVSr measurement location 1

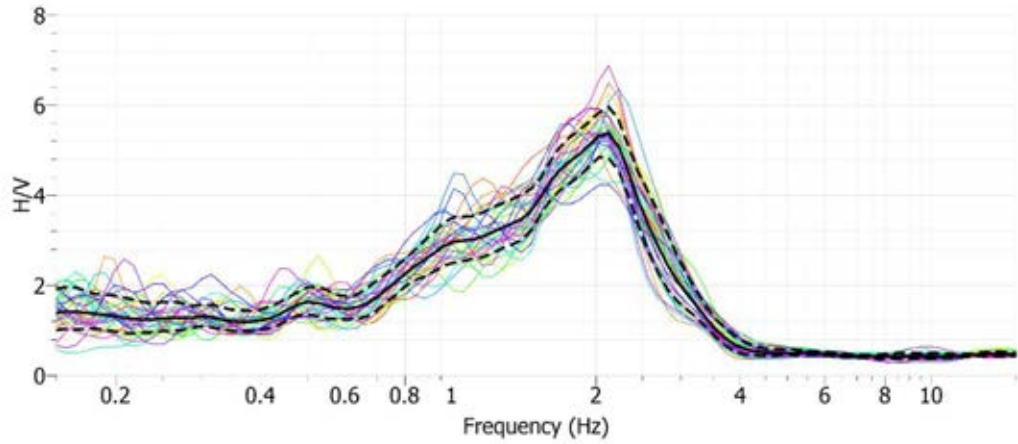


Looking southeast along MASW Array 2

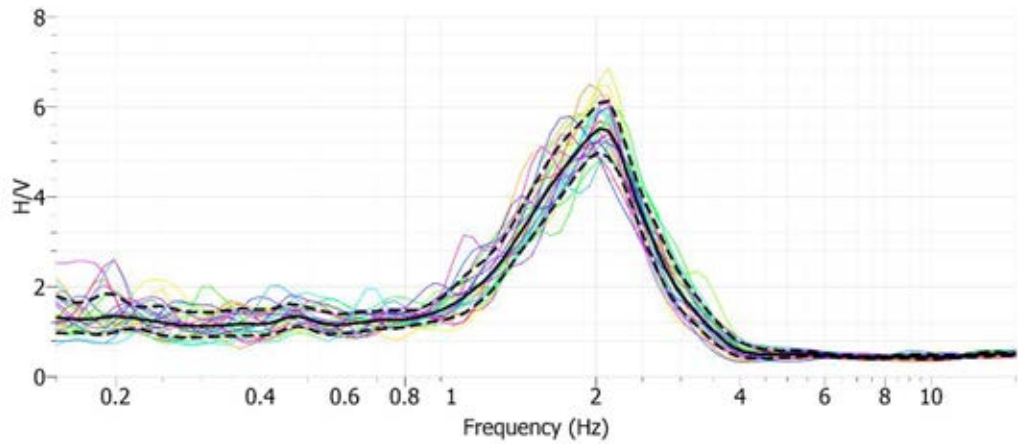


Looking northeast towards the location of the corner of L-shaped Array 1

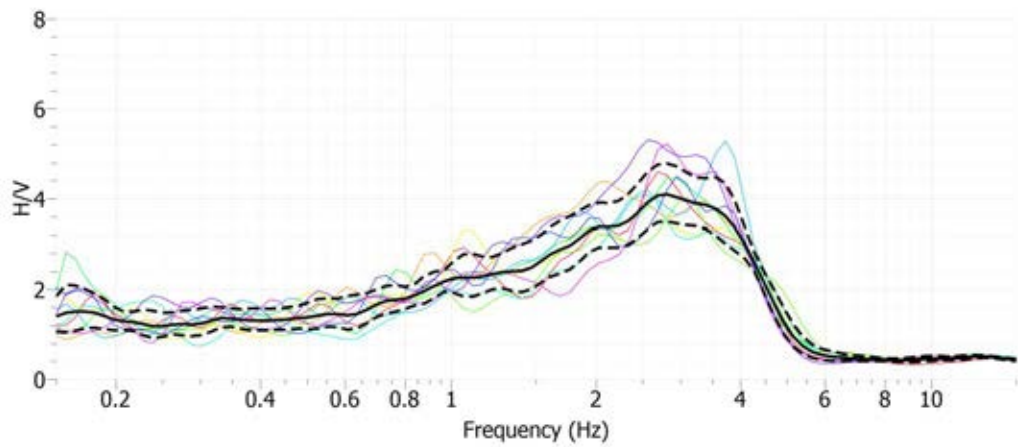
Figure 3 Site CE.57371 Photographs



Site CE.57371, HVSr Location 1, Nanometrics Trillium Compact Sensor



Site CE.57371, HVSr Location 1, MOHO Tromino ENGR Sensor



Site CE.57371, HVSr Location 2, MOHO Tromino ENGR Sensor

Figure 4 H/V Spectral Ratio of Ambient Vibration Data – Measurement Location 1, Site CE.57371

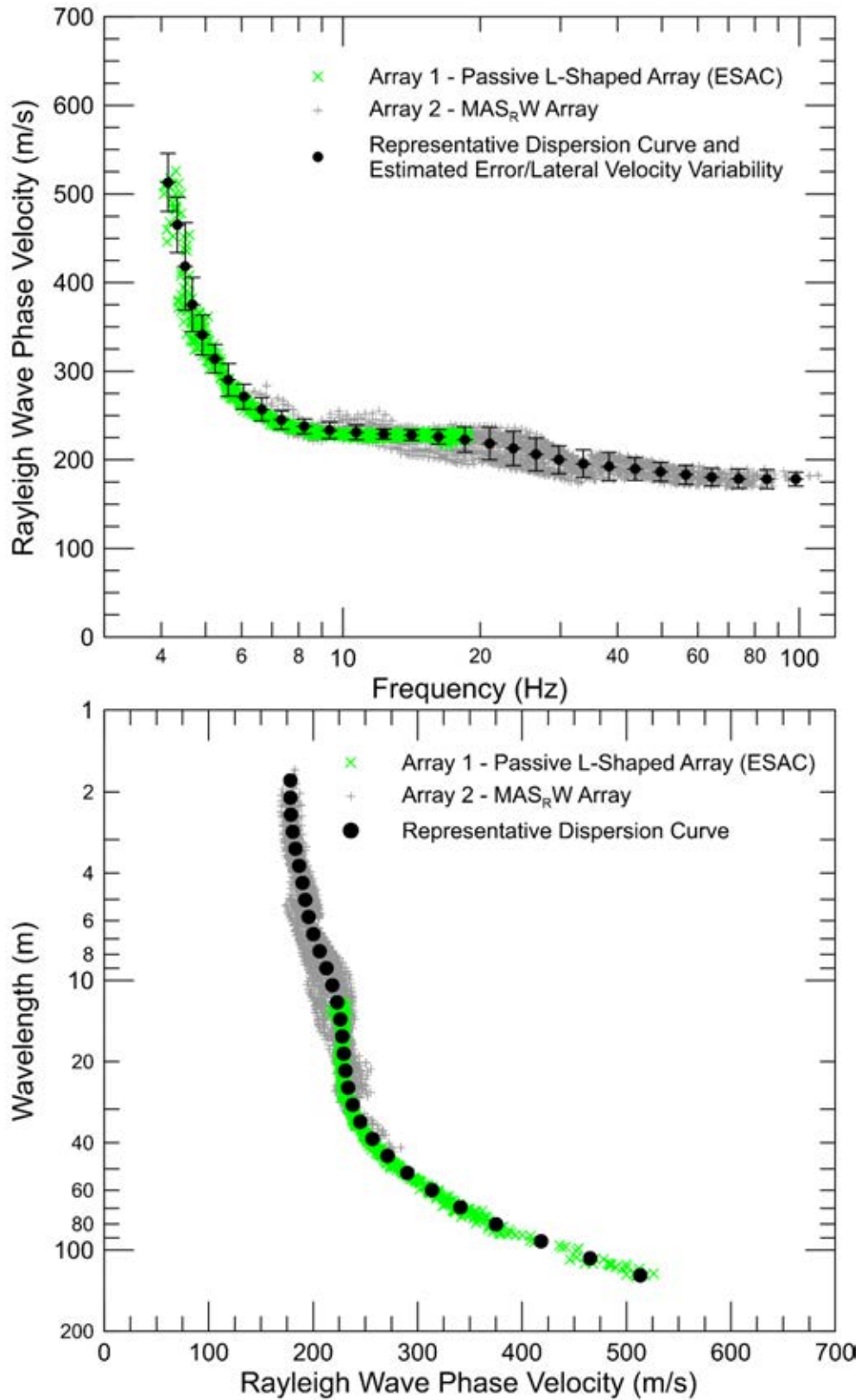


Figure 5 CE.57371 – Rayleigh wave dispersion curves derived from active- and passive-source surface wave data

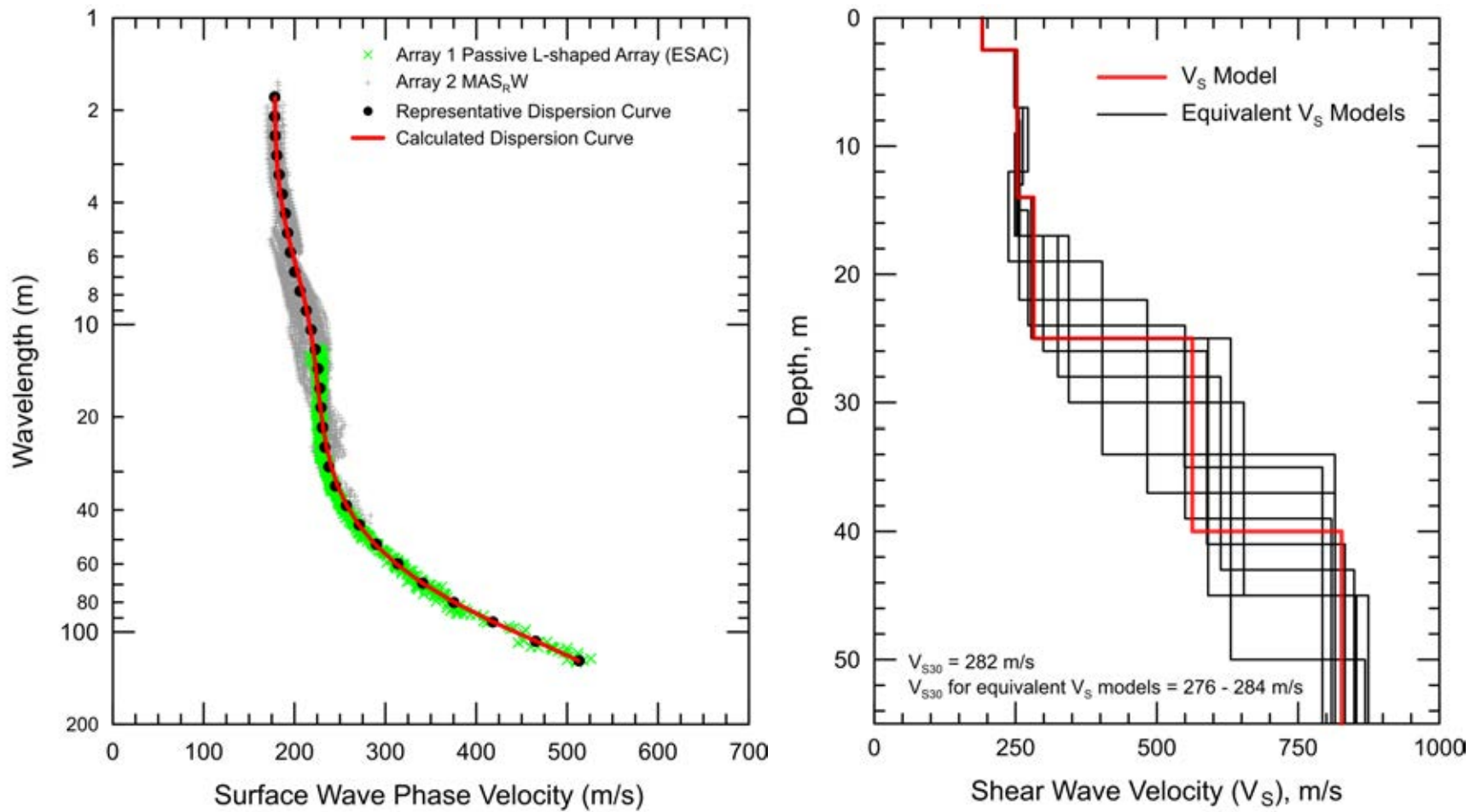
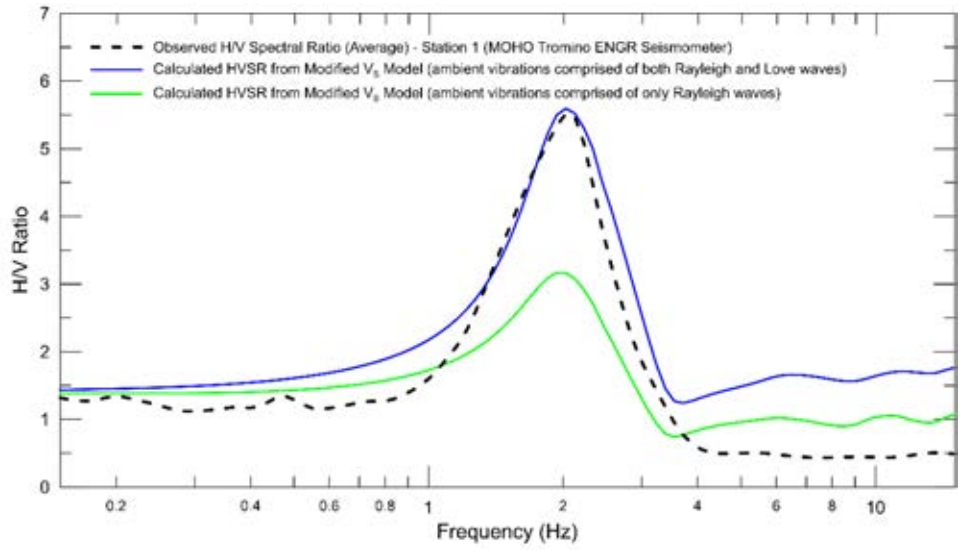
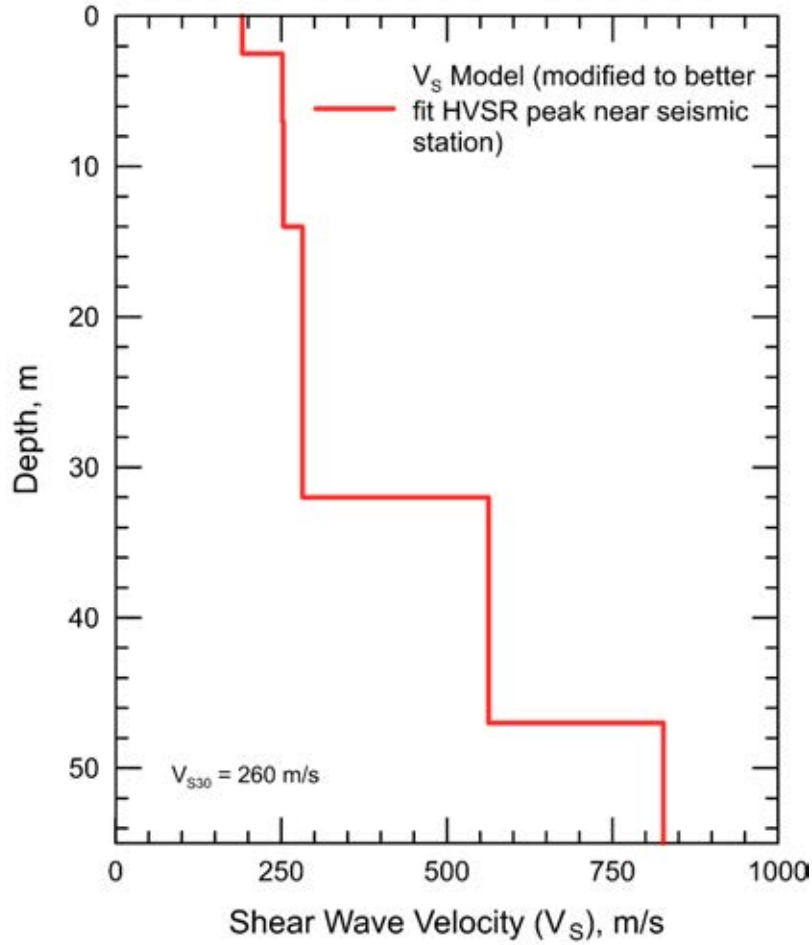


Figure 6 CE.57371 - Field, representative and calculated surface wave dispersion data (left) and associated V_S models (right)



Site CE.57371, Calculated HVSR Response for V_s Model Shown Below



V_s Model Modified to Better Fit HVSR Peak at Location 1 Near Seismic Station

Figure 7 V_s Model Modified (Depth to Bottom Two Layers Increased) to Fit HVSR Peak from Measurement Location Closest to Seismic Station CE.57371

Report Geophysical Site Characterization SMIP Station CE.58135

Station Name: Santa Cruz – UCSC Lick Electric Shop

Location: UC Santa Cruz, Lick Electronics Lab, Mclaughlin Drive, Santa Cruz, CA

Latitude: 37.0014

Longitude: -122.0615

V_{s30}: 408 m/s

Estimated Error in V_{s30}: ± 35 m/s

NEHRP Site Class: C

Geomatrix Code: AHB/ANB

HVSR Peak Frequency: 3.6 – 4.0 Hz

Site Geology: Station located on geologic unit mapped as Mesozoic/Paleozoic metamorphic and intrusive rock, 1 km from Ben Lomond fault. Field inspection reveals that residual soil overlies rock.

Site Conditions: Site located on university campus with minimal vehicular and pedestrian noise during geophysical testing. Gently undulating terrain in site vicinity.

Geophysical Methods Utilized: MAS_RW, array microtremor, HVSR

Geophysical Testing Arrays:

1. Array 1: 48 channel MAS_RW array utilizing 4.5 Hz vertical geophones spaced 2 m apart for a length of 94 m, forward and reverse shot locations with multiple source offsets (2 to 10 m) and multiple interior source locations. Four (4) and 12-lb hammers were used at the near-offset and interior source locations. An accelerated weight drop (AWD) and 20-lb hammer were used for the off-end source locations. The array also used to collect passive surface wave data (Figure 1).
2. Two HVSR locations, one near seismic station and the other near midpoint of Array 1 (Figure 1).

Table 1 Location of Geophysical Testing Arrays

Location	Latitude	Longitude
Seismic Station CE.58135	37.0014	-122.0615
Array 1 MASW/Passive, West End of Array	37.00142	-122.06301
Array 1 MASW/Passive, East End of Array	37.00151	-122.06196
HVSR Location 1	37.00140	-122.06241
HVSR Location 2	37.00145	-122.06108

Notes: 1) WGS84 Coordinate System (decimal degrees)
 2) Seismic station moved to building housing sensor and coordinates adjusted

S-Wave Velocity Model:

Table 2 V_s Model

Depth to Top of Layer (m)	Layer Thickness (m)	S-Wave Velocity (m/s)	Inferred P-Wave Velocity (m/s)	Assumed Poisson's Ratio	Assumed Density (g/cm ³)
0	1.5	286	535	0.300	1.90
1.5	3	301	563	0.300	1.90
4.5	6	315	589	0.300	1.90
10.5	10.5	492	920	0.300	2.00
21	14	502	939	0.300	2.05
35	>5	978	1830	0.300	2.20

Notes: 1) Depth of investigation is about 30 m.
 2) Velocity increase added at 35 m depth to better fit HVSR data.
 2) Bottom layer is a half space.

Observations/Discussion:

H/V Spectral Ratio

HVSR data was collected at two locations using a Nanometrics Trillium Compact (Trillium) seismograph as shown in Figure 1 and Table 1. About 80 min of ambient vibration data was acquired at HVSR Location 1, near the center of Array 1, and 55 min of data was acquired at HVSR Location 2, located adjacent to the building housing the seismic station. The HVSR peak frequency is 3.6 and 4 Hz at Locations 1 and 2, respectively (Figure 4).

Array Microtremor Data

There was insufficient space at the site to deploy a two-dimensional array for array microtremor measurements; however, over 60 minutes (129, 30 second seismic records) of ambient vibration data were acquired into MASW Array 1. Noise conditions at the site (multi-directional noise sources) were not adequate for successful application of passive surface wave techniques, and useful data was not obtained from the array microtremor measurements.

MASW Data

MASW data acquisition was conducted using a 94 m long receiver array (Array 1). Rayleigh wave dispersion data were interpreted from 19 MAS_RW seismic records collected at 11 different source locations using 4-lb hammer, 12- and 20-lb sledgehammer, and AWD energy sources. Maximum source offset was 10 m at both ends of the array. Using the 19 seismic records and variable receiver offset ranges, over 90 dispersion curves were extracted and combined for analysis. To minimize near field effects, the maximum wavelength Rayleigh wave extracted from the MAS_RW data set was set equal to the lesser of 1.3 times the distance between the source and midpoint of the active receiver array or 71 m. There is nominally about 25 to 40 m/s of scatter in MAS_RW dispersion data, which is likely in part due to lateral velocity variation. The minimum wavelength Rayleigh wave extracted from a 48-channel MAS_RW receiver gather is in the 4 to 15 m range. Reducing data from smaller hammer sources using a limited offset range receiver gather (i.e. less active geophones) allowed for extraction of surface wave dispersion data to a minimum wavelength of about 3.5 m.

Modeling

The phase velocity of a 40 m wavelength Rayleigh wave (V_{R40}) averages 393 m/s with a coefficient of variation (COV) of 2.5 % from 46 dispersion curves reduced from MASW data collected along Array 1. A representative dispersion curve was generated for the surface wave data set using a moving average, polynomial curve fitting routine. Error bars for the representative dispersion curve were estimated based on the scatter in the dispersion data. Figure 5 presents the Rayleigh wave dispersion data and representative dispersion curve.

The representative dispersion curve was inverted using an iterative non-linear least squares (local search) inversion routine with the fundamental mode Rayleigh wave assumption to derive V_S models. Realistic estimates of Poisson's ratio and density were used to make models as accurate as possible. There was no evidence of saturated sediments in the seismic refraction first arrival data. Model layer thicknesses increased with depth to reflect the reduction in model resolution with depth. Multiple V_S models were developed with almost identical calculated dispersion curves to demonstrate the non-uniqueness inherent in the inversion of surface wave dispersion data; especially at layer boundaries where an abrupt change in seismic velocity occurs or associated with high velocity layers or velocity inversions.

Theoretical HVSR, based on the diffuse field assumption, was computed for V_S models using the software package *HV-Inv* Release 2.3 and the assumption that the noise field consists of only Rayleigh waves and both Rayleigh and Love waves. Initially, V_S models were limited to the upper 30 m based on expected depth of investigation but had to be extended to slightly greater depth to better match HVSR data.

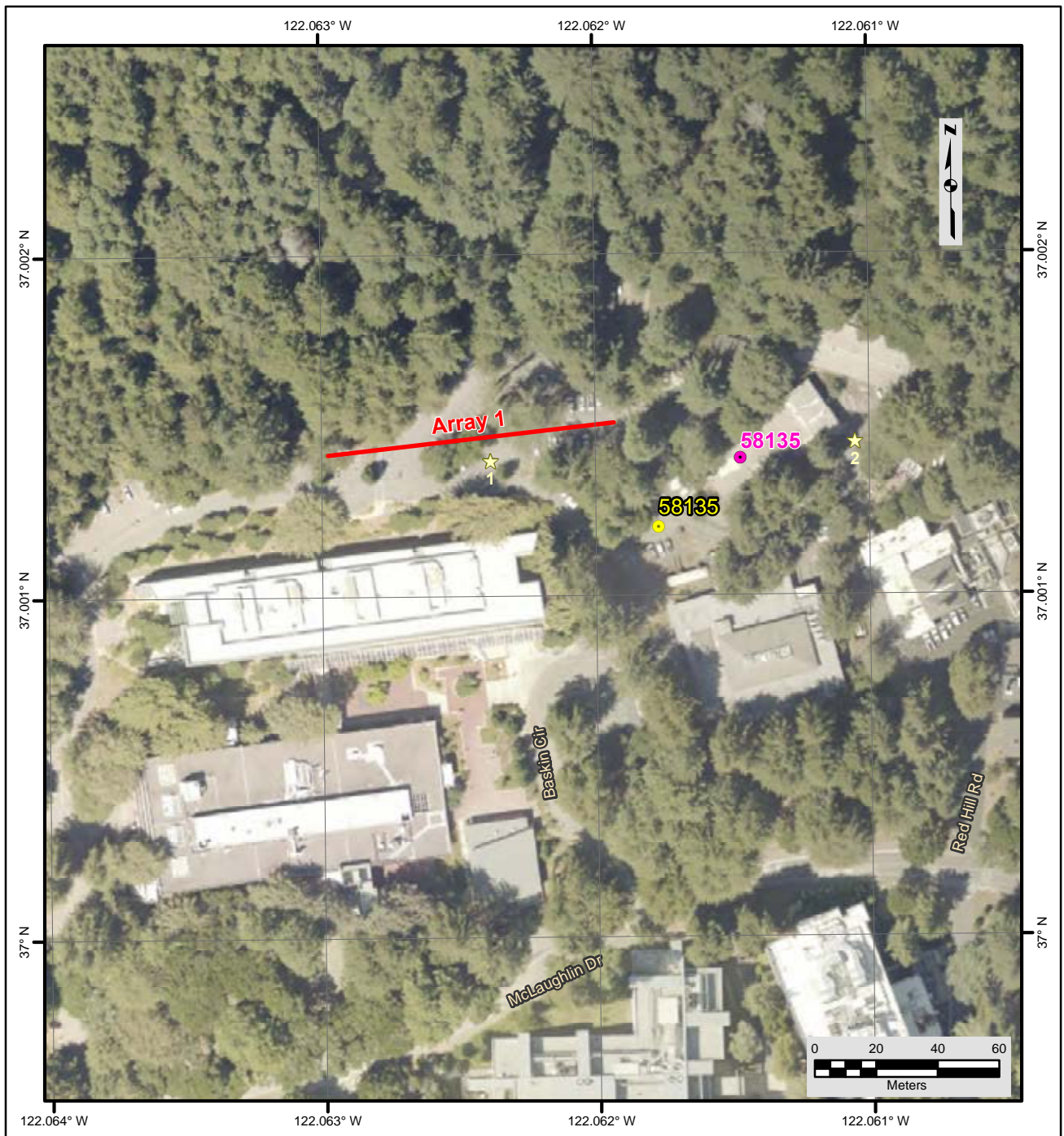
Results

V_S models are presented in Figure 6 and the V_S model selected for purpose of site characterization is presented in Table 2. V_S exceeds 400 m/s at a depth of about 10 m; this is likely the top of very intensely weathered to decomposed rock. Surface wave depth of investigation is about 30 m based on $\lambda_{\max}/2$ to $\lambda_{\max}/2.5$.

None of the V_S models presented in Figure 6 with the half space above 30 m depth have calculated HVSR response that is in good agreement with the observed HVSR response. This indicates that deeper geologic structure may partially contribute to the HVSR response. Therefore, additional V_S models were developed with a sharp increase in V_S between a depth of 30 and 40 m to better match the amplitude and frequency of the HVSR peak. Figure 7 presents the calculated HVSR response for the ensemble of V_S models presented in Figure 6. The V_S model with calculated HVSR response best matching the observed HVSR frequency (Figure 7) was selected for site characterization.

V_{S30} is 408 m/s (NEHRP Site Class C). The estimated error in V_{S30} , which includes some effects of the lateral velocity variability beneath the testing arrays, is about 35 m/s. This is computed based on the sum of the following rounded to the nearest 5 m/s: an estimated error of 3% from the realistic assumed layer Poisson's ratios in the model, 1% error from the realistic assumed layer densities in the model, 2% for the variation in V_{S30} associated with non-uniqueness, and the 2.5 % COV in V_{R40} from the passive-source surface wave dispersion data. The HVSR peak frequency near the seismic station (4 Hz) is slightly higher than that near the center of Array 1 (3.6 Hz). This indicates that the weathered rock may be slightly shallower near the seismic station. Shifting the lower high velocity layer in the V_S model (Table 2) from 35 to 30 would account for the different HVSR peak frequency with no change in V_{S30} .

Interestingly, V_{S30} estimated from V_{R40} using the Brown et al., 2000 relationship ($V_{S30} \cong 1.045V_{R40}$, assuming V_{R40} represents the fundamental mode Rayleigh wave) is 411 m/s, less than 1% higher than that estimated from the V_S model.



File Name: 18045_58135

Date: 6/7/2018

Legend

- Corrected CSMIP Station
- CSMIP Station and Number
- ★ H/V Spectral Ratio Measurement Location
- MASW Array

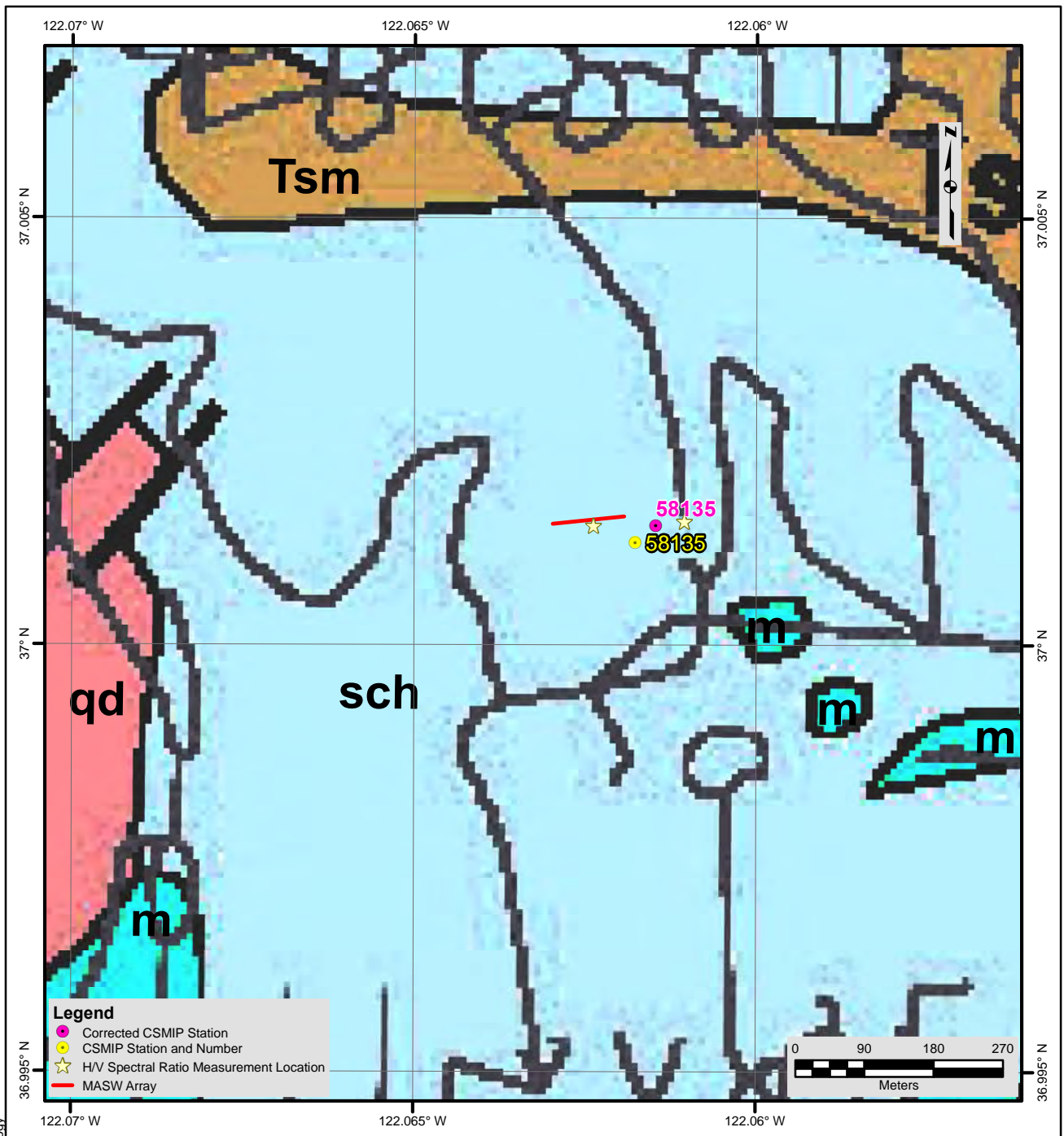
NOTES:

1. WGS 1984 Coordinate System
2. Image Source: Esri, DigitalGlobe, GeoEye, Earthstar Geographics, CNES/Airbus DS, USDA, USGS, AEX, Getmapping, Aerogrid, IGN, IGP, swisstopo, and the GIS User Community



**FIGURE 1
SITE MAP
CE • 58135**





File Name: 18045_58135-Geology

Date: 6/7/2018



**FIGURE 2
 GEOLOGIC MAP
 CE • 58135**





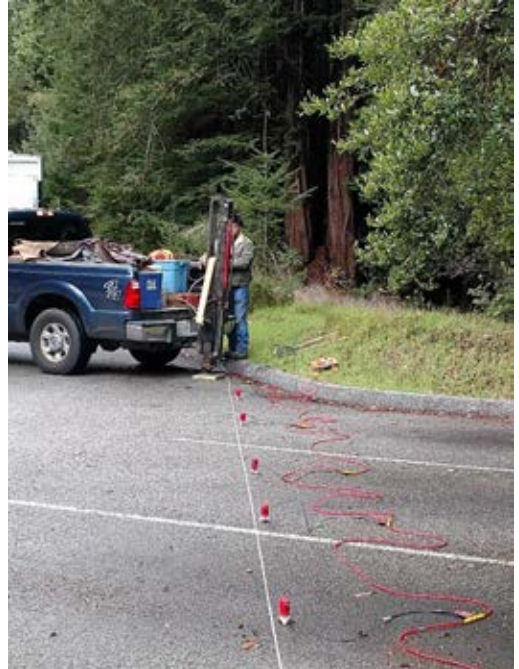
Looking northwest towards HVSR measurement location 2 and building housing seismic station CE.58135



Looking towards HVSR measurement location 1

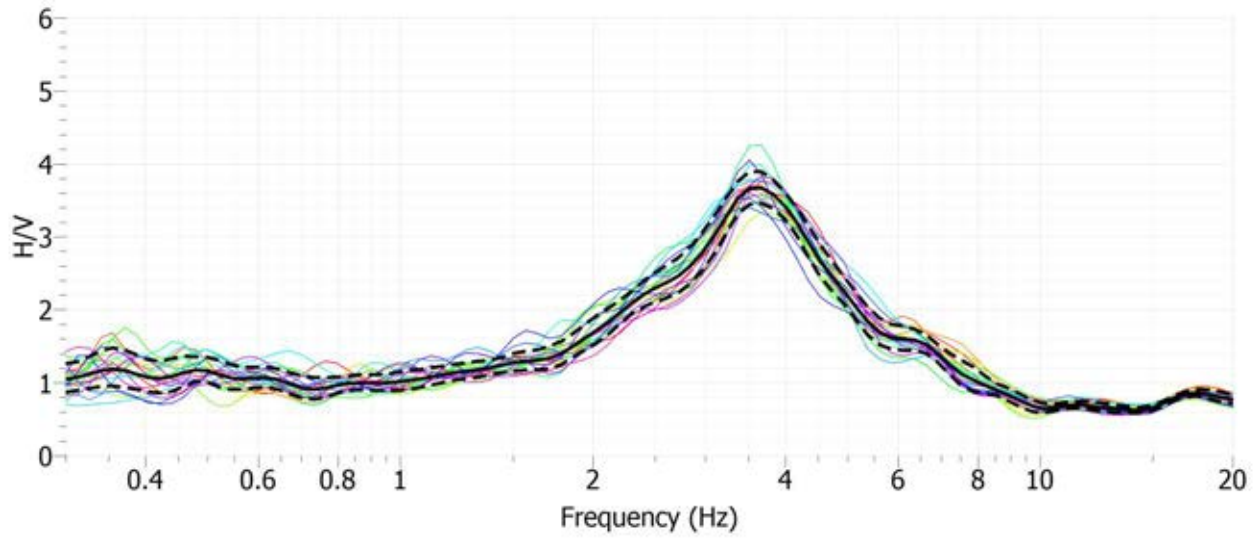


Looking east along MASW Array 1

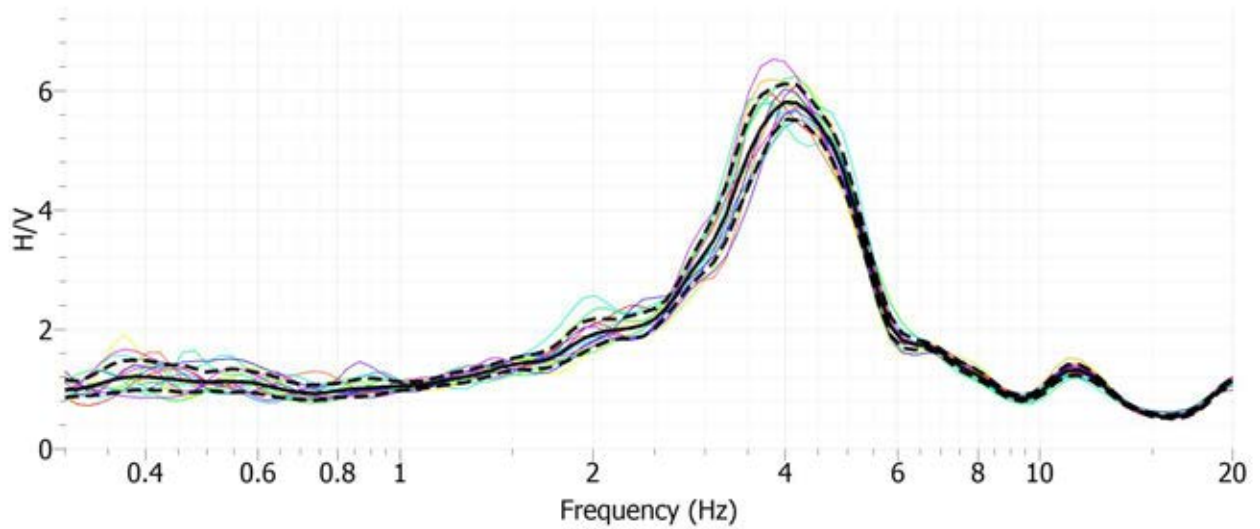


Looking west along MASW Array 1 and accelerated weight drop energy source

Figure 3 Site CE.58135 Photographs



Site CE.58135, HVSr Location 1, Nanometrics Trillium Compact Sensor



Site CE.58135, HVSr Location 2, Nanometrics Trillium Compact Sensor

Figure 4 H/V Spectral Ratio of Ambient Vibration Data – Site CE.58135

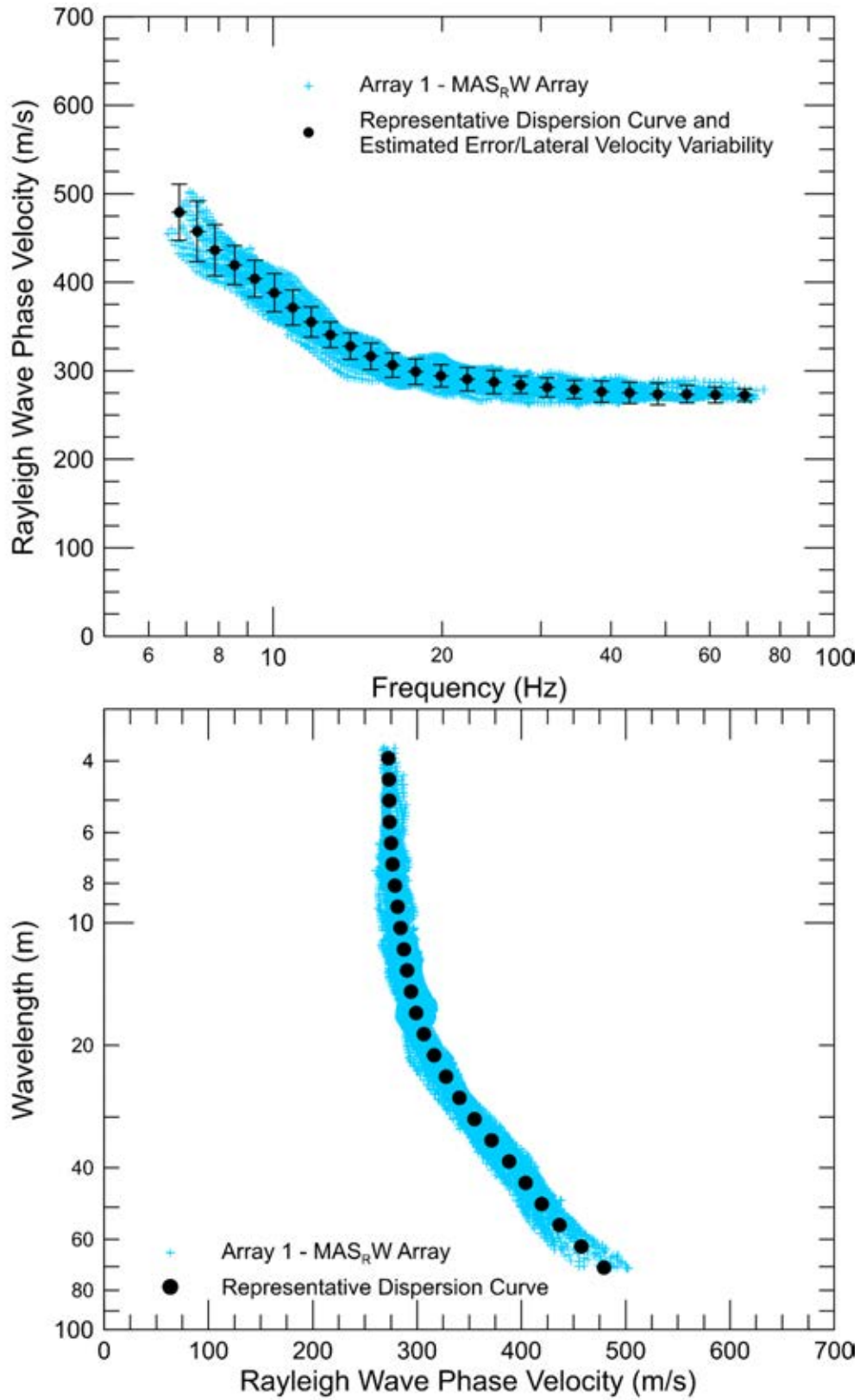


Figure 5 CE.58135 – Rayleigh wave dispersion curves derived from active-source surface wave data

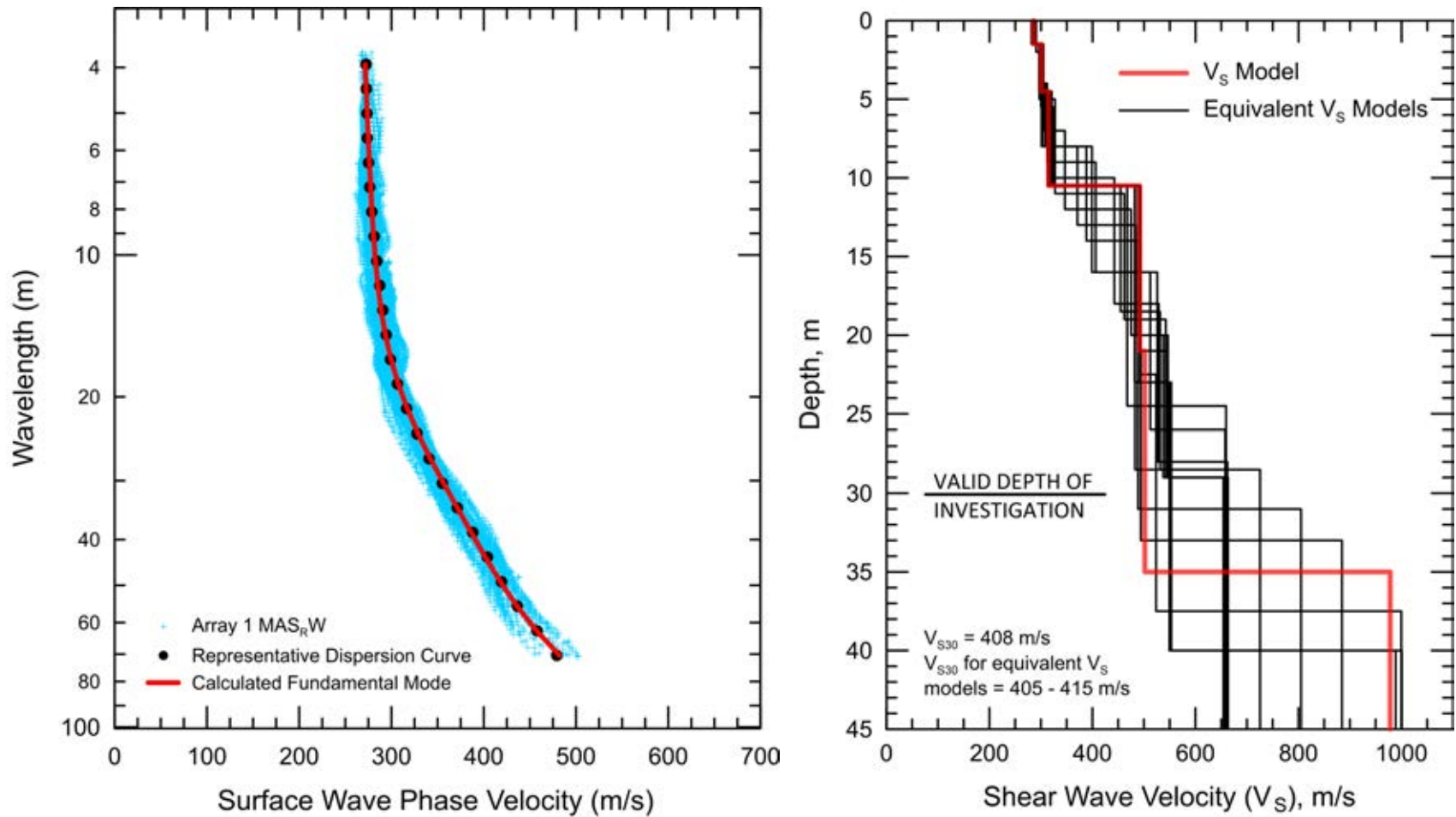


Figure 6 CE.58135 - Field, representative and calculated surface wave dispersion data (left) and associated V_s models (right)

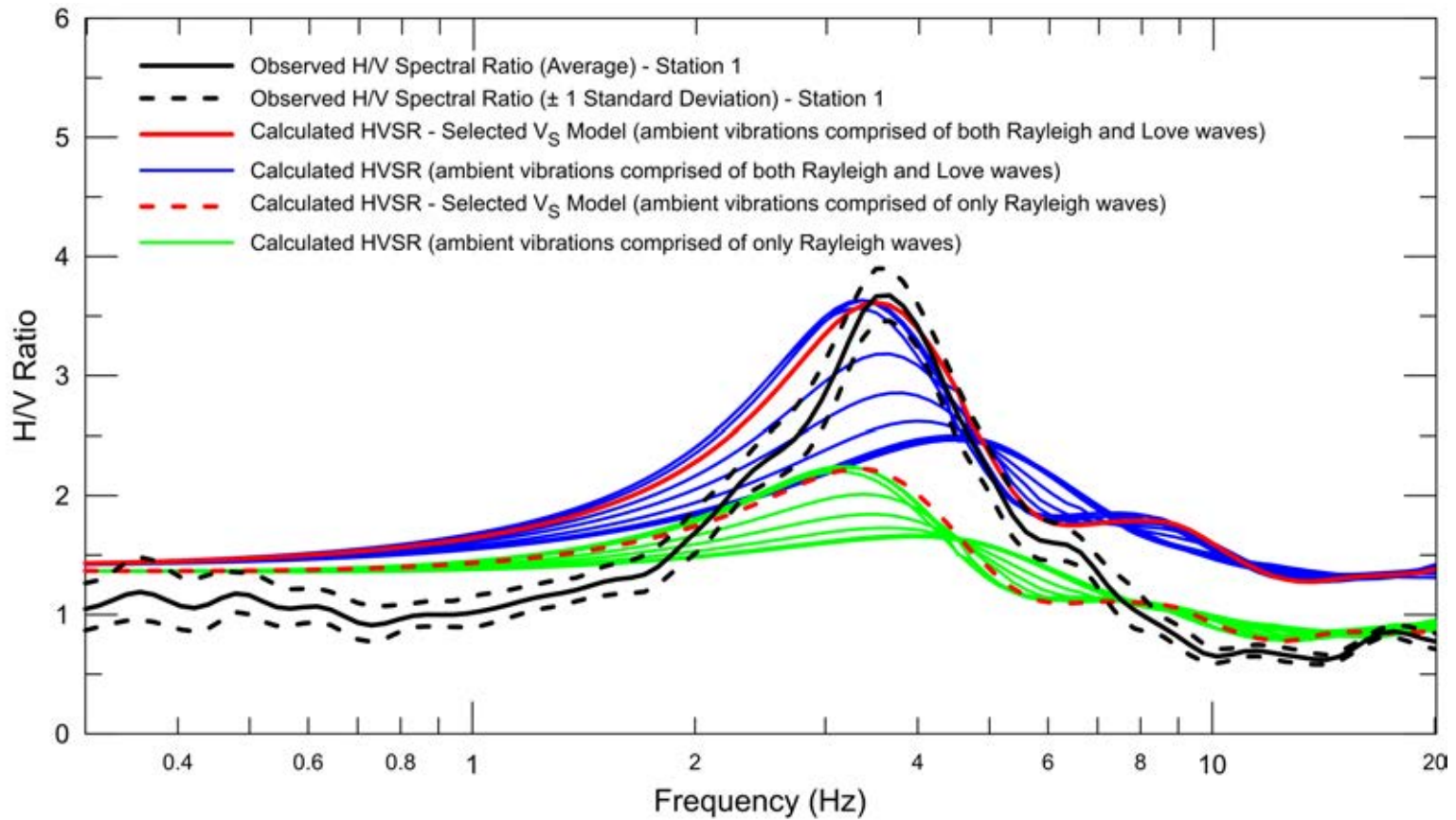


Figure 7 CE.58135 – Calculated HVSR response for V_S models based on diffuse field assumption. V_S models were developed with abrupt increase in velocity at depth greater than expected depth of investigation to better fit frequency and amplitude of HVSR peak.